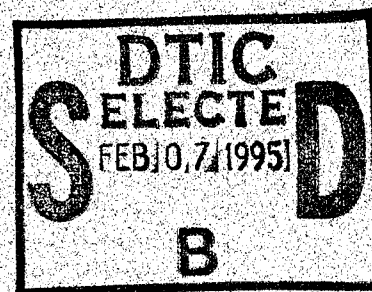
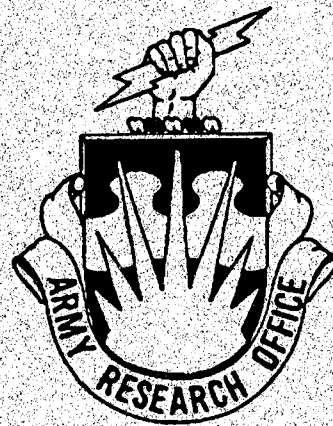
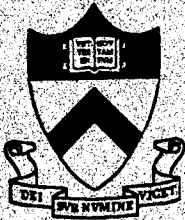


# UNITED STATES ARMY RESEARCH OFFICE

## *11<sup>th</sup>* *ENGINE WORKSHOP*

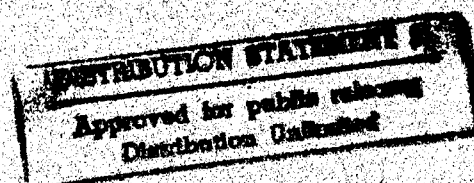


March 14 - 15, 1994



Princeton University  
Princeton, New Jersey

19950203 015



# REPORT DOCUMENTATION PAGE

Form Approved  
OMB No. 0704-0188

Public reporting burden for this collection of information is estimated to average 1 hour per response, including the time for reviewing instructions, searching existing data sources, gathering and maintaining the data needed, and completing and reviewing the collection of information. Send comments regarding this burden estimate or any other aspect of this collection of information, including suggestions for reducing this burden, to Washington Headquarters Services, Directorate for Information Operations and Reports, 1215 Jefferson Davis Highway, Suite 1204, Arlington, VA 22202-4302, and to the Office of Management and Budget, Paperwork Reduction Project (0704-0188), Washington, DC 20503.

1. AGENCY USE ONLY (Leave blank)		2. REPORT DATE 10/19/94	3. REPORT TYPE AND DATES COVERED Final 1 Mar 94 - 31 Jul 94	
4. TITLE AND SUBTITLE ELEVENTH ARMY RESEARCH OFFICE ENGINE WORKSHOP			5. FUNDING NUMBERS DAAH04-94-G-0059	
6. AUTHOR(S) C.K. Law				
7. PERFORMING ORGANIZATION NAME(S) AND ADDRESS(ES) Princeton University Department of Mechanical & Aerospace Engineering E-Quad D325 Princeton, NJ 08544			8. PERFORMING ORGANIZATION REPORT NUMBER	
9. SPONSORING/MONITORING AGENCY NAME(S) AND ADDRESS(ES) U.S. Army Research Office P.O. Box 12211 Research Triangle Park, NC 27709-2211			10. SPONSORING/MONITORING AGENCY REPORT NUMBER ARO 33033.1-EG-CF	
11. SUPPLEMENTARY NOTES The views, opinions and/or findings contained in this report are those of the author(s) and should not be construed as an official Department of the Army position, policy, or decision, unless so designated by other documentation.				
12a. DISTRIBUTION/AVAILABILITY STATEMENT Approved for public release; distribution unlimited.			12b. DISTRIBUTION CODE	
13. ABSTRACT (Maximum 200 words) The Eleventh Engine Workshop sponsored by the Army Research Office was held at Princeton University on March 14-15, 1994. A total of nineteen presentations were conducted in four half day sessions, covering the topics of ignition chemistry, soot formation, atomization and spray, turbulent combustion, and advanced diagnostics as related to diesel engine combustion. This Proceeding consists of the summary of the presentations.				
14. SUBJECT TERMS			15. NUMBER OF PAGES	
			16. PRICE CODE	
17. SECURITY CLASSIFICATION OF REPORT UNCLASSIFIED	18. SECURITY CLASSIFICATION OF THIS PAGE UNCLASSIFIED	19. SECURITY CLASSIFICATION OF ABSTRACT UNCLASSIFIED	20. LIMITATION OF ABSTRACT UL	

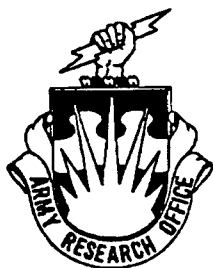
Proceedings of the

**ELEVENTH**

**ARMY RESEARCH OFFICE**

**ENGINE WORKSHOP**

Sponsored by



U.S. Army Research Office



Princeton University

ALL QUALITY INSPECTED 4

## Table of Contents

	Page
Agenda	iii
List of Presentations	vi
Abstracts of Presentations	1
List of Invitees	20

<b>Accession For</b>	
NTIS GRA&I	<input checked="" type="checkbox"/>
DTIC TAB	<input type="checkbox"/>
Unannounced	<input type="checkbox"/>
Justification	
By _____	
Distribution _____	
Availability Codes	
Dist	Avail and/or Special
A-1	

## Agenda

### Monday, March 14th

10:00 - 12:00	Registration
10:15 - 12:00	Lab Tour 1
12:00 - 1:00	Lunch
1:00 - 1:10	D.M. Mann and C.K. Law Welcome and Announcements
1:10 - 1:45	W. Bryzik, TARDEC "Army Tank-Automotive Propulsion Activities"
1:45 - 2:25	R. Bill, ARL-VPD "Vehicle Propulsion Directorate Engine, Combustion and Reacting Flow Interests"
2:25 - 3:00	M. Valco, NASA-Lewis "DOE/NASA Engine Research Program"
3:00 - 3:15	Break
3:15 - 4:00	J.M. Clarke, Caterpillar "Requirements for the Next Generation Diesel Engine"
4:00 - 4:30	N.P. Cernansky, Drexel University "High Pressure Preignition Chemistry of Hydrocarbons and Hydrocarbon Mixtures"
4:30 - 5:00	C.K. Law, Princeton University "Ignition in Convective-Diffusive Systems"
5:00 - 5:30	J. Trolinger, MetroLaser "Resonant Holographic Interferometry"
6:30 - 7:00	Social Hour
7:00	Banquet

## Tuesday, March 15th

- |               |   |
|---------------|---|
| 8:00 - 8:30   | Registration  |
| 8:30 - 9:00   | R.A. Dobbins, Brown University<br>"Control of Soot Formation"   |
| 9:00 - 10:00  | D.E. Foster, University of Wisconsin<br>"Soot Modeling and Experiments at the ERC"  |
| 10:00 - 10:30 | S.P. Lin, Clarkson University<br>"Jet Breakup Phenomena"  |
| 10:30 - 10:45 | Break   |
| 10:45 - 11:15 | L.A. Melton, University of Texas<br>"Fluorescent Diagnostics and Fundamental Droplet Processes"   |
| 11:15 - 11:45 | D.A. Santavicca, Penn State University<br>"The Effect of Turbulence on Vaporization and Mixing in Dense Sprays"                             |
| 11:45 - 12:45 | Lunch   |
| 12:45 - 1:15  | J. Abraham, University of Minnesota<br>"Computations of Sprays in a Very High Pressure, Constant Volume Chamber"                            |
| 1:15 - 2:00   | P.V. Farrell, University of Wisconsin<br>"Spray Research at the ERC"  |
| 2:00 - 2:30   | F.V. Bracco, Princeton University<br>"Advanced Diesel Injection Strategies"   |
| 2:30 - 3:00   | K.T. Rhee, Rutgers University<br>"High Speed, Four Color Infrared Digital Imaging for Studying In-Cylinder Processes in a DI Diesel Engine" |
| 3:00 - 3:15   | Break   |

**Tuesday, March 15th**

- 3:15 - 3:45      N.A. Henein, Wayne State University  
                     "Diesel Spray Dynamics, Ignition, Combustion, and Soot  
                     Formation"
- 3:45 - 4:15      D.E. Klett, North Carolina A & T University  
                     "Collaborative Research in Diesel Engine Combustion"
- 4:15 - 5:00      C.J. Rutland, University of Wisconsin  
                     "Diesel Combustion Modeling at the ERC"
- 5:00              Lab Tour 2

## List of Presentations

		Page
W. Bryzik, TARDEC	"Army Tank-Automotive Propulsion Activities"	1 -
R. Bill, ARL-VPD	"Vehicle Propulsion Directorate Engine, Combustion and Reacting Flow Interests"	2 -
M. Valco, NASA-Lewis	"DOE/NASA Engine Research Program"	3 -
J.M. Clarke, Caterpillar	"Requirements for the Next Generation Diesel Engine"	4 -
N.P. Cernansky, Drexel U.	"High Pressure Preignition Chemistry of Hydrocarbons and Hydrocarbon Mixtures"	5 -
C.K. Law, Princeton U.	"Ignition in Convective-Diffusive Systems"	6 -
J. Trolinger, MetroLaser	"Resonant Holographic Interferometry"	7 -
R.A. Dobbins, Brown U.	"Control of Soot Formation"	8 -
D.E. Foster, U. of Wisconsin	"Soot Modeling and Experiments at the ERC"	9 -
S.P. Lin, Clarkson U.	"Jet Breakup Phenomena"	10 -
L.A. Melton, U. of Texas	"Fluorescent Diagnostics and Fundamental Droplet Processes"	11 -
D.A. Santavicca, Penn State U.	"The Effect of Turbulence on Vaporization and Mixing in Dense Sprays"	12 -
J. Abraham, U. of Minnesota	"Computations of Sprays in a Very High Pressure, Constant Volume Chamber"	13 -
P.V. Farrell, U. of Wisconsin	"Spray Research at the ERC"	14 -
F.V. Bracco, Princeton U.	"Advanced Diesel Injection Strategies"	15 -
K.T. Rhee, Rutgers U.	"High Speed, Four Color Infrared Digital Imaging for Studying In-Cylinder Processes in a DI Diesel Engine"	16 -



N.A. Henein, Wayne State U.	"Diesel Spray Dynamics, Ignition, Combustion, and Soot Formation"	17 -
D.E. Klett, N C A&T U.	"Collaborative Research in Diesel Engine Combustion"	18 -
C.J. Rutland, U. of Wisconsin	"Diesel Combustion Modeling at the ERC"	19 -

## **INVITED PRESENTATION**

### **Army Tank-Automotive Propulsion Activities**

**W. Bryzik  
US Army Tank-Automotive RDE Center (TARDEC)  
Warren, MI 48397-5000**

The propulsion system forms a critical building block for present and future military ground vehicles. Characteristics of particular importance to TARDEC's ground propulsion systems include: low system volume (including engine, cooling system, air handling system, turbomachinery, ducts, etc.), low system weight, improved fuel economy or vehicle range, rapid acceleration, reduced signature (including thermal acoustic, visual/smoke, etc.), high reliability and survivability, and improved cost effectiveness. Innovative integration of the propulsion system components, when combined with individual component technology gains, produce an exceptional opportunity for optimizing the above listed characteristics.

Various propulsion system activities at TARDEC are discussed during this briefing from an overall perspective standpoint. Representative example projects dealing with: 1) low heat rejection combustion, 2) cold start characteristics, 3) engine finite element analysis procedures, 4) advanced diesel technology, 5) engine wear analysis and life prediction, 6) thin ceramic coating performance optimization, 7) multi-fuel adaptation to two-stroke engines, and 8) a number of other efforts aimed at optimizing the characteristics given above are discussed. In addition, the importance of TARDEC's leveraging of propulsion activities being funded by sources such as the Army Research Office (ARO), Army Research Laboratory (ARL), ARPA, DOE, NSF, and others is noted with a few examples given.

## **INVITED PRESENTATION**

**Vehicle Propulsion Directorate Engine,  
Combustion and Reacting Flow Interests**

**R. Bill  
U.S. Army Vehicle Propulsion Directorate/ARL  
Lewis Research Center, Cleveland, Ohio 44135**

## **INVITED PRESENTATION**

### **DOE/NASA Engine Research Program**

**M. Valco  
NASA Lewis Research Center  
Vehicle Propulsion Directorate, Army Research Laboratory  
Cleveland, OH 44135-3127**

## **INVITED PRESENTATION**

### **Requirements for the Next Generation Diesel Engine**

**J.M. Clarke  
Engine Research Department  
Caterpillar Inc.  
Peoria, IL 61629**

The common goals of the ARO, universities and the heavy duty engine industry are discussed. It is apparent that understanding emission mechanisms, evolving the next generation of design optimization methods and identifying potential revolutions in engine design should be highlights of engine related research.

The chemical kinetic and fluid dynamics modeling of heterogeneous combustion processes remains beyond the reach of engine designers and developers. The low speed, uncertain accuracy and high cost of current physically based simulations takes them outside the design and development cycles. This is the area which needs the most development of physical insight leading to efficiently formulated models.

Current engine design is an extremely complex decision process based on information from marketing, raw materials costs, manufacturing costs, and analyses related to durability and reliability, performance and emissions. Much of the data is subject to uncertainty and some of it is based on experience in the form of "rules of thumb". In spite of this informal process (some might say because of its informality) engines have improved enormously. Additional improvement is anticipated based on up-to-date information processing and rational optimizing procedures. For instance, we are a long way from the genetic programming of optimum engine designs. Anticipated computer performance increase seems to bring procedures of this type into the realm of possibility. Efforts to move in this direction will continue to attract industry interest.

Since the diesel engine matured in its current form there have been many "breakthroughs" in technical capability. Looking at the "breakthrough" list it becomes tempting to try new engine designs based on recognizing the role such capability might play in radical approaches to a new generation of ecologically benign and economically attractive engines. Here is a chance for universities to challenge their multi-disciplined(?) eager(?) young engineers. A table of required and desired functional features in any new design is included.

## High Pressure Preignition Chemistry of Hydrocarbons and Hydrocarbon Mixtures

N.P. Cernansky and D.L. Miller  
Department of Mechanical Engineering and Mechanics  
Drexel University  
Philadelphia, PA 19104

An experimental program to study the effects of pressure on preignition chemistry of hydrocarbon fuels is currently underway. Experiments are being conducted over a range of operating conditions, including temperatures which encompass the low and intermediate temperature regimes (500-1000 K), and pressures ranging from less than 1 atm to 20 atm. Three experimental test facilities are being used to perform this study: a pressurized flow reactor (PFR), an atmospheric flow reactor (APFR), and a static reactor (SR). Results are being used to provide much needed kinetic and mechanistic information in these regimes over a range of pressures. Additionally an effort to develop in situ diagnostic capabilities in the laboratory has received partial funding under this contract.

Recent efforts have concentrated on the SR, PFR, diagnostic development and modeling. Studies of n-pentane in the SR have identified important steps which control product formation. Results on 1-pentene indicate that long alkenes exhibit negative temperature coefficient behavior similar to alkanes. Experimental studies of n-butane, iso-butane and n-pentane oxidation at elevated pressures using the PFR have confirmed that branched chains are less reactive than straight chains and have provided species distribution data for use in modeling. The newly installed on-line FTIR measured significant levels of formic acid, a species difficult to measure by other techniques, from the reaction of n-butane, iso-butane and n-pentane. DFWM development continues with measurements of OH and continued work on HO<sub>2</sub>. All of these data are used to develop detailed chemical mechanistic information and elucidate the effects of pressure on the mechanisms. We have recently adopted a two temperature sensitivity method to test for the effect of reaction rate changes on NTC behavior.

---

Research supported by the Army Research Office Under  
Contract No. DAAH04-93-G-0042; Proposal No. 30782-EG

# Motivation

---

- Preignition fuel chemistry plays a critical role in diesel engine combustion
  - Low temperature phenomena are important (e.g., region of negative temperature coefficient, cool flames)
  - Significant in engine operations (e.g., diesel cold start, use of low cetane number fuels)
  - Consists of hydrocarbon oxidation at low and intermediate temperature ( $T < 1000\text{ K}$ ) and high pressure ( $1 < P < 30\text{ atm}$ )
- Detailed studies of hydrocarbon oxidation chemistry at low temperature and high pressure are limited
- Comprehensive chemical kinetic mechanisms are incomplete
  - Based largely on high temperature experimental results
  - Not easily extended to lower temperatures ( $< 1000\text{ K}$ ) and higher pressures (15-30 atm)
- Data needed to extend and validate models

## Effects of Temperature and Pressure on Overall Kinetic Mechanism

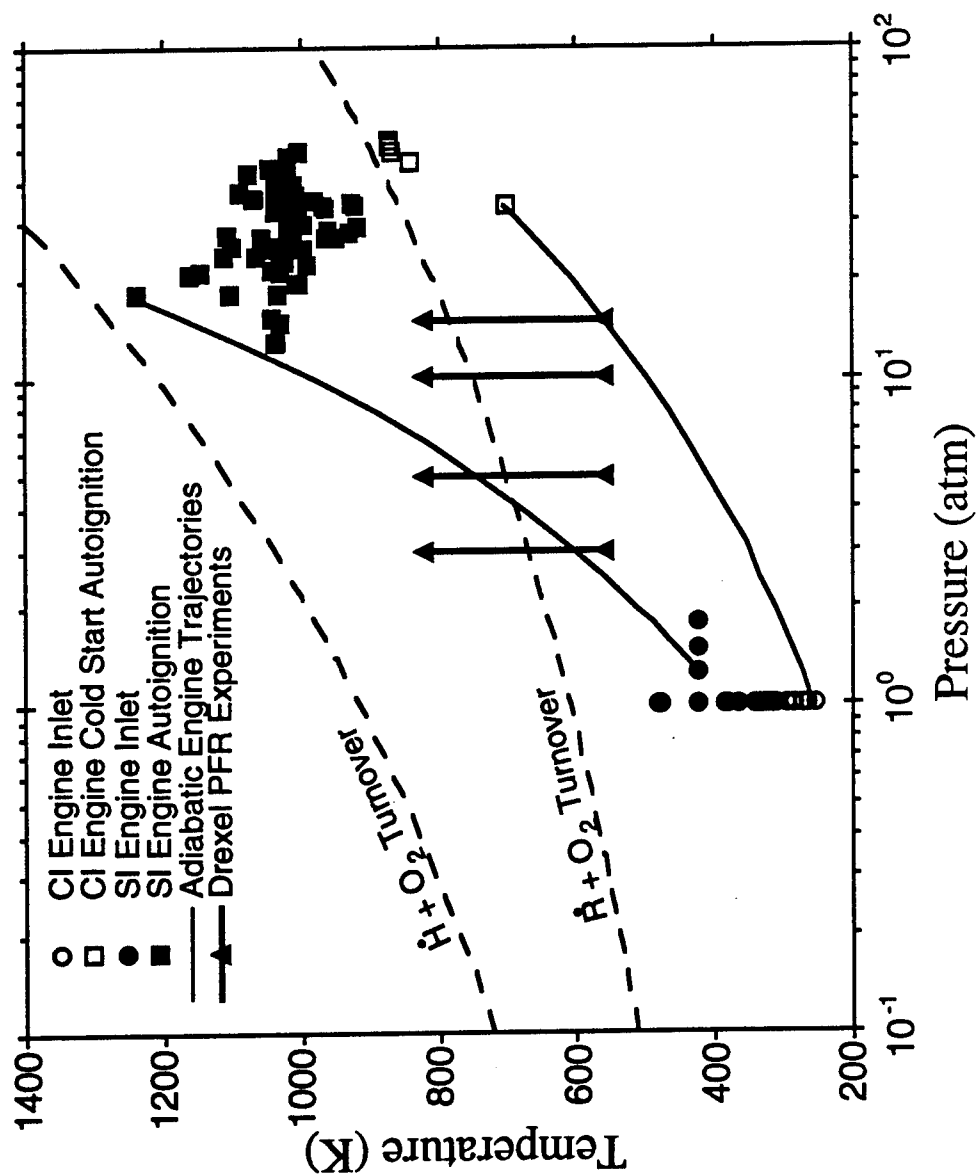
---

- Temperature and pressure changes can cause an exchange of dominance between competing chemical kinetic pathways
  - Certain "pathways" are preferred within a detailed chemical kinetic mechanism
  - Multiple pathways may lead to and proceed from intermediate compounds
  - For certain key intermediates, the preferred pathway shifts with changes in conditions (T, P,  $\Phi$ )
- $\dot{\text{R}} + \text{O}_2$  turnover marks the transition between the low and intermediate temperature regimes
- $\dot{\text{H}} + \text{O}_2$  turnover marks the transition between the intermediate and high temperature regimes



# The Low and Intermediate Temperature Regimes in Diesel Engines

Adiabatic (T,P)-Histories in Internal Combustion Engines Showing the Importance of the Low and Intermediate Temperature Regimes and Comparing the Experimental Conditions of Studies of Hydrocarbon Oxidation at Elevated Pressures



# Program Overview

---

- Objectives
  - Obtain mechanistic information for the oxidation of pure hydrocarbons at varying pressures in the low and intermediate temperature regimes
  - Determine effects of fuel components within multicomponent fuel mixtures on the ignition and emissions characteristics of engines
  - Formulate hypotheses on ignition mechanisms and develop a method for predicting the ignition characteristics of actual fuels based on their composition
- Approach
  - Three bench scale reactor facilities
    - Static Reactor (SR) (T: 500-750 K; P: 600 torr)
    - Atmospheric Pressure Flow Reactor (APFR) (T: 600-900 K)
    - Pressurized Flow Reactor (PFR) (T: 600-900 K; P: 2-20 atm)
  - Extracted gas samples for detailed chemical analysis (NDIR, FTIR, GC)
  - Development of optical diagnostics for on-line and in situ analysis
  - Chemical kinetic modelling

# **Summary of Prior Work**

---

- Static Reactor Activities
  - Experimental mechanistic studies with ethene, propene, propene oxide, n-butane, isobutane and n-pentane
  - Chemical kinetic modeling (with Westbrook and Pitz of LLNL)
  - Liquid fuel ignition studies on C7-C12 hydrocarbons:
    - Pure fuels in air (straight & branched chain alkanes, alkenes, aromatics)
    - Two and three component mixtures
- Atmospheric Pressure Flow Reactor Activities
  - Chemistry of aldehyde formation from diesel-type fuel components
  - Fuel structure/blending interaction effects for C5-C10 hydrocarbons
  - Investigation of the potential for a correlation between  $[\text{CO}]_{\text{max}}$  and octane number for PRF blends
- Pressurized Flow Reactor Activities
  - Reactivity mapping of C2-C4 alkanes and alkenes
  - Detailed species measurements of propane and n-butane oxidation
  - Examined the effect of pressure on the turnover between the low and intermediate temperature regimes

## **Summary of Recent Work**

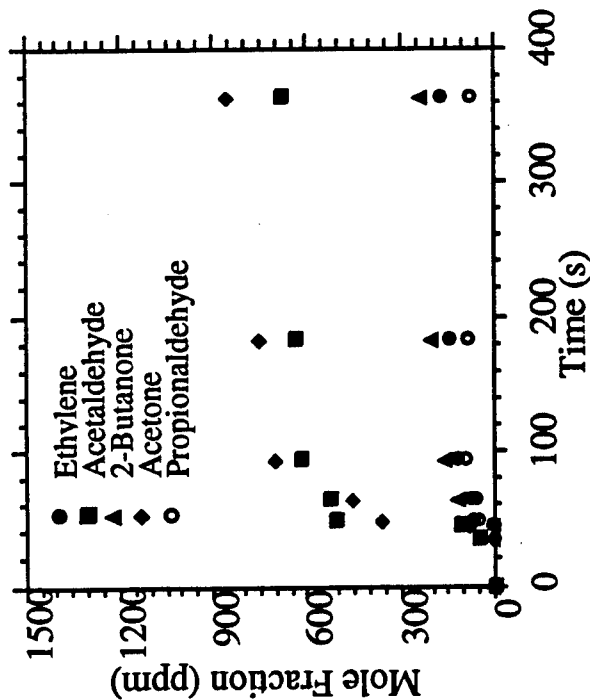
- Static Reactor Activities (T: 500-775 K; P: 200-400 torr)
  - Experimental studies to determine mechanism of 1-pentene oxidation and effect of 1-pentene on n-pentane oxidation
- Pressurized Flow Reactor Activities (T: 600-850 K; P: 4-15 atm)
  - Facility was upgraded to handle liquid fuels and for on-line FTIR
  - Experimental studies of n-butane, iso-butane and n-pentane oxidation
- Optical Diagnostic Technique Development
  - Species measurements by FTIR spectroscopy
  - Species measurements by DFWM
- Chemical Kinetic Modeling

## **Static Reactor Recent Work**

---

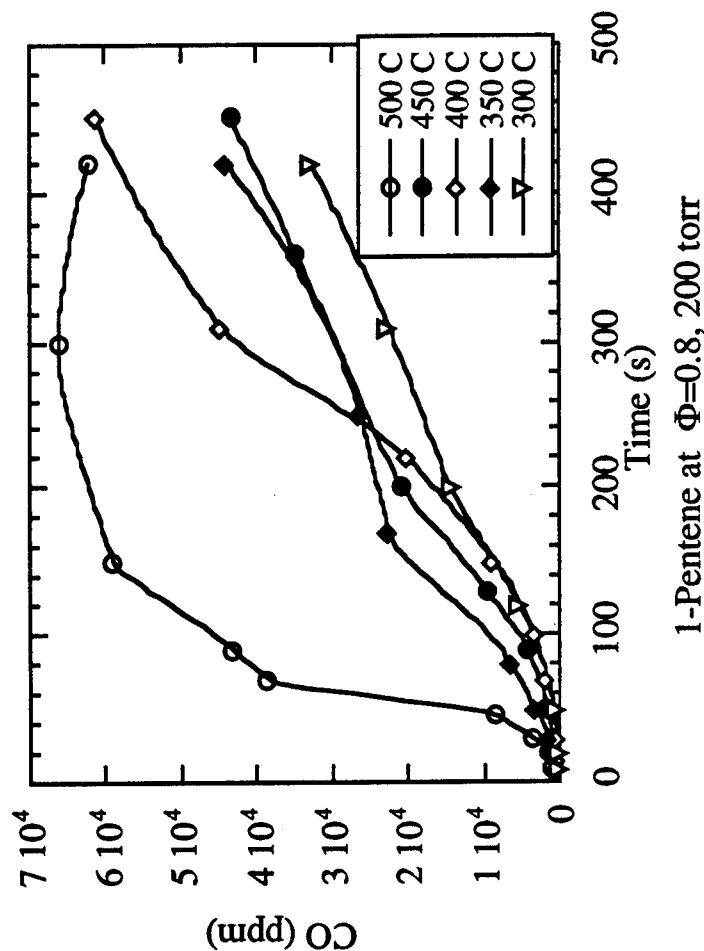
- Facility Upgraded & Verified
  - Modified Mac II based data acquisition system
  - Enhanced temperature measurement capability to check for temperature gradients within the reactor
- Experimental Studies
  - n-Pentane oxidation studies (Prabhu, M.S. thesis, March 1994)
  - 1-Pentene oxidation studies
  - 1-Pentene & n-pentane mixtures
  - Collected T and P vs time data to characterize induction time and general reactivity
  - Extracted gas samples for GC analysis

## Static Reactor Results



5-9

- Longstanding argument whether gas-phase or surface reactions cause acetone formation
- Results indicate gas-phase dihydroperoxy radical decomposition explains acetone formation



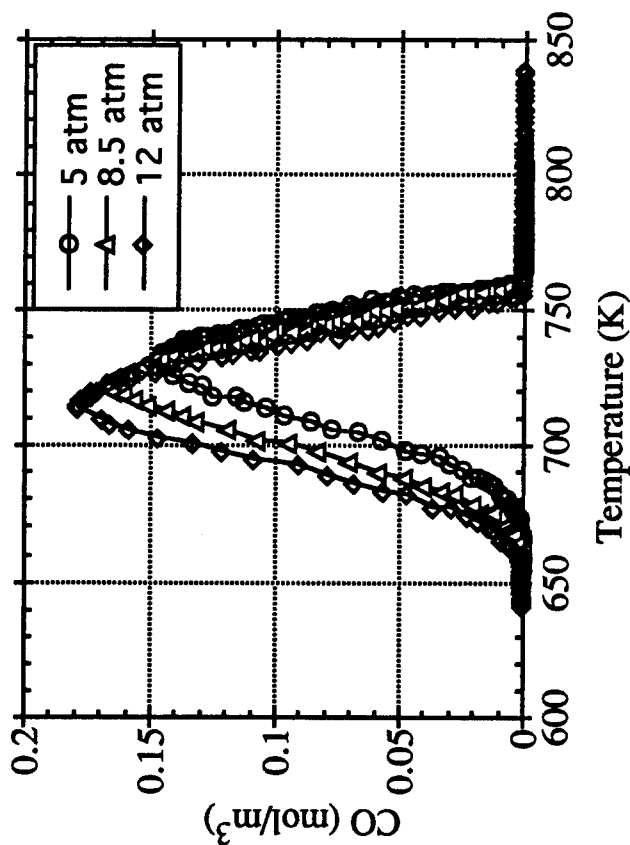
- NTC behavior observed in CO profiles
- Further analysis will provide insight on NTC region transition in olefins

## **Pressurized Flow Reactor Recent Work**

---

- Liquid Fuel Delivery System Designed and Implemented
- Species Measurements by FTIR Spectroscopy
  - Samples extracted from PFR and analyzed via FTIR spectroscopy
  - Measurements of water, formaldehyde and methanol now possible in addition to other stable species
  - Formic acid detected in significant concentrations
  - H and C atom balances within  $\pm 2\%$
- Experimental Studies
  - Completed detailed species measurements for propane
    - Koert et al., **Comb. Flame**, **96**: 34-49, January 1994
    - Modeling with LLNL underway
  - Completed detailed species measurements for n-butane
    - Anand et al., WSSCI 94-39, 1994
    - Anand, M.S. thesis, March 1994
  - Iso-butane oxidation studies
    - McCormick, M.S. thesis, June 1994
  - n-Pentane oxidation studies
    - Wood, M.S. thesis, August 1994

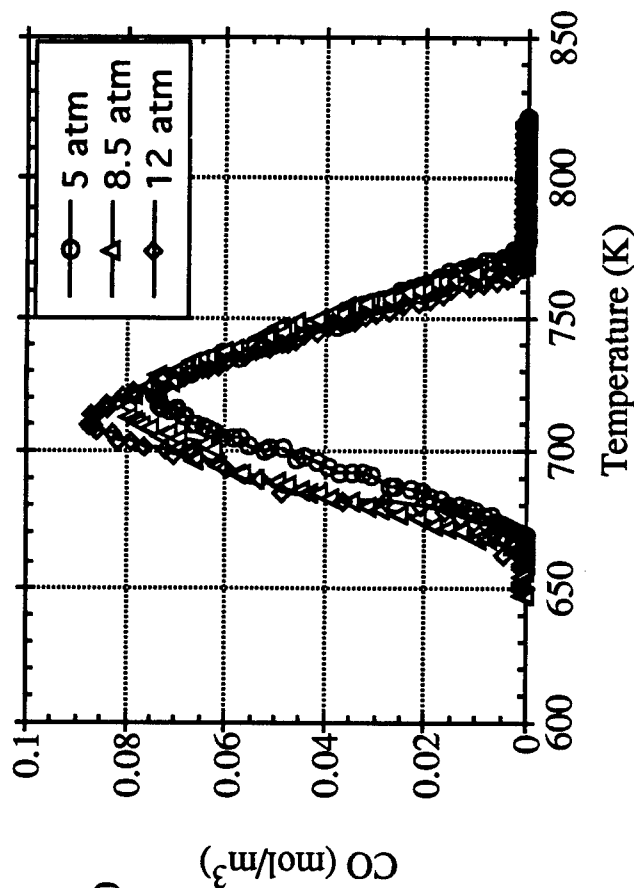
# PFR Results - N-Butane and Iso-Butane Cool Down



n-Butane at  $\Phi=0.3$ ,  $[C]=1.64 \text{ mol/m}^3$

- n-Butane more reactive than iso-butane
- Oxygenates favored in the low temperature region and alkenes favored in the NTC region
- Formic acid detected in significant concentration

- Each set of experiments are at constant C and O atom concentration



Iso-butane at  $\Phi=0.3$ ,  $[C]=2.08 \text{ mol/m}^3$



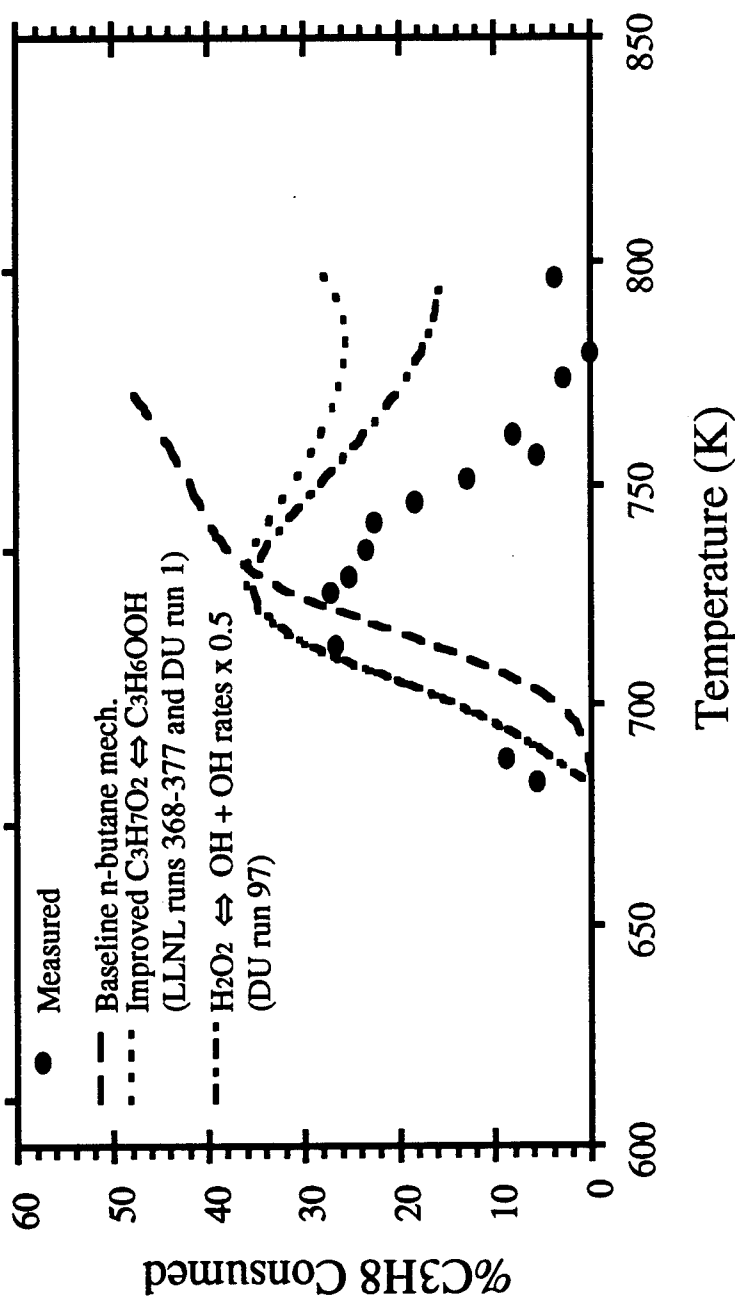
# **Optical Diagnostic Technique Development**

---

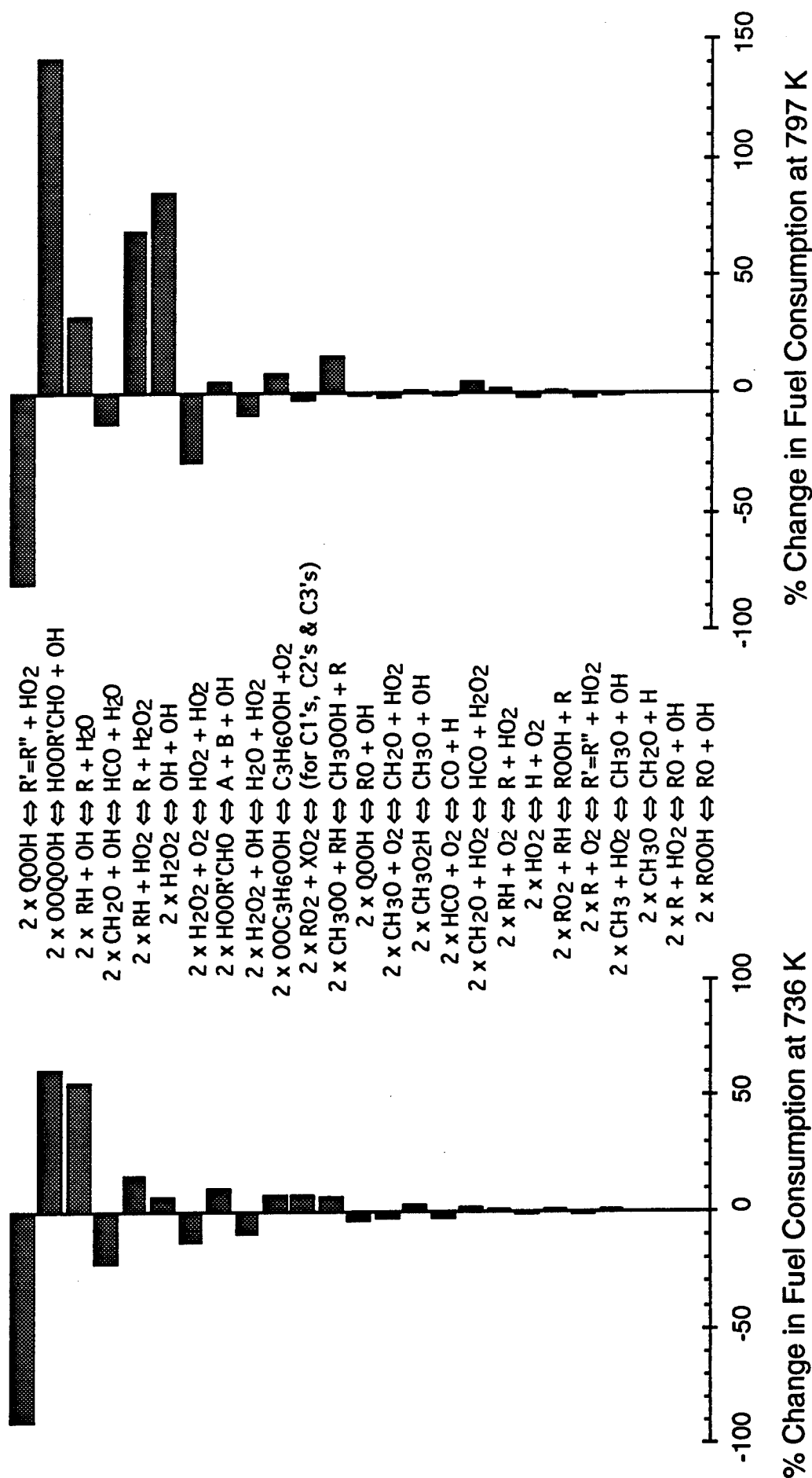
- Species Measurements by FTIR Spectroscopy
  - Constructed reactor using an optical multipass gas cell in sample compartment of FTIR spectrometer
  - Developed technique to measure stable products
  - Studied oxidation of methyl radicals generated by UV photolysis of azomethane at 298 K and 1 atm
  - Unable to determine IR signature of methylperoxy radicals
  - More dynamic range required to simultaneously measure both stable and radical species
- Species Measurements using DFWM
  - Acquired DFWM signals for OH from different sources and conditions:
    - Propane/Air bunsen burner flame
    - Hydrogen/Oxygen/Nitrogen slot burner flame
    - Low pressure/concentration discharge chamber
  - Optimizing beam tilting technique to increase sensitivity
  - Working on CN and HO<sub>2</sub> measurements
  - Developing a technique for HO<sub>2</sub> calibration using electrical discharge under low pressure in a discharge flow reactor

## Chemical Kinetic Modeling

- Current detailed kinetic models have difficulty reproducing experimental data that span multiple reaction regimes (e.g., the NTC region)
- In cooperation with LLNL we are working to improve these models by:
  - Providing new and challenging experimental data
  - Suggesting appropriate sub-mechanism modifications and changes
  - Employing techniques such as two temperature sensitivity analysis
- Some recent modeling results



# Sensitivity to a Factor of Two Increase in Rates as Indicated by %Fuel Consumed



## **Status and Issues**

---

- There is a growing body of data at pressures of practical importance for alkanes and alkenes; the framework for interpreting alkane chemistry is well advanced
  - Alkene chemistry still uncertain
  - Component interactions not well understood
- Importance of low and intermediate temperature chemistry is well accepted; mechanisms are now available which include these steps and they are under continued development
  - HO<sub>2</sub> radicals still appear to be the key species
  - Rate parameters for coupled RO<sub>2</sub> mechanism are uncertain
  - Dihydroperoxide chemistry appears essential for explaining observed product distributions
- Measurement of key radical intermediates may simplify the puzzle
  - DFWM has reasonable potential for measuring HO<sub>2</sub> radicals

## **Current and Planned Activities**

---

- Static Reactor
  - Complete study of 1-pentene and its effect on the oxidation of n-pentane
  - Study oxidation of other C5 hydrocarbon fuels and fuel blends
- Pressurized Flow Reactor
  - Complete detailed species measurements for iso-butane and n-pentane
  - Study pressure effects on the oxidation chemistry of 1-butene, 1-pentene, cis-2-butene and trans-2-butene
- Optical Diagnostic Techniques
  - Continue work on developing a DFWM technique for CN and HO<sub>2</sub> radical measurement in combustion sources
  - Apply and extend techniques for in situ species measurements
- Chemical Kinetic Modeling
  - Continue mechanistic development activity
  - Continue collaborative efforts with LLNL

## Ignition in Convective-Diffusive Systems

C. K. Law and T. G. Kreutz

Department of Mechanical and Aerospace Engineering  
Princeton University  
Princeton, NJ 08544

Autoignition in non-premixed hydrocarbon/air combustion has been experimentally, numerically, and analytically investigated in counterflowing jets of fuel against hot air. Details of the ignition process are studied by examining the *steady-state* situation as the air temperature is raised to a point *just prior* to ignition. Experimental measurements of the ignition temperature have been made as a function of system pressure, aerodynamic strain rate, and fuel concentration for fuels such as hydrogen, methane, propane, n-butane, and iso-butane. These studies are augmented by numerical modelling using detailed chemistry that elucidates the nature of underlying ignition 'kernel', a spatially-localized zone of high chemical reactivity.

In the  $H_2$ -air system, both experiments and calculations show that the ignition temperature, when plotted as a function of pressure, exhibits a characteristic 'Z'-shape similar to that seen in the explosion limits of homogeneous  $H_2$ -air mixtures. The three sections of this Z-curve are denoted the first, second, and third ignition limits in analogy with the three explosion limits. Numerical analysis indicates that, for each limit, the dominant chemistry is identical in both the explosion and ignition situations. Aerodynamic straining is found in all cases to increase the ignition temperature due to the decreased size of the ignition kernel and the decreased residence time of active radicals within it. Ignition in the first and third limits are found to be sensitive to aerodynamic straining because loss of radical species via mass transport plays an important role in these two ignition regimes. In contrast, the second ignition limit is governed primarily by fast chemical reactions and is thus relatively insensitive to variations in the strain rate.

The chemistry governing the  $H_2$ -air ignition process has been distilled by means of careful analysis and verified by means of 'skeletal' chemical reaction mechanisms consisting of a minimal number of elementary reaction steps. The skeletal mechanisms have been further compressed to 'reduced' mechanisms, consisting of non-elementary reactions, via techniques such as the steady-state approximation. These methods and reaction schemes are validated by means of comparison with the results of computations using the full kinetic mechanism.

In the  $H_2$ -air system, the role of heat release in providing 'thermal feedback' at the ignition turning point has been examined in detail for all three ignition limits. Contrary to classical notions based upon one-step overall chemistry, thermal feedback is shown to play essentially *no*, or minimal, role in the steady-state solution at the ignition turning point - either in its character or parametric dependence. In most cases, turning point and S-curve behavior are found to exist in the complete absence of heat release, driven solely by 'kinetic' feedback provided by algebraic nonlinearities in the coupled chemical kinetics. As a result, the location of the ignition turning points are found to be essentially governed by the kinetics of gain versus loss of key radicals in the ignition kernel which depend parametrically upon global variables such as air temperature, strain rate, pressure, and fuel concentration.

Experimental and calculated ignition temperatures for methane, as well as measured ignition temperatures for n-butane and iso-butane, are found to be quite sensitive to the strain rate. Sensitivity to aerodynamic straining is found to occur when at least one critical ignition reaction proceeds at a rate which is relatively slow and thus comparable to the rates of mass transport out of the localized region of the ignition kernel.

## *Background*

- Ignition in Diesel engines is expected to involve inhomogeneous mixtures:
  - Premixed reactants
  - Nonpremixed reactants
  - Temperature nonuniformity
- Presence of temperature and concentration gradients implies the importance of diffusive transport.
- Ignition states determined from homogeneous experiments may not be directly applicable.

## *Objectives*

- To study the dynamics and chemical kinetics of hydrocarbon/air ignition in the presence of diffusive mixing.
- Experimentally and computationally determine:
  - 1) Bulk ignition parameters such as ignition temperature and strain rate;
  - 2) Identify the critical kinetic steps and species governing diffusive ignition.
- Analytically derive:
  - 1) Reduced mechanisms relevant to diffusive ignition;
  - 2) Ignition Damköhler number and criteria.
- Conceptually understand/unify:
  - 1) Homogeneous versus diffusive ignition;
  - 2) Thermal versus kinetic ignition.

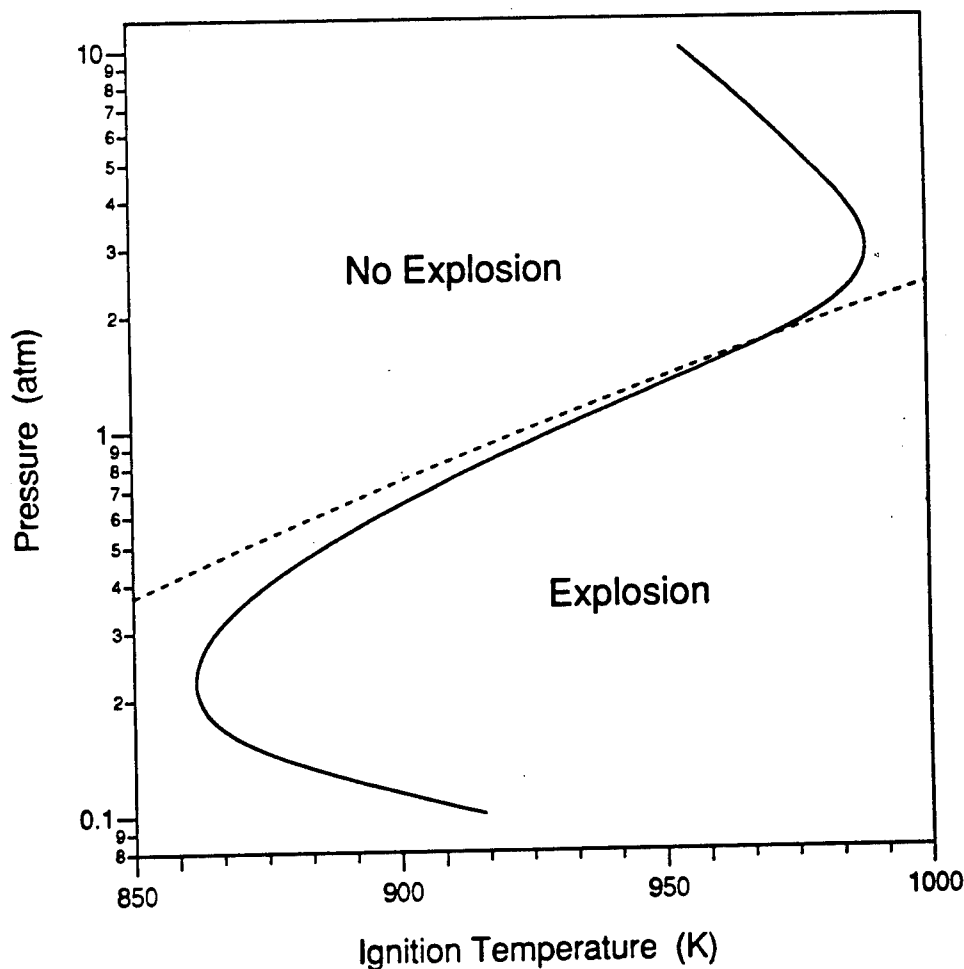


## *Approach*

- Counterflow configuration: well-defined strain rate and hence characteristic flow time
- Steady-state ignitability studies
- Transient ignition
- Nonpremixed ignition: cold fuel against hot air
- Premixed ignition: cold fuel/air against hot inert
- Investigate/manipulate ignitability for different:
  - Fuels (e.g.  $\text{H}_2$ ,  $\text{CH}_4$ ,  $\text{C}_3\text{H}_8$ ,  $n\text{-C}_4\text{H}_{10}$ ,  $i\text{-C}_4\text{H}_{10}$ )
  - Fuel concentration
  - Temperature of the hot jet
  - System pressure
  - Flow strain rate

## *Diffusive Ignition of Hydrogen/Oxygen Mixtures*

- Homogeneous ignition of hydrogen/oxygen mixture is characterized by three explosion limits.
- How is this behavior modified by diffusion and aerodynamic straining in a nonuniform, flowing mixture?



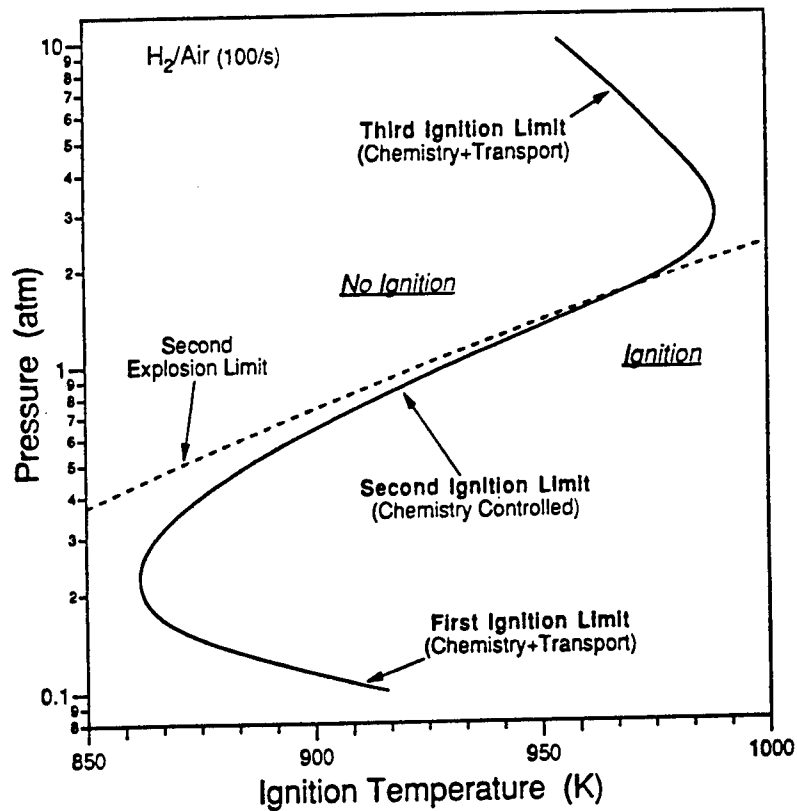
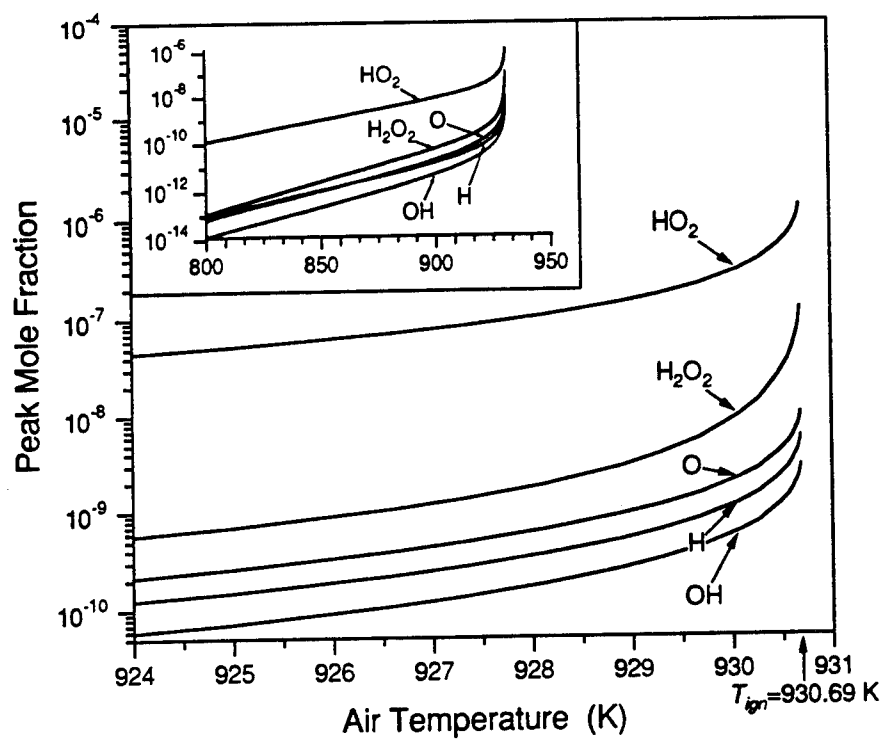
## *H<sub>2</sub>/Air Reaction Mechanism*

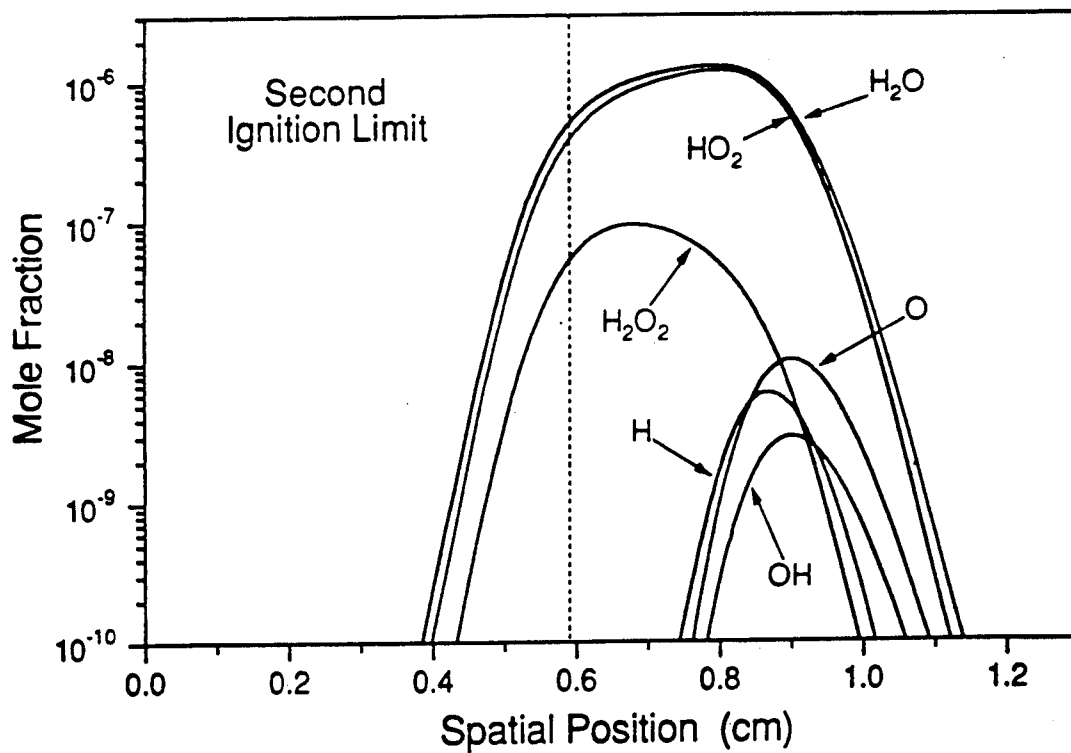
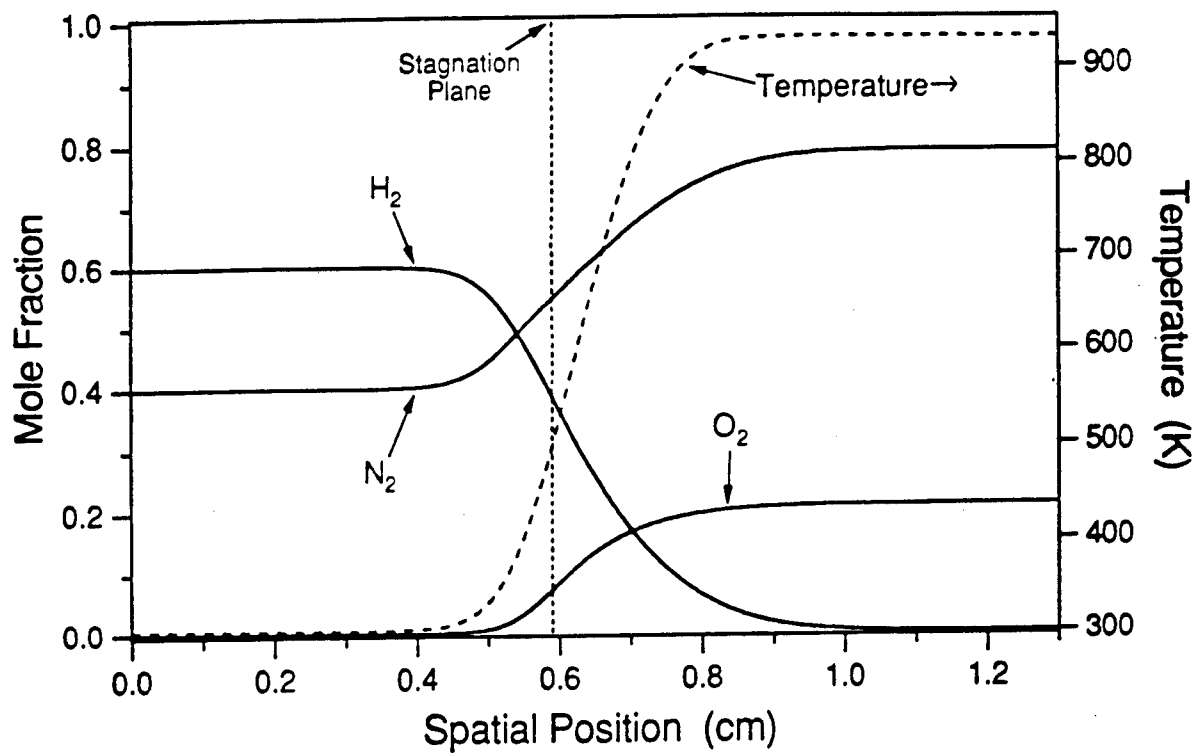
(Yetter, Dryer, Rabitz, 1991)

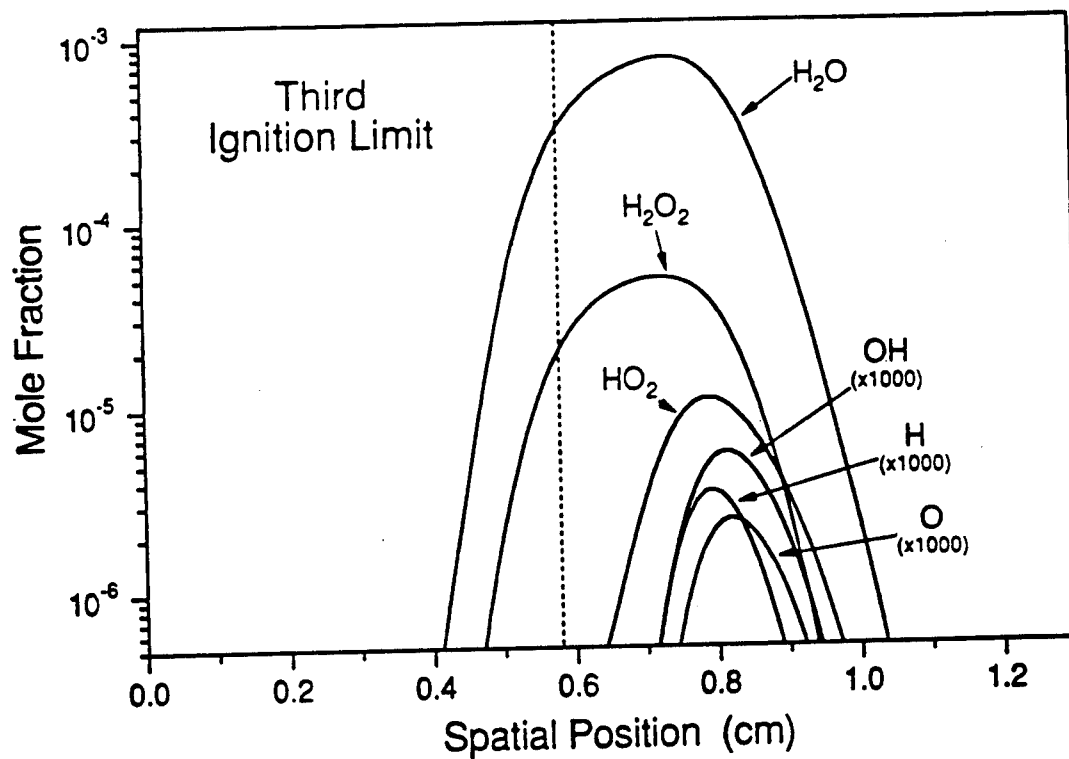
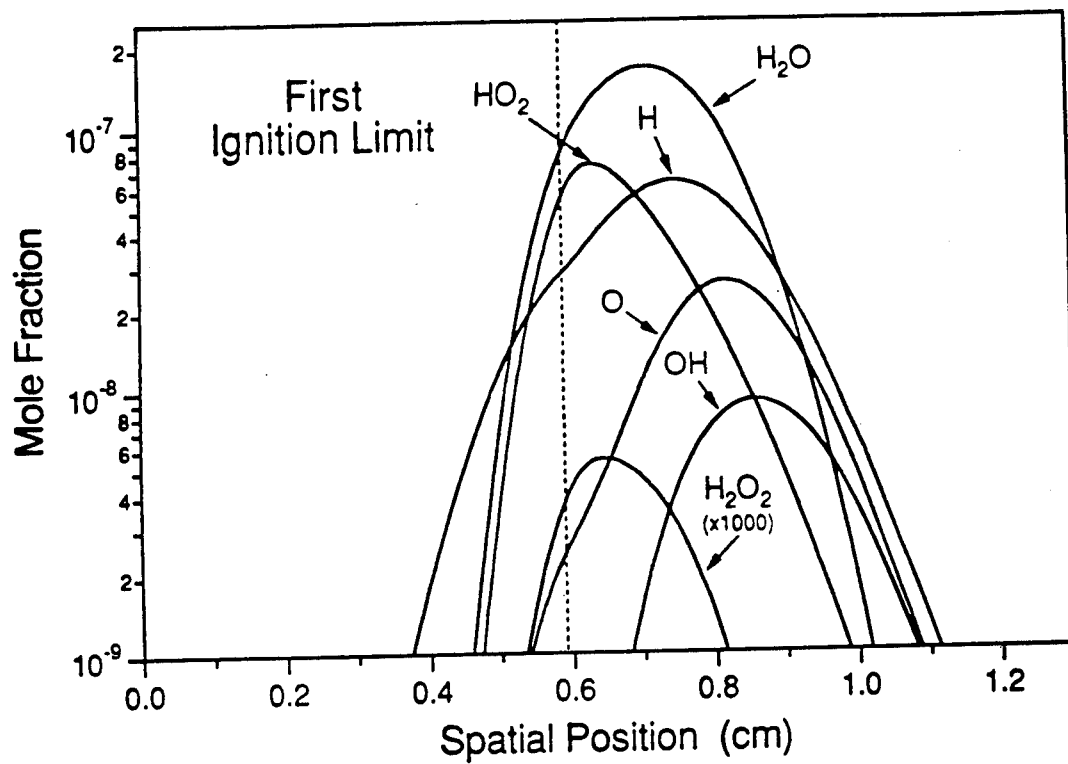
	Reaction	A	n	E <sub>a</sub>
1.	$\text{H} + \text{O}_2 \rightleftharpoons \text{O} + \text{OH}$	$1.92 \times 10^{14}$	0.0	16.44
2.	$\text{O} + \text{H}_2 \rightleftharpoons \text{H} + \text{OH}$	$5.08 \times 10^4$	2.67	6.29
3.	$\text{OH} + \text{H}_2 \rightleftharpoons \text{H} + \text{H}_2\text{O}$	$2.16 \times 10^8$	1.51	3.43
4.	$\text{OH} + \text{OH} \rightleftharpoons \text{O} + \text{H}_2\text{O}$	$1.23 \times 10^4$	2.62	-1.88
5.*	$\text{H}_2 + \text{M} \rightleftharpoons \text{H} + \text{H} + \text{M}$	$4.57 \times 10^{19}$	-1.4	104.4
6.*	$\text{O} + \text{O} + \text{M} \rightleftharpoons \text{O}_2 + \text{M}$	$6.17 \times 10^{15}$	-0.5	0.0
7.*	$\text{O} + \text{H} + \text{M} \rightleftharpoons \text{OH} + \text{M}$	$4.72 \times 10^{18}$	-1.0	0.0
8.*	$\text{H} + \text{OH} + \text{M} \rightleftharpoons \text{H}_2\text{O} + \text{M}$	$2.25 \times 10^{22}$	-2.0	0.0
9.*	$\text{H} + \text{O}_2 + \text{M} \rightleftharpoons \text{HO}_2 + \text{M}$	$6.17 \times 10^{19}$	-1.42	0.0
10.	$\text{HO}_2 + \text{H} \rightleftharpoons \text{H}_2 + \text{O}_2$	$6.63 \times 10^{13}$	0.0	2.13
11.	$\text{HO}_2 + \text{H} \rightleftharpoons \text{OH} + \text{OH}$	$1.69 \times 10^{14}$	0.0	0.87
12.	$\text{HO}_2 + \text{O} \rightleftharpoons \text{OH} + \text{O}_2$	$1.81 \times 10^{13}$	0.0	-0.4
13.	$\text{HO}_2 + \text{OH} \rightleftharpoons \text{H}_2\text{O} + \text{O}_2$	$1.45 \times 10^{16}$	-1.0	0.0
14.	$\text{HO}_2 + \text{HO}_2 \rightleftharpoons \text{H}_2\text{O}_2 + \text{O}_2$	$3.02 \times 10^{12}$	0.0	1.39
15.*	$\text{H}_2\text{O}_2 + \text{M} \rightleftharpoons \text{OH} + \text{OH} + \text{M}$	$1.20 \times 10^{17}$	0.0	45.5
16.	$\text{H}_2\text{O}_2 + \text{H} \rightleftharpoons \text{H}_2\text{O} + \text{OH}$	$1.00 \times 10^{13}$	0.0	3.59
17.	$\text{H}_2\text{O}_2 + \text{H} \rightleftharpoons \text{H}_2 + \text{HO}_2$	$4.82 \times 10^{13}$	0.0	7.95
18.	$\text{H}_2\text{O}_2 + \text{O} \rightleftharpoons \text{OH} + \text{HO}_2$	$9.55 \times 10^6$	2.0	3.97
19.	$\text{H}_2\text{O}_2 + \text{OH} \rightleftharpoons \text{H}_2\text{O} + \text{HO}_2$	$7.00 \times 10^{12}$	0.0	1.43

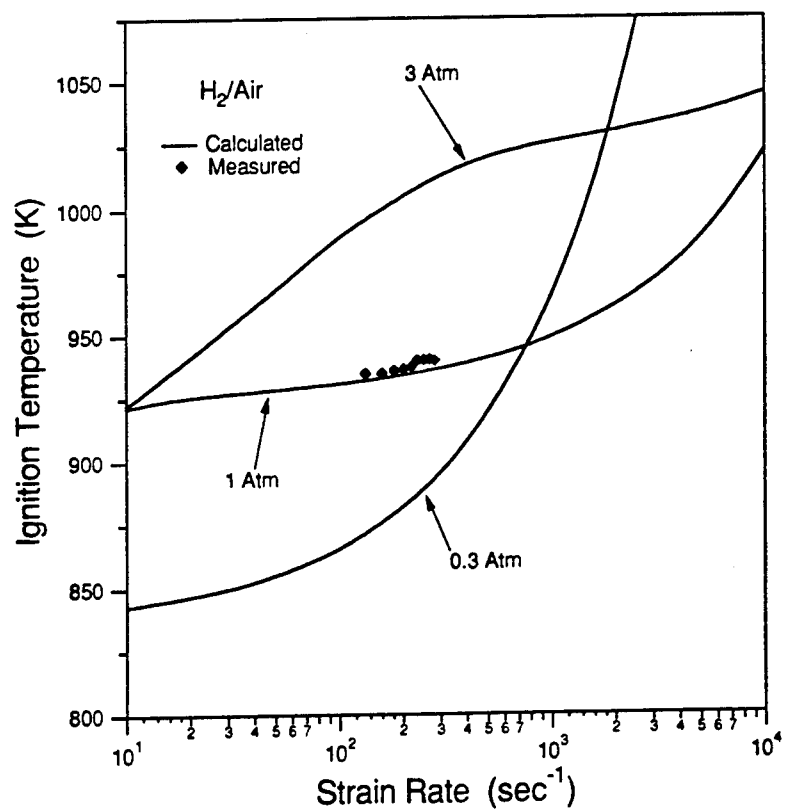
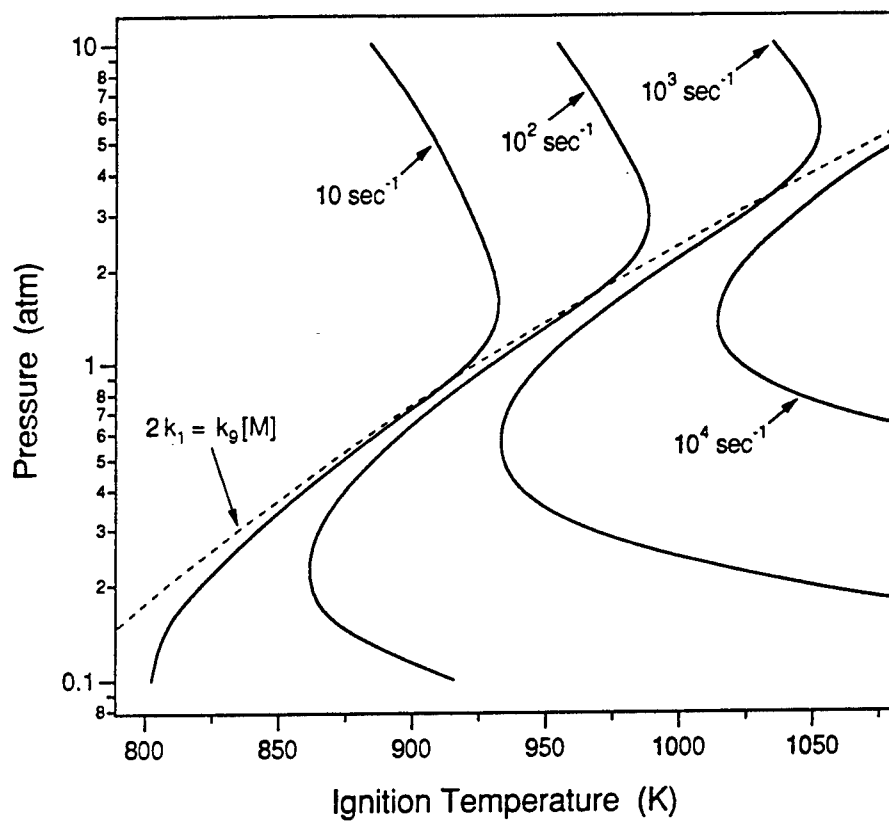
Third body enhancement factors: H<sub>2</sub>O: 12; H<sub>2</sub>: 25

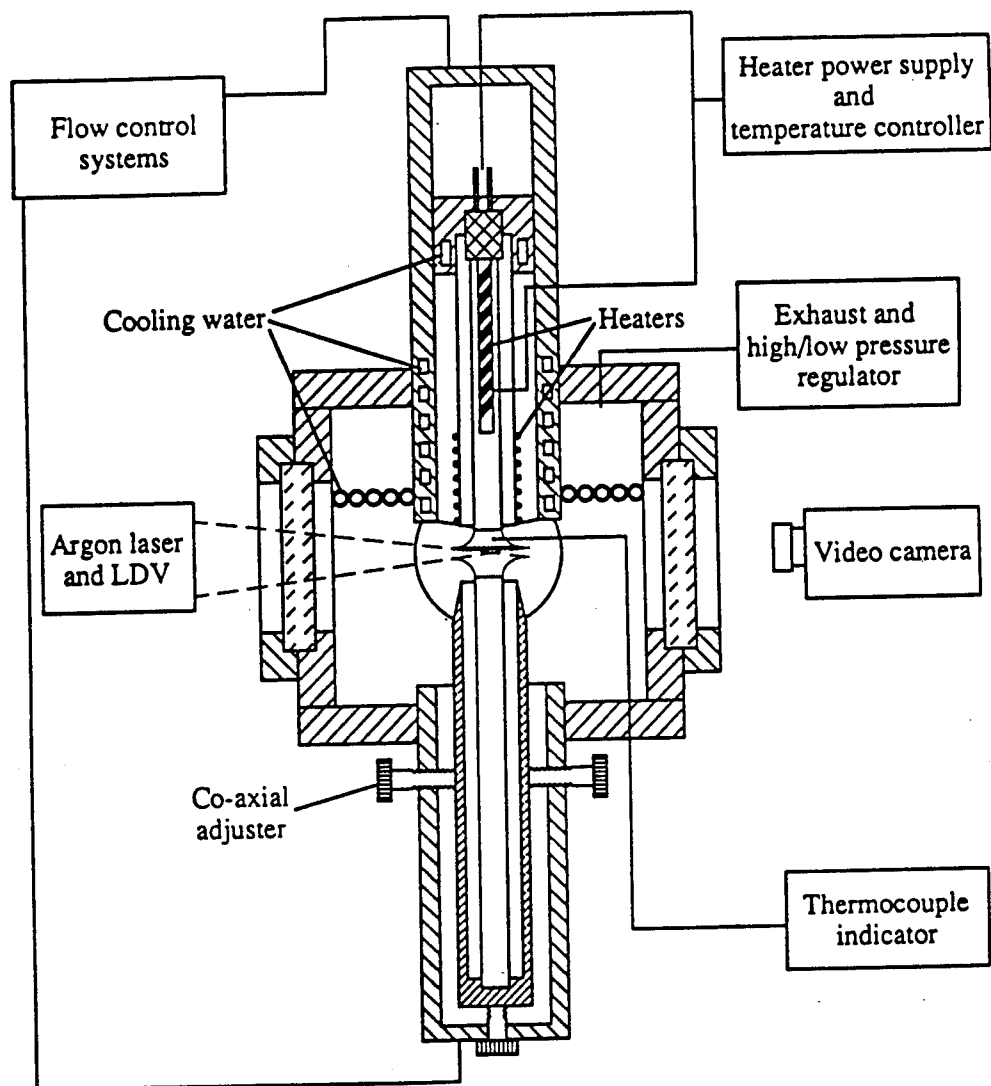
Units: cm, mole, sec, kcal



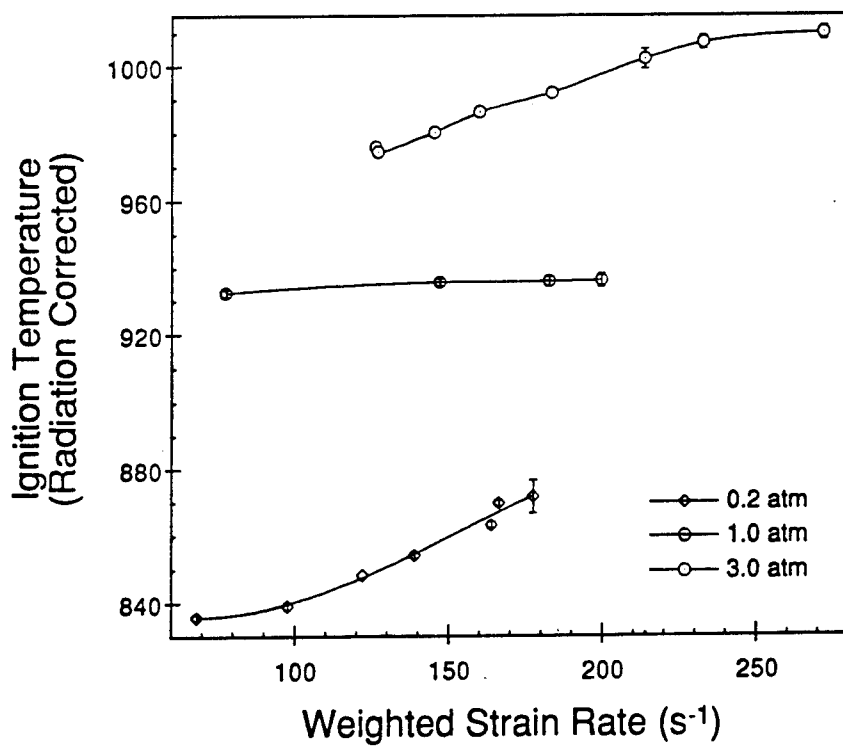
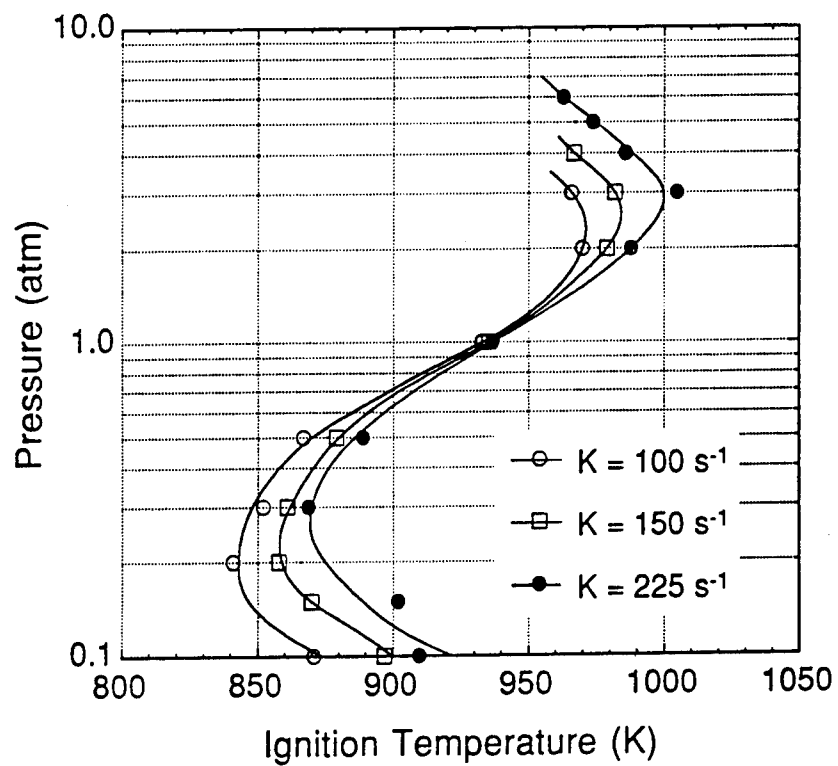






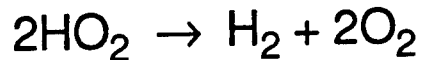
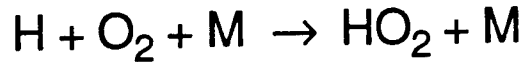
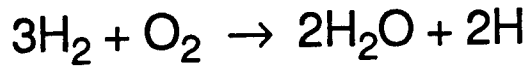






## *Reduced Mechanisms for Hydrogen/Oxygen Ignition*

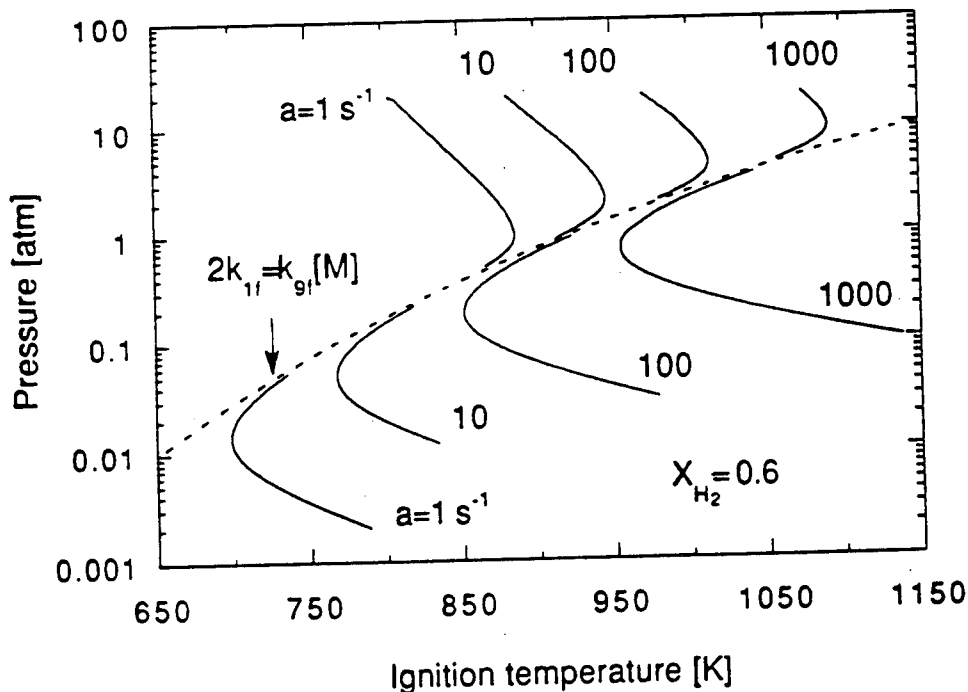
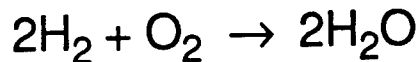
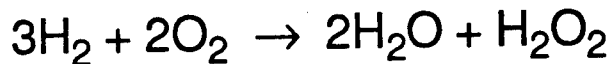
- First Limit: O and OH in steady state

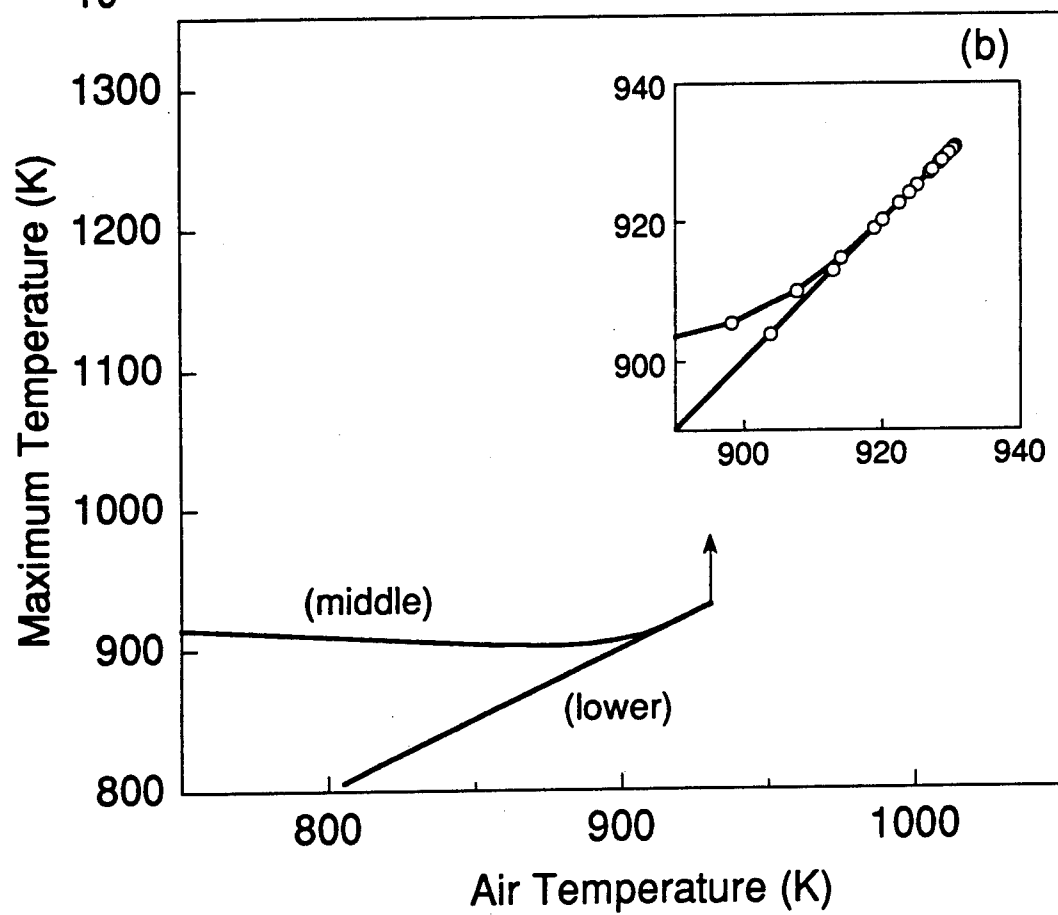
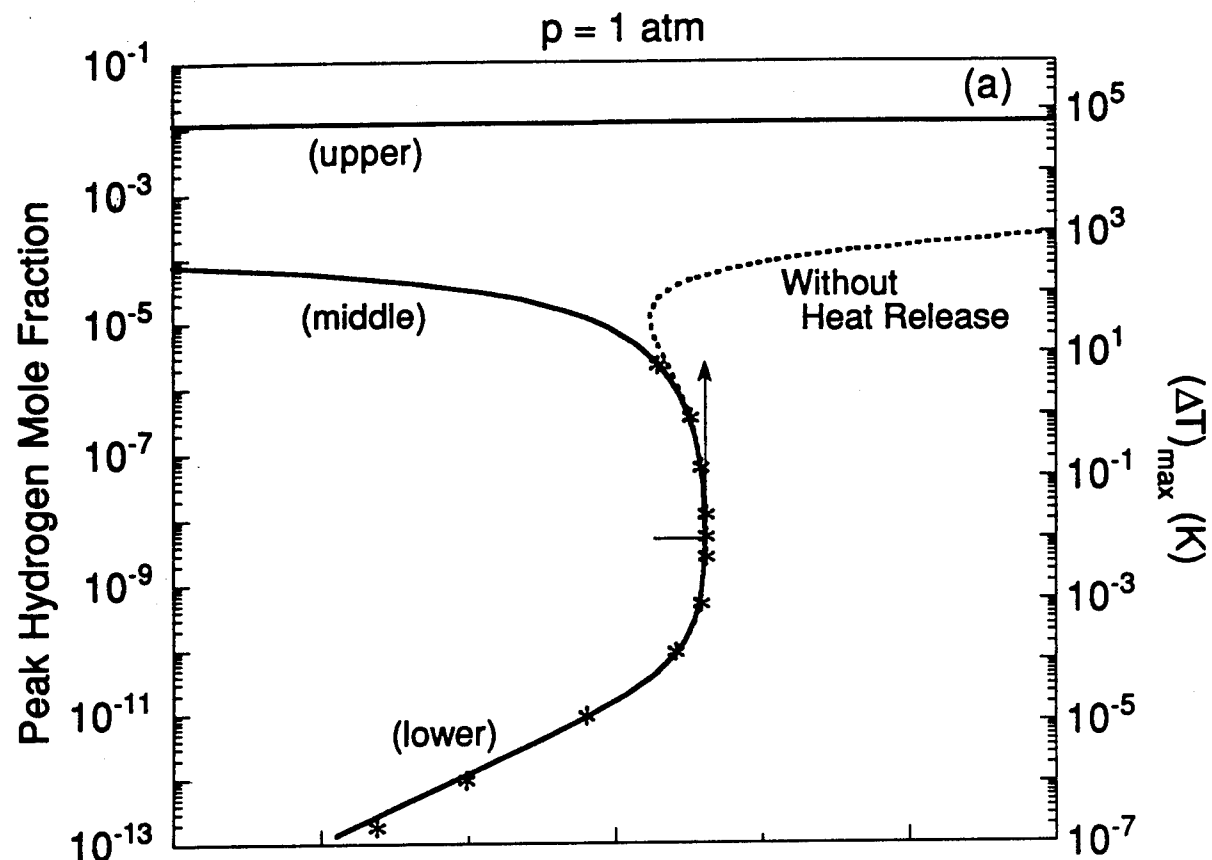


- Second Limit: H, O, and OH in steady state;  $2\omega_a \sim \omega_b$

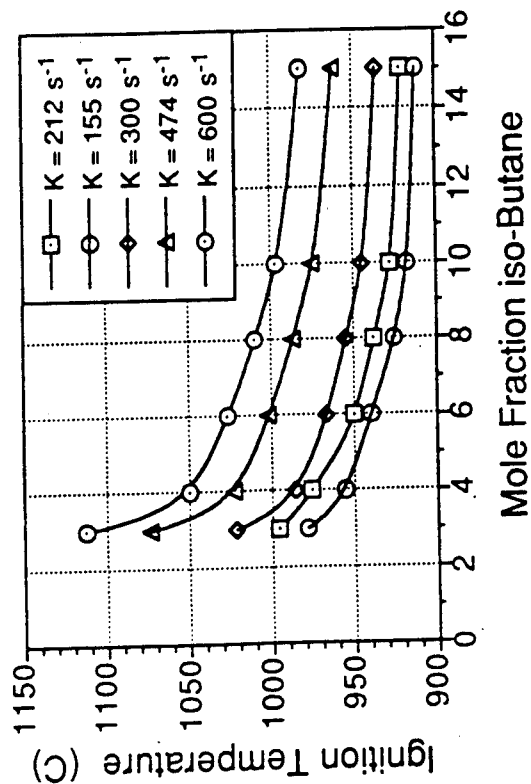
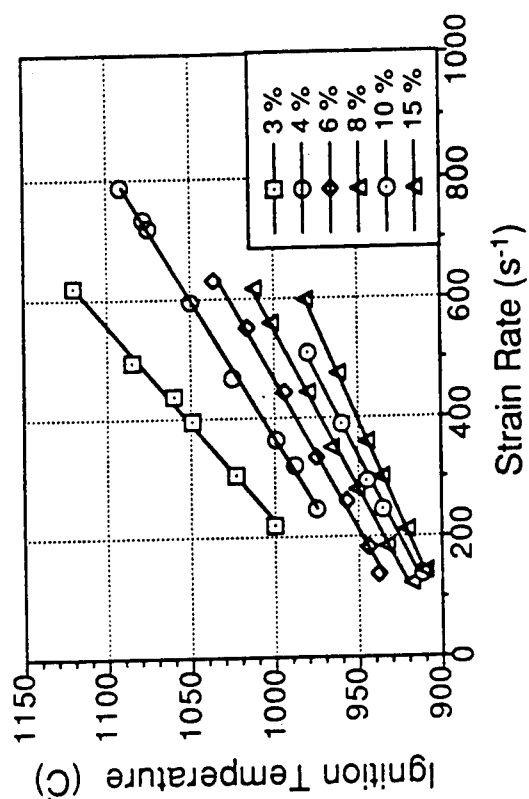


- Third Limit: H, O, OH, and  $\text{HO}_2$  in steady state

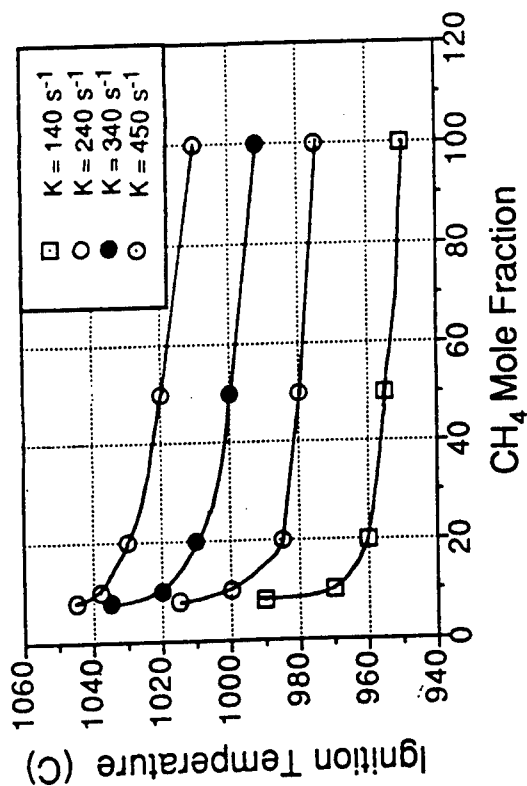
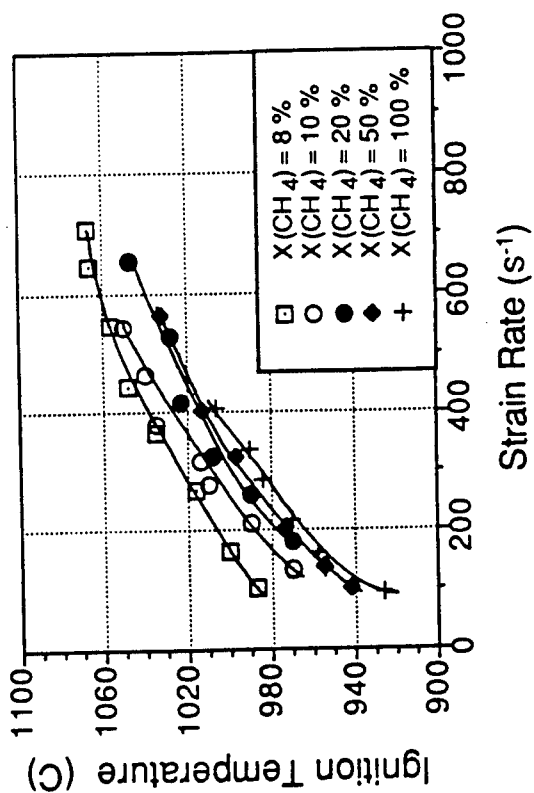




## *i*-Butane/Air Ignition:



## Methane/Air Ignition:



## *Summary of Accomplishments*

- Nonpremixed ignition of hydrogen/air extensively studied;
  - Unified chain-transport interpretation of ignition phenomena;
  - Role of thermal versus kinetic ignition identified;
  - New numerical algorithm developed for the study of ignition/extinction phenomena.
- 

## *Current and Future Work*

- Premixed systems
- Transient ignition
- Methane and methane/hydrogen ignition
- C<sub>4</sub>-hydrocarbon ignition

## Resonant Holographic Interferometry

P.A. DeBarber, N.J. Brock, M.S. Brown, C.F. Hess, and J.D. Trolinger

MetroLaser

18006 Skypark Circle, Suite 108

Irvine, CA 92714

This presentation discusses a novel, nonintrusive, spectroscopic tool to explore combustion and flames. This tool is called **Resonant Holographic Interferometric Spectroscopy (RHIS)**. RHIS is a completely nonintrusive optical diagnostic. As the *RHIS* acronym implies, RHIS is a hybrid technique. It brings together the three-dimensional imaging capability of *holography*, the phase sensitive detection of *interferometry*, and the species specificity of *spectroscopy* to form a powerful, versatile diagnostic package. RHIS is a holographic interferometric technique which may be combined with tomography to provide three dimensional characterization and quantitative measurement to species number density, temperature, velocity, pressure, molecular mixing, and other thermophysical quantities.

Conceptually, a single RHIS measurement records the concentration of a resonant absorbing chemical species in the form of a spatially resolved interferogram. This is achieved by holographically recording the phase shift due to the resonant species simultaneously with the phase shift due to all other nonresonant species. Upon reconstruction, the phase shift produced nonresonantly is subtracted out leaving a neat interferogram which contains information only about the resonant species. In practice, this is achieved in the following way. The output beams of two lasers operating at different frequencies are spatially and temporally overlapped to form a single two-color beam. One of the lasers is tuned to a molecular resonance of the species of interest. The other laser is tuned off-resonance. The two-color beam is then split into the standard object and reference legs of a conventional holographic interferometer. Light from each leg is then recombined on a film plate to form two holograms simultaneously at each frequency. Both of the two electric fields at the two different frequencies in the object arm are phase shifted by the same amount due to density fluctuations. However, the resonantly-tuned electric field receives an additional phase shift. Upon reconstruction, the two holographically recorded images interfere with each other resulting in a cancellation of all phase information that was common to the two electric fields. Therefore resulting in an interferogram which preserves only the phase shift fringes attributable to the resonant species. This, in effect, is a background-free recording of the spatially resolved density of the resonant species. Since phase shifts are largest near resonance, the RHIS technique is far more sensitive to low species concentrations than conventional nonresonant interferometry. The detected phase shifts are linearly dependent on concentration which makes the RHIS technique also linearly dependent on concentration.

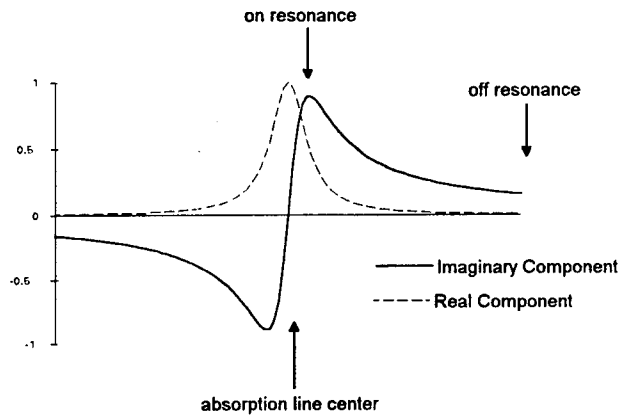


**Figure 1.** Plot of Real and Imaginary components of the index of refraction near an absorption line.

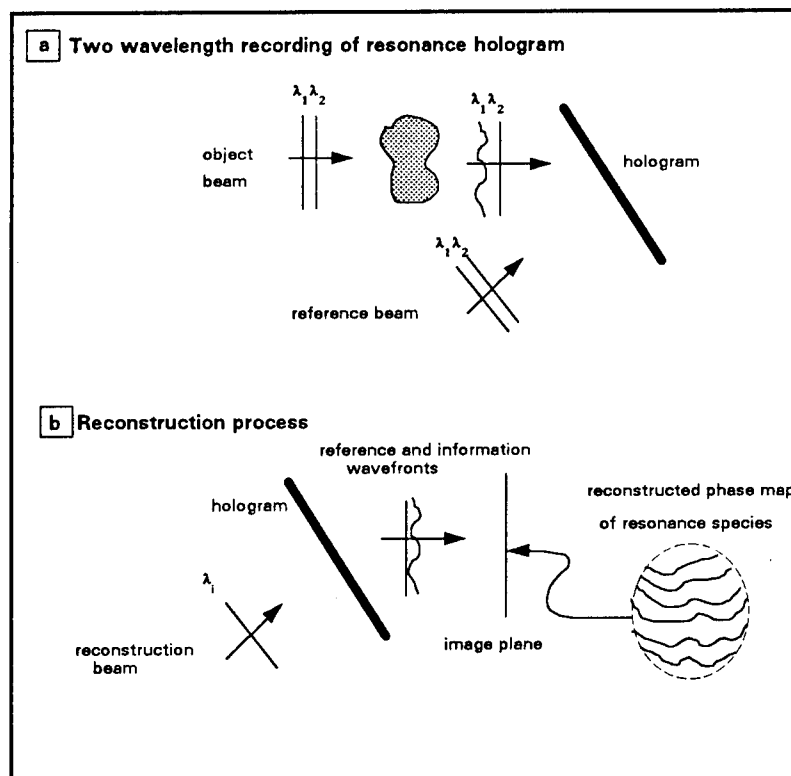


**Figure 2.** Two wavelength RHIS procedure. Panel (a) illustrates the recording procedure.  $\lambda_1$  corresponds to the laser tuned "on resonance";  $\lambda_2$  corresponds to the laser tuned "off resonance". Panel (b) outlines the reconstruction process. Note that the reconstruction can be accomplished with almost any available laser  $\lambda_i$ .

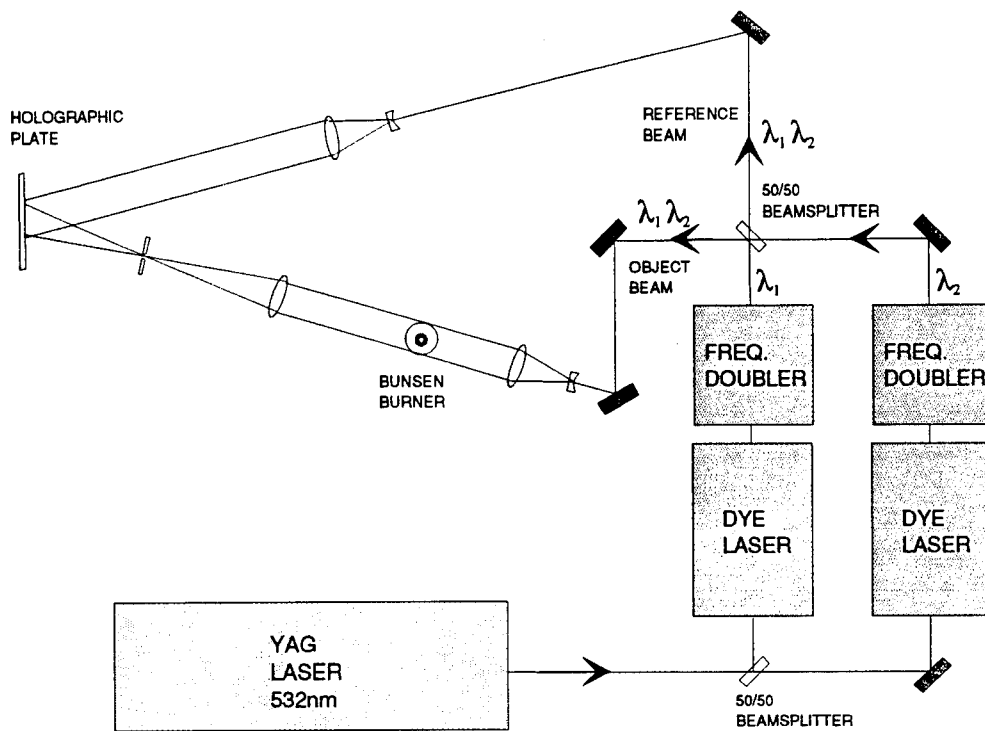


**Figure 3.** Schematic diagram of the two-laser RHIS system. In this case, the object probed is the flame produced in a laboratory burner.

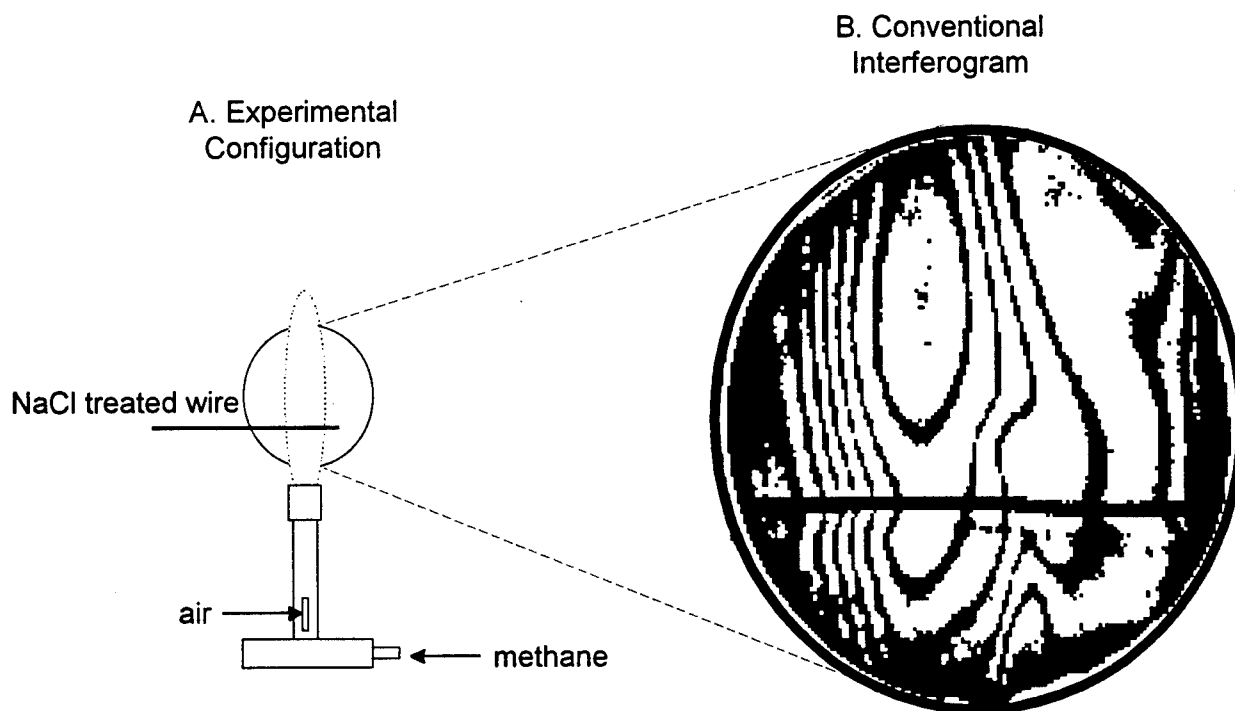


**Figure 4.** (a) Experimental configuration. (b) Conventional holographic interferogram.



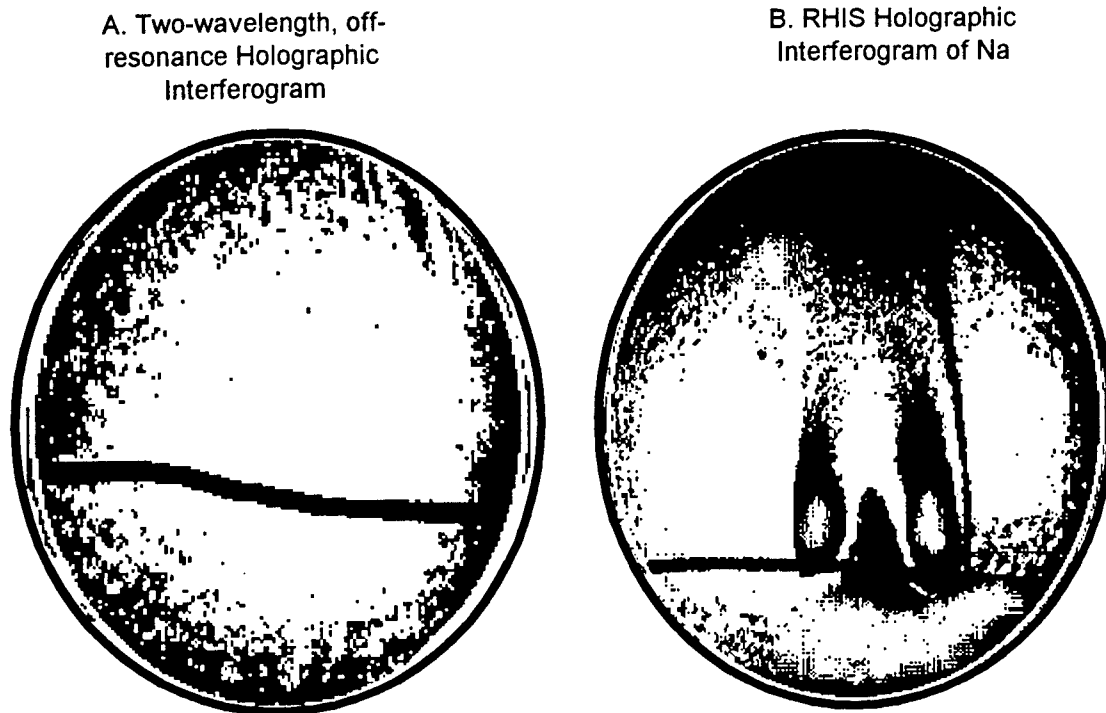


**Figure 5.** (a) two-wavelength off-resonance interferogram illustrating total subtraction inherent in holographic reconstruction. (b) RHIS interferogram of Na seeded into a methane/air diffusion burner flame.

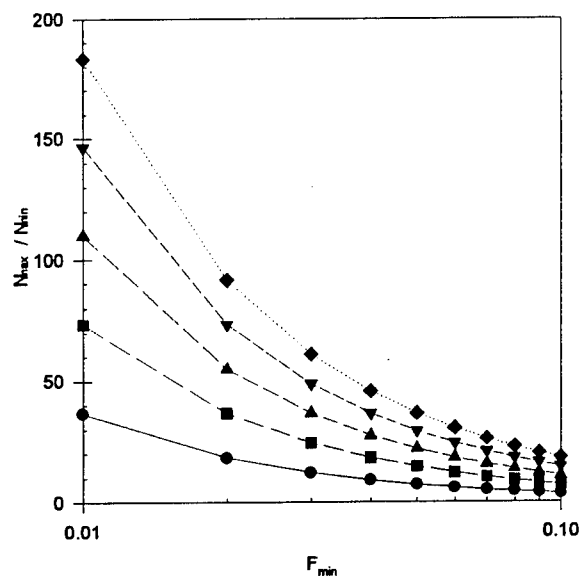


**Figure 6.** Predictions for the dynamic range of an individual RHIS hologram as a function of the minimum detectable fringe shift.

## CONTROL OF SOOT FORMATION

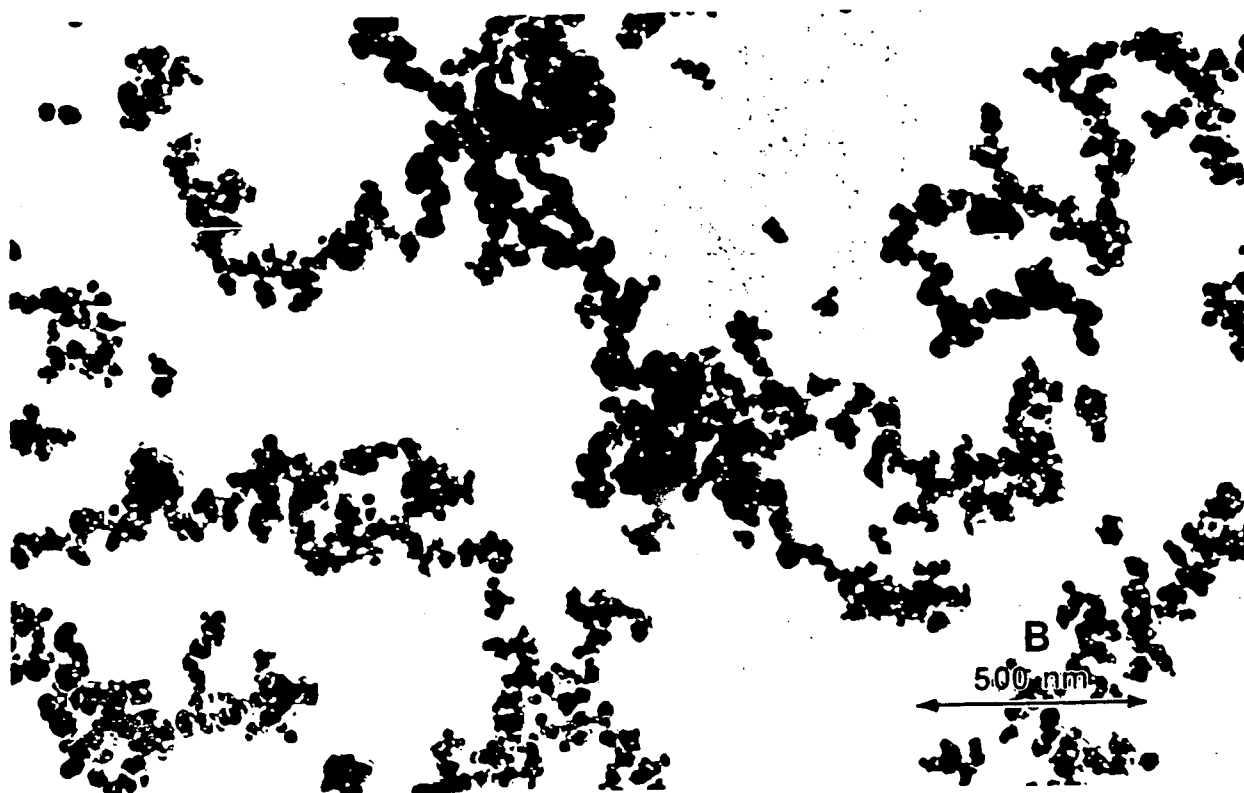
R.A. Dobbins  
Division of Engineering  
Brown University  
Providence, RI 02912

Micrographs (TEM) obtained by thermophoretic sampling of soot particles from diffusion flames have revealed two contrasting morphologies. On the fuel side of the lower diffusion flame front, many small singlet precursor particles are found that are nearly transparent to the electron beam. In the higher temperature regions the particles are found to consist of opaque, carbonaceous aggregates made up of monodisperse spherules. Our studies and reference to the literature lead to the conclusion that the precursor stage observed in diffusion flames is a common, if not universal, stage in the formation of the carbonaceous materials in shock tubes, in premixed and diffusion flames, and in droplets in microgravity.

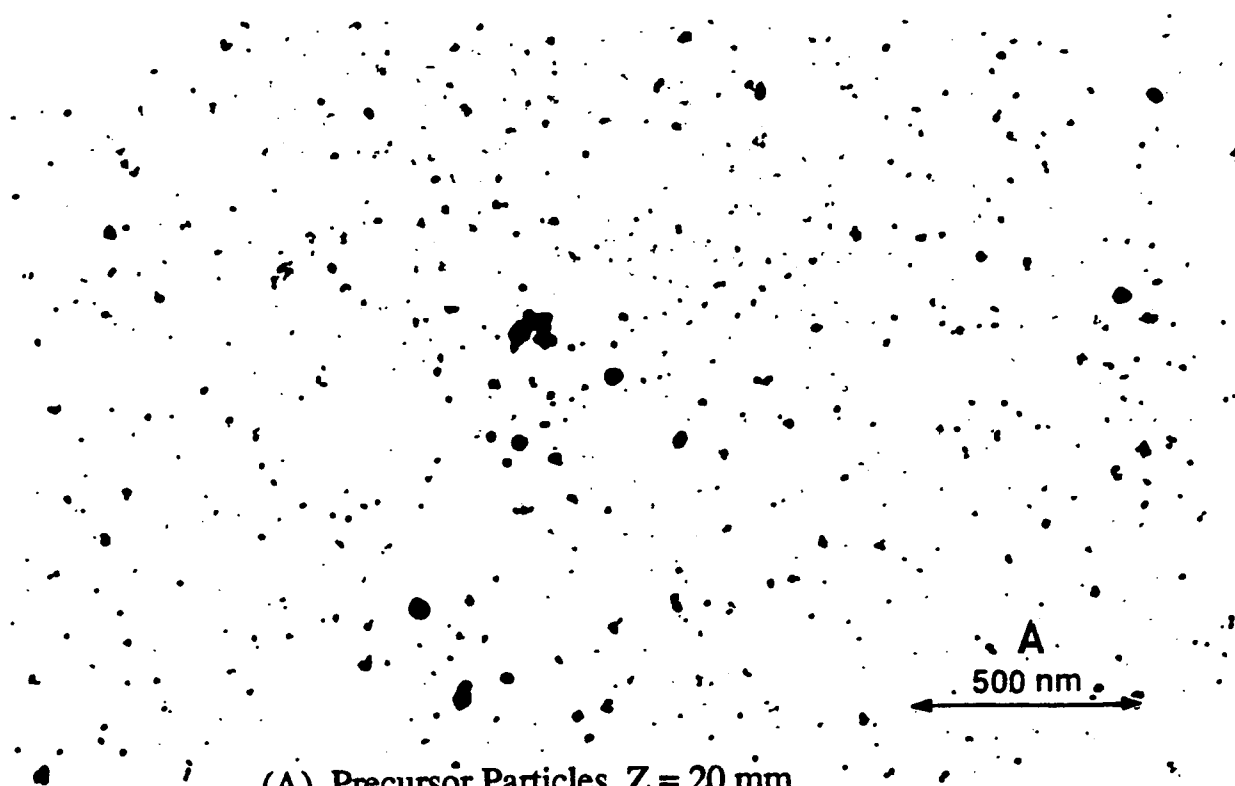
The nature of the precursor particle recently has been explored by laser microprobe mass spectrometry (LMMS). This research has been a collaboration with R.A. Fletcher of the NIST using the LAMMA-500 instrument available there. The advantages and drawbacks of the LMMS method and the results of testing samples of pure and mixed polycyclic aromatic hydrocarbons are reviewed. LMMS mass spectra of precursor material from low on the axis of the diffusion flame reveals many ion masses corresponding to PAHs in the 200 to 300 amu range. The most prominent of these are the mass numbers are 252, e.g., benzo(a)pyrene; 276, e.g., benzo(ghi)perylene; and 300, coronene. Of striking significance is that these PAH masses were predicted by Stein and Fahr (1985) to be among the most thermodynamically stable species ("stabilimers") in typical flame conditions of pressure and temperature. Mass spectra of the carbonaceous material from the upper flames show many carbon clusters with typically with 0, 1, or 2 hydrogen atoms. Small quantities of ion masses in the 418 to 444 amu range are also found in the carbonaceous materials along with traces of fullerene-like ions - 600, 720, 840 and 1105 amu. The values of hydrogen mole fraction, or C/H ratio, of both precursor and carbonaceous material are found by the LMMS to conform to prior expectations.

The rate of carbonization of precursor materials is an important parameter in the understanding and intervention in the process of soot formation. In nitrogen-diluted ethene diffusion flames the onset of carbonization is delayed and occurs over a range of temperatures according to the amount of dilution. Thermocouple measurements are conducted using the rapid insertion technique to eliminate the influence of soot deposition on sensor emissivity. The observed locations of carbonization and the observed temperature profiles lead to carbonization rate measurements when first order kinetics are assumed. Two methods of data reduction are employed and give similar results. An activation energy of 21 kcal/mole is found for the rate of carbonization of precursor particles. The implications of this carbonization rate on soot formation in combustion processes are discussed.

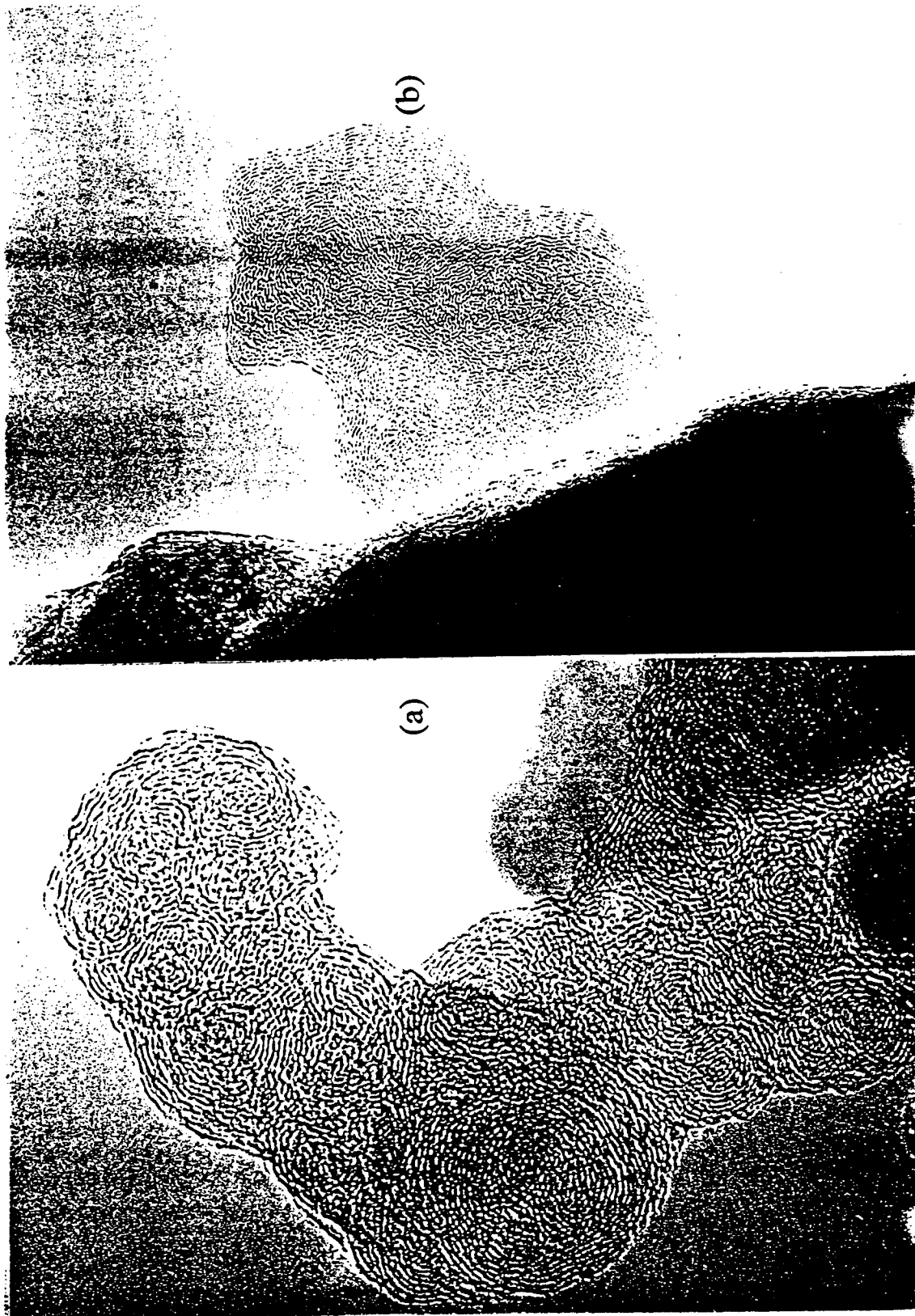
ARO Grant DAAL03-92-G-0023



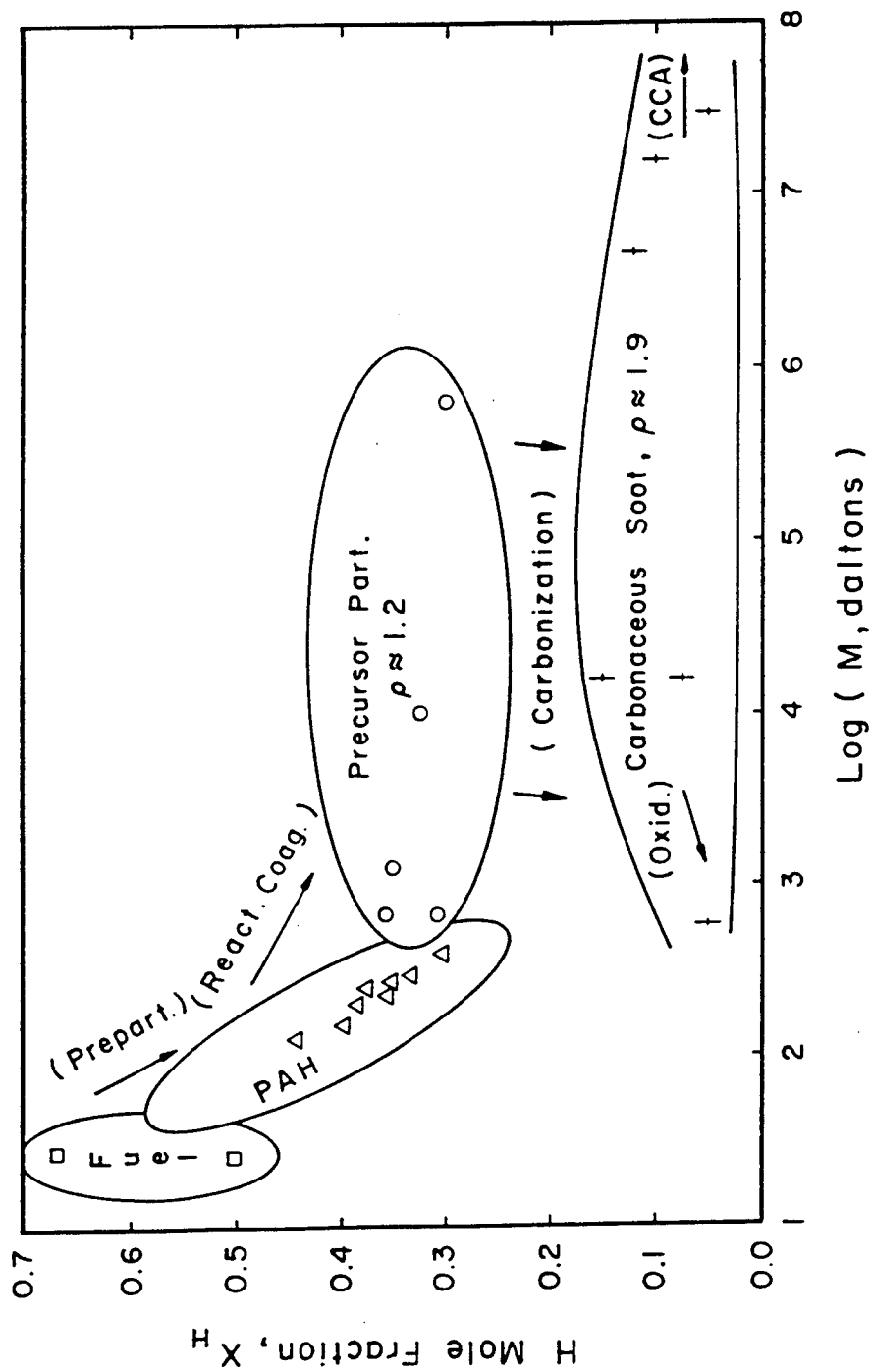
(B) Carbonaceous Aggregates,  $Z = 50$  nm



(A) Precursor Particles,  $Z = 20$  nm



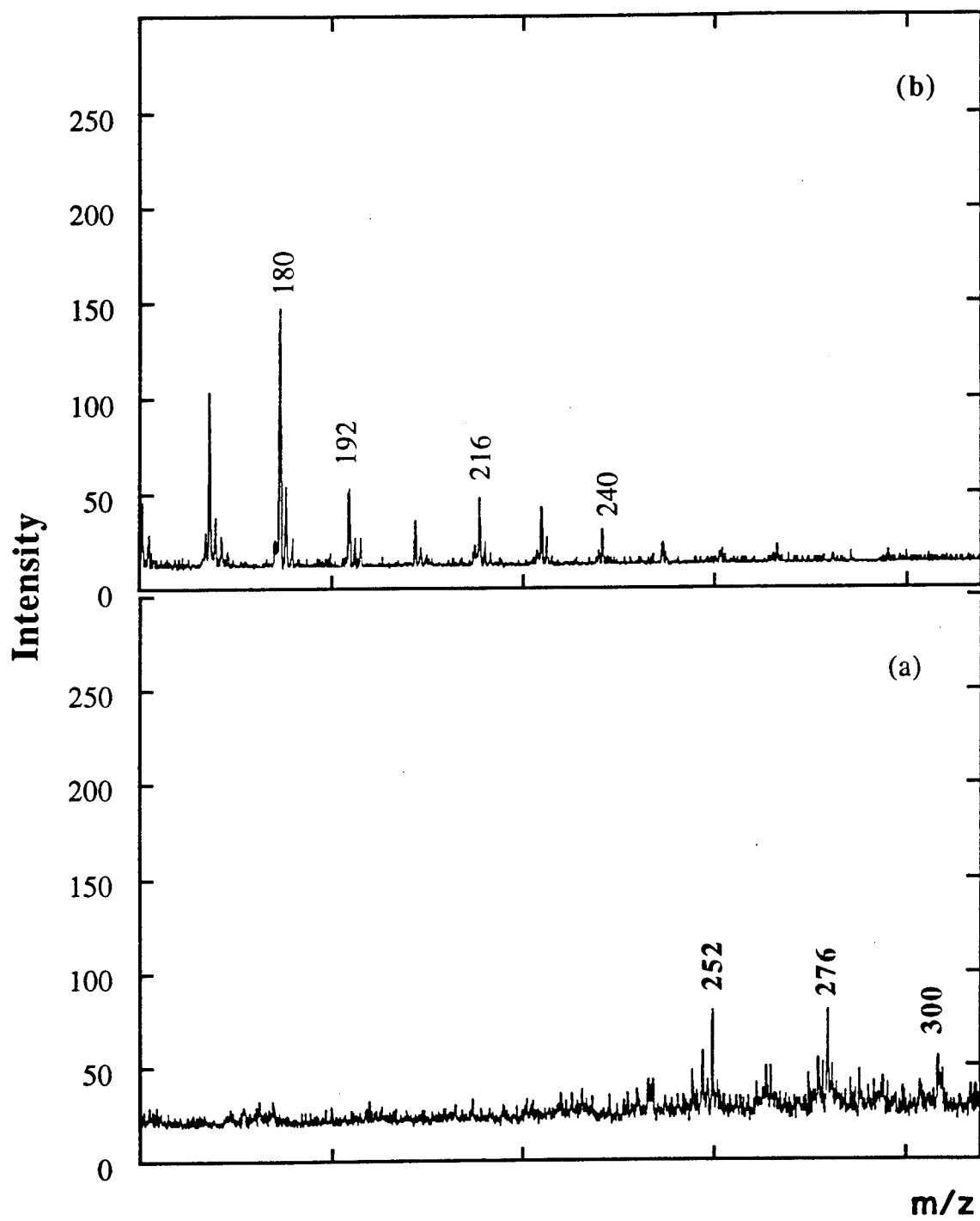
HRTEM of (a) Mature Carbonaceous Aggregate and (b) Young Microparticle



Evolution of Soot in Flames

## LASER MICROPROBE MASS SPECTROMETRY

- 265 NM LASER OUTPUT FOCUSED ON SAMPLE - 1 TO 100 MICROJOULES, 10ns PULSE.
- BEAM DEFOCUSSED TO 50 - 100 MICRON DIAMETER,  $10^{+8}$  W/m<sup>2</sup>.
- VACUUM OF  $10^{-4}$  PA.
- MATERIAL IS SIMULTANEOUSLY ABLATED AND IONIZED.
- IONIZED PRODUCTS MASS ANALYZED, 0 TO 5700 AMU,  $M/\Delta M \sim 500$  @  $M/Z = 200$ ,  $M=1$  TO 5700 AMU.
- REPRODUCIBILITY LOW BECAUSE MICROSCOPIC VARIABILITY OF SAMPLE COMPOSITION AND THICKNESS & VARIABILITY OF LASER PULSE.



### LMMS Spectra

(a) Precursor Material Z = 20 mm

(b) Carbonaceous Materials Z = 50 mm

LMMS Analysis - Soot from  $C_2H_4$  diffusion flame.

$Z = 50$  mm

$T = 1570$  K

Many  $C_xH_y$        $x = 4$  to  $24$   
                          $y = 0, 1, 2$

$X_h \geq 0.14$        $C/H \approx 6.1$

Small amounts of PAH-like species 418-444

Trace levels of masses corresponding to  $C_{50}$ ,  $C_{60}$ ,  $C_{70}$ ,  $C_{92}$

$Z = 20$  mm

$T = 1430$  K

PAH-like ions (count fraction)

252 (0.16)      276 (0.20)      300 (.090)

$X_H \geq 0.35$        $C/H \approx 1.9$

Many  $C_xH_y$  Clusters

Ten PAHs-like ions reported by others  
Five PAHs-like ions not reported



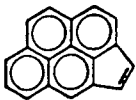
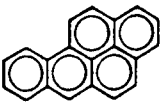
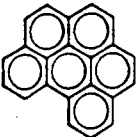
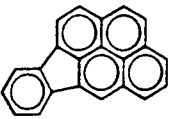
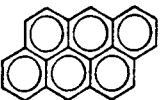
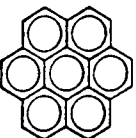
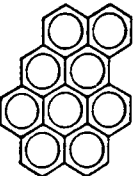
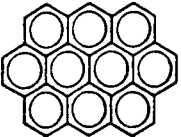
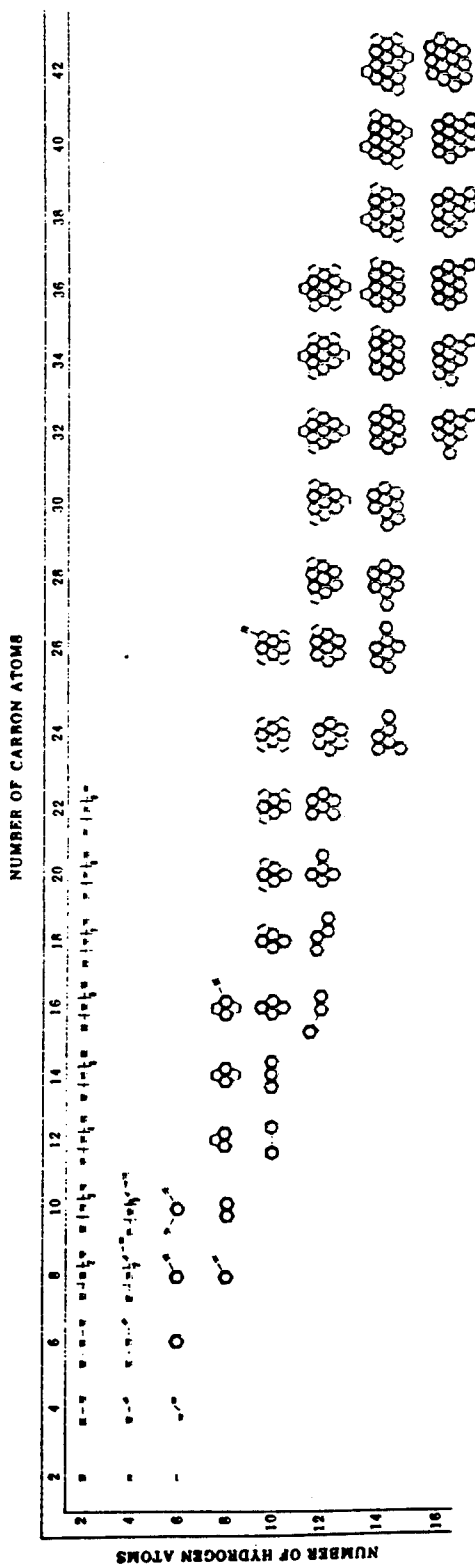
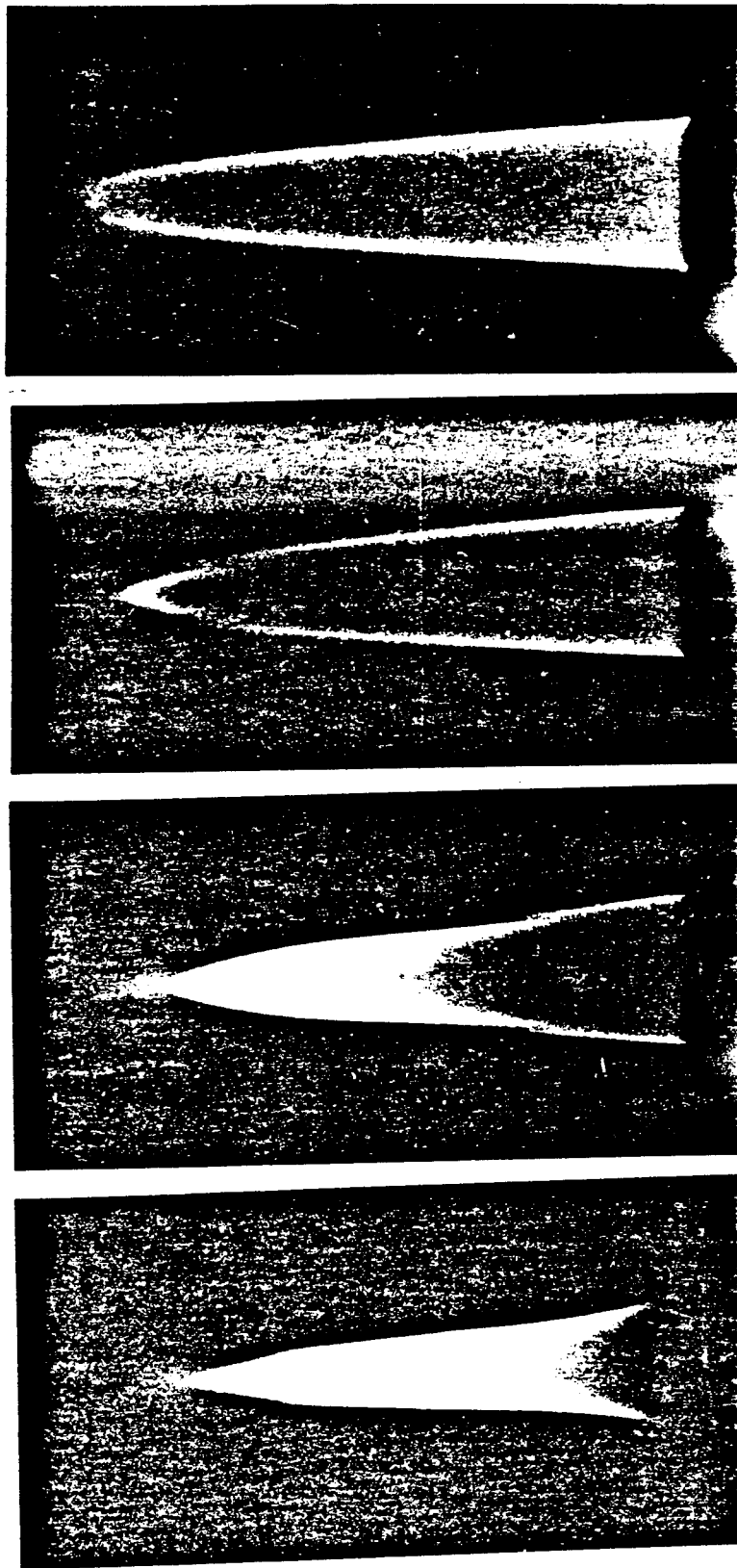
Species	Formula	<i>M</i> (g/mole)	Structure
Cyclopenta( <i>cd</i> )pyrene	C <sub>18</sub> H <sub>10</sub>	226	
Benzo( <i>a</i> )pyrene	C <sub>20</sub> H <sub>12</sub>	252	
Benzo( <i>ghi</i> )perylene	C <sub>22</sub> H <sub>12</sub>	276	
Indeno(1,2,3- <i>cd</i> )pyrene	C <sub>22</sub> H <sub>12</sub>	276	
Anthanthrene	C <sub>22</sub> H <sub>12</sub>	276	
Coronene	C <sub>24</sub> H <sub>12</sub>	300	
Naphtho(8,1,2- <i>abc</i> )coronene	C <sub>30</sub> H <sub>14</sub>	374	
Ovalene	C <sub>32</sub> H <sub>14</sub>	398	

Table 3.6-2: PAH species identified in flame samples using liquid chromatography. Pyrene and fluoranthene, which were also detected by gas chromatography, are not listed in this table. Many peaks which appeared in the chromatographs were not identified.

(From Feitelberg, Ph.D. Thesis, MIT, 1990)

### PAHs Found in C<sub>2</sub>H<sub>4</sub> Premixed Flame

Figure 1. Structures of the most stable isomers in the most stable classes of  $C_nH_m$  molecules ("isoblowers").(From Stein & Fahr, *J. Phys. Chem.* 89, 3714 (1985))



(0.0)

(4.0)

(6.8)

(>8.0)

(Moles  $N_2 / C_2H_4$ )

Ethene Diluted with Nitrogen ( $Q$  of  $C_2H_4 = 2.1 \text{ cm}^3/\text{s}$ )

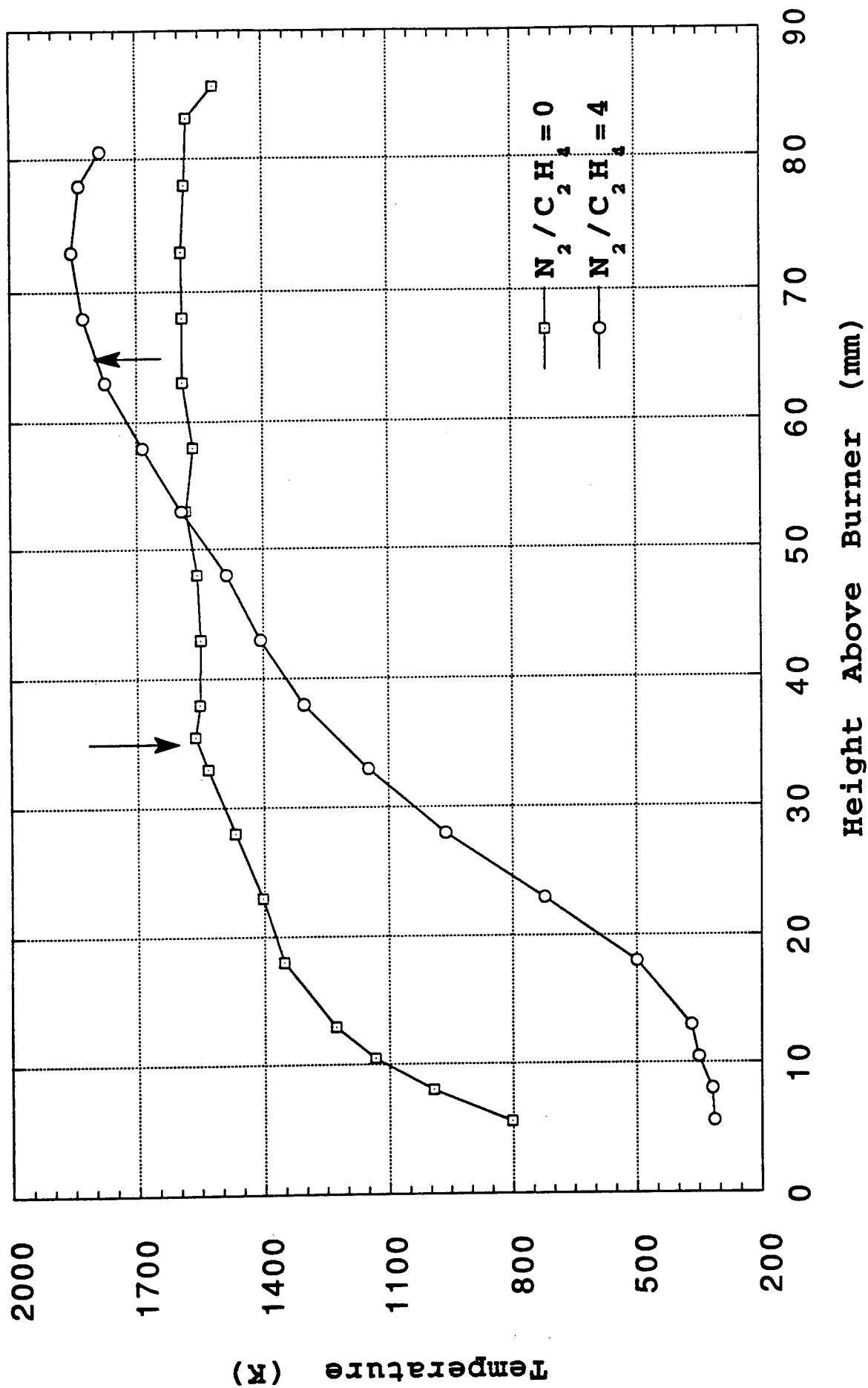


Figure 1. Diffusion Flame Axial Temperature Profiles for Pure and Diluted Ethene

## CARBONIZATION RATE

### METHOD I

$$K_{ca} = \left[ t(Z_2) - t(Z_1) \right]^{-1}$$

$Z_1, Z_2$ , observed, 5 mm resol.

$T(z)$  for Six Dilution Ratios

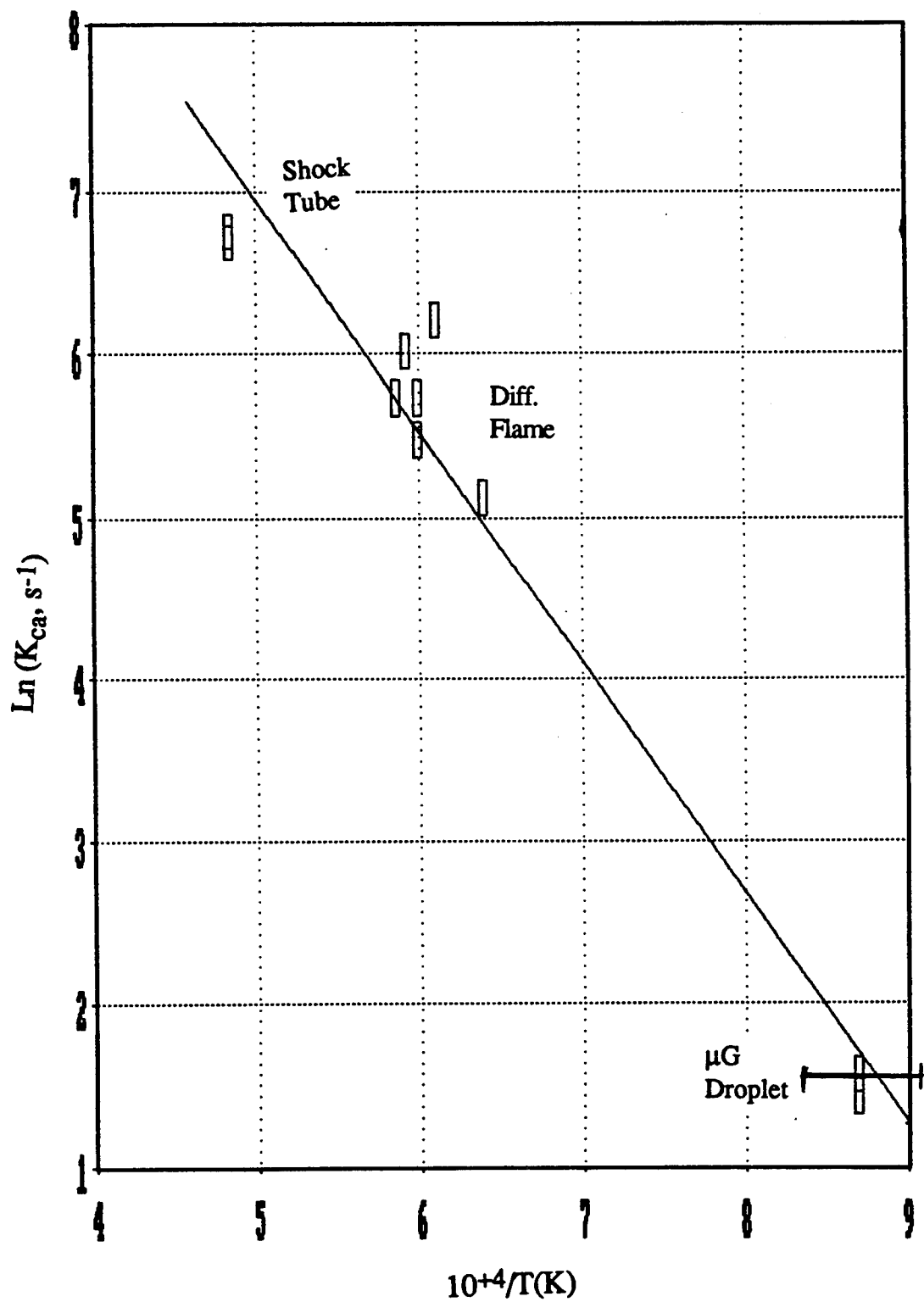
Plot  $\ln(K_{ca})$  vs.  $T^{-1}$ , find A & E

### METHOD II

$$K_{ca} = Ae^{-E/RT}$$

$$\frac{M}{M_0} = 1 - A \int_{t_1}^{t_2} e^{-E/RT(t)} \frac{M(t)}{M_0} dt$$

Given  $t_1, T(t)$ , assume E, reiterate to find A to give  $\frac{M}{M_0} = e^{-1}$  when  $t = t_2$ .



CARBONIZATION RATE (PRELIMINARY)

## Soot Modeling and Experiments at the ERC

D.E. Foster  
Engine Research Center  
University of Wisconsin - Madison

In this presentation the Engine Research Center's experimental and modeling work relative to soot emissions from diesel engines will be reviewed. First an overall picture of the work will be presented which will be followed by a focused discussion on three specific projects. The three projects being: in-situ measurements of soot particle size, volume fraction and number density via a combination two wavelength scattering/extinction technique, the development of a phenomenological soot model for the purpose of inclusion into three dimensional computational diesel simulations and the effort to predict soot emission with simplistic soot models taken from the literature and applied to the KIVA II simulation.

The scattering extinction technique was built on our experience of installing windows into an operating diesel engine by introducing a laser, via fiber optic transmission, into the cylinder next to the window. The technique was compared to a scattering-two color radiant emission technique and the results for particle size, number density and volume fraction were found to be consistent. The measurement system was then applied to the engine operating under different conditions.

The phenomenological soot model describes the processes of inception, nucleation, surface growth, oxidation and coagulation with global kinetic reactions. The rate constants for each global reaction is taken to be consistent with those for similar types of reactions from published data. The model has been applied for conditions of a laminar flame published in the literature and the results were encouraging. Next the model has been exercised for a computational cell from a KIVA diesel engine simulation. The profiles of fuel, oxygen and temperature were scaled in a parametric study to examine the response of the model. No parameters were adjusted during these variations. The model predicts the expected soot emission behavior.

Finally the results of our efforts to incorporate the Hiroyasu soot model into the KIVA II diesel engine will be discussed. Hiroyasu's model has been modified to include the Nagle Strickland-Constable oxidation. The results have been tuned for a single operating condition and the model used to assess whether it predicts the correct trends with changes in engine operating conditions. The results reinforce the strong coupling between the combustion model and the emission models. It has been determined that the NOx model demonstrates the highest level of sensitivity to small variations in the combustion model.

# **"Soot Modeling and Experiments at the ERC"**

Dave Foster  
Engine Reserach Center  
University of Wisconsin - Madison

Eleventh ARO Engine Workshop  
March 15, 1994

ERC Faculty: Gary Borman, Mike Corradini, Pat Farrell, Dave Foster, Jay  
Martin, Rolf Reitz and Chris Rutland

## **Overview of Current Work:**

### **Experiments:**

- Two dimensional two color optical pyrometry
- In-situ measurement of particle size, number density, volume fraction and temperature via scattering and extinction
- Interaction between multiple, split injection scenarios and the soot NOx trade-off

### **Modeling Efforts:**

- Development of a phenomenological soot model
- Incorporation of literature models into KIVA
- Implimentation of the more detailed models into KIVA



## **In-situ Measurement of Particle Size, Number Density, Volume Fraction and Temperature via Scattering and Extinction**

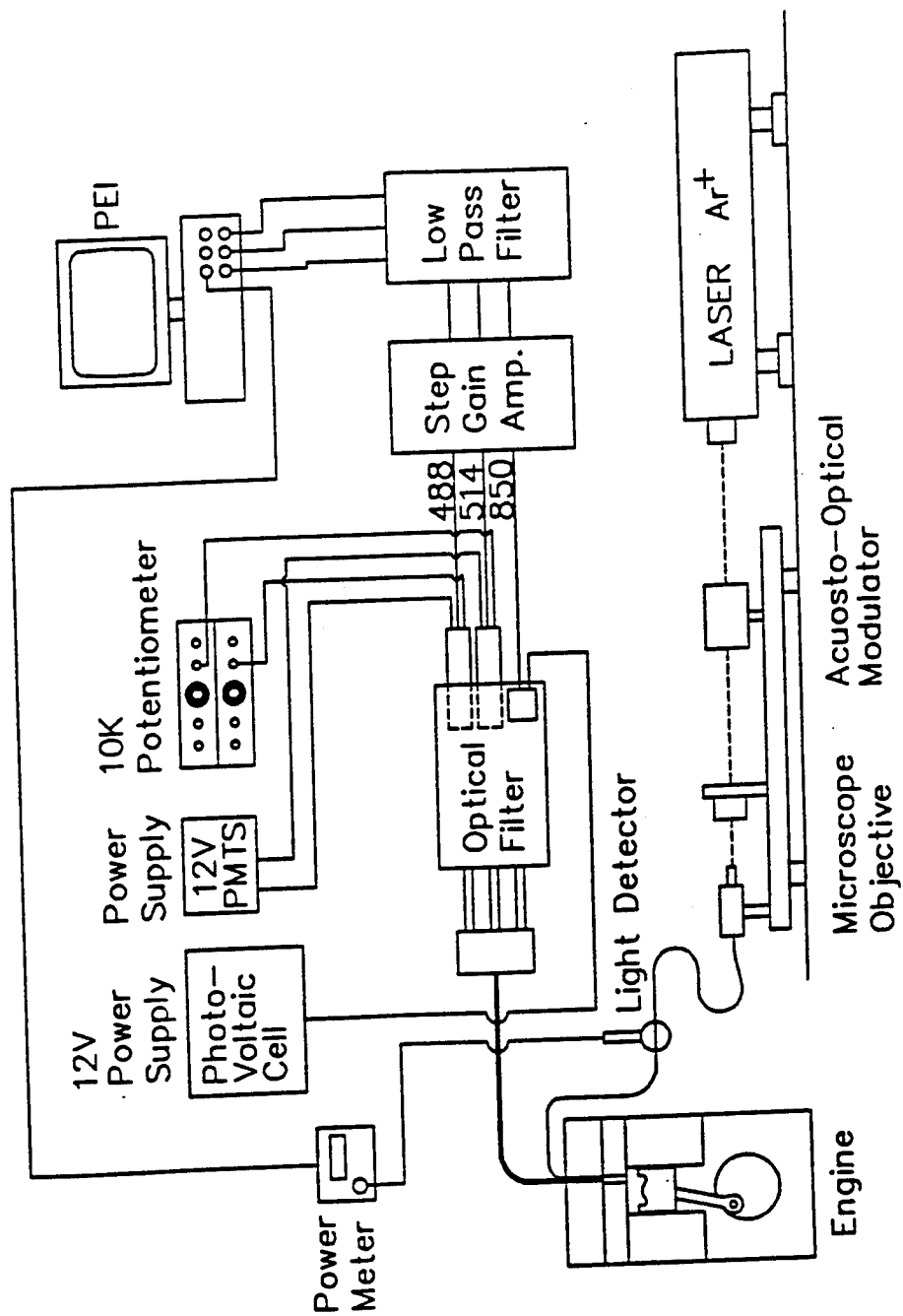
- Point measurement in the cylinder of an operating DI diesel engine
- Simultaneous measurement of light scattering/extinction and radiant emission from engine soot cloud
- Different engine operating conditions were investigated

### **Phenomenological soot model**

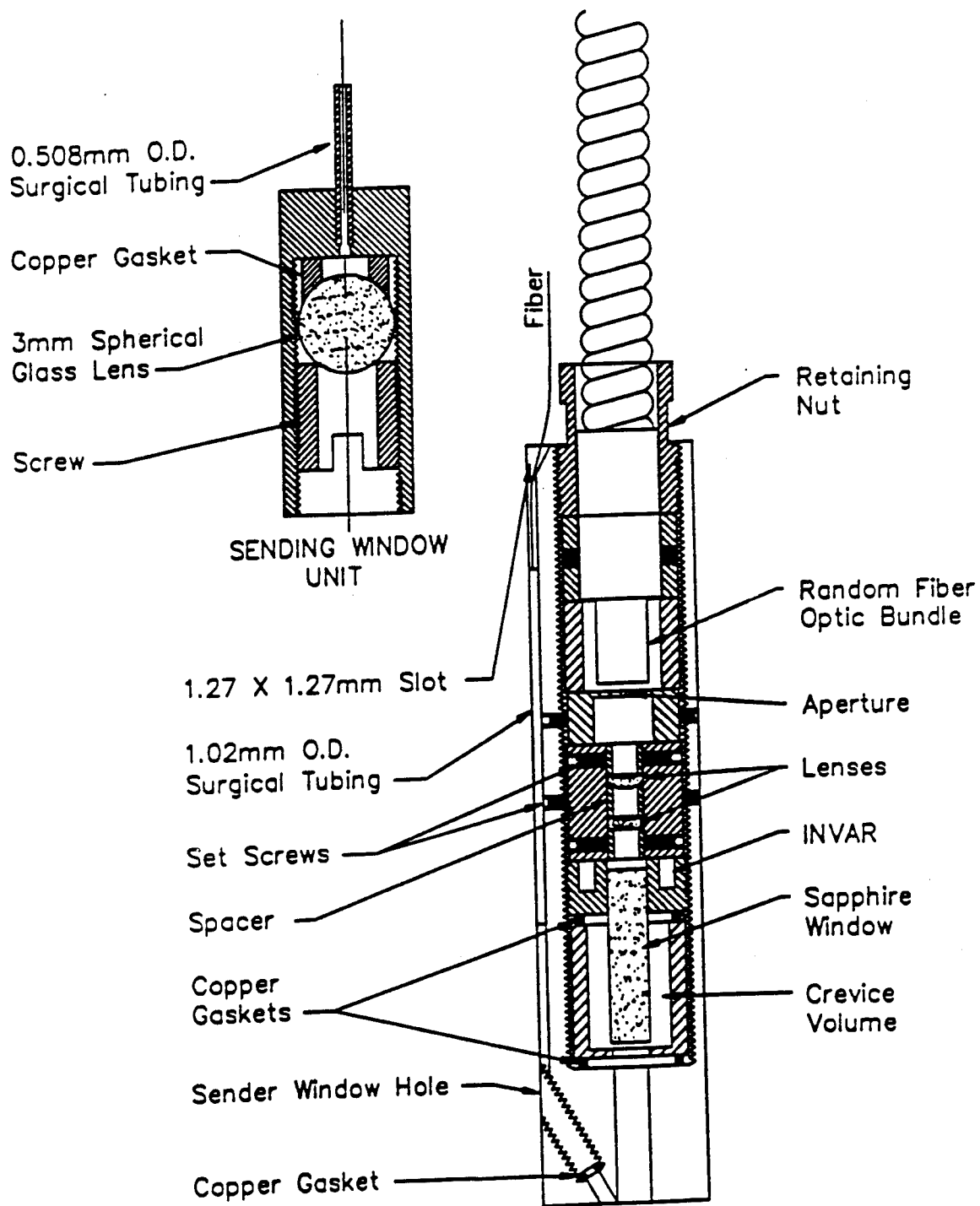
- Global kinetic expressions for the physical processes of:
  - inception
  - surface growth
  - oxidation
  - coagulation
- Rate constants for the global kinetic expressions are consistent with literature
- Compared to laminar flame data
- Implemented in a KIVA computational cell

## **Incorporation of literature models into KIVA**

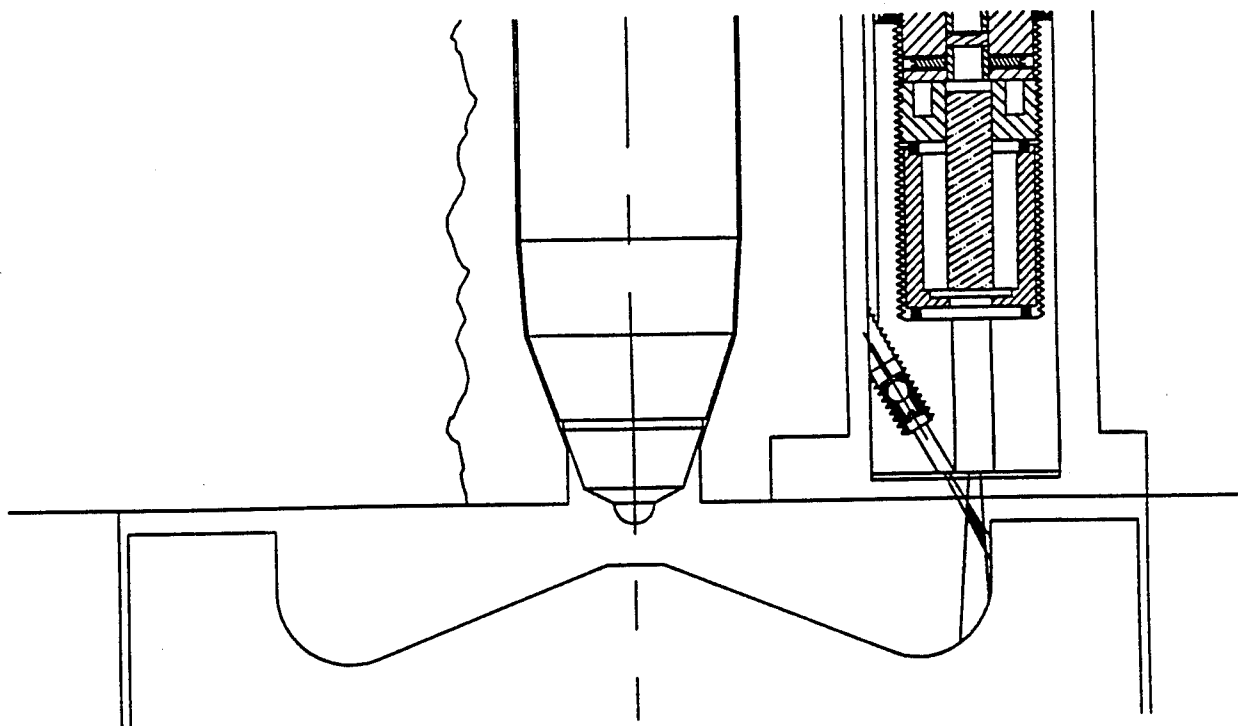
- Hiroyasu model with NSC oxidation implimented into KIVA II diesel engine simulation
- Preparations for more detailed models to be implimented into the simulation



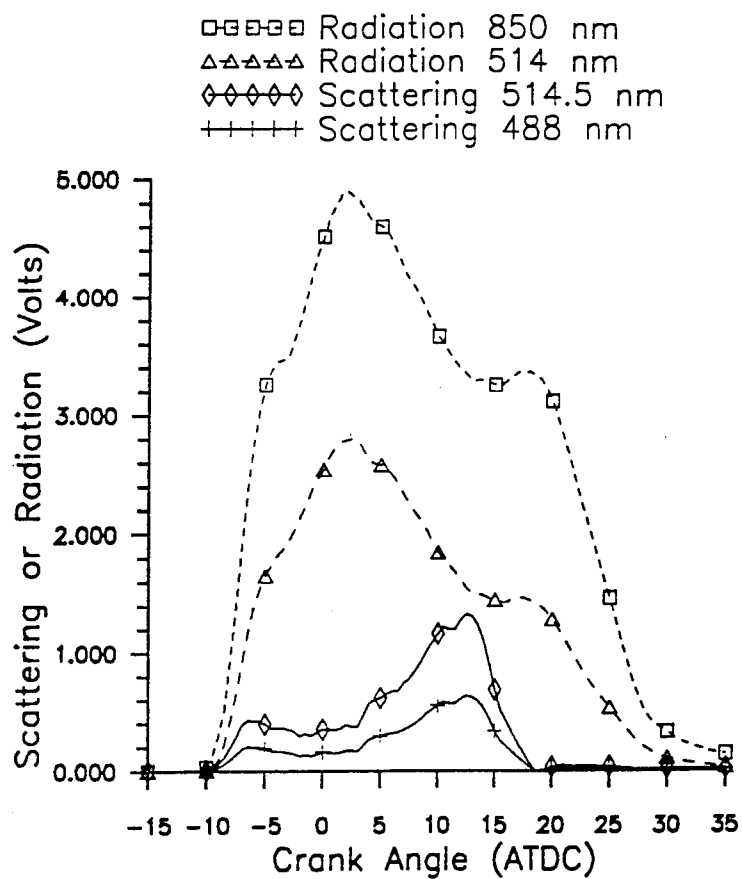
Schematic diagram of optical set-up and engine.



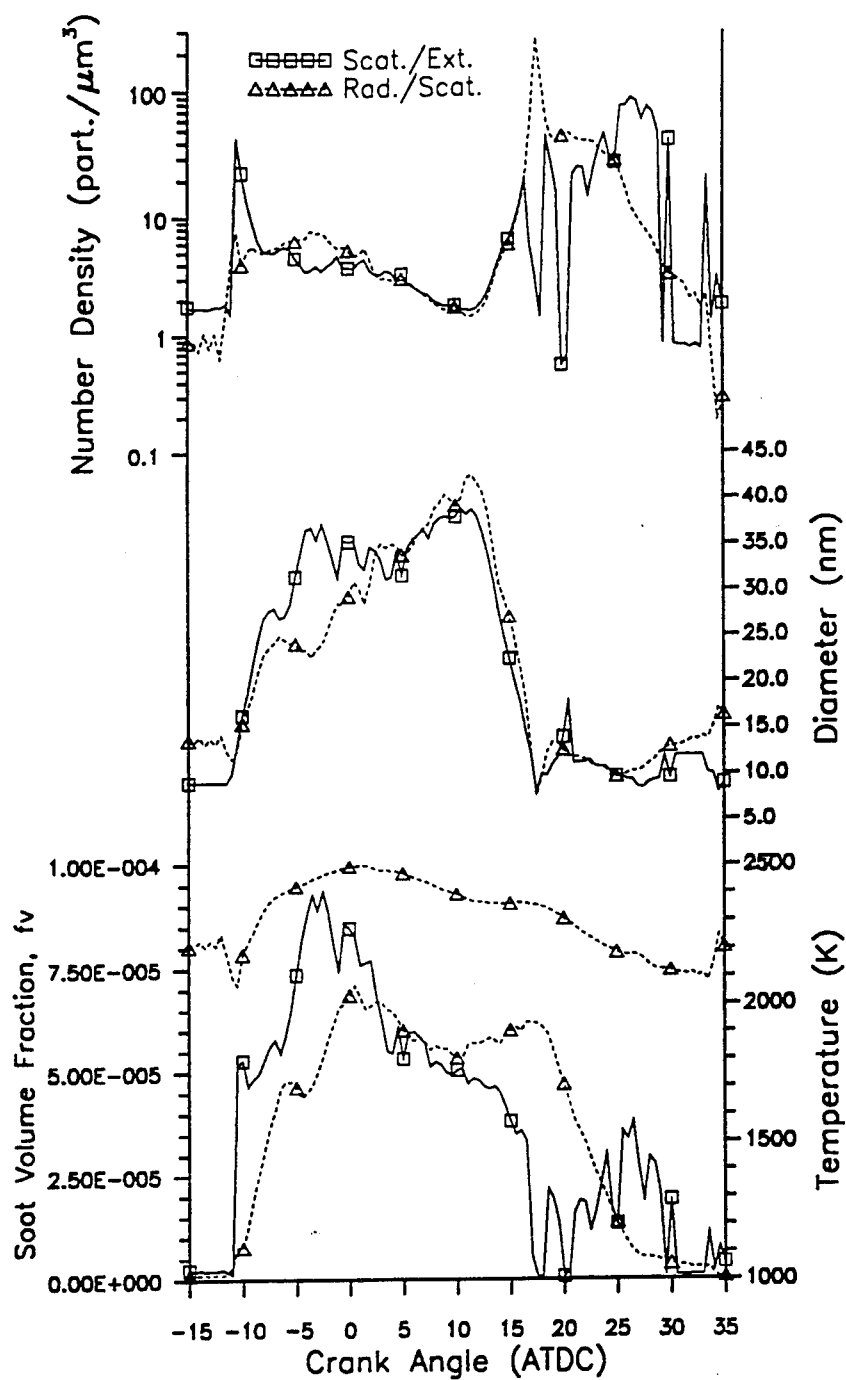
Cross section of the optical probe.



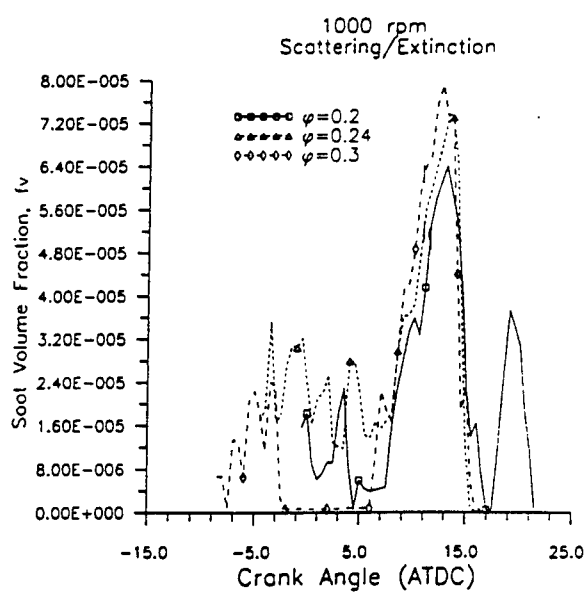
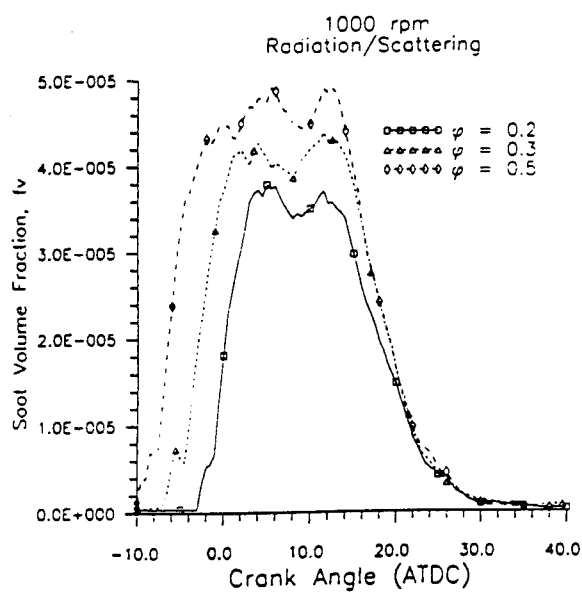
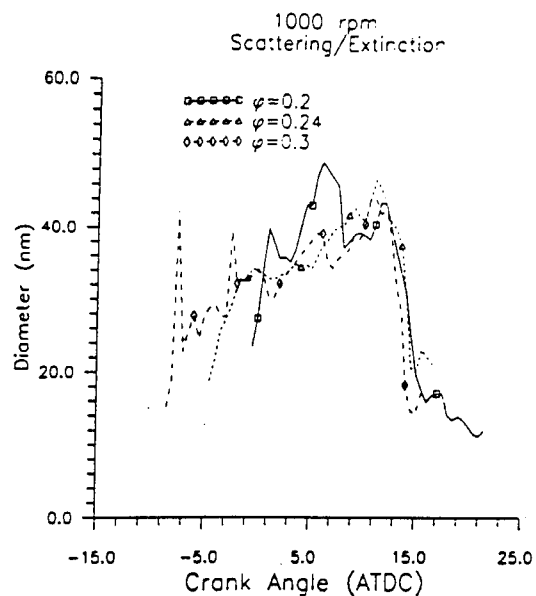
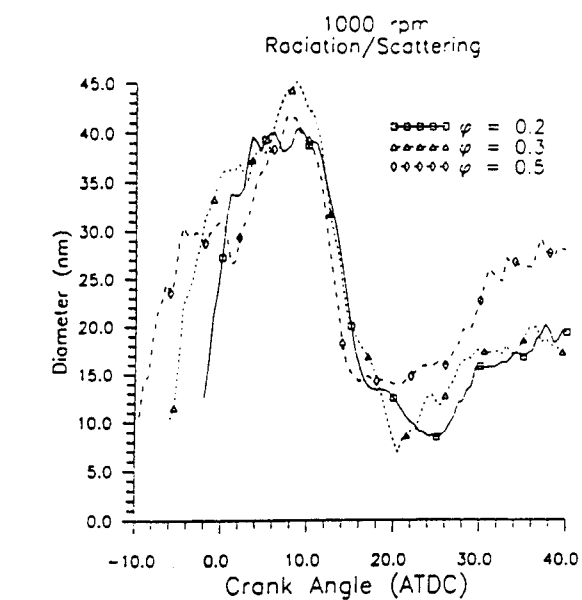
Cross section of the engine head, piston bowl, and measurement volume location.



Separated radiation and scattering signals after ensemble averaging at the three measured wavelengths.

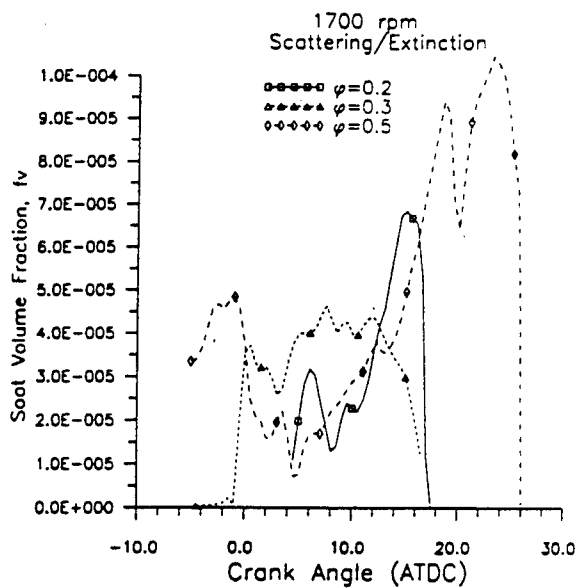
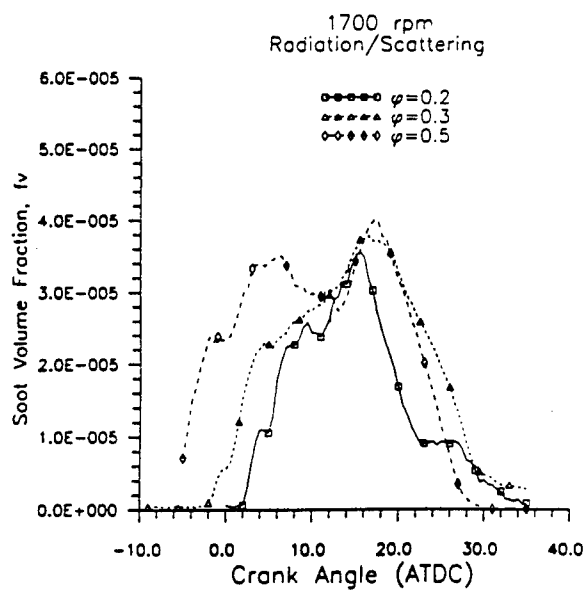
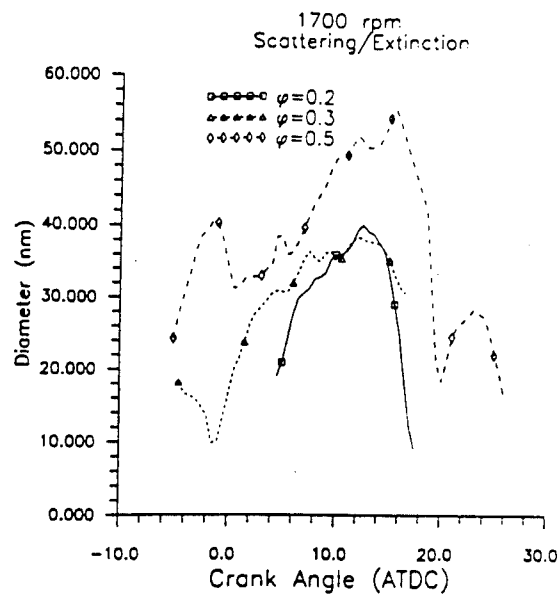
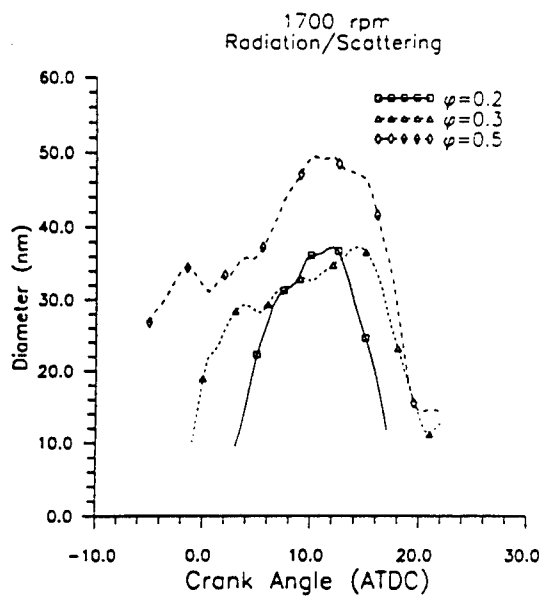


Soot particle diameter, number density, and soot volume fraction for both the scattering / extinction and radiation / scattering methods. Also soot particle temperature obtained from radiation two-color pyrometry.

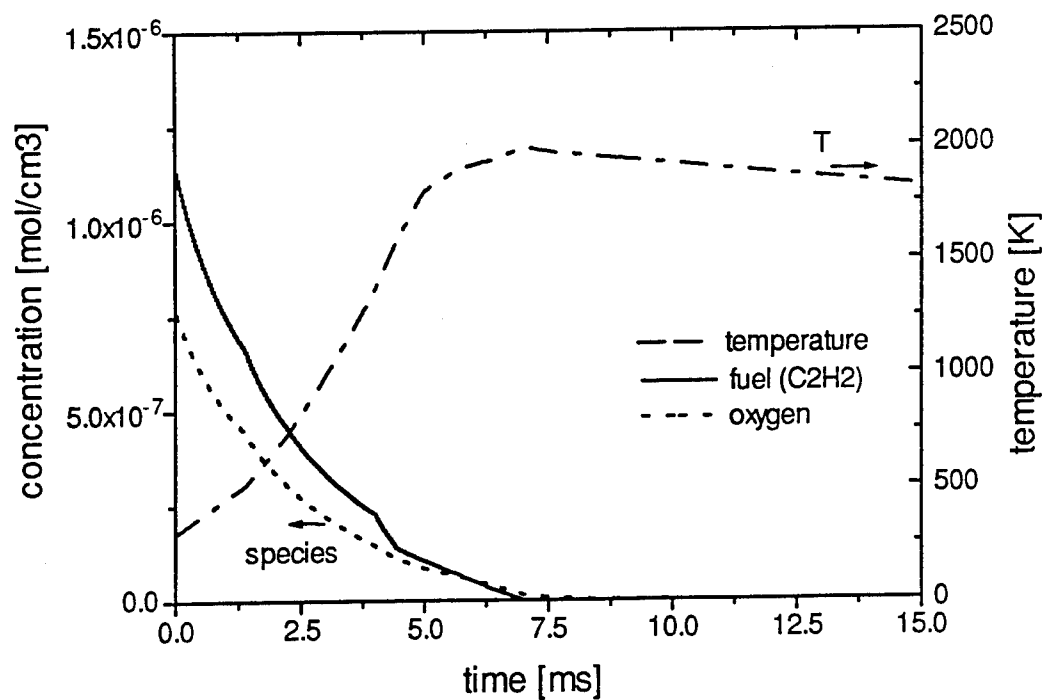
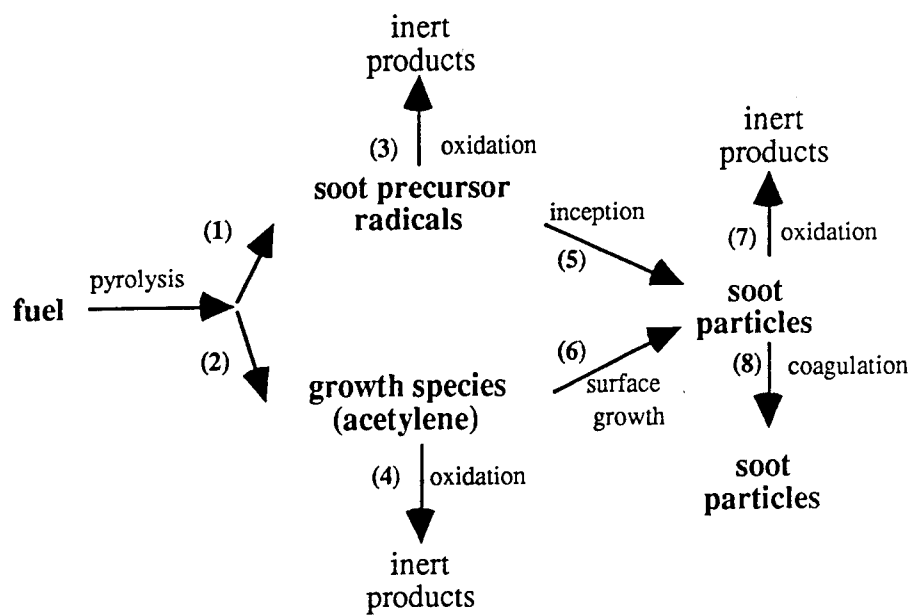


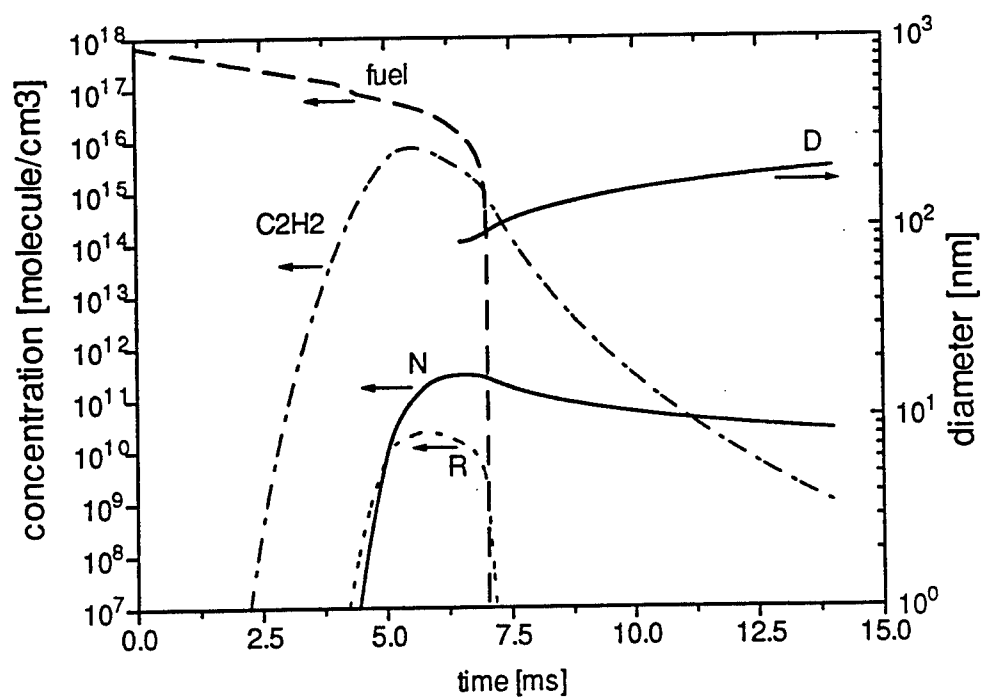
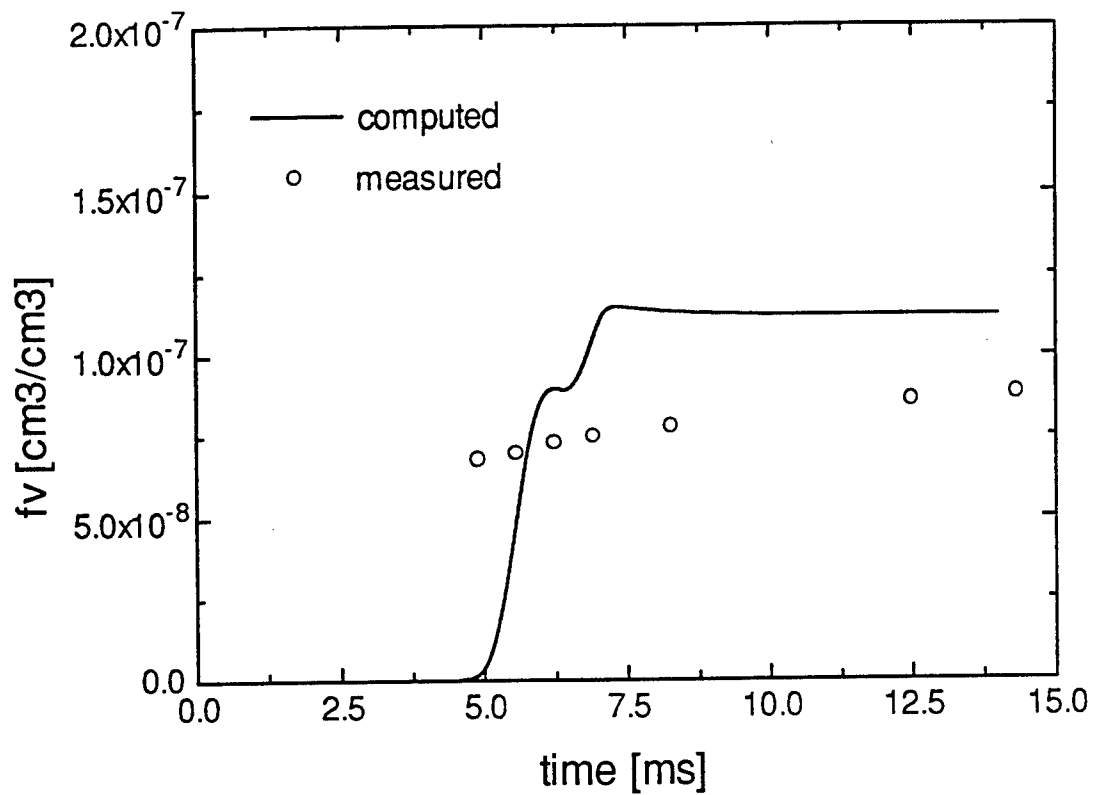
Crank angle resolved soot volume fraction and diameter at 1000 rpm and  $\phi = 0.2, 0.24, \text{ and } 0.3$  for both the scattering/extinction and radiation/scattering methods.

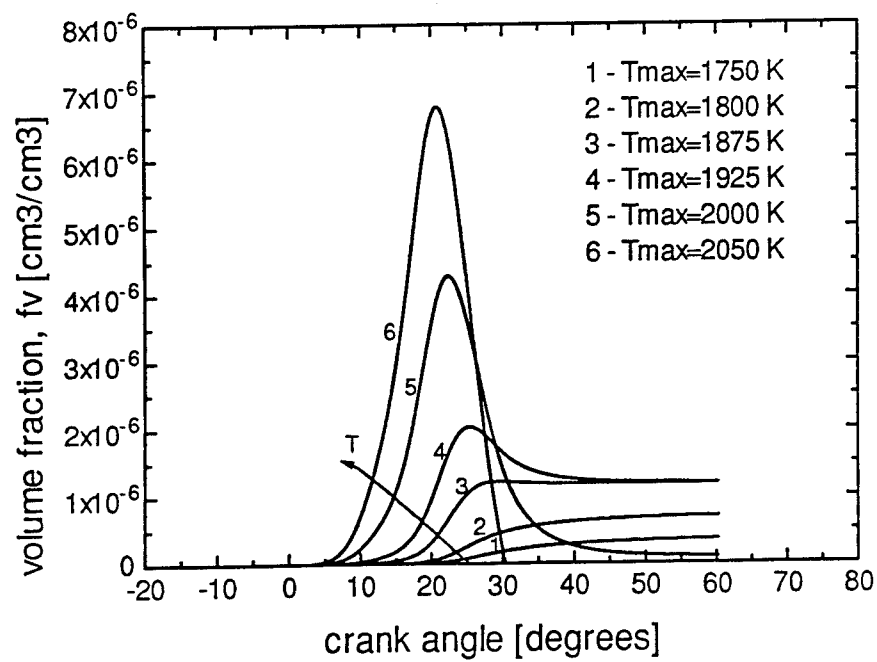
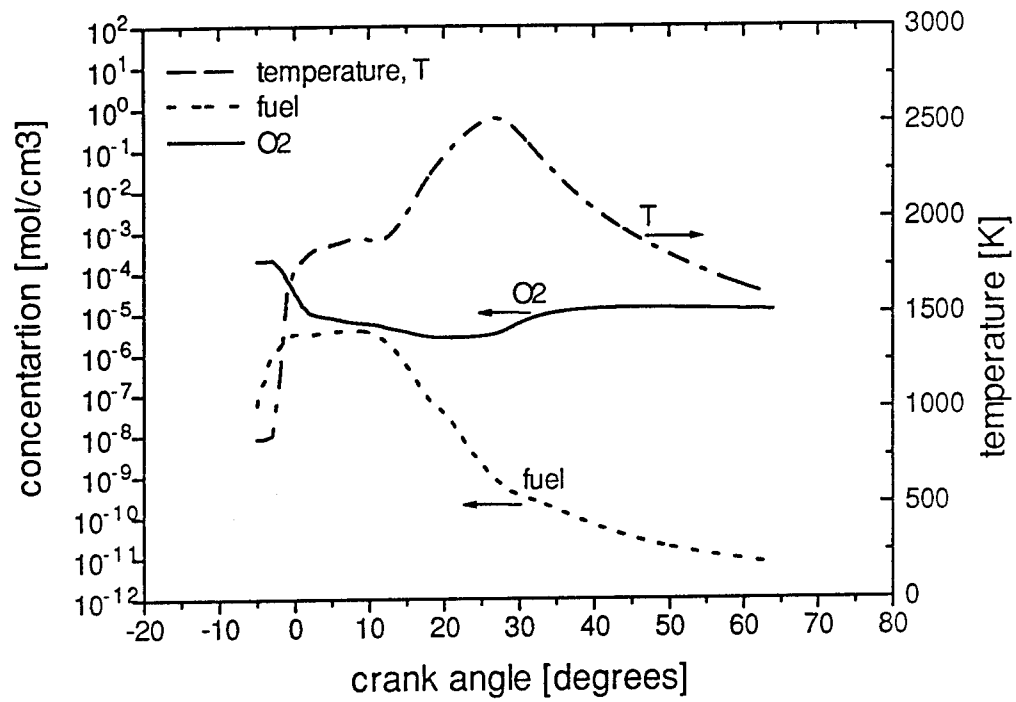


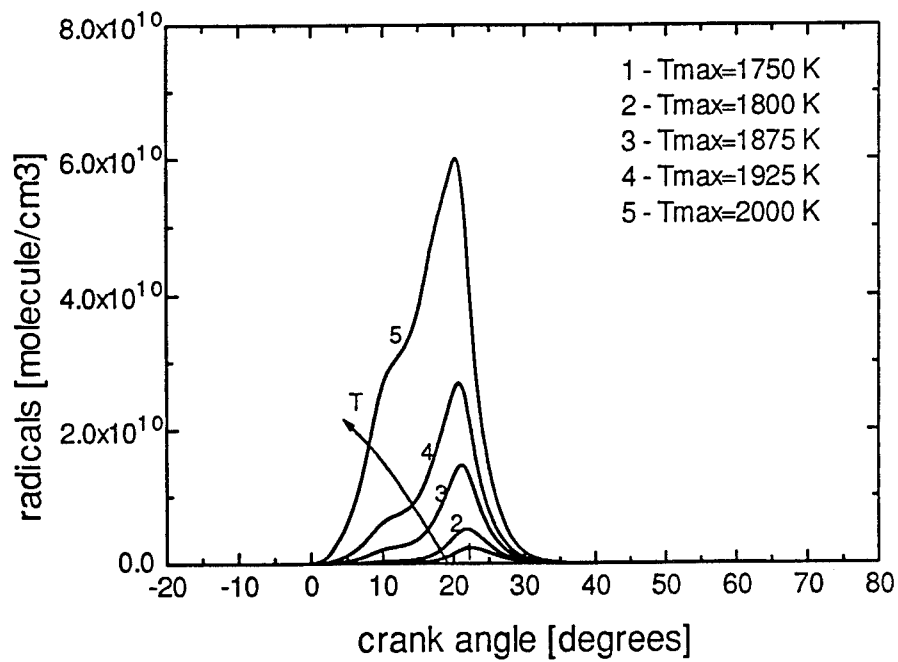
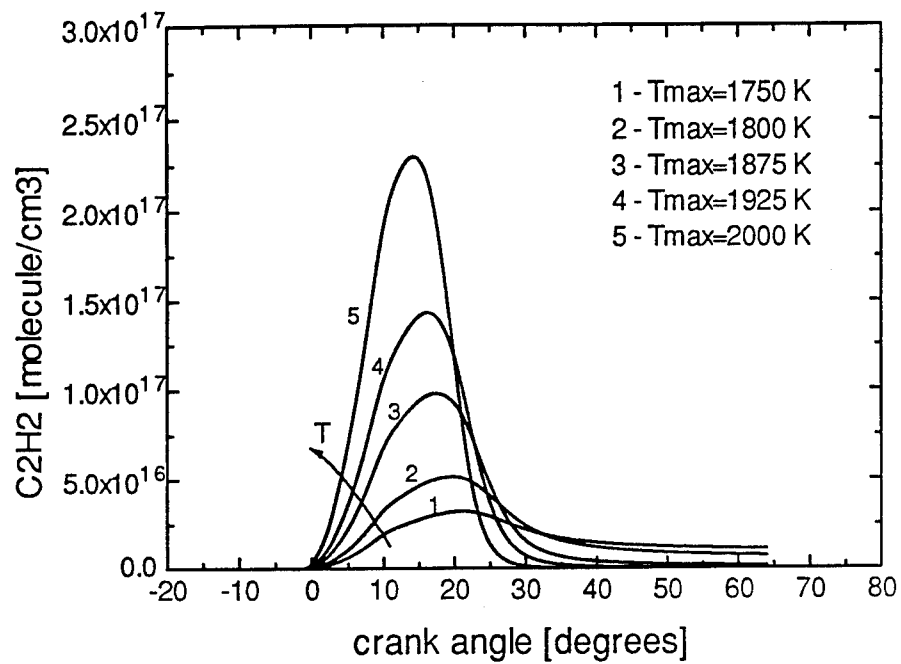


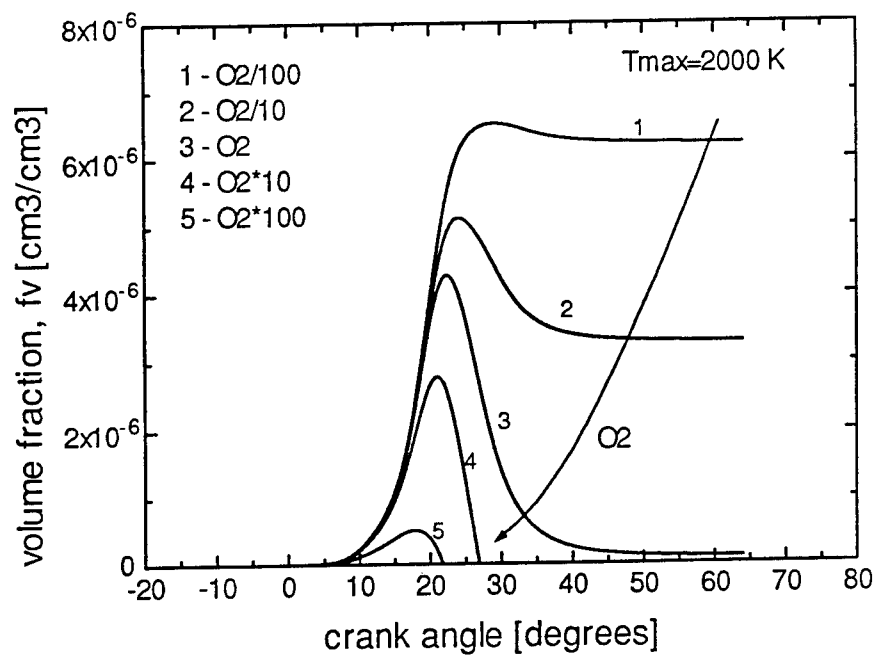
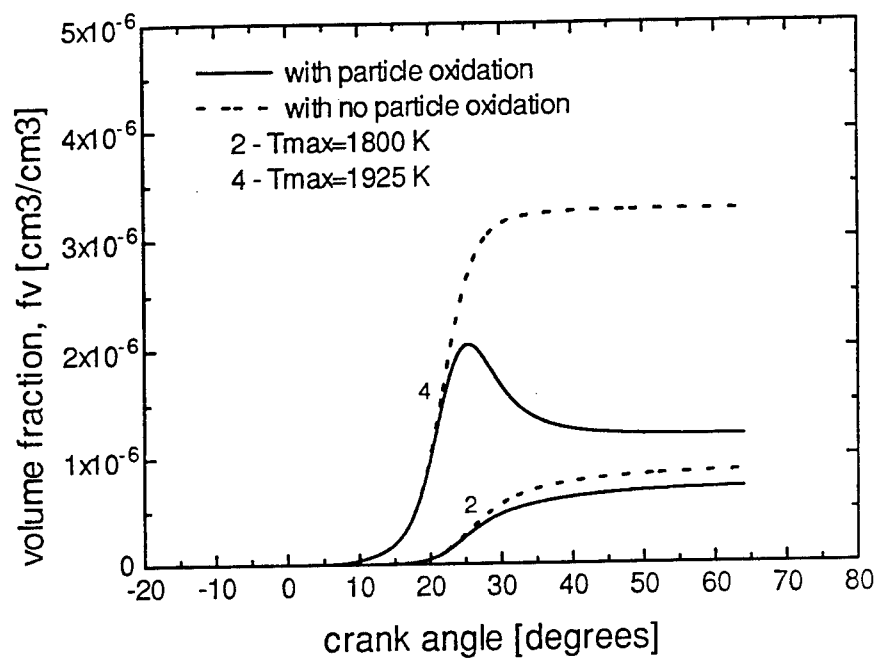
Crank angle resolved soot volume fraction and diameter at 1700 rpm and  $\phi=0.2, 0.3$ , and  $0.5$  for both the scattering/extinction and radiation/scattering methods.











## **REGIMES OF JET BREAKUP**

S.P. Lin and Michael D. Hudman

Mechanical and Aeronautical Engineering Department

Clarkson University

Potsdam, NY 13699-5725

### **ABSTRACT**

The regimes of jet breakup including the first-wind induced, second wind-induced, and atomization regimes are elucidated by use of a single equation. The equation is obtained by use of linear stability analysis. The equation relates the dimensionless intact length  $L$  to the dimensionless velocity  $U$  for relevant flow parameters. The results are plotted in the  $L$  vs  $U$  space to elucidate the regimes and mechanism of the jet breakup. The theory compares well with some experiments.

### **INTRODUCTION**

The atomization process is widely used in the formation of sprays for various industrial applications, including fuel spray. The process can be achieved by breaking up a liquid jet or a liquid sheet emanating from a nozzle of various geometries. The main cause of atomization is known to be due to the pressure fluctuation [1,2]. The jet may also be broken up by the Rayleigh mode of capillary pinching which produces droplets of diameter much larger than that of atomized droplets [3]. For a given jet breaking up in a given gas, the Rayleigh mode occurs at low jet speed and the atomization process takes place at relatively large velocity. In the Rayleigh mode of breakup, the actual breakup does not take place until some finite distance down stream of the nozzle. This distance is called intact length. The intact length increase with the jet speed up to a critical speed, and then decreases as the speed is increased further. This transition takes place in so called first wind-induced breakup regime [4] which follows the Rayleigh breakup regime. After the transition, the jet continues to shorten and numerous small ligaments emanate from the liquid-gas interface in the so called second wind-induced breakup regime. Finally the intact length vanishes, and the spray of small droplets is formed. Attempts have been made to explain the change of the intact length with the jet speed in different regimes, based on the first principle. Weber [5] attempted to explain the first wind-induced regime on the basis of a simplified characteristic equation obtained from linear stability analysis. His theory predicted a considerably smaller critical velocity for the maximum intact length. Stirling and Sleicher [6] improved Weber's theory by use of an empirical correlation. However, a theory which explains all regimes of the jet breakup from a single equation has not yet appeared. Here we offer such a theory.

## THEORY

The starting point of our explanation is the following equation

$$\begin{aligned}
 & (\omega - ik)^2 + \frac{2k^2}{R_e} \left( \frac{I_1'(k)}{I_0(k)} - \frac{2k\lambda}{\lambda^2 + k^2} \frac{I_1(k)I_1'(\lambda)}{I_0(k)I_1(\lambda)} \right) \\
 & \times (\omega - ik) + \omega^2 Q \frac{\lambda^2 - k^2}{\lambda^2 + k^2} \frac{K_0(k)I_1(k)}{K_1(k)I_0(k)} \\
 & - \frac{1}{We} k(1 - k^2) \frac{\lambda^2 - k^2}{\lambda^2 + k^2} \frac{I_1(k)}{I_0(k)} = 0,
 \end{aligned} \tag{1}$$

$R \equiv$  Reynolds number  $= U_0 r_0 / \nu_1$

$We \equiv$  Weber number  $= \rho_1 U_0^2 r_0 / S$

$Q =$  Density ratio  $= \rho_2 / \rho_1$

$\lambda = k^2 - Re(\omega - ik)$

Eq. (1) is the characteristic equation obtained [4] from the stability analysis of a liquid jet subject to disturbances whose Fourier components have a factor  $\exp[i k y + \omega t]$ , where  $k = k_r + ik_i$  is the complex wave number,  $\omega = \omega_r + i\omega_i$  is the complex wave frequency,  $y$  is axial distance measured from the nozzle tip. In Eq. (1),  $K$  and  $I$  are the modified bessel functions of orders indicated by their subscripts,  $\rho$  is the density,  $\nu$  is the kinematic viscosity,  $S$  is the surface tension,  $U_0$  is the average jet velocity,  $r_0$  is the jet radius and the subscripts 1 and 2 associated with the physical properties denote respectively the liquid and gas phases. Weber used a drastically simplified equation of Eq. (1). His results did not enjoy agreement with experiments. For a given jet at different  $U_0$ , Sterling and Sleicher [6] multiply the  $Q$ -term in Eq. (1) by 0.175 and solve the equation numerically for  $[\omega_r(k)]_{\max}$  assuming  $k_i = 0$ . The intact length  $L$  is then obtained from the relation  $L = \text{constant}/[\omega_r(k)]_{\max}$ . The factor 0.175 was used so that their theoretical prediction agrees best with the experiments. They argued that this multiplication factor is necessary because the air viscosity which may have a damping effect, is neglected in the theory. They also quoted the related work of Benjamin and stated that the air viscosity effect is much smaller than the inertia force effect of gas at the interface. Thus there is an apparent inconsistency. If the air viscosity effect is small, then the reduction of the gas inertia force represented by the  $Q$ -term in Eq. (1) should not have been reduced by a large factor of  $(1 - 0.175)$ .

Here we will not multiply the  $Q$ -term by any empirical factor. However we shall use a rational approximation to simplify the mathematics, and bring out the physical mechanisms of the jet breakup. Since both phenomena of first and second wind-induced regimes are due



to the interfacial pressure fluctuation [1,2], and the viscosities play minor roles [3], we shall neglect the  $Re$ -term in Eq. (1). This is justifiable for the large Reynolds number jet which is encountered in most of the applications. With this approximation, Eq. (1) is reduced to

$$\omega_2 + (\omega + ik)^2 QA = We^{-1}k(i - k^2) B = 0, \quad (2)$$

where

$$A = \frac{k_0(k)I_1(k)}{K_1(k)I_0(k)},$$

$$B = \frac{I_1(k)}{I_0(k)}.$$

We define the intact length  $L$  to be the distance from the nozzle tip to a downstream position where the disturbance amplitude has grown from the initial value  $a_0$  to an amplitude  $a$  for breakup. Then  $a = a_0 \exp(k_i L)$  and thus

$$L = k_i^{-1} \ln(a/a_0). \quad (3)$$

$k_i$  in Eq. (3) must be found from Eq. (2) as the maximum amplification rate for a given  $Q$  and  $We$ . The numerical task required is very considerable since the complex  $k$  appears in the arguments of the modified Bessel functions. Fortunately, the spatial and temporal growth rates are related [7] by

$$k_i = \omega_r + 0(We^{-2}), \quad (4)$$

$$k_r = \omega_i + 0(We^{-2}). \quad (5)$$

Moreover, both the first and second wind-induced breakup occur at  $We^{-1} \leq Q$ , [1]. For a water jet in air,  $Q = 0.13$  at 100 atm. Thus we may write Eq. (3) as

$$L = \omega_r^{-1} \ln(a/a_0),$$

with an error of less than 2% if the jet is issued into air of pressure less than 100 atm.  $\omega_r$  must be obtained from Eq. (2) as the maximum temporal growth rate  $\omega_m$  for given  $Q$  and  $We$ . The real and imaginary parts of Eq. (2) are

$$(\omega_r^2 - \omega_i^2)(1 + QA) - kQA(2\omega_i + k) - We^{-1}k(1 - k^2)B = 0 \quad (6)$$

$$\omega_i(1 + QA) + kQA = 0 \quad (7)$$

Substitution of  $\omega_i$  from Eq. (7) into Eq. (6) yields

$$\omega_r^2 = We^{-1} k(1 - k^2) b + k^2 a = 0, \quad (8)$$

where

$$a = QA/(1 + QA)^2, \quad b = B/(1 + QA).$$

The extrema of  $\omega_r$  in Eq. (8) must satisfy

$$We^{-1} (1 - 3k^2)b + 2ka + We^{-1} k (1 - k^2) b' + k^2 a' = 0. \quad (9)$$

where primes denote differentiation with  $k$ . For given  $We$  and  $Q$ , the solution of (9) gives  $k_m$  the wave number corresponding to the most amplified disturbances. Substitution of  $k_m$  for  $k$  in Eq. (8) yields  $(\omega_r)_{max}$ . Substituting this value for  $k_i$  in Eq. (3), we have

$$L = \omega_r^{-1} \ell n(a/a_0) \quad (10)$$

## RESULTS

The dimensionless intact length  $L$  obtained from Eq. (10) with  $\ell n(a/a_0) = 1$  is plotted against the dimensionless jet speed  $U = WeQ$  in Fig. 1, for three different values of  $Q$ . The Rayleigh regime I where  $QWe < 0.8$ , the first wind-induced regime II where  $0.8 < QWe < 1.2$ , the second wind-induced regime III where  $1.2 < QWe < 5$  and the atomization regime IV are also indicated in the same figure. These parameter ranges are consistent with the results obtained in the author's previous investigations [1-3], on the mechanism of jet breakup. The dotted lines near  $U = 0$  correspond to the dripping jet. The dripping jet arises from absolute instability [8]. Some experimental results taken from sterling and Sleicher for large Reynolds number are also given in the same figure for comparison. It should be pointed out that the intact length discussed here refers to the intact liquid-gas interface. It does not refer to the intact core length [4,9], the determination of which requires nonlinear theory.

## CONCLUSION

Five regimes of jet breakup have been recognized from the solution of a single equation. These regimes are dripping jet, the Rayleigh capillary pinching, first wind-induced breakup, second wind-induced breakup, and atomization. The dripping jet regime occurs when the Weber number is smaller than the critical Weber number [9]. The Rayleigh regime occurs when  $QWe < 0.8$ . The first wind-induced regime takes place in  $0.8 < QWe < 1.2$ . The second wind-induced regime occurs in  $1.2 < QWe < 10$ . Both the first and second wind-induced breakup are due to pressure fluctuation at the interface. Finally, the atomization regime starts when  $QWe > 10$ . The present classification of the breakup regimes refers to the jet interface, but does not refer to the jet core. The classification of the regimes of jet core breakup requires nonlinear theories.

## ACKNOWLEDGEMENTS

This work was supported in part by Grants No. DAAL 03-89-K-0179 of ARO, and No. NAG3-1402 of NASA.

## NOMENCLATURE

$a$  , disturbance amplitude  
 $k$  , complex wave number  
 $L$  , intact length  
 $Q$  , Density ratio  
 $r_o$  , nozzle radius  
 $Re$  , Reynolds number  
 $S$  , Surface tension  
 $We$  , Weber number

## Greek symbols

$\lambda$  , argument of Bessel function  
 $\omega$  , complex wave frequency  
 $\nu$  , kinematic viscosity

## Subscripts

0 , initial value  
1 , liquid phase  
2 , gas phase  
 $i$  , imaginary part  
 $r$  , real part

## REFERENCES

1. S.P. Lin and Z.W. Lian, Mechanism of Atomization, *AIAA Journal*. Vol. 28, pp. 120-126, 1989.
2. S.P. Lin and B. Creighton, Energy Budget in Atomization, *J. Aerosol Science Technology*, Vol. 12, pp. 630-636, 1990.
3. S.P. Lin and E.A. Ibrahim, Instability of a Viscous Liquid Jet Surrounded by a Viscous Gas in a Vertical Pipe, *J. Fluid Mech.*, Vol. 218, pp. 641-658, 1990.
4. R.D. Reitz and F.V. Braco, Mechanism of Breakup of Round Liquid Jets in N.P. Cheremisinoff (ed.) *Encyclopedia of Fluid Mechanics*, Chap. 10, Gulf Publishing Co. Houston, 1986.
5. C. Weber, On the Breakdown of a Fluid Jet, *Z.A.M.P.*, Vol. 11, pp. 136-154, 1931.
6. A.M. Stirling and C.A. Sleicher, The Instability of Capillary Jets, *J. Fluid Mech.*, Vol. 68, pp. 477-495, 1975.
7. J.B. Keller, S.I. Rubinow and Y.O. Tu, Spatial Instability of a Jet, *Physics of Fluid A*, Vol. 16, pp. 2052-2055, 1972.
8. S.P. Lin and Z.W. Lian, Absolute and Convective Instability of a Viscous Liquid Jet Surrounded by a Viscous Gas in a Vertical Pipe, *Phys. Fluids A*, Vol. 5, pp. 771-773, 1993.

9. H. Hiroyasu, Experimental and Theoretical Studies of the Structure of Fuel Sprays in Diesel Engines, *Proc. Symp. ICLASS-91*, pp. 17-31, 1991.

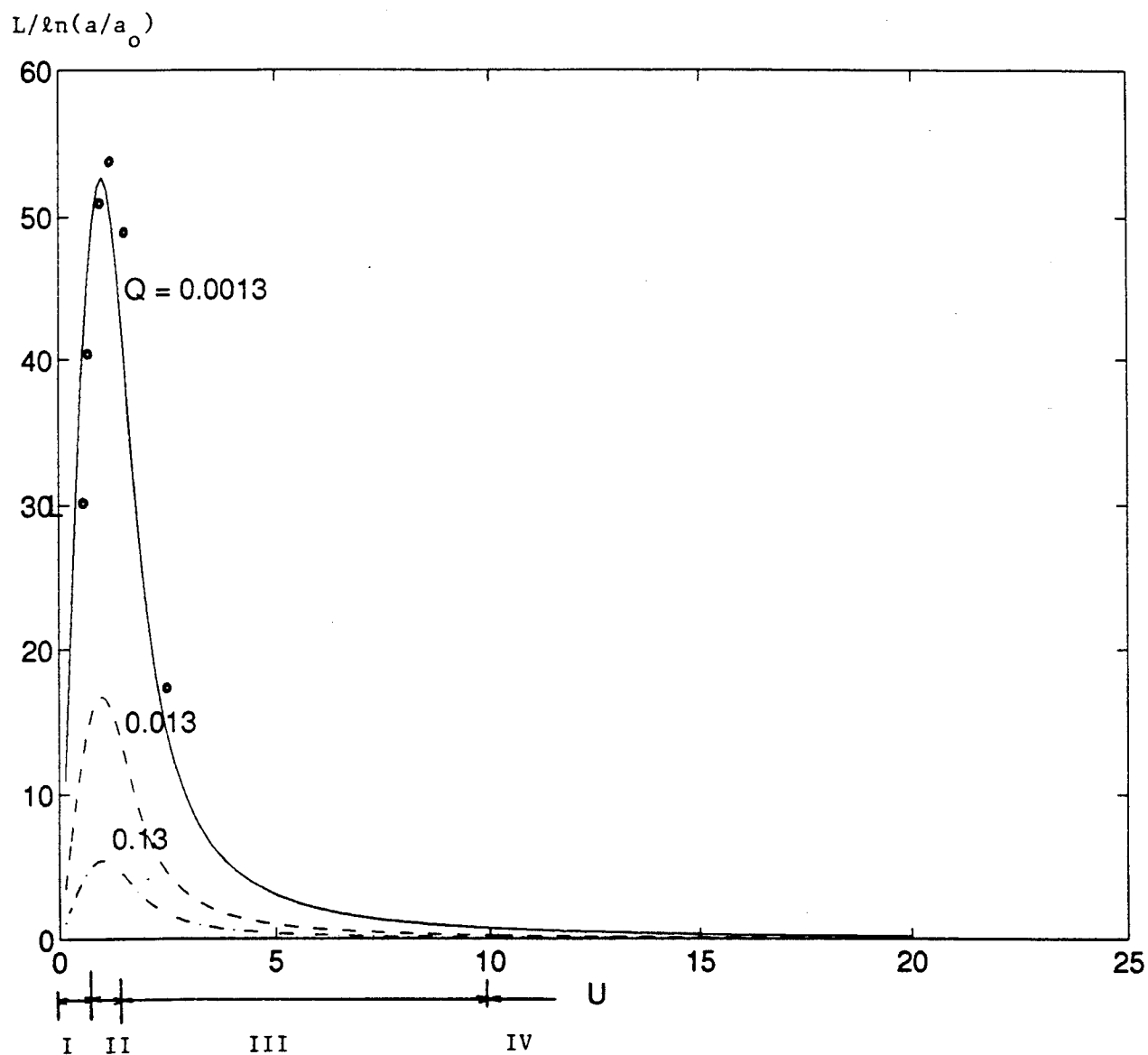


Fig. 1 . Jet breakup regimes

## **Restoration of Laser Droplet Slicing Images**

Jingyi Zhang and L.A. Melton  
Department of Chemistry  
University of Texas at Dallas  
Richardson, TX 75083-0688

and

## **Novel Droplet Slicing Techniques**

Michael Winter  
United Technologies Research Center  
East Hartford, CT 06108

In droplet slicing imaging, a technique in which the midplane of a sub-millimeter droplet is illuminated with a laser sheet and the fluorescence is viewed (usually) at  $90^\circ$  to the sheet, the image is significantly distorted, with the central portion being magnified and the outer portion being compressed at the droplet edge. At UTD, algorithms and programs for the removal of these distortions have been developed and tested.

The numerical restoration process involves several steps. (1) The mapping which takes the actual fluorescence pattern within the droplet (object image) to that measured by the CCD camera (camera image) is constructed. (2) The inverse mapping, which takes the camera image to the restored object image, is constructed. (3) These mappings are used on numerically constructed images to test the degree to which the restored object image matches the object image. (4) For experimental data, it is necessary to include steps involving the conversion from Cartesian coordinates to polar coordinates and vice versa.

The image restoration process is highly unstable numerically. While it is possible to restore simulated  $90^\circ$  droplet slicing images which have extremely high signal-to-noise ratios, when low levels of random noise (1%) or perturbations in the index of refraction are added, the numerical results become meaningless because of unconstrained oscillations. The numerical instability can be suppressed significantly by fitting the object image to a set of basis functions and performing a least squares fit for the best coefficients in this expansion.

The best way to recover the image all the way to the edge of the droplet is to carry out measurements at approximately  $60^\circ$  to the laser sheet. In this manner, the image on the acute side is recovered easily because the numerical restoration is stable, while the information on the oblique side is lost completely.

AT UTRC, aerodynamic droplet generators have been used (1) to reveal the interactions between internal liquid motions in the droplet and the motions in the surrounding vapor and (2) to generate "layered droplets" in which fluorescent acetone vapor condenses on a decane droplet and reveals the streamlines through its fluorescence (bright on a dark background).

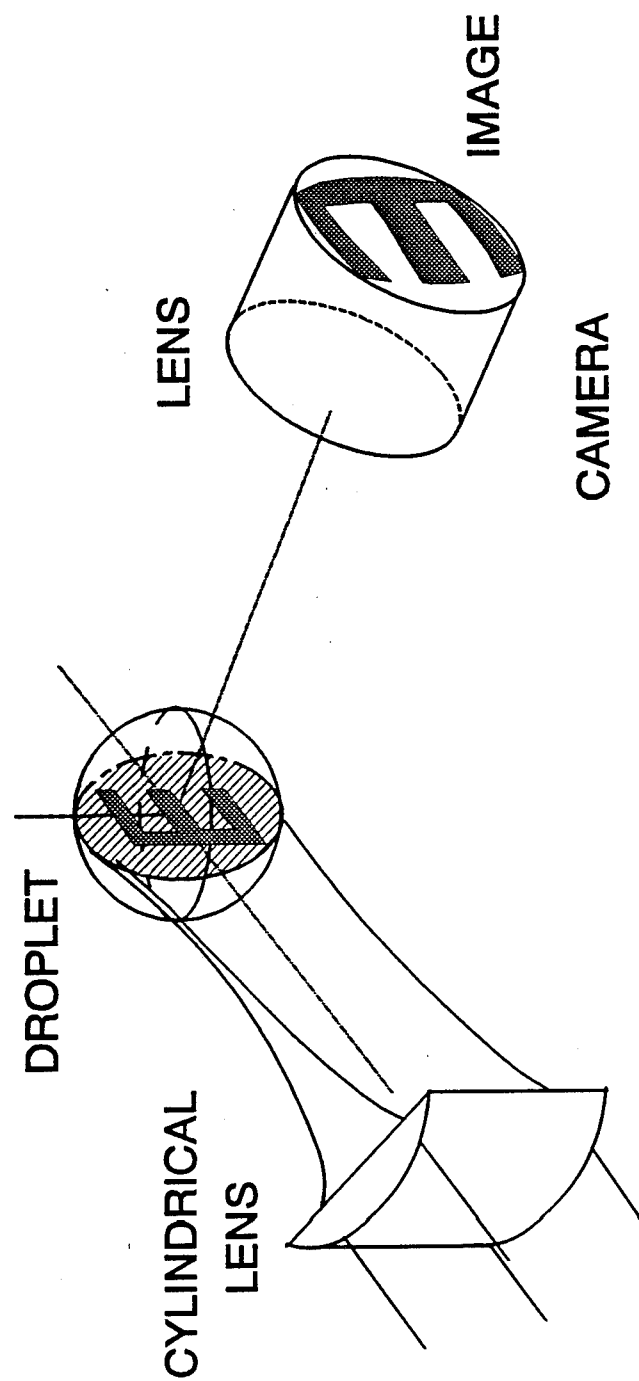
# **RESTORATION OF LASER DROPLET SLICING IMAGES**

**Jingyi Zhang and Lynn A. Melton  
Chemistry Department  
University of Texas at Dallas**

**Army Research Office  
Contract No. DAAL03-91-G-0033**

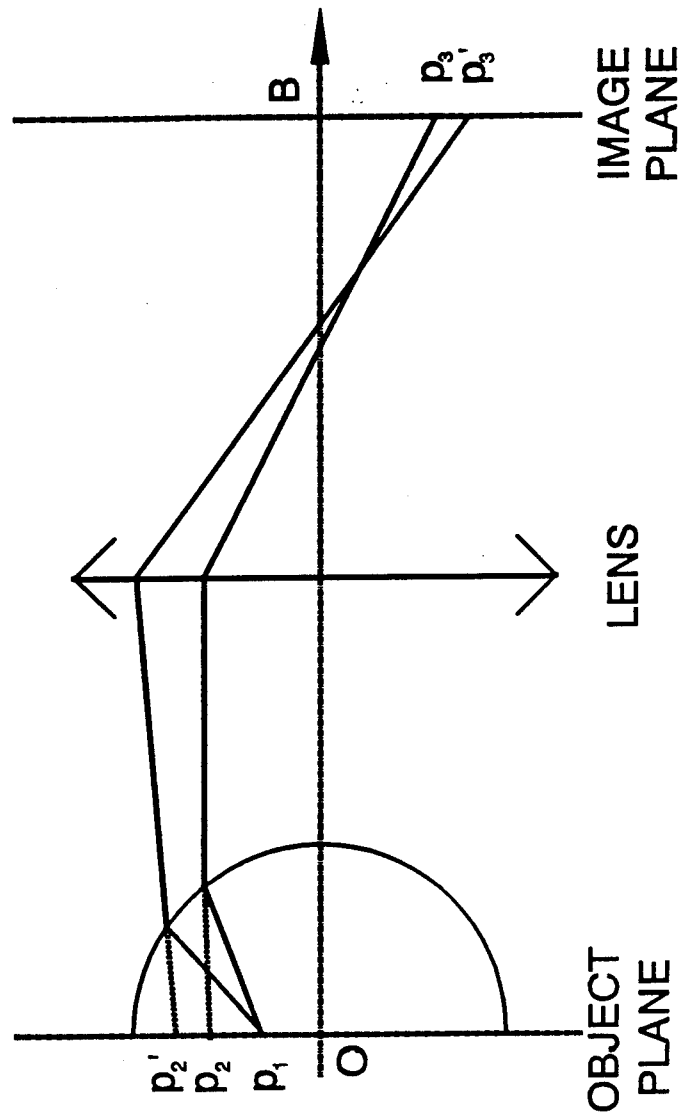
# LASER DROPLET SLICING IMAGING

WINTER - MELTON'S EXPERIMENTS

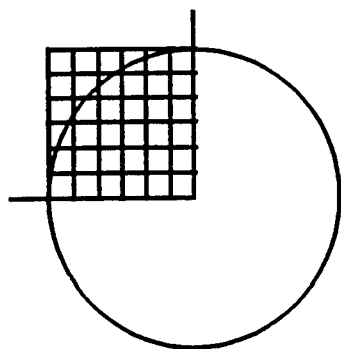




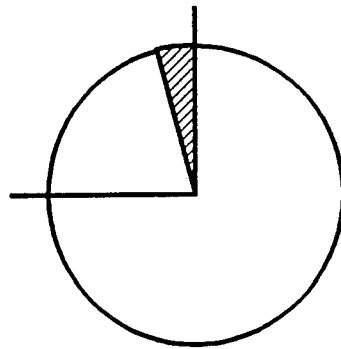
# GEOMETRICAL OPTICS RAY TRACING



# COORDINATE SYSTEMS



ORIGINAL IMAGE IN  
CARTESIAN COORD.



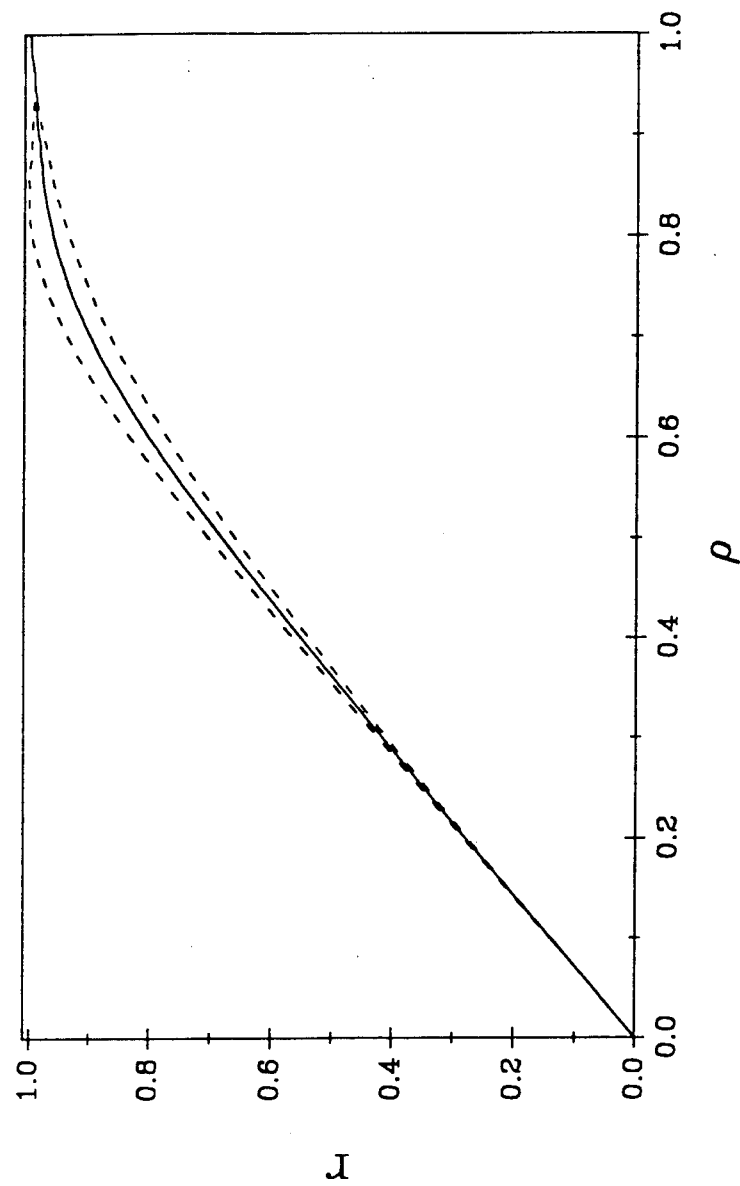
MAPPED INTO  
POLAR COORD.

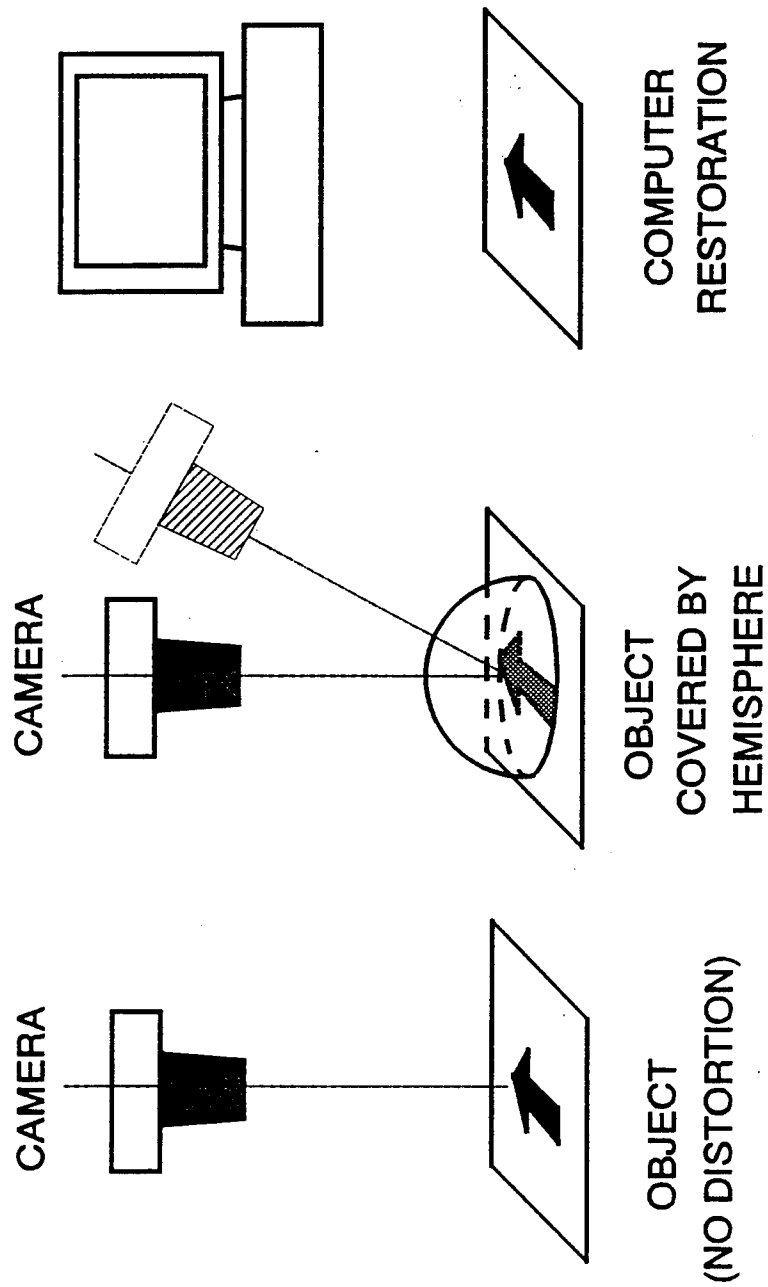


WEDGE



# COMPUTED RADIAL COORDINATES MAPPING SHOWING SPATIAL DISTORTIONS





## MATHEMATICAL FORMULATIONS

- $[A] \cdot [F] == [G]$

$[A]$  : Mapping Matrix (Point Spread Function)

$[F]$  : Object Matrix

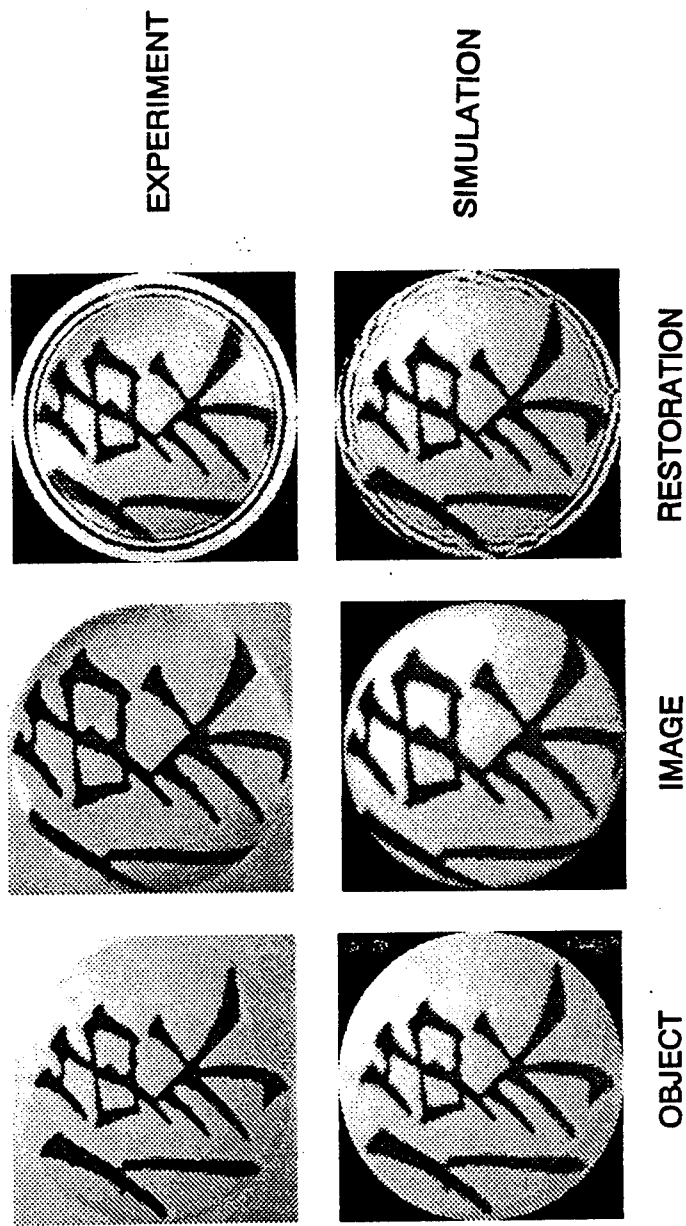
$[G]$  : Image Matrix

- Forward mapping: Simulation of Image Formation
- Inverse mapping: Image Restoration
- Direct Inversion (Restoration): failed
- Least Squares Inversion: with success
- Basis Functions:

$$1, x, \sin x, \cos x, \sin 2x, \cos 2x, \dots, \sin \frac{K-2}{2}, \cos \frac{K-2}{2}$$

# IMAGE DISTORTION AND RESTORATION 90 DEGREE OBSERVATION

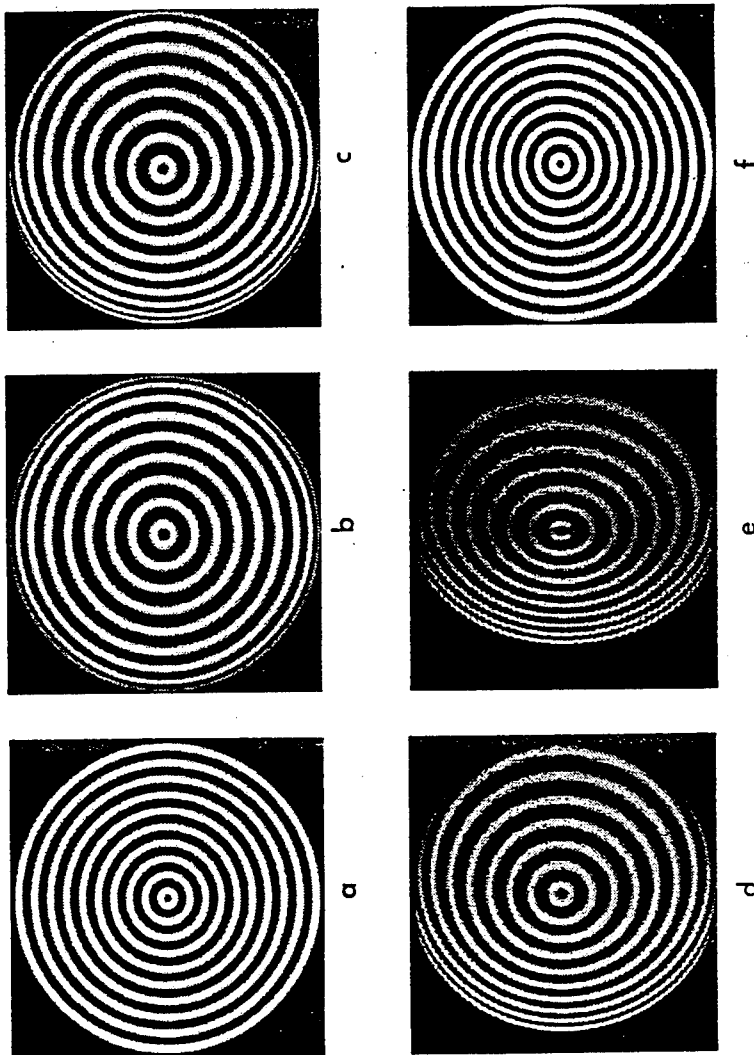
- NUMERICAL SIMULATION OF IMAGING PROCESS
- NUMERICAL IMAGE RESTORATION



## OFF - 90 DEGREE OBSERVATIONS

- 90 DEGREE OBSERVATION  
DIFFICULT TO RESTORE OUTER REGION
- OFF - 90 DEGREE OBSERVATION  
SUCCESS IN RESTORING OUTER REGION

# NUMERICAL SIMULATION OF OFF-90 DEGREE OBSERVATIONS

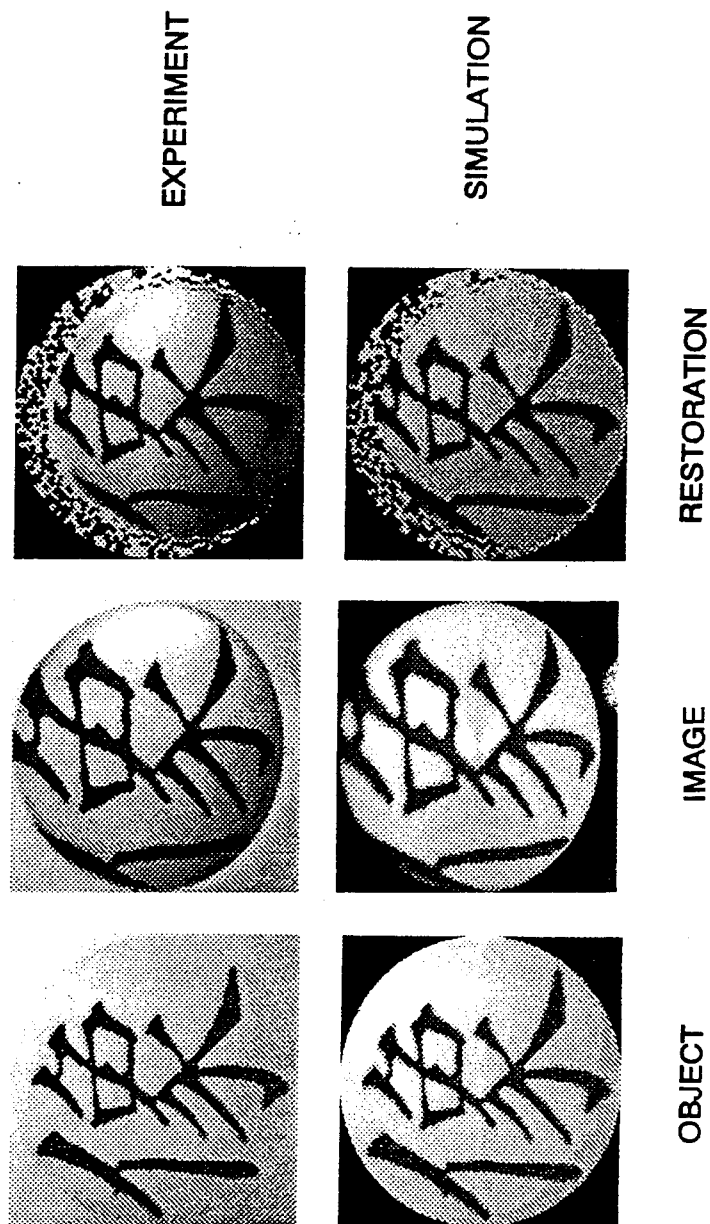


(a) Object (b)  $0^\circ$  (c)  $15^\circ$  (d)  $30^\circ$  (e)  $44^\circ$  Images' (f) Restoration ( $30^\circ$ )



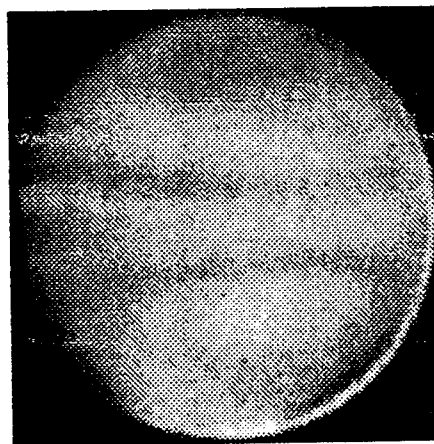
# IMAGE DISTORTION AND RESTORATION

## OFF - 90 DEGREE OBSERVATION

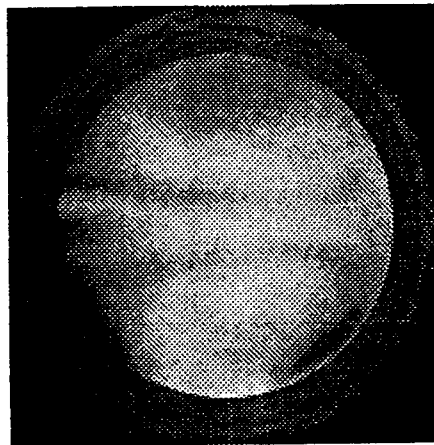


# DROPLET - SLICING IMAGE AND RESTORATION

90 DEGREE OBSERVATION



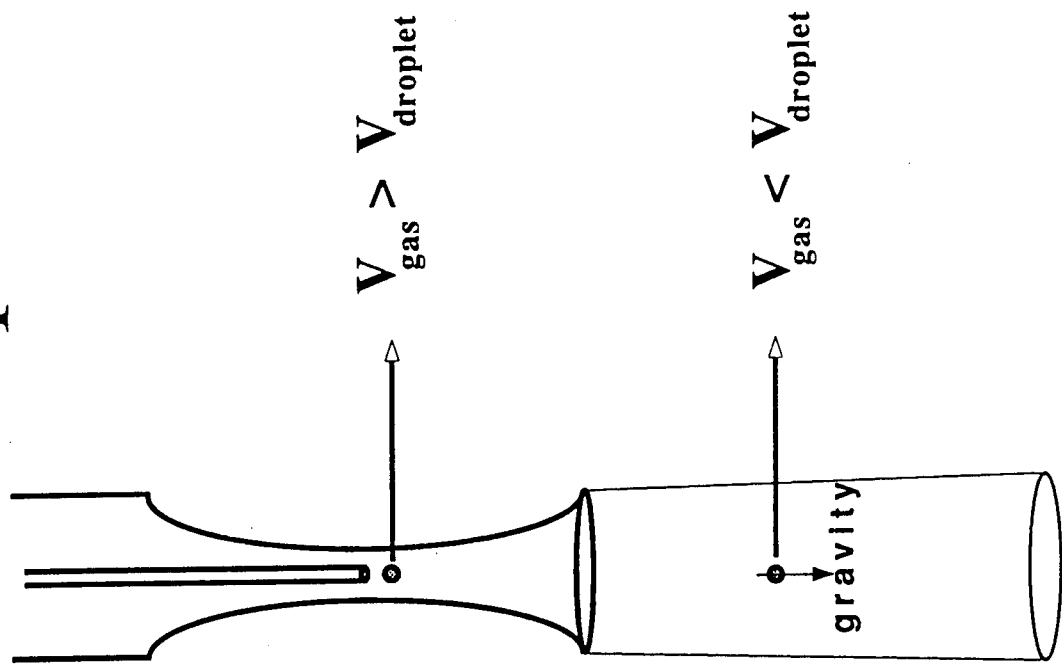
IMAGE



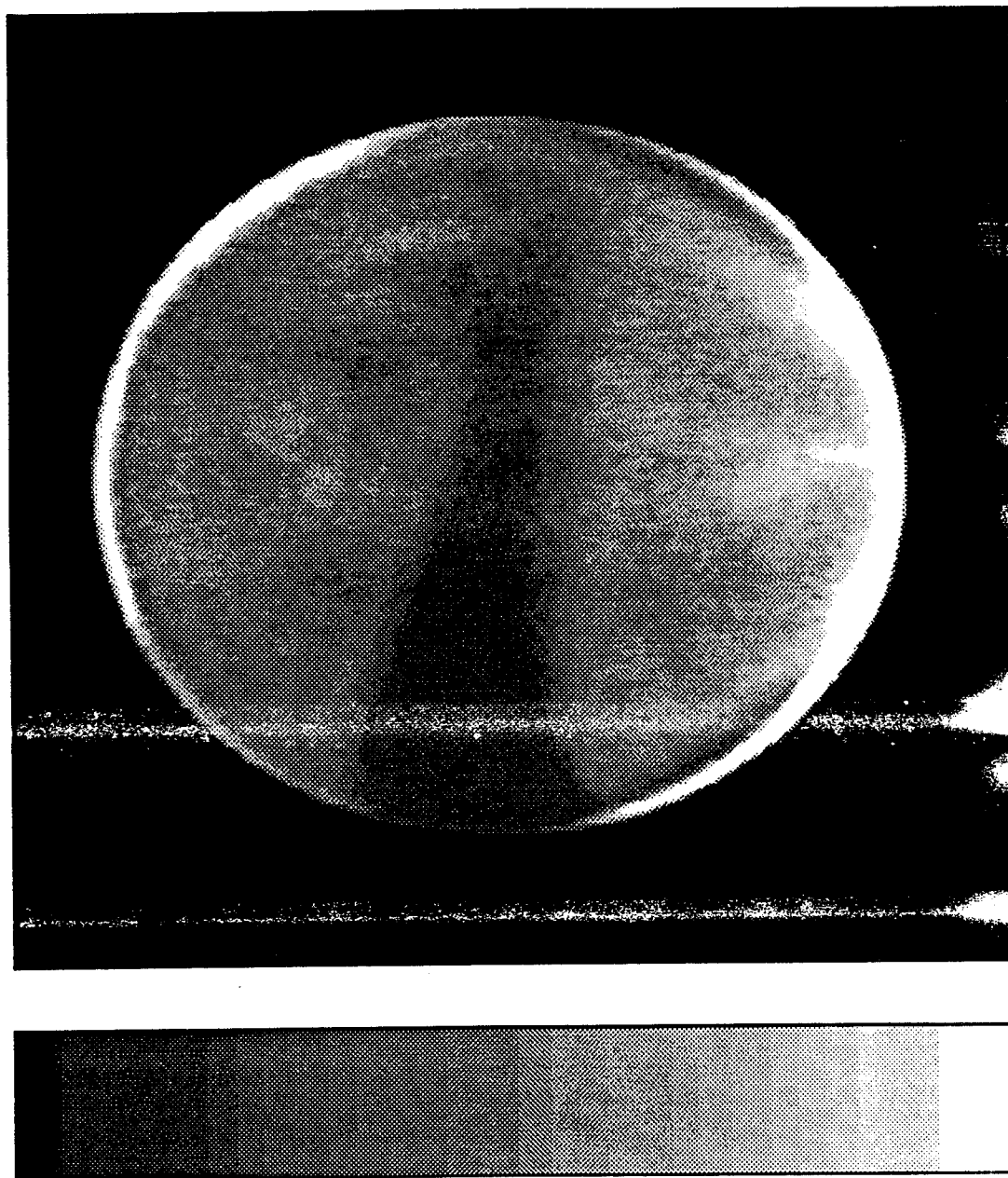
RESTORATION

Left photo courtesy M. Winter, UTRC, East Hartford, CT

# Aerodynamic Droplet Generator



# INTERNAL STRUCTURE OF A BICOMPONENT DROPLET



# **The Effect of Turbulence on Vaporization and Mixing in Fuel Sprays**

**D. A. Santavicca  
Department of Mechanical Engineering  
Penn State University  
University Park, PA 16802**

The objective of this research is to obtain an improved understanding of the behavior of droplets in vaporizing sprays, particularly under conditions typical of those in high swirl, direct injection Diesel engines. Experiments are conducted in a high pressure, high temperature, optically-accessible flow system which is capable of operation at pressures up to 70 atm, temperatures up to 600 K, gas velocities up to 20 m/sec and turbulence intensities up to 40%. Single droplets, 50 to 500 micron in diameter, are produced by an aerodynamic droplet generator and transversely injected into the flow. Measurements are made of the droplet position, size, velocity and temperature from which droplet drag, dispersion, heating, vaporization and breakup are characterized.

To date, the main results from this study are the following:

1. Under laminar flow conditions, vaporization was found to reduce droplet drag, in quantitative agreement with the drag correlation of Chiang and Sirignano.
2. Under laminar flow conditions, droplet drag was not affected by unsteady curvilinear motion.
3. Under laminar flow conditions, unsteady curvilinear motion was found to result in small but non-negligible droplet lift ( $C_L/C_D \approx 0.1$ ), but only at relatively high droplet Reynolds numbers ( $20 < Re < 38$ ).
4. Turbulence was found to result in an apparent increase in droplet drag, however, this can be accounted for by properly defining the mean relative velocity.
5. Turbulence was found to result in an apparent decrease in the critical Weber number for secondary droplet breakup, however, this can be accounted for by properly defining the mean relative velocity.
6. The phenomenological nature of secondary breakup was observed to be fundamentally different in turbulent and laminar flows.

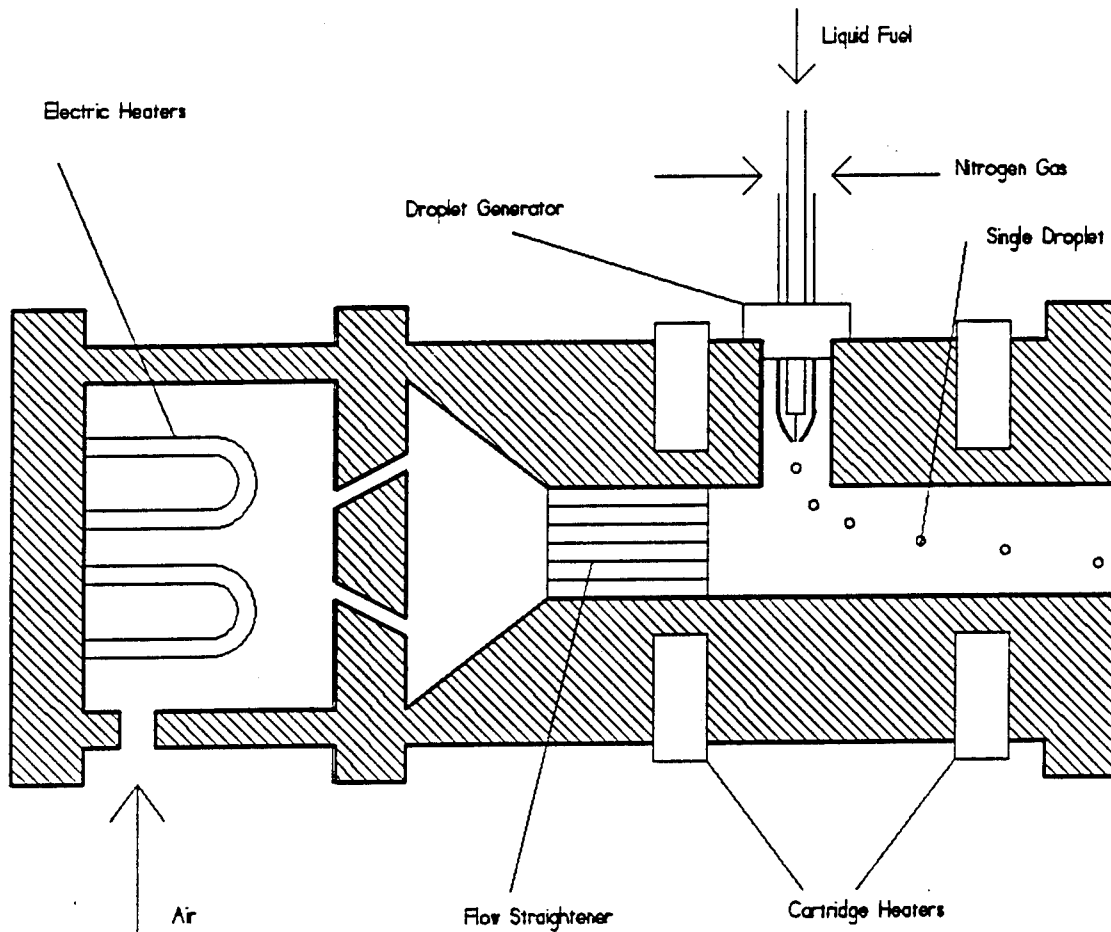
## **OBJECTIVE**

- **TO CHARACTERIZE THE BEHAVIOR OF LIQUID FUEL DROPLETS IN HIGHLY CONVECTIVE FLOWS TYPICAL OF THOSE IN DIESEL FUEL SPRAYS.**
- **TO CHARACTERIZE AND QUANTIFY DROPLET DRAG, DISPERSION, HEATING, VAPORIZATION, DISTORTION AND BREAKUP.**
- **OF PARTICULAR INTEREST ARE THE EFFECTS OF TURBULENCE AND SUPERCRITICAL CONDITIONS.**

## APPROACH

- **EXPERIMENTS ARE CONDUCTED WHERE SINGLE DROPLETS ARE TRANSVERSELY INJECTED INTO A LAMINAR OR TURBULENT, SUB- OR SUPER-CRITICAL FLOW.**
- **MEASUREMENTS ARE MADE OF THE DROPLET POSITION, TEMPERATURE, SIZE, SHAPE AND CONCENTRATION, AS A FUNCTION OF TIME, FROM WHICH DROPLET DRAG, LIFT, DISPERSION, HEATING, VAPORIZATION, DISTORTION AND BREAKUP ARE DETERMINED.**

## HIGH PRESSURE, HIGH TEMPERATURE TURBULENT FLOW SYSTEM



### OPERATING RANGE

**PRESSURE**  
**TEMPERATURE**  
**GAS VELOCITY**  
**TURBULENCE INTENSITY**  
**DROPLET SIZE**

**UP TO 70 ATM**  
**UP TO 600 K**  
**UP TO 20 M/SEC**  
**UP TO 40%**  
**50 TO 500 MICRONS**



**DROPLET PARAMETER**

**MEASUREMENT TECHNIQUE**

**SIZE, SHAPE**

**DIRECT PHOTOGRAPHY**

**POSITION→VELOCITY, ACCELERATION**

**PARTICLE TRACKING**

**TEMPERATURE**

**EXCIPLEX FLUORESCENCE**

**SIZE, SHAPE, CONCENTRATION  
(SUPERCritical)**

**2-D RAMAN IMAGING**

## STATUS

- **RAMAN IMAGING OF JET BREAKUP IN A SUPERCRITICAL ENVIRONMENT**
- **CALIBRATION OF DROPLET THERMOMETRY**
- **VISUALIZATION OF DROPLET VAPOR WAKE**

## RESULTS

- **EFFECT OF VAPORIZATION ON DROPLET DRAG (LAMINAR)**
- **EFFECT OF UNSTEADY CURVILINEAR MOTION ON DROPLET DRAG AND LIFT (LAMINAR)**
- **EFFECT OF TURBULENCE ON DROPLET DRAG**
- **EFFECT OF TURBULENCE ON SECONDARY BREAKUP**
- **EFFECT OF TURBULENCE ON DROPLET DISPERSION**

## LAMINAR EXPERIMENTS -

## THE EFFECT OF VAPORIZATION AND UNSTEADY CURVILINEAR MOTION

### EXPERIMENTAL CONDITIONS

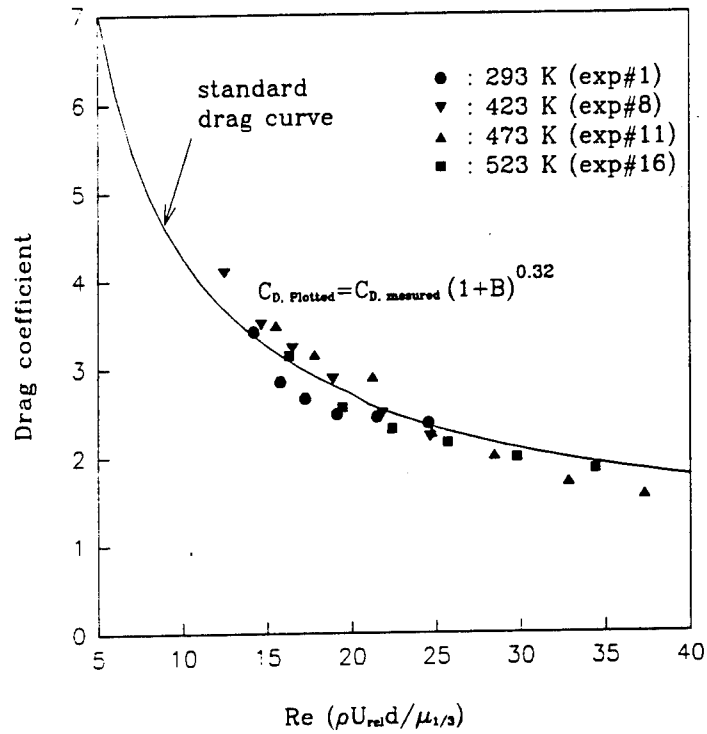
Exp.No.	D <sub>init</sub> (μm)	T <sub>air</sub> (K)	P (atm)	U <sub>gas</sub> (m/s)	Re	B <sub>steadv</sub>
1	90	293	2.7	1.25	12-25	0.2
8	90	423	4.4	1.40	10-25	0.6
11	90	473	4.4	2.80	15-38	0.9
16	103	523	5.76	2.15	13-37	1.2

### DATA ANALYSIS

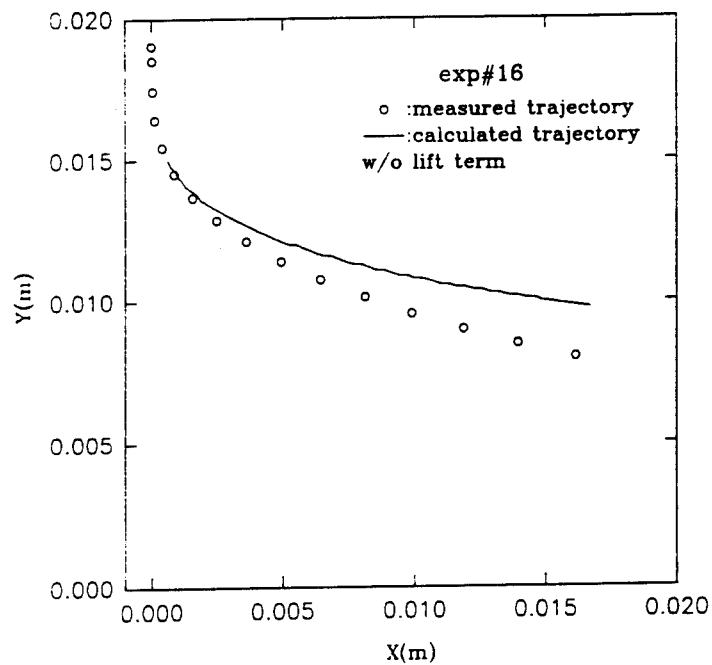
$$m \frac{dU_{x,d}}{dt} = \frac{1}{2} \rho_g |\bar{U}_g - \bar{U}_d| \frac{\pi}{4} d^2 [-C_L (U_{g,y} - U_{d,y}) + C_D (U_{g,x} - U_{d,x})]$$

$$m \frac{dU_{y,d}}{dt} = \frac{1}{2} \rho_g |\bar{U}_g - \bar{U}_d| \frac{\pi}{4} d^2 [C_L (U_{g,x} - U_{d,x}) + C_D (U_{g,y} - U_{d,y})] - mg$$

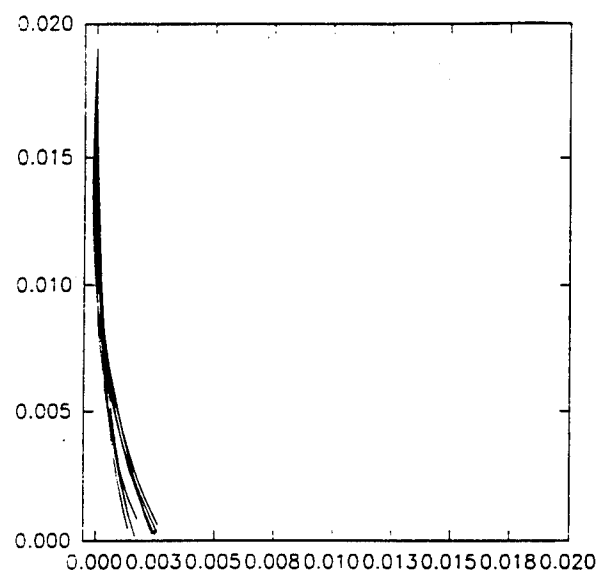
## EFFECT OF VAPORIZATION ON DROPLET DRAG



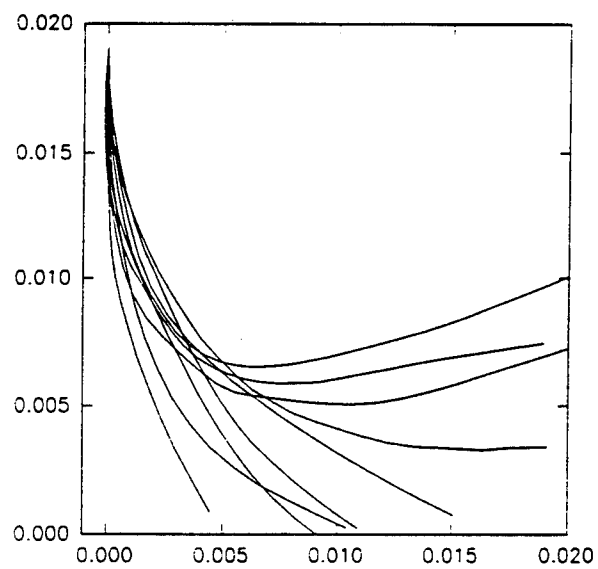
## EFFECT OF UNSTEADY CURVILINEAR MOTION ON DROPLET LIFT



## DROPLET TRAJECTORIES IN TURBULENT FLOWS

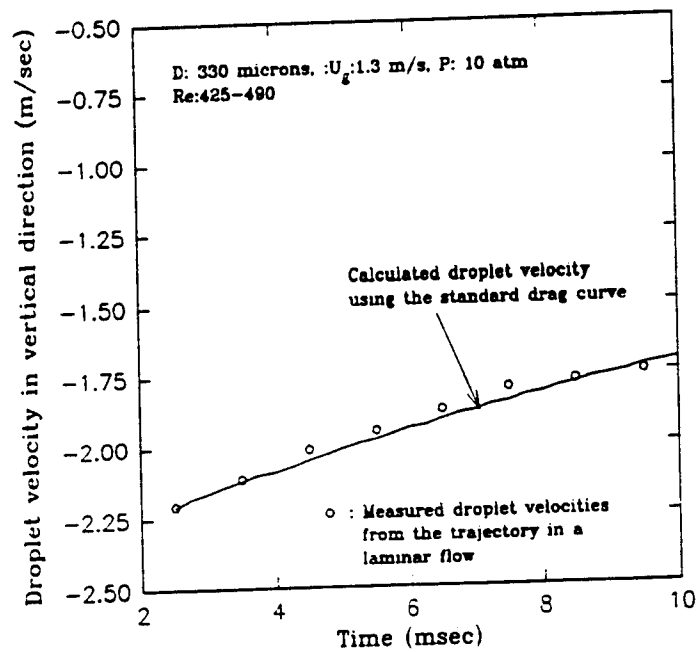


LOW DISPERSION CASE

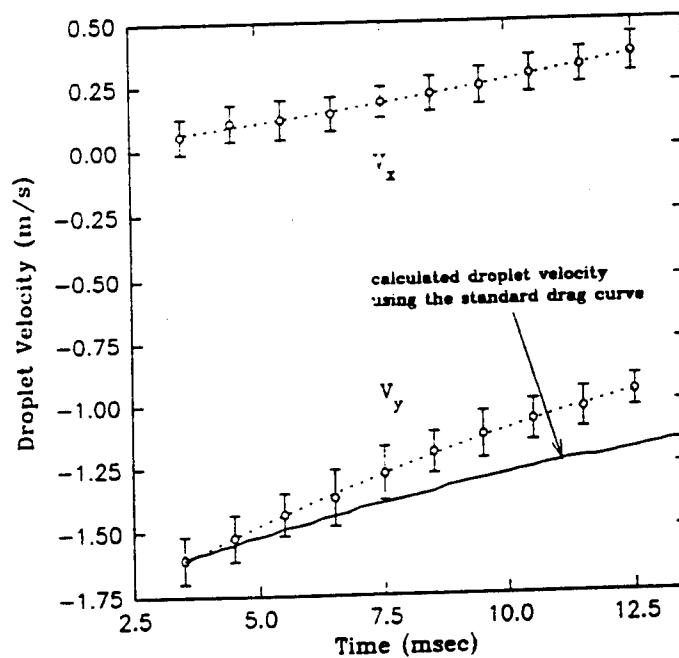


HIGH DISPERSION CASE

## THE EFFECT OF TURBULENCE ON DROPLET DRAG



## DROPLET VELOCITY IN A LAMINAR FLOW



## DROPLET VELOCITY IN A TURBULENT FLOW

## **Computations of Sprays in a Very High-Pressure, Constant Volume Chamber**

**J. Abraham  
Mechanical Engineering Department  
University of Minnesota  
Minneapolis, MN 55455**

In recent years, several Diesel engine manufacturers have initiated efforts to explore ways of achieving increased power-density in engines through the use of extremely high cylinder pressures (up to 30 MPa). The engine configurations and geometries being considered are unique and it is apparent that rapid progress can only be made if models for the in-cylinder flows, sprays and combustion are used to optimize the engine geometry. However, the accuracy of such models have not been assessed at the conditions being proposed. In this work, comparisons of computed and measured penetrations for vaporizing and non-vaporizing sprays in a fixed-volume chamber will be presented. The ratio of ambient gas density to liquid density varies in the range 0.005 - 0.25. It will be shown that adequate agreement of computed and measured penetrations may be obtained if sufficiently high numerical resolution is used. It is also shown that as the ratio of chamber density/liquid density is increased, the flammable fraction of the vapor fuel increases.

## **OBJECTIVE:**

To assess the accuracy of a 3-D model for flows, sprays and combustion in diesel engines under very high-pressure (density of ambient gas/density of liquid is relatively very high) engine operating conditions.

## **THE MODEL:**

### Numerics

KIVA (Los Alamos)

### Physics

1. Turbulence - k- $\epsilon$
2. Boundary layers - wall functions
3. The spray model - (Princeton)
  - (a) atomization
  - (b) line source
  - (c) turbulence dispersion
  - (d) drop breakup (O'Rourke & Amsden, Los Alamos)
  - (e) collisions & coalescence
4. Autoignition model
5. Combustion model

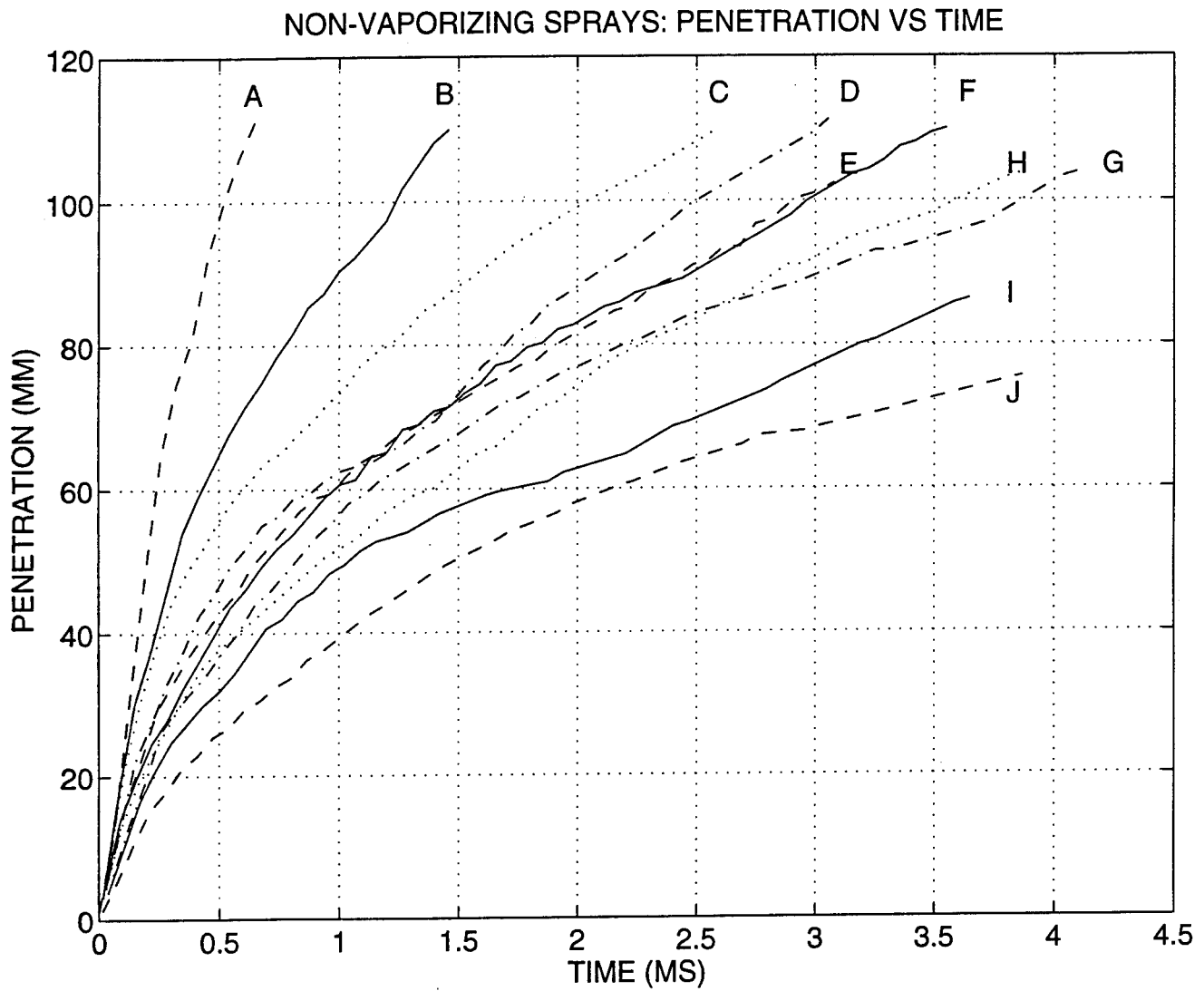


# EXPERIMENTAL DATA: (SANDIA NATIONAL LABORATORY)

Non-Vaporizing Sprays			
Case	$\rho_{\text{air}}/\rho_{\text{fuel}}$	$T_c$ (K)	$P_{\text{fuel}}$ (MPa)
A	0.005	300	142
B	0.019	300	145
C	0.033	300	142
D	0.047	300	139
E	0.061	300	142
F	0.075	300	143
G	0.089	300	143
H	0.103	300	139
I	0.148	300	142
J	0.243	300	138

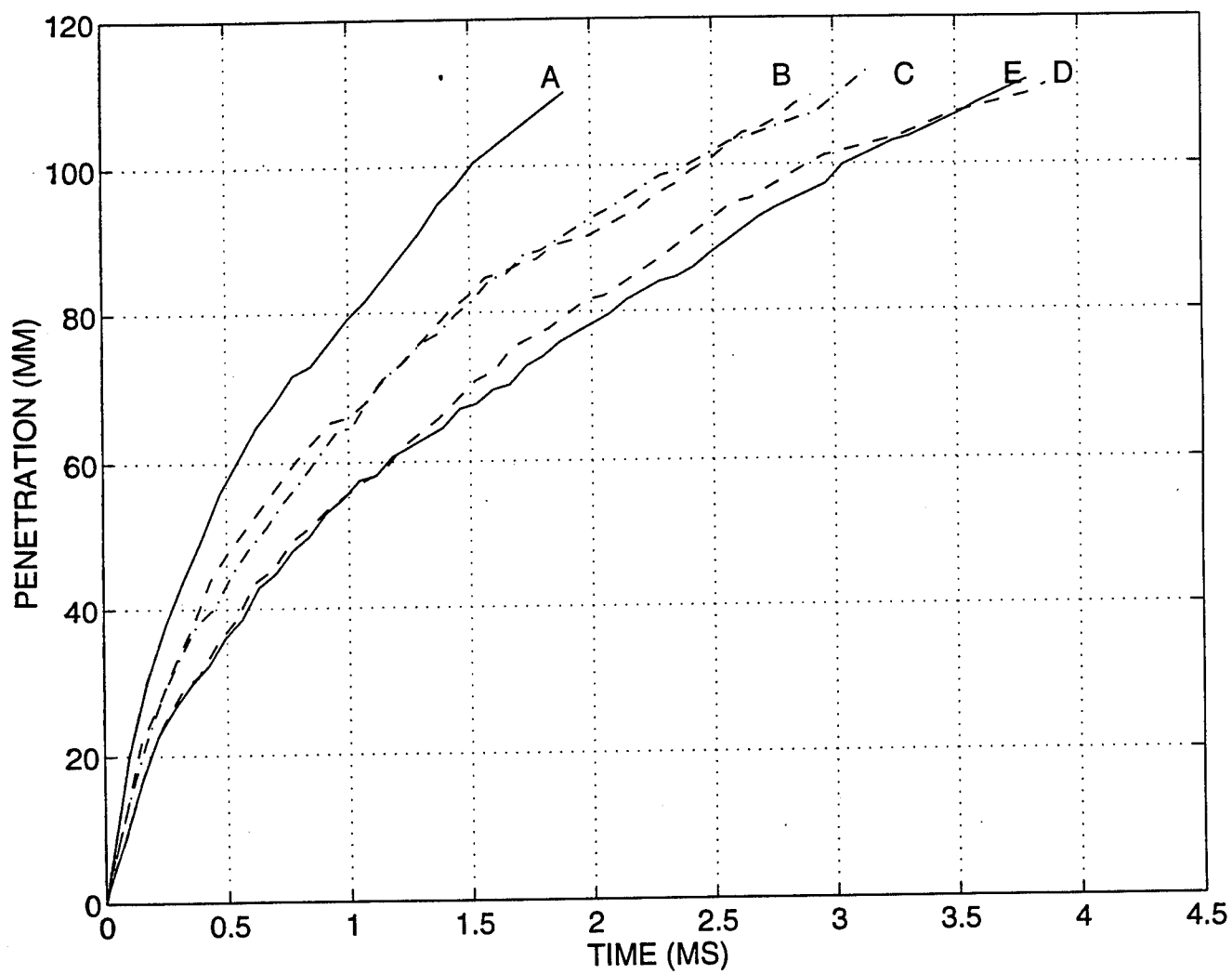
Vaporizing Sprays			
Case	$\rho_{\text{air}}/\rho_{\text{fuel}}$	$T_c$ (K)	$P_{\text{fuel}}$ (MPa)
A	0.019	900	138
B	0.032	899	131
C	0.046	908	140
D	0.061	896	142
E	0.075	895	145

## Measurements



## Measurements

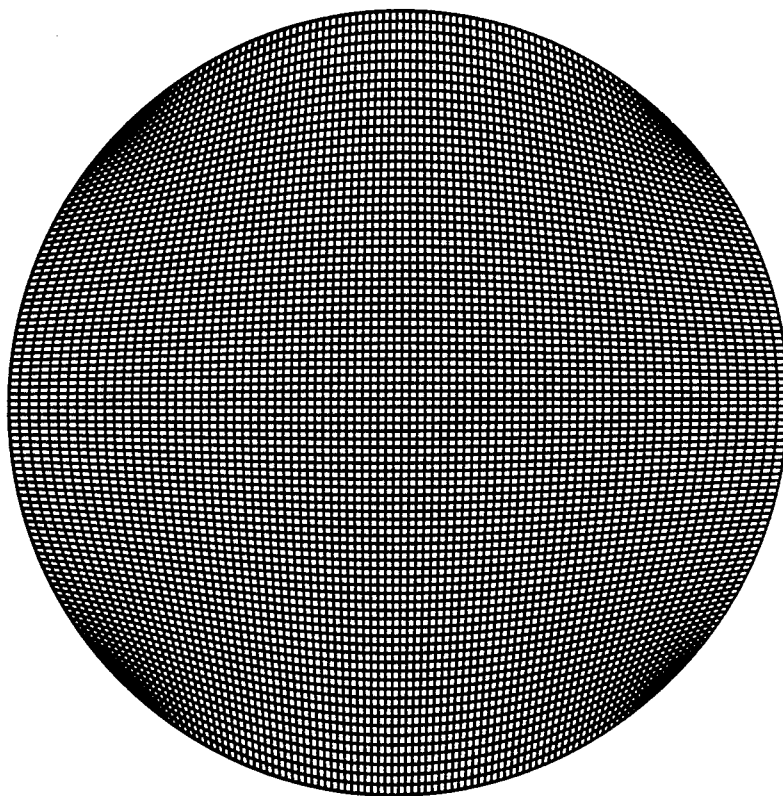
PENETRATION VS TIME: VAPORIZING SPRAYS



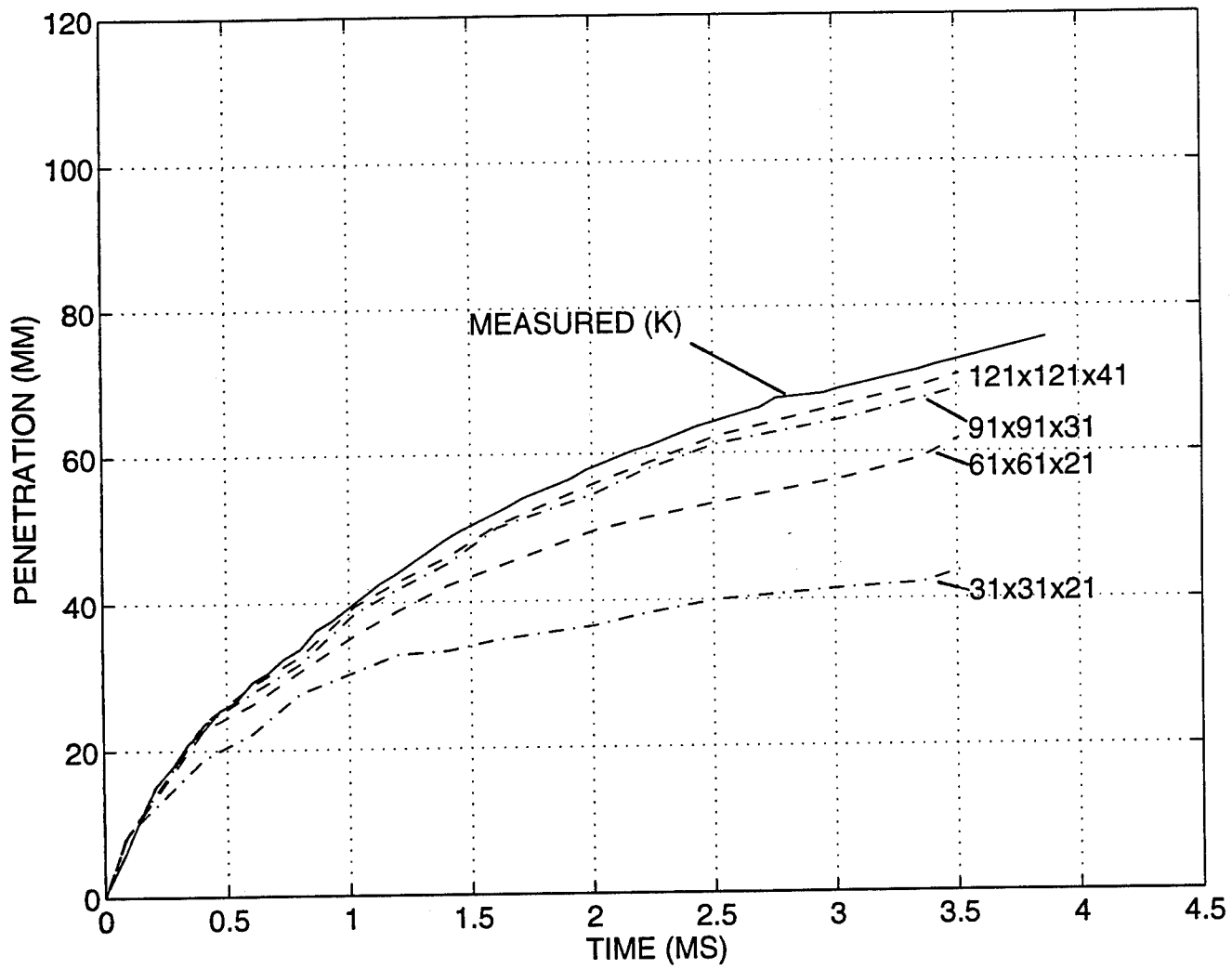
## Computational Grid

$NX*NY*NZ = 91*91*31$

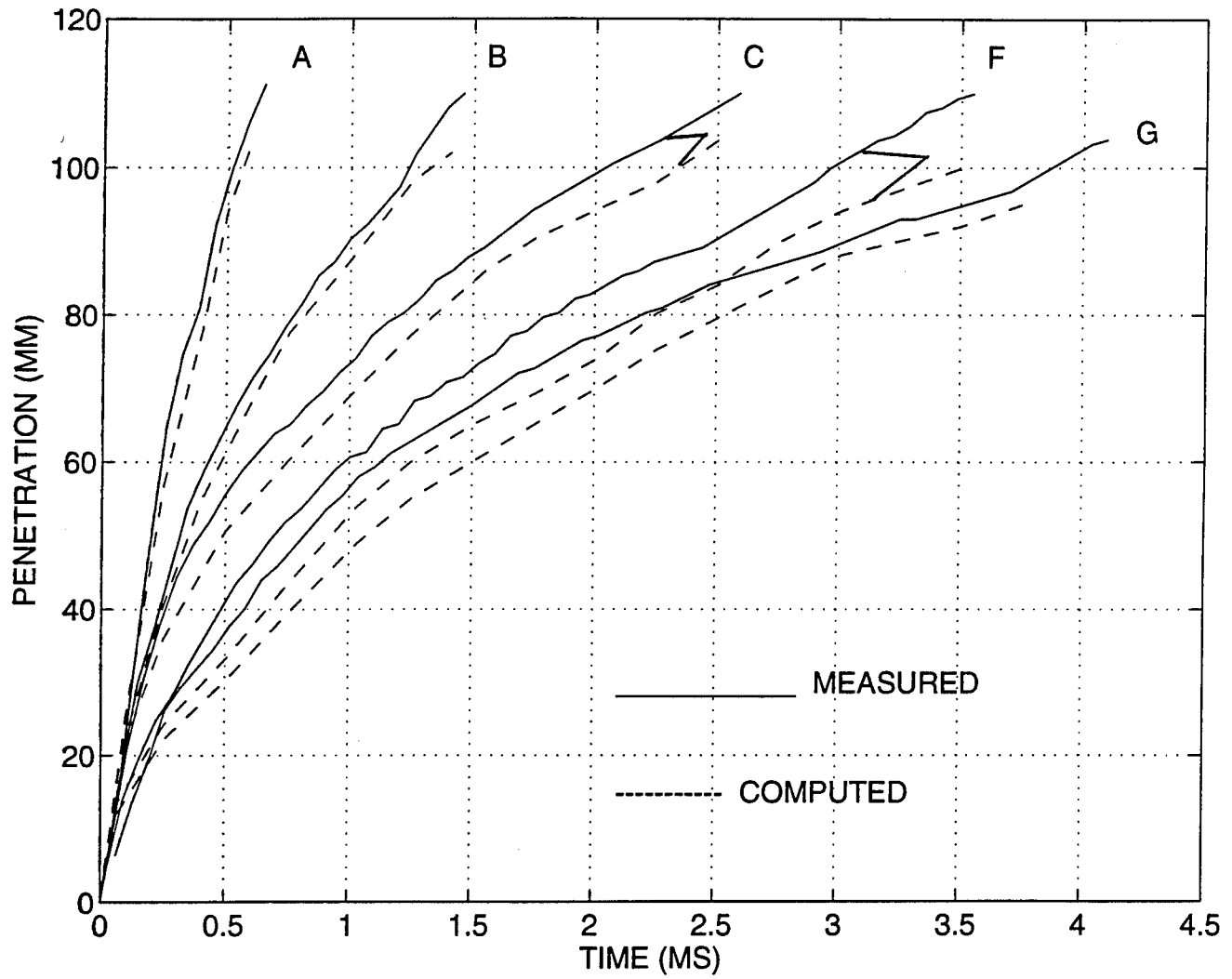
plane  $k = 17$



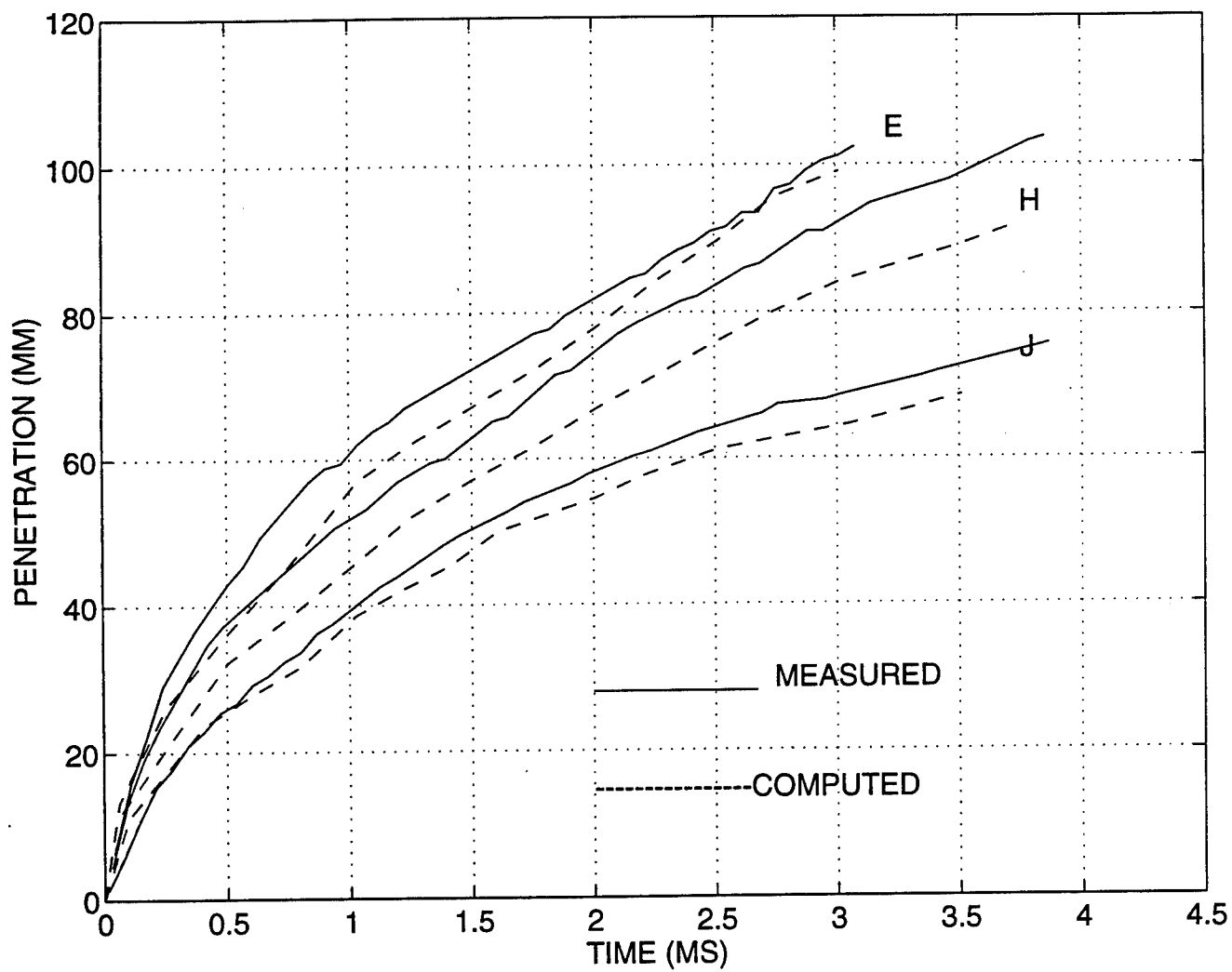
# EFFECT OF GRID RESOLUTION



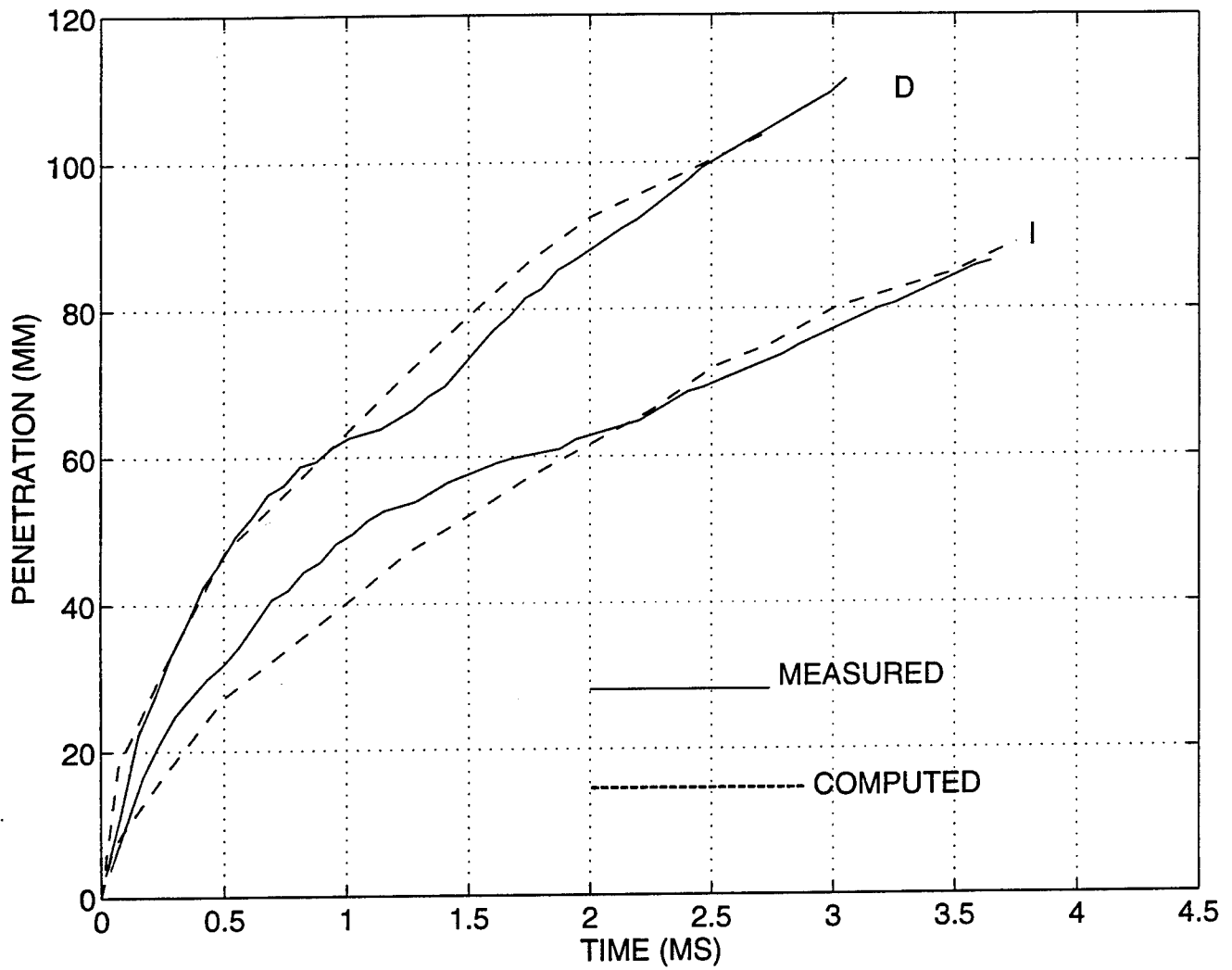
# NON-VAPORIZING SPRAYS: PENETRATION VS TIME



# NON-VAPORIZING SPRAYS: PENETRATION VS TIME

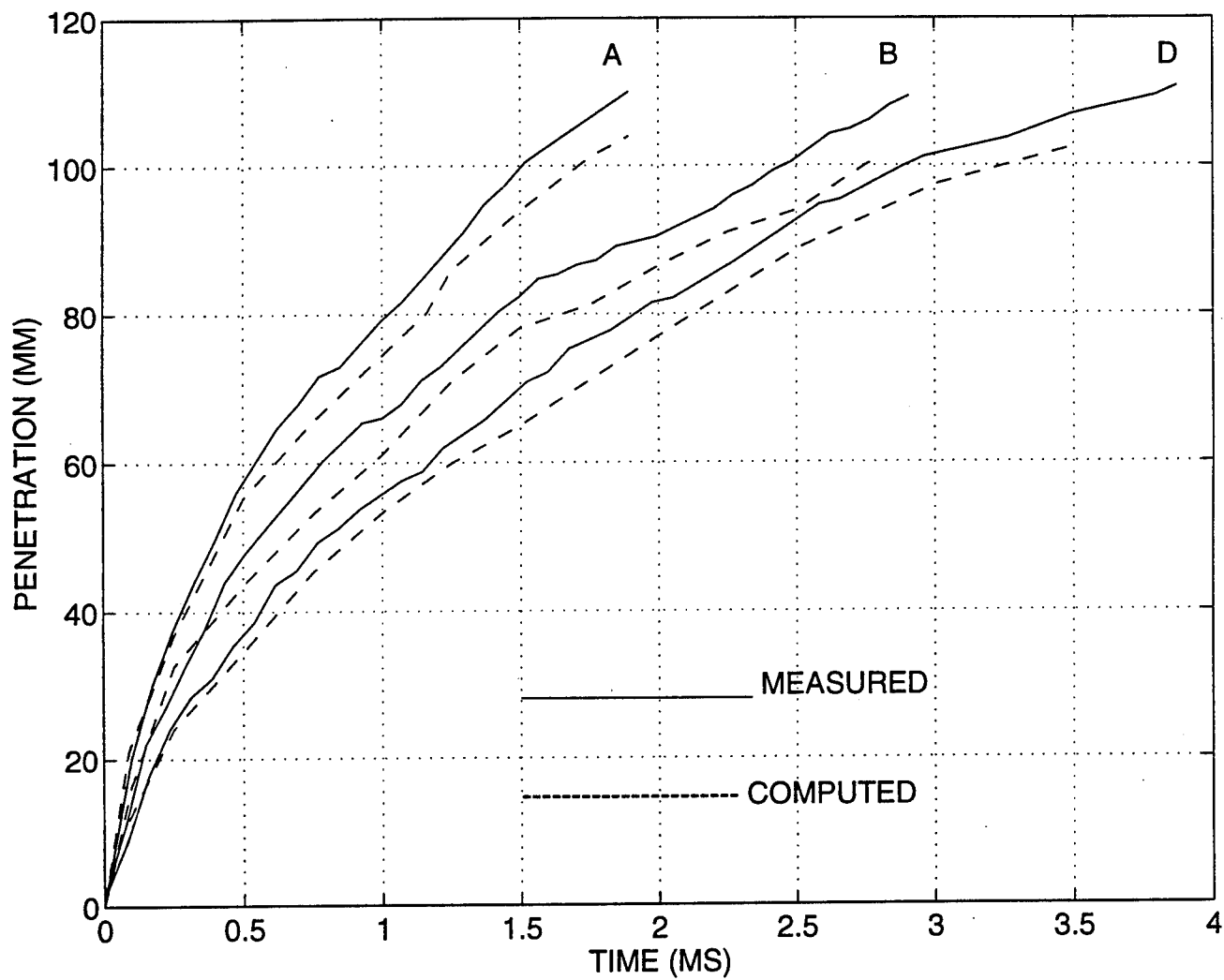


# NON-VAPORIZING SPRAYS: PENETRATION VS TIME

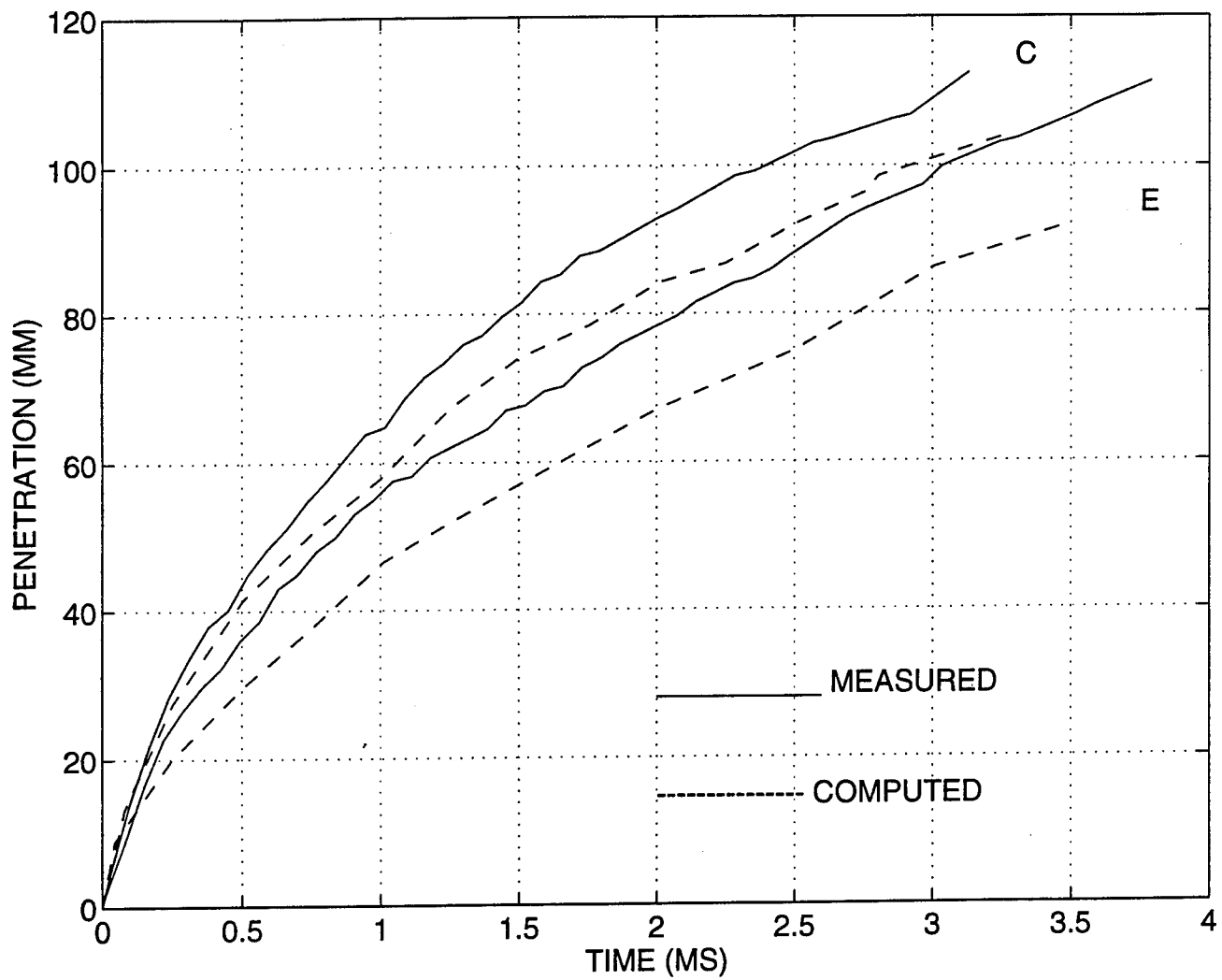




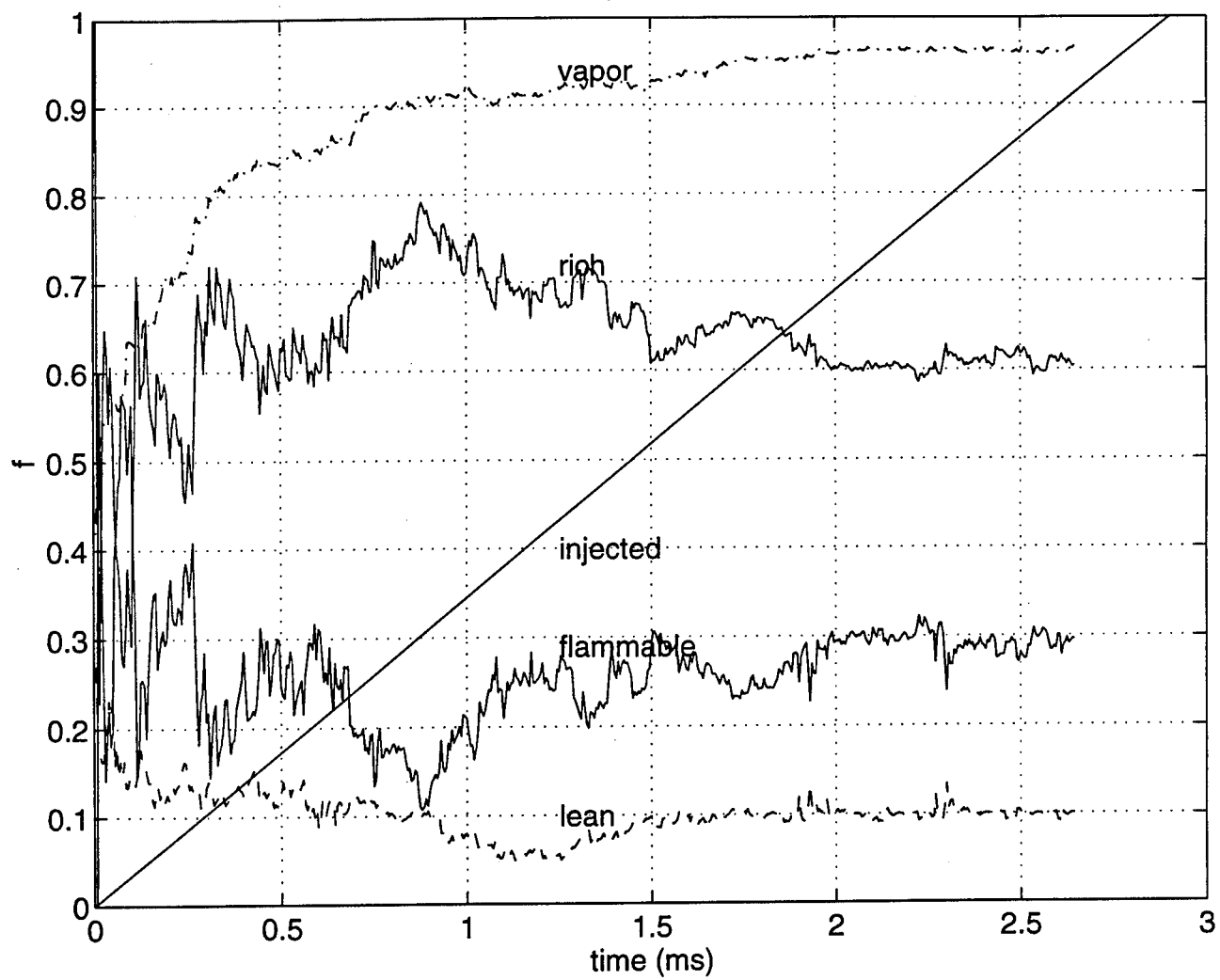
# VAPORIZING SPRAYS: PENETRATION VS TIME



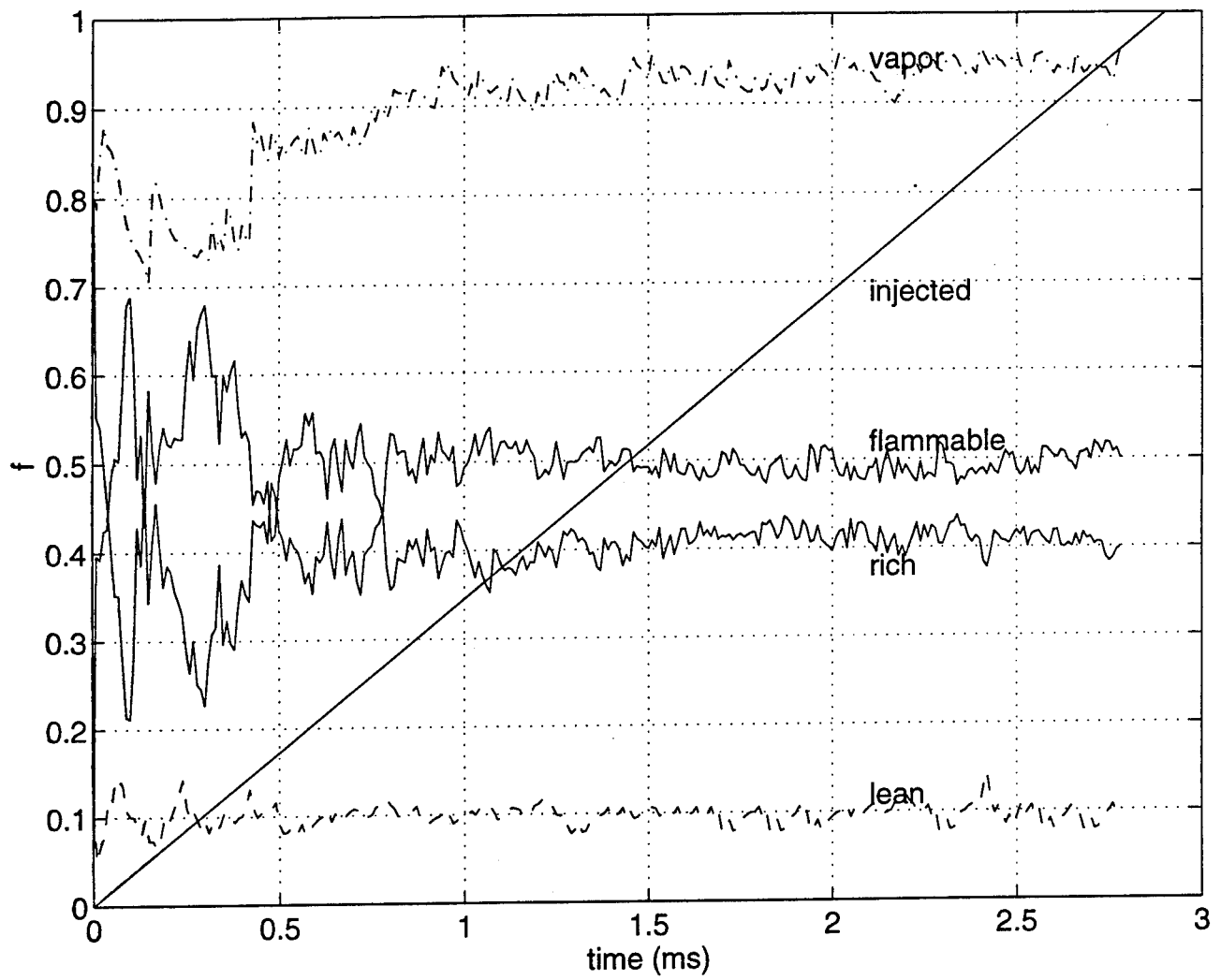
VAPORIZING SPRAYS: PENETRATION VS TIME



f vs time plot for CASE A



f vs time plot for CASE D



## **CONCLUSIONS:**

1. Comparisons of computed and measured penetration rates of sprays injected into high-pressure ambient gas show adequate agreement provided sufficient numerical resolution is used.
2. As chamber pressure density is increased, the flammable fraction of the vapor fuel increases and the rich fraction decreases. If this persists during combustion, the combustion will be faster as the chamber density is increased.

## **Spray Research at the Engine Research Center**

P. V. Farrell  
with

G. L. Borman, D. E. Foster, J. K. Martin, R. D. Reitz, C. J. Rutland and lots of graduate students

Engine Research Center  
University of Wisconsin-Madison  
Madison, WI 53706

A large number of two-phase flow and related spray projects are underway at the University of Wisconsin-Madison Engine Research Center. For diesel engines, the spray projects are aimed at issues which include: increasing power density (power/package size); examining cold start spray effects; studies of fuel effects on spray behavior; sprays in some special application engines; and studies of spray effects on emissions. For spark ignited engines spray work emphasizes spray effects on mixing.

At the Engine Research Center (ERC) a variety of methods are employed to investigate the issues outlined. These methods include an extensive range of experiments, from engine experiments to specialized off-engine investigations of specific phenomena, and a large effort in applying and improving computer models of spray events. The diesel injectors studied include moderate pressure injectors (500 bar), high pressure experimental injectors (1000 - 2000 bar), and high pressure commercial or production injectors (1500 bar).

The experimental tools currently applied to spray studies include conventional measurements (mass flow rate, needle lift, pressures,...), optical methods (photography, PDPA, diffraction based sizing, LIF,...), and some developing optical methods (PIV and DSIV).

The modeling tools center around KIVA as the core of the model, with emphasis for the spray on the submodels most connected to the spray predictions. The submodel developments generally parallel experimental efforts in the same area. Modelers can directly tell experimenters what kinds of data they need, and experimenters can discuss with modelers what can be delivered. A very important part of the ERC activities involves this interaction between model development and validation and experimental focus, design, and operation. We think it is vital that students and faculty recognize the value, requirements, and limitations of each of these approaches in order to progress on all fronts.

This presentation will attempt to outline the range of projects currently underway at the ERC and to indicate the general objectives of the projects and what we hope will be the impact of these projects. Many of the projects described are funded by ARO, however for completeness, some non-ARO funded projects will also be mentioned. In addition to the project survey, two areas of projects will be examined in somewhat more detail in order to present a little more detail for these topics and some results.

## **Spray Research at the Engine Research Center**

**P. V. Farrell  
Engine Research Center  
University of Wisconsin-Madison**

**with  
G. L Borman, D. E. Foster, J. K.  
Martin, R. D. Reitz, C. J. Rutland  
and lots of graduate students**

## **Introduction to Sprays Focus Areas at ERC**

- **Diesel Engine Issues Include:**
  - power density (power/package size)
  - cold start
  - fuel effects
  - special application engines
  - emissions (soot vs. NOx trade-off)
- **Spark-Ignited Engine Issues Include:**
  - mixing and improved lean-burn limit
  - reduced HC

## Methods for Spray Studies at ERC

- Experiments
  - Environments
    - » Engines
      - » High temperature and pressure vessels
      - » Low temperature, high pressure vessels
    - » atmospheric conditions
  - Injectors
    - » moderate pressure diesel
    - » high pressure experimental diesel(main, pilot, split)
    - » high pressure commercial diesel(main, pilot, split)
    - » moderate pressure SI
  - Measurement tools
    - » mundane--but effective (rate of injection, emissions, ...)
    - » optical methods (photography, PDPA, diffraction-based sizing, ...)
    - » more exotic optical methods (PLIF, PIV and DSIV, two-color, Exciplex,...)

## Methods for Spray Studies at ERC

- Modeling
  - KIVA based models
  - Spray model development and improvement
    - » different injectors
    - » different operating conditions (pressure, timing, duration, ...)
    - » different geometries (spray angles, impingement, size of combustion chamber,...)
    - » different vaporization characteristics (gas temperature, fuel,...)
  - Effects of spray models on combustion
    - » combustion predictions
    - » emission predictions



## Methods for Spray Studies at ERC

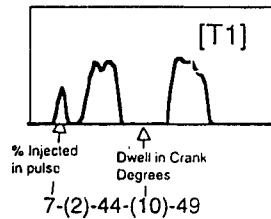
- **Integration of Experiments and Modeling**
  - Essential for designing useful experiments and reliable validated models
  - Many of the experiments are motivated by modeling issues
  - Modeling applied to experimental conditions

## Project Areas

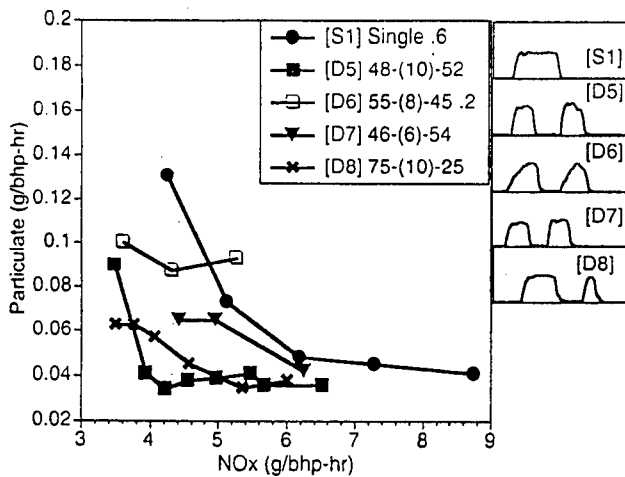
- **High pressure injection studies: (power density, cold start, fuel effects, emissions)**
  - high pressure spray distribution and geometric variations --ARO/Caterpillar (A. Knox-Kelec, D. Schmidt, J. Su)
  - delivery rate variations--Caterpillar (T. Tow, A. Pierpont, J. Su)
  - fuel-air ratio distributions (K. Carabell)
  - fuel vapor visualization (G. Bower)
  - multicomponent droplet vaporization modeling (N. Ayoub)
- **Wall Impingement Studies (cold start, emissions)**
  - spray-wall hydrodynamics and heat transfer (J. Naber, M. Al-Roub)
  - direct impingement sprays (J. Naber, R. Booth, J. Eckhouse)

# Fuel System

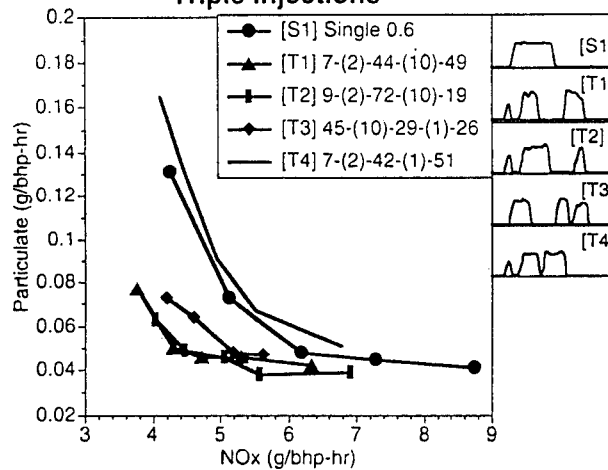
Injector Type	Common Rail - Electronically Controlled independent control of the duration and timing of up to 4 injections per cycle
Injection Pressure (variable)	90 MPa (13,230 psia)
Number of nozzle orifices	6
Nozzle diameter	0.26 mm
Spray Angle (included)	125°
Nozzle Cd	0.78
Fuel Type	Amoco 1994 Low Sulfur Emissions Certification Fuel



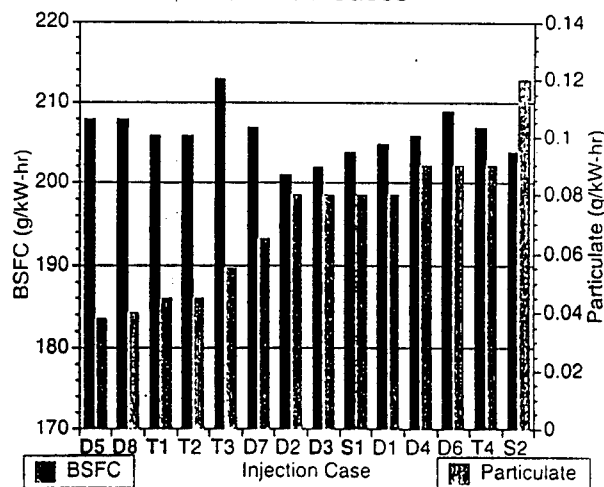
Particulate vs. NOx 75% Load

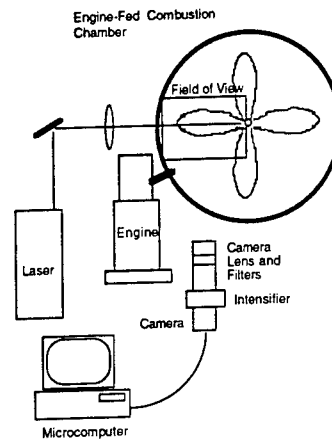
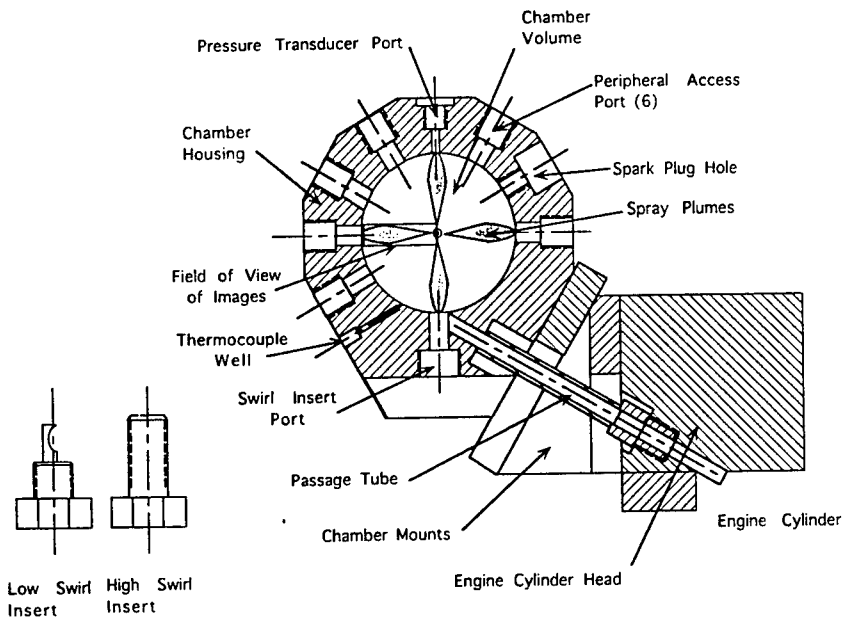


Particulate vs. NOx 75% Load  
Triple Injections



BSFC and Particulate at NOx = 5 g/bhp-hr  
75% Load Cases





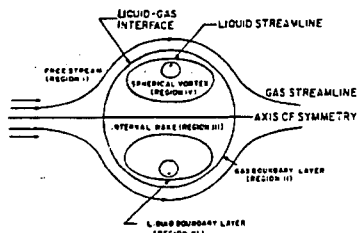
## Multicomponent Model

$$f_i^L = f_i^V$$

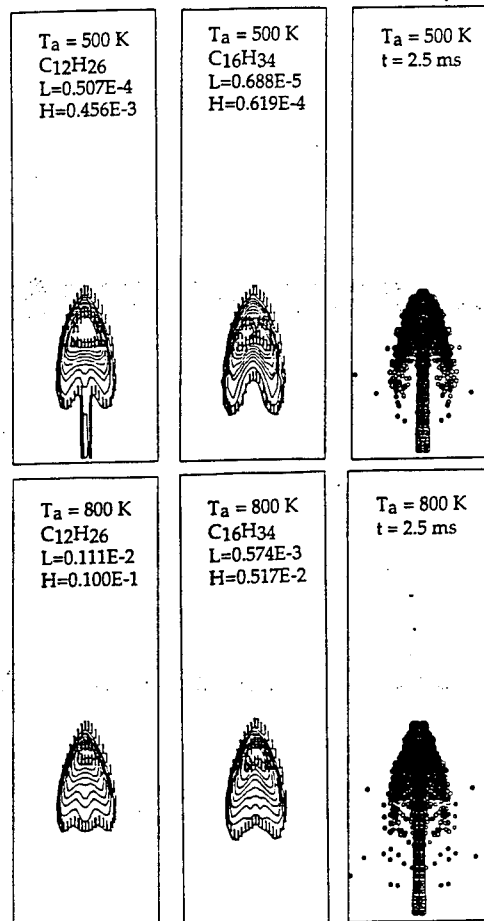
$$\Gamma^2 \frac{\partial T}{\partial \tau} = \frac{\partial^2 T}{\partial \omega^2} + \left( \frac{2}{\omega} + \omega \Gamma \frac{d\Gamma}{d\tau} \right) \frac{\partial T}{\partial \omega}$$

$$Le \Gamma^2 \frac{\partial x_i}{\partial \tau} = \frac{\partial^2 x_i}{\partial \omega^2} + \left( \frac{2}{\omega} + Le \omega \Gamma \frac{d\Gamma}{d\tau} \right) \frac{\partial x_i}{\partial \omega}$$

$$\tau = \frac{\alpha t}{r_{i0}^2} \quad \omega = \frac{r}{r_i} \quad \Gamma = \frac{r}{r_{i0}}$$



[Model based on Jin & Borman (SAE 850264)]

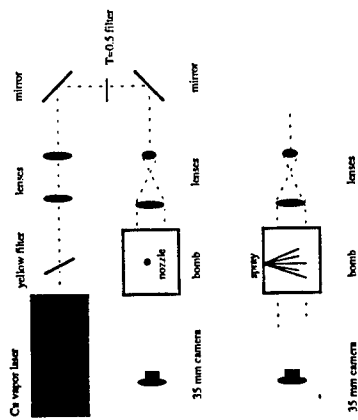


## Project Areas

- **Alternative Injection Strategies**  
(power density, special application engines, fuel effects)
  - air Injection for Increased atomization--S. C. Johnson (H. Snyder)
- **Measurement Development**  
(emissions, fuel effects)
  - Full field droplet sizing and velocity measurements--AASERT/NSF (M. Coll)
  - 3-D PIV and DSIV methods (K. Sholes)
- **Spark-Ignited (mixing, HC production)**
  - direct Injection for stratified charge HC control--Ford (S. Parrish and S. Majors)
  - DI 2-Stroke engines--WSEC

## Extended Review of Projects

- **High pressure injection studies:**  
(power density, cold start, fuel effects, emissions)
  - high pressure spray distribution and geometric variations --ARO/Caterpillar (A. Knox-Kelecy, D. Schmidt, J. Su)



## AERATED ATOMIZATION

H. Snyder  
R. Reitz

### OBJECTIVE:

Liquid Atomization with  $<1\%$  air to liquid mass ratio  
(compared to  $>300\%$  for conventional air-assist atomizers)

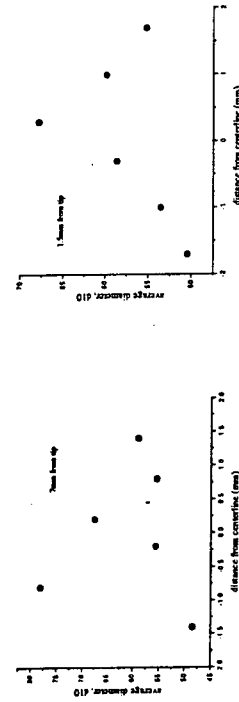
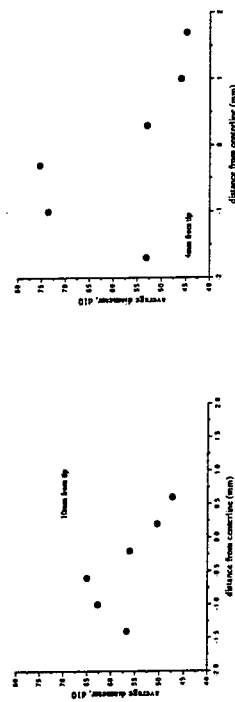
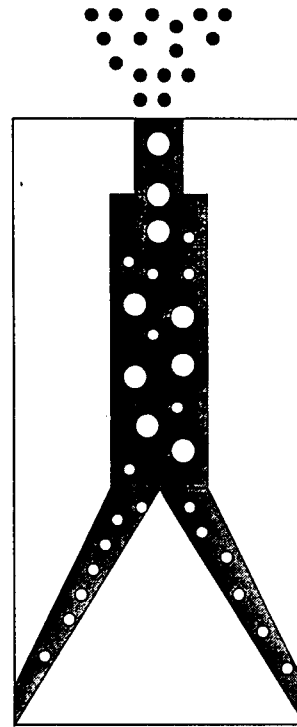
### KEY:

Internal 2-phase flow which effectively couples energy from the  
expanding gas to the liquid break-up process

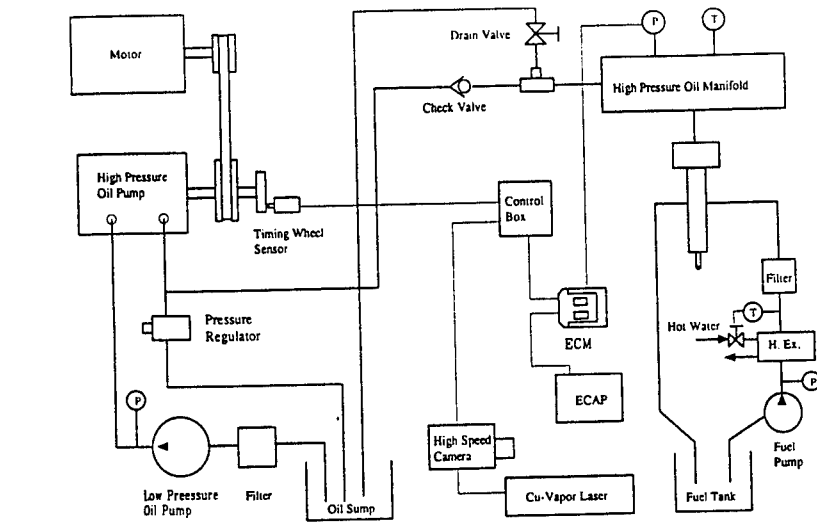
STATUS: 2/94

Initial testing of 1 g/s research atomizer with flexible geometry and  
optical access to the internal two phase flow region

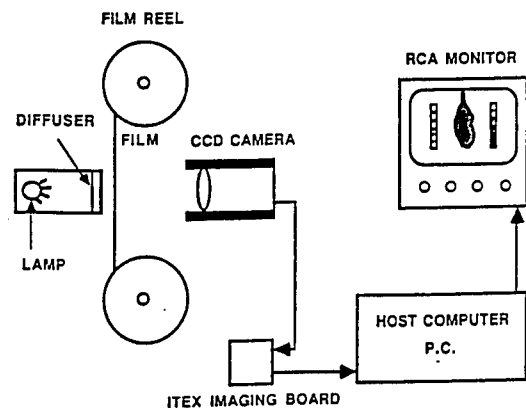
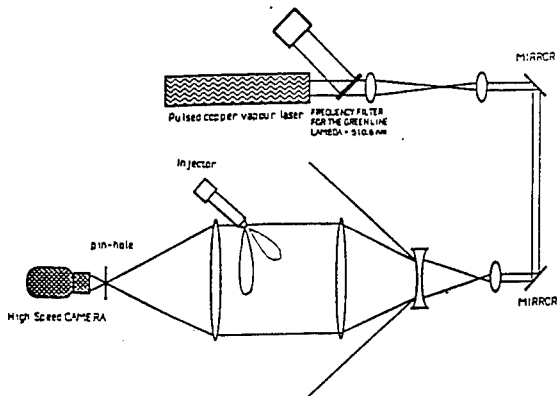
### RESEARCH AERATED ATOMIZER



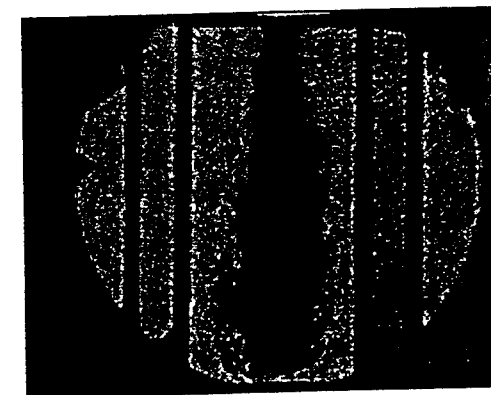
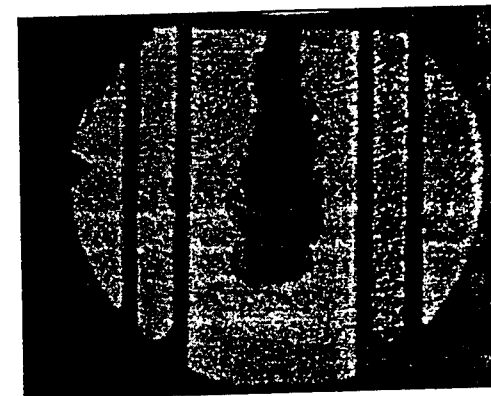
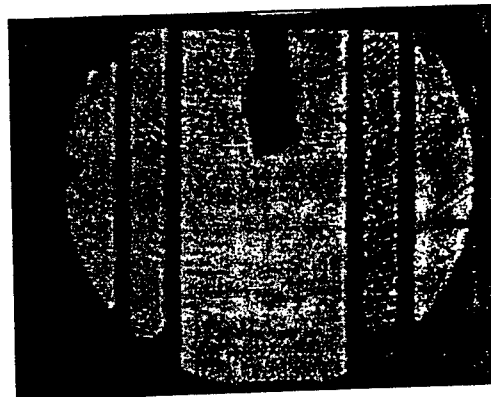
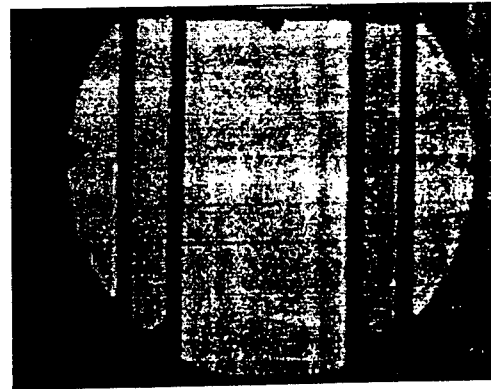
Schematic Diagram of Spray Visualization System



BEAM CUP FOR THE YELLOW LINE (WAVELENGTH = 578 nm)



Schematic diagram of the digital imaging system.



## Extended Review of Projects

- Wall Impingement Studies (cold start, emissions)
  - spray-wall hydrodynamics and heat transfer (J. Naber, M. Al-Roub)
  - direct impingement sprays (J. Naber, R. Booth, J. Eckhouse)

## Summary

- The major themes of spray work at UW-Madison ERC are a focus on realistic sprays in realistic environments and the parallel development and integration of spray modeling and experiments.
- The results of ERC spray work will be:
  - Accurate, validated spray models for use in KIVA
  - Experiments revealing fundamental physics of spray behaviour for engine conditions.

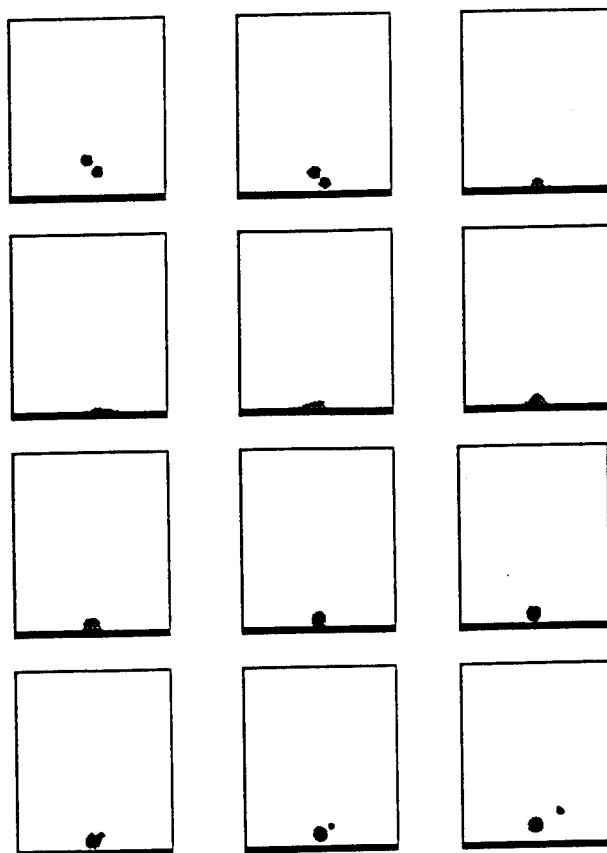
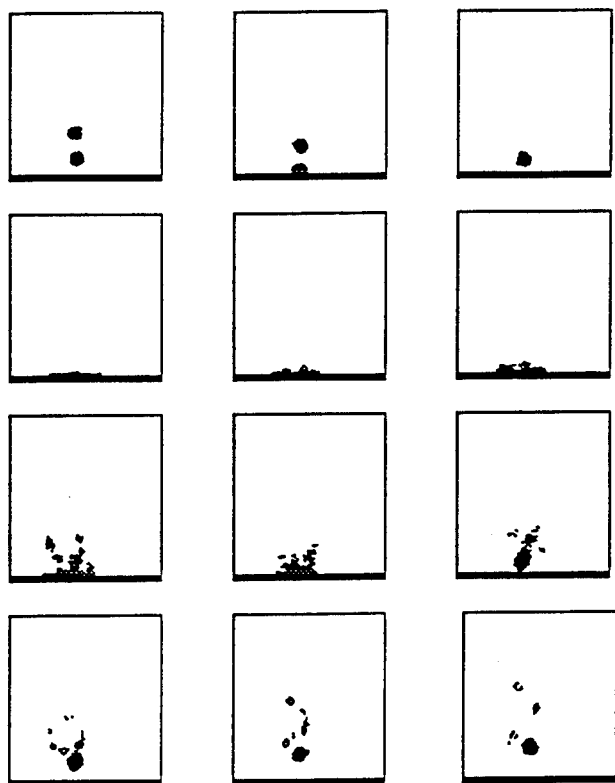
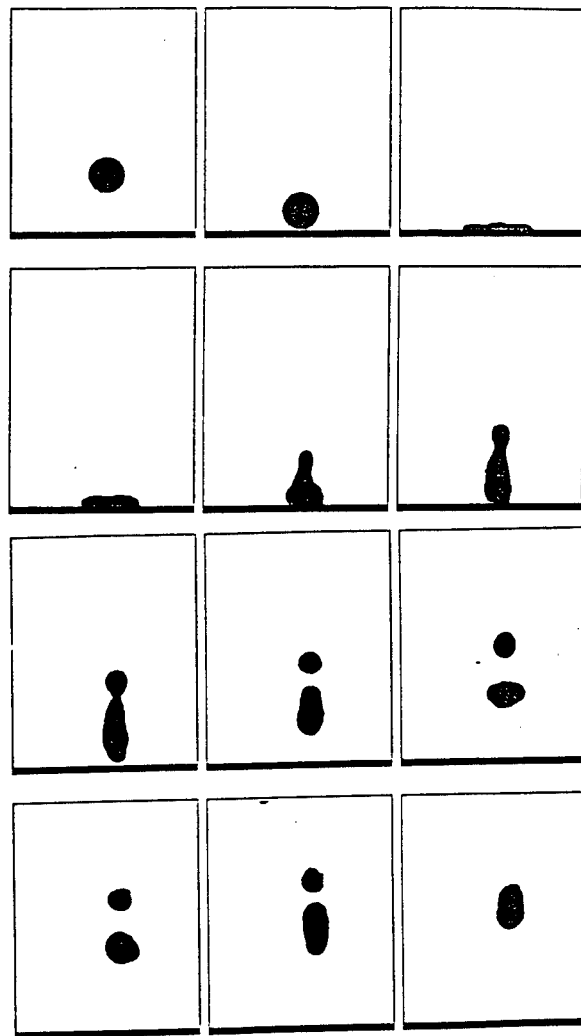
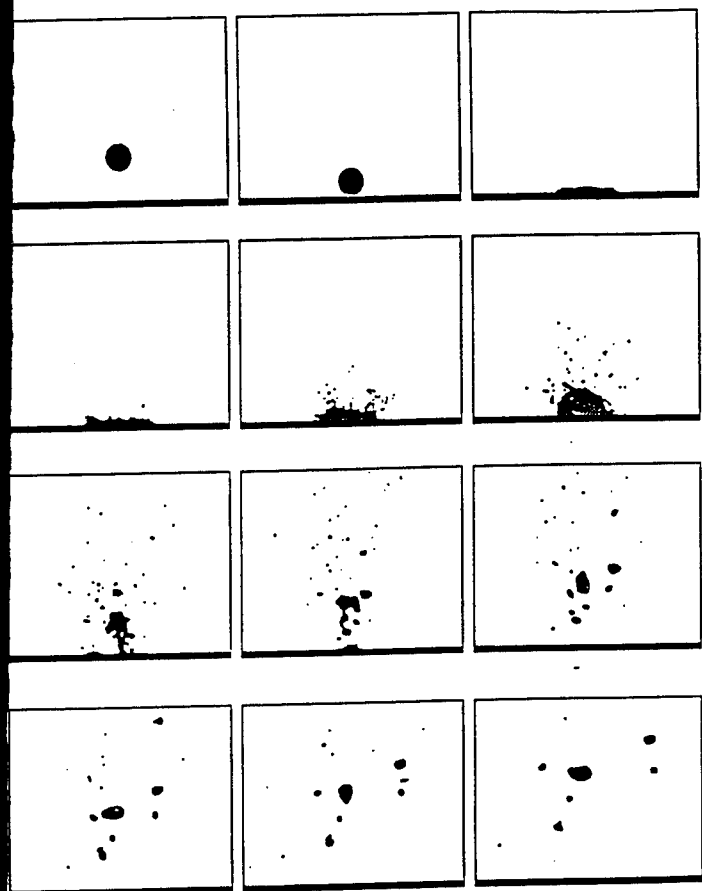


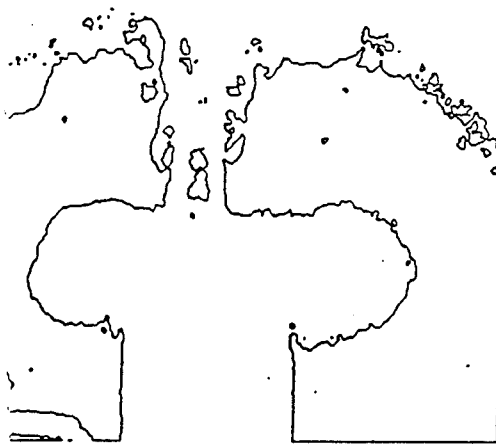


Table 4.1. Injector Calibration Parameters

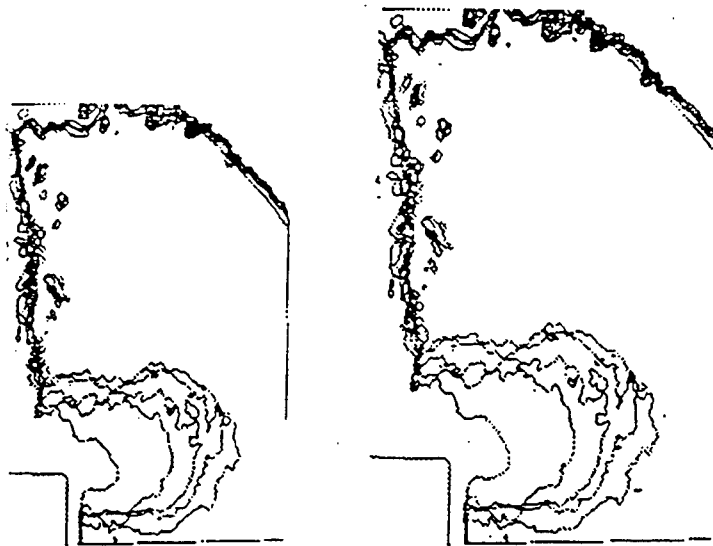
Parameter	Lombardini specifications	Large nozzle D-2 fuel	Large Nozzle Jet-A fuel	Small Nozzle D-2 Fuel
Injected mass (mg)	≈20	19.7	19.7	7.7
Nozzle Open. Press. (Mpa)	19-21	19.0	19.0	19.0
Mean Injection Press. (Mpa)		25.1	25.4	25.1
Peak Injection Press. (Mpa)		33.8	33.8	40.4
Injection Duration (ms)		1.7	1.7	1.8
Mean Inj. Velocity (m/s)		186.3	192.6	198.7

Table 4.3. System Specifications for the Laser Interrupt Test and Variables Studied with Ranges.

Injection System Specification:	Lucas CAV injector with Bosch injection pump.
Pump Speed	1500 RPM
Radial Penetration Distances $R_r$ (mm)	10, 15, 20, 30
Nozzle Diameter, $d$ (mm)	0.180 (+), 0.306 (-)
Impingement Distance, $L_i$ (mm)	6, (-) 38 (+)
Target Diameter, $D_t$ (mm)	14.7 (-), 18.3 (+)
Target Temperature, $T$ (°C)	150 (-), 315 (+)
Ambient Density, $\rho_a$ (kg/m <sup>3</sup> )	14.34 (-), 22.07 (+)
Ambient Pressure, $P_a$ (Mpa)	1.23 / 1.93 N <sub>2</sub> (-), 1.51 / 2.31 80% N <sub>2</sub> (+)
Target Materials Conductivity (W/m <sup>2</sup> K @ 400K)	16.6 (-), 197 (+)
Fuel Type	Amoco Low Sulfur D-2, Commercial Jet-A

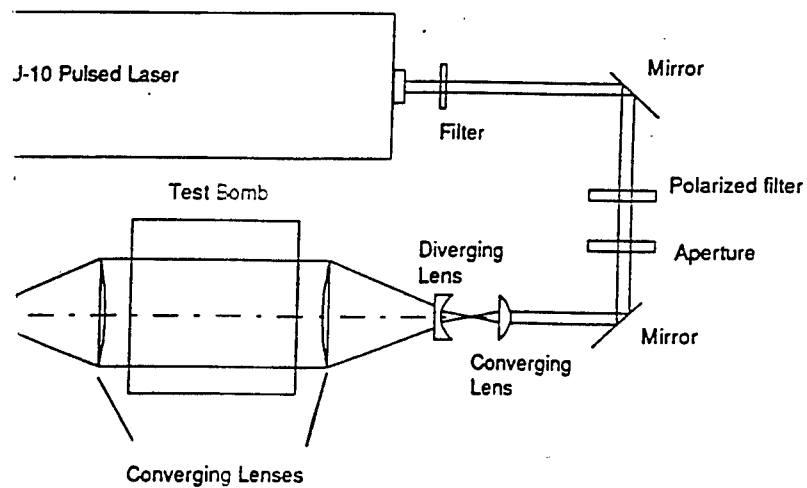


(a)



(c)

pray image film 4 frame 6. (b) and (c) Super-imposed edged spray  
spray and cropped spray development diagrams.



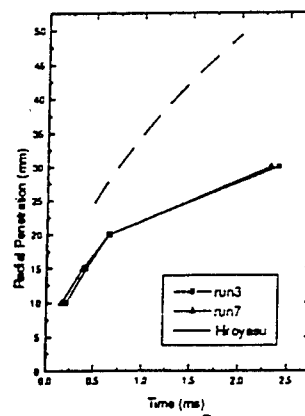
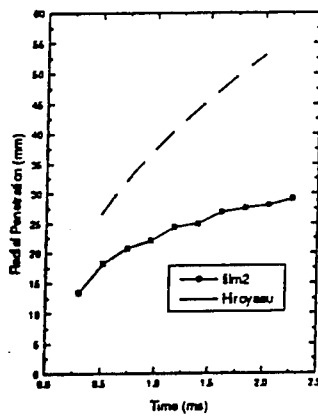
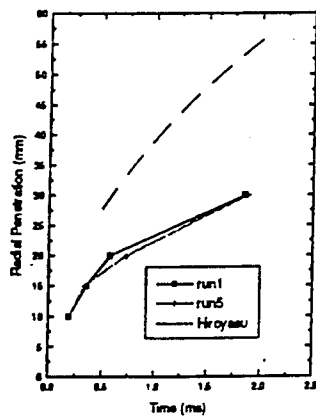
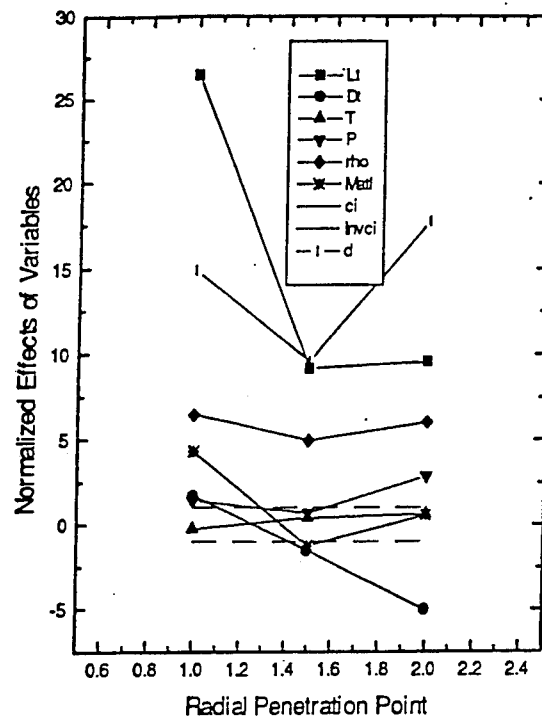
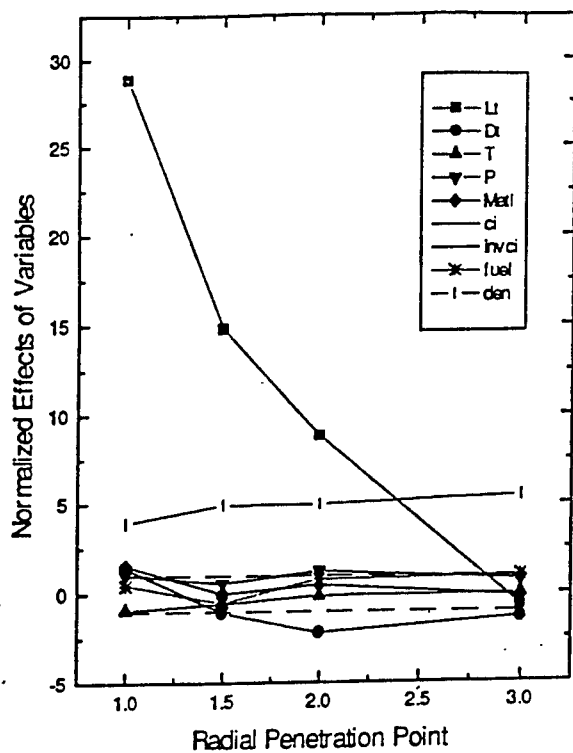


Figure 6.40. (a-c) Comparisons of spray penetration of a normal cone spray and a spray impinged against a raised target

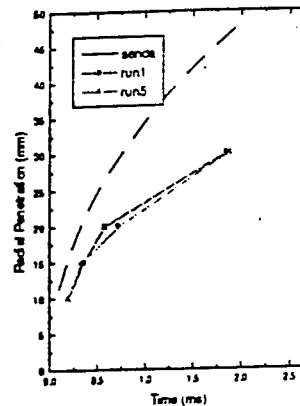
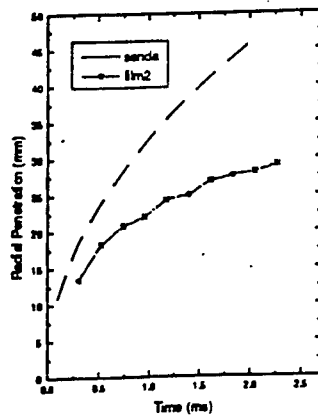
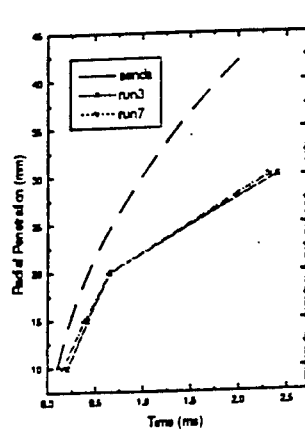
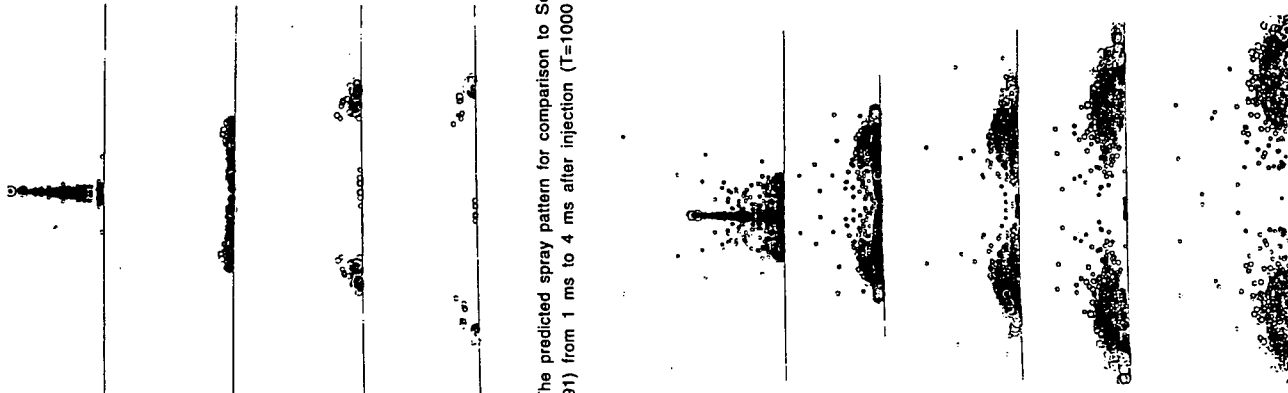
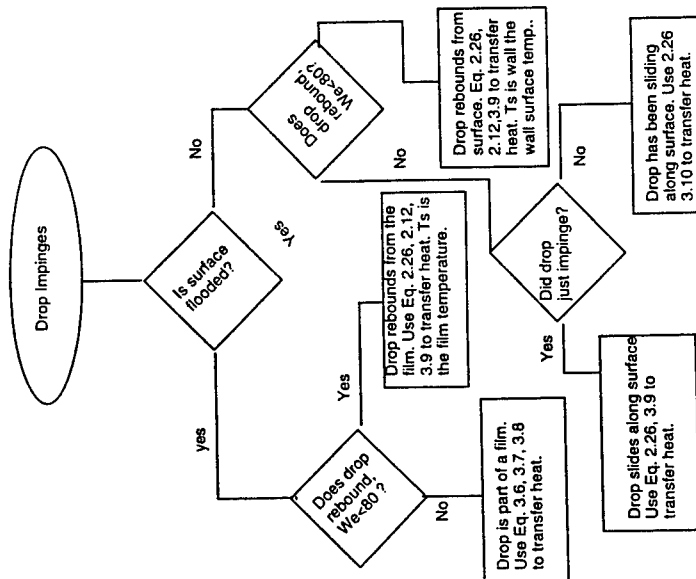


Figure 6.38.(a-c). Comparisons of penetration of a spray impinged upon a flat wall and a spray impinged against a raised target



The predicted spray pattern for comparison to Senda et al. (1991) from 1 ms to 4 ms after injection ( $T=1000$  K).

The predicted spray pattern for comparison to Senda et al. (1991) at 1 ms, 2 ms, 3 ms, 6 ms, and 9 ms after injection ( $T = 500$  K)



The model flowchart.

## **Advanced Diesel Injection Strategies**

F.V. Bracco  
Princeton University

Direct injection of natural gas in Diesel engines by several engine companies has yielded the surprising result that combustion time is much longer with natural gas than with Diesel fuel (the ignition delay time is not much longer). Natural gas also yields unexpectedly high soot emission. These trends are surprising because it has always been assumed that the faster the vaporization the faster the combustion and the limit of very fast vaporization is the gas jet.

Results are presented of 3-D computations of direct injection of gaseous methane and of liquid tetradecane through a multi-hole injector into a Diesel engine. The study focusses on the distribution of fuel/air ratio within the resulting gas and spray jets under typical Diesel conditions prior to ignition. It is shown that for a significant time after start of injection, the fraction of the vapor fuel which is in richer-than-flammable mixtures is greater in gas jets than in sprays. For methane injection, it is also shown that changing some of the flow conditions in the engine or going to a poppet-type injector, does not result in improved mixing. It is concluded that in general a spray mixes faster than a gas jet in direct-injection Diesel engines and possible explanations for this unexpected result are provided. An experiment is also in progress to check the proposed explanations.

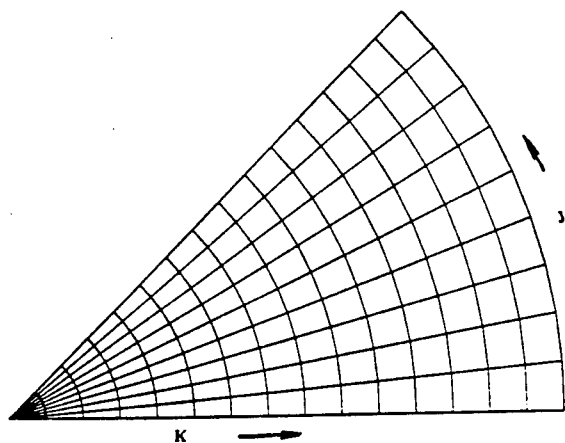


Fig.1: Computational grid layout in a 45° sector.

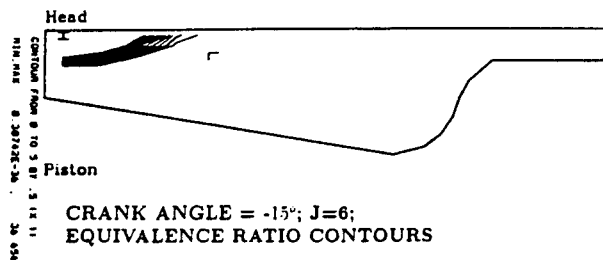
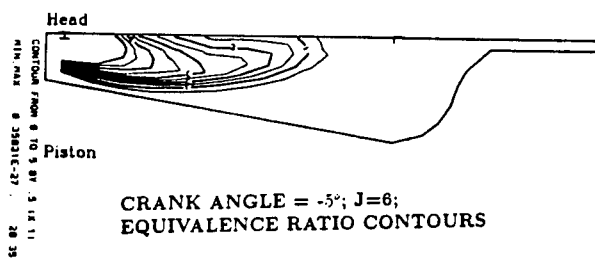
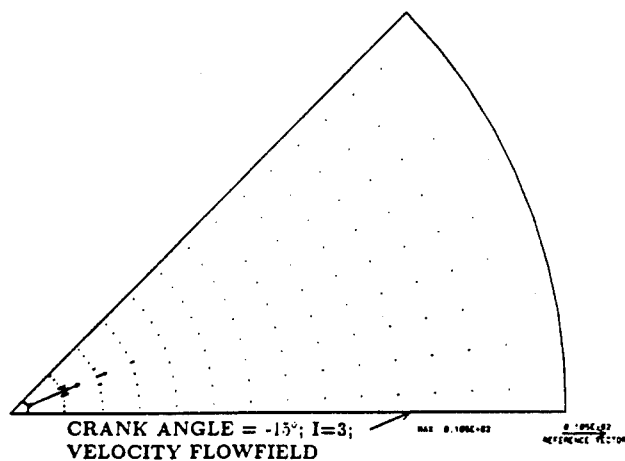
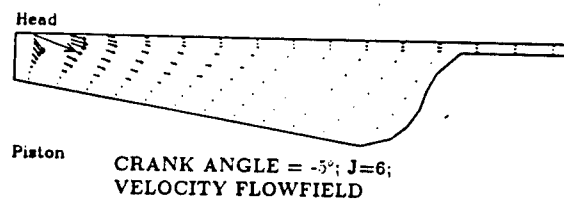
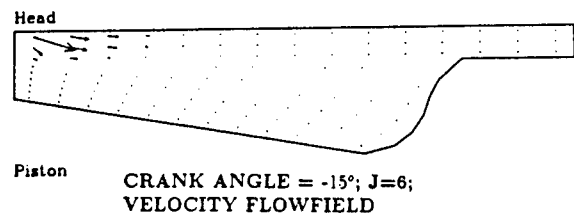


Fig.2: Velocity flowfield and equivalence ratio contour plots for the baseline case.

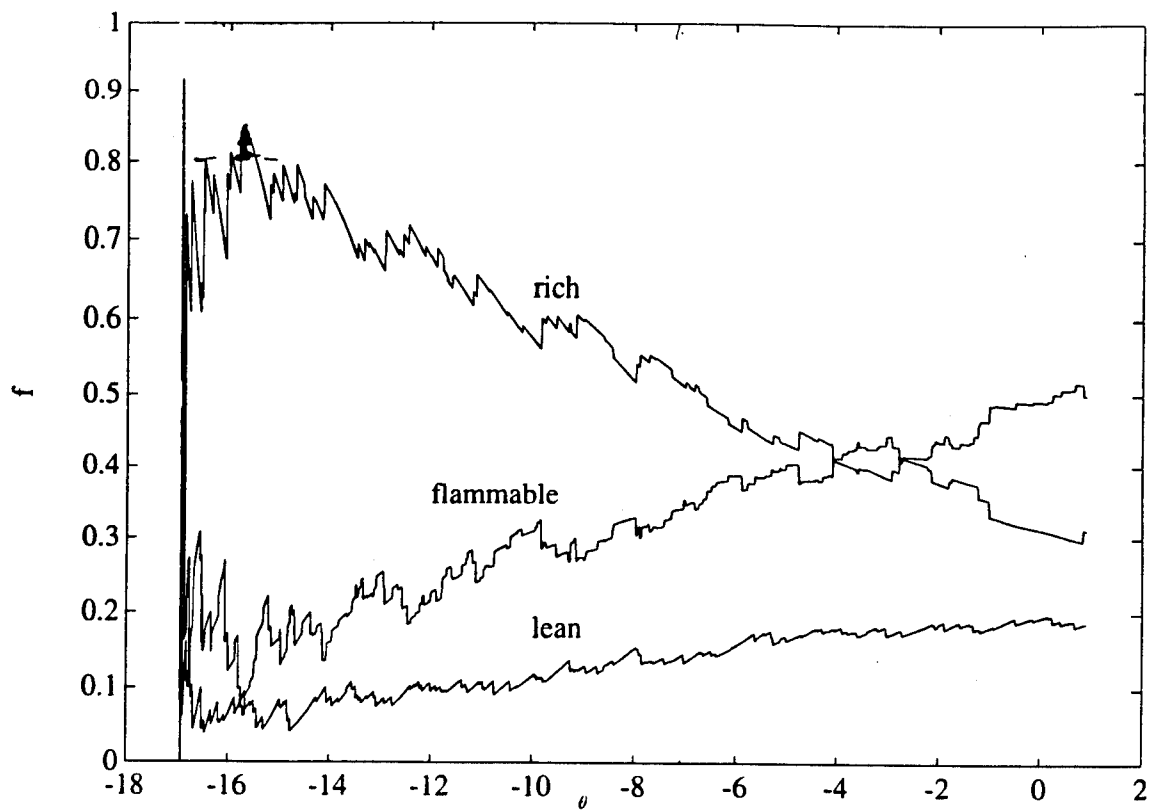


Fig.3: "f -  $\theta$ " plot for the baseline case.

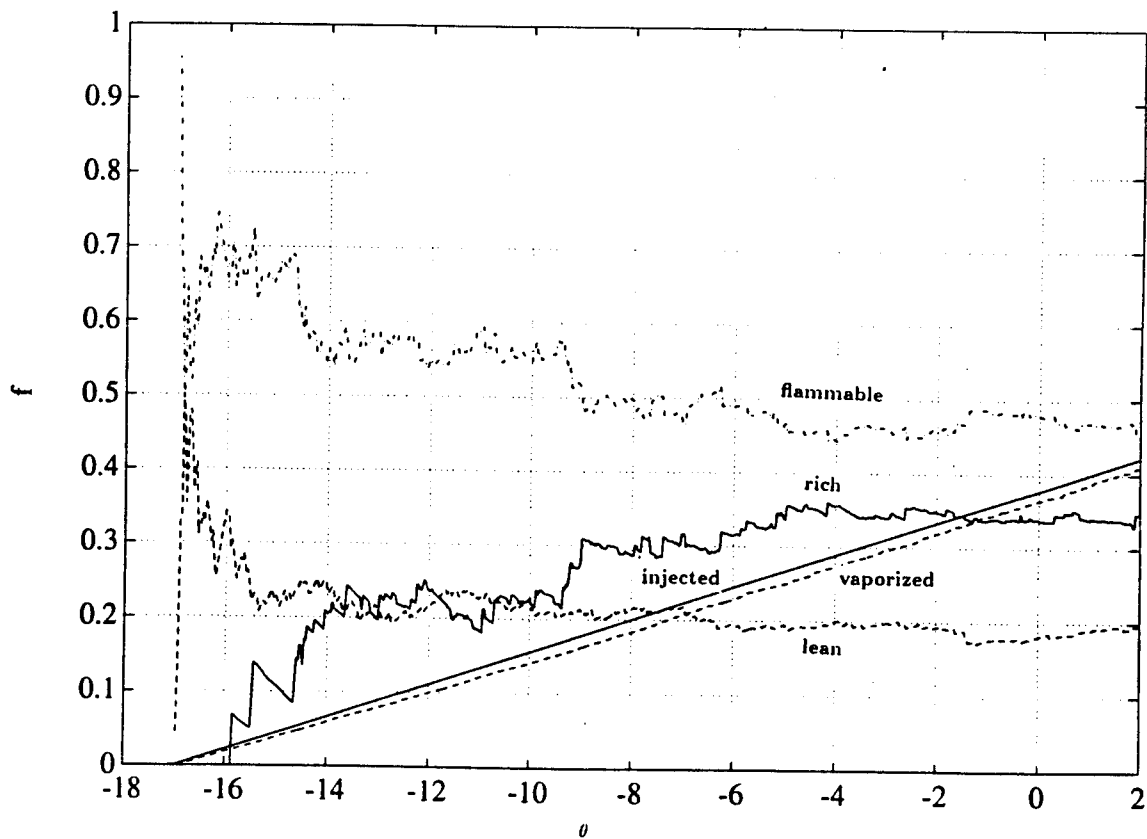


Fig.4: "f -  $\theta$ " plot for the spray.

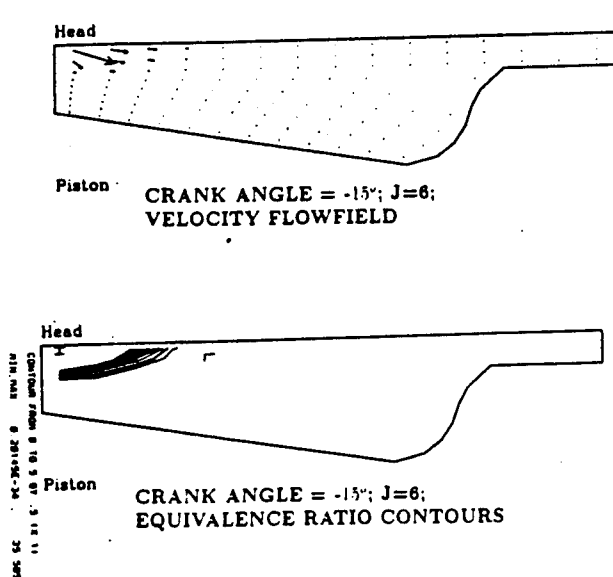


Fig.5: Velocity flowfield and equivalence ratio contour plots for the case with swirl.

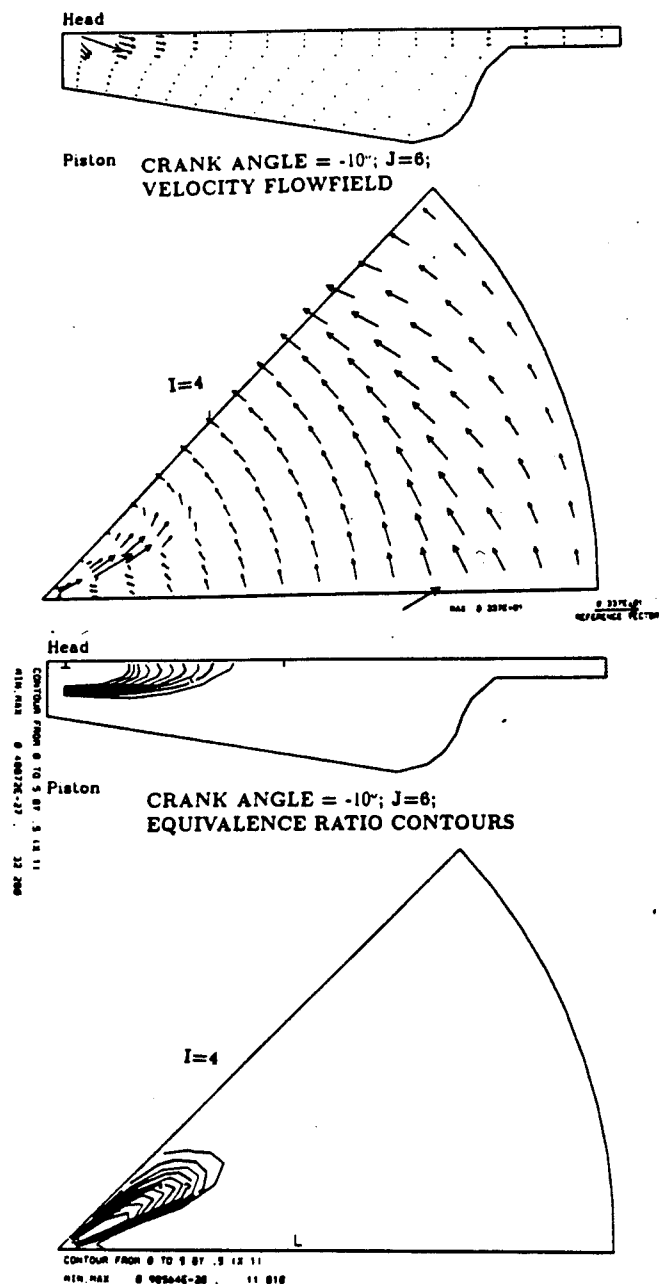
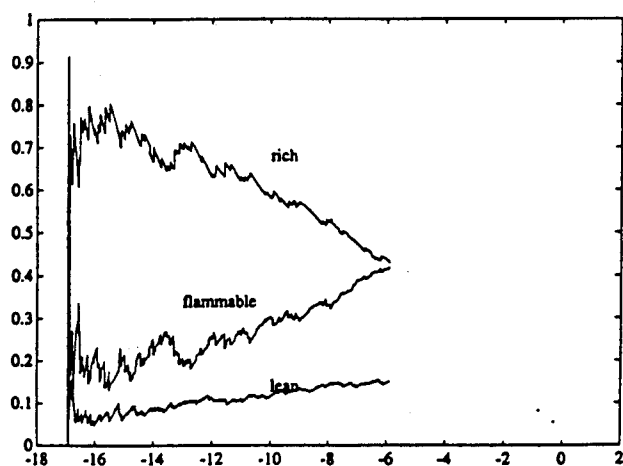
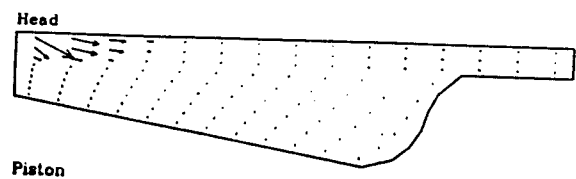


Fig.6: "f -  $\theta$ " plot for the case with swirl.

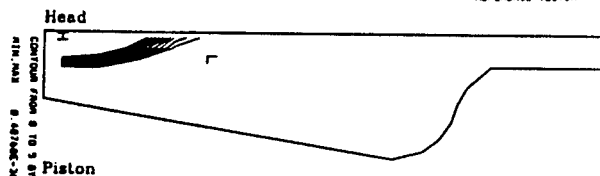




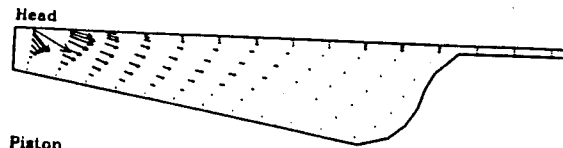


CRANK ANGLE =  $-15^\circ$ ;  $J=6$ ;  
VELOCITY FLOWFIELD

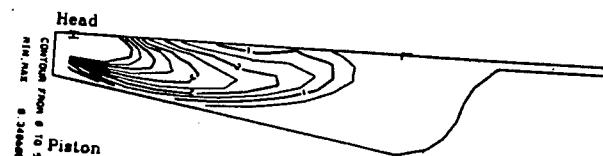
0.722E+01  
REFERENCE VECTOR



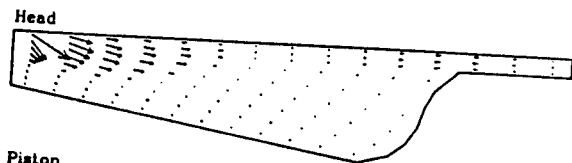
CRANK ANGLE =  $-15^\circ$ ;  $J=6$ ;  
EQUIVALENCE RATIO CONTOURS



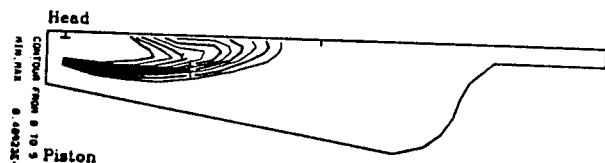
CRANK ANGLE =  $0^\circ$ ;  $J=6$ ;  
VELOCITY FLOWFIELD



CRANK ANGLE =  $0^\circ$ ;  $J=6$ ;  
EQUIVALENCE RATIO CONTOURS



CRANK ANGLE =  $-10^\circ$ ;  $J=6$ ;  
VELOCITY FLOWFIELD



CRANK ANGLE =  $-10^\circ$ ;  $J=6$ ;  
EQUIVALENCE RATIO CONTOURS

Fig.7: Velocity flowfield and equivalence ratio contour plots for the case with a  $15^\circ$  angle between the engine head and injector hole orientation.

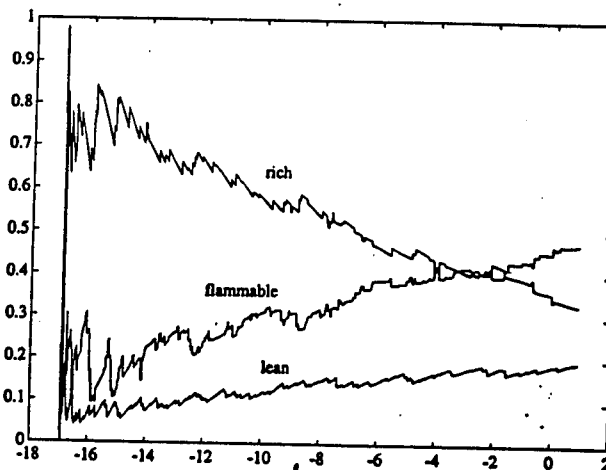
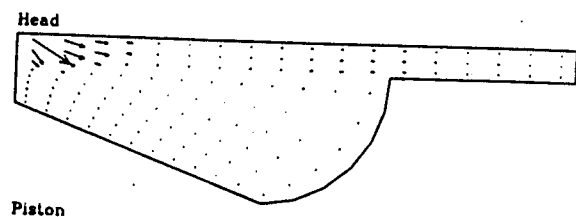
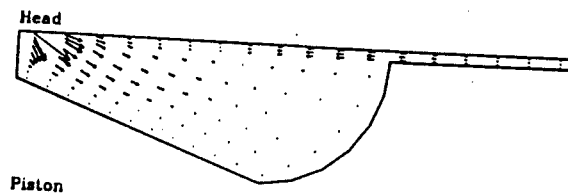


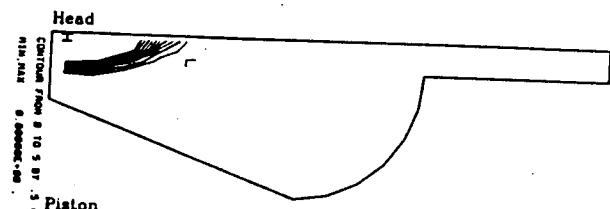
Fig.8: "f -  $\theta$ " plot for the case with a  $15^\circ$  angle between the engine head and injector hole orientation.



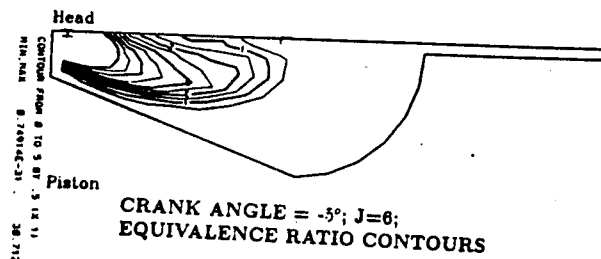
CRANK ANGLE =  $-15^\circ$ ;  $J=6$ ;  
VELOCITY FLOWFIELD



CRANK ANGLE =  $-5^\circ$ ;  $J=6$ ;  
VELOCITY FLOWFIELD



CRANK ANGLE =  $-15^\circ$ ;  $J=6$ ;  
EQUIVALENCE RATIO CONTOURS



CRANK ANGLE =  $-5^\circ$ ;  $J=6$ ;  
EQUIVALENCE RATIO CONTOURS

Fig.9: Velocity flowfield and equivalence ratio contour plots for the case with increased squish.

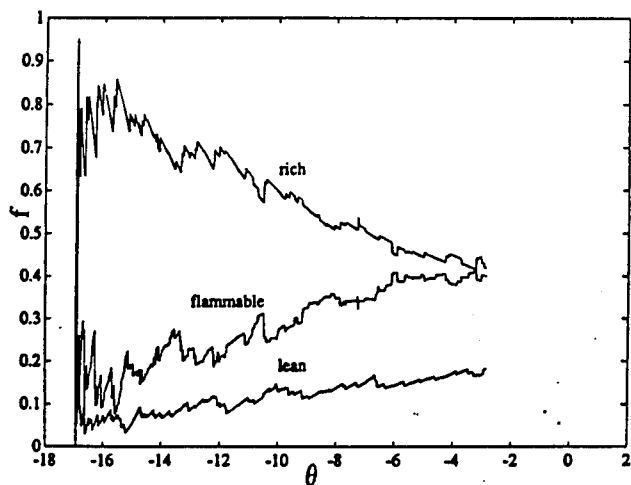
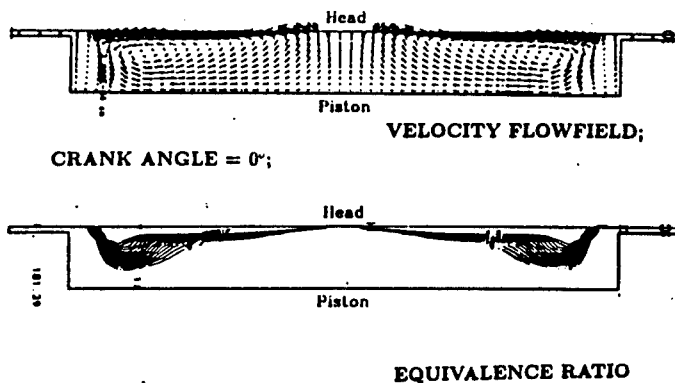


Fig.10: "f -  $\theta$ " plot for the case with increased squish.



CRANK ANGLE =  $0^\circ$ ;

EQUIVALENCE RATIO

Fig.11: Velocity flowfield and equivalence ratio contour plots for gas injection into a cylindrical bowl with a conical gas jet.

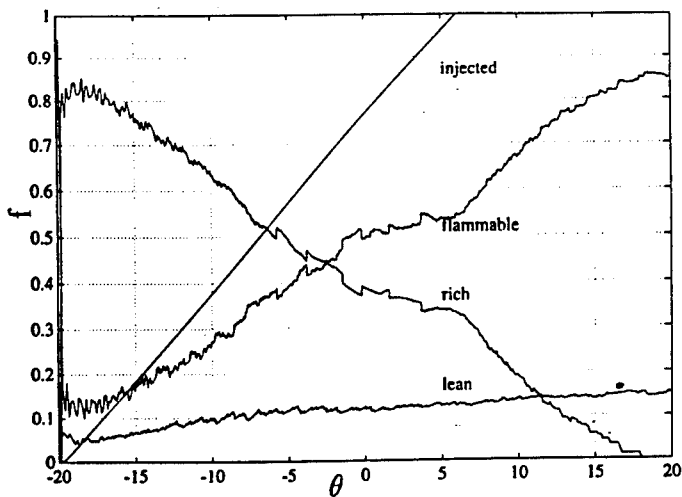


Fig.12: "f -  $\theta$ " plot for gas injection into a cylindrical bowl with a conical gas jet (reference case).

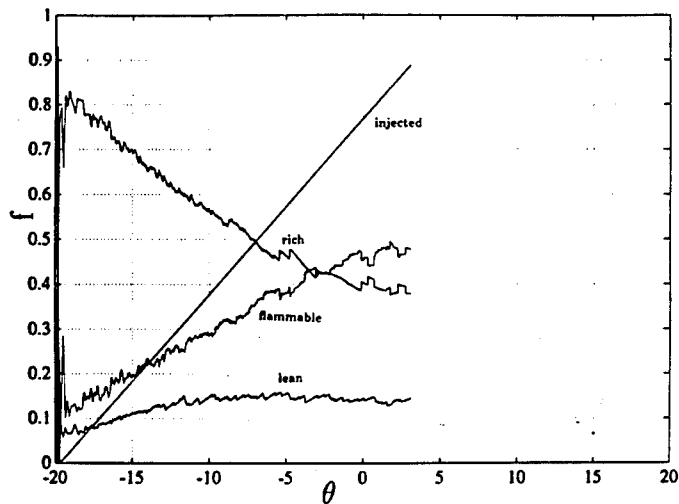


Fig.13: "f -  $\theta$ " plot for gas injection into a cylindrical bowl with a conical gas jet and with the turbulence intensity increased by a factor of 2 over the reference case.

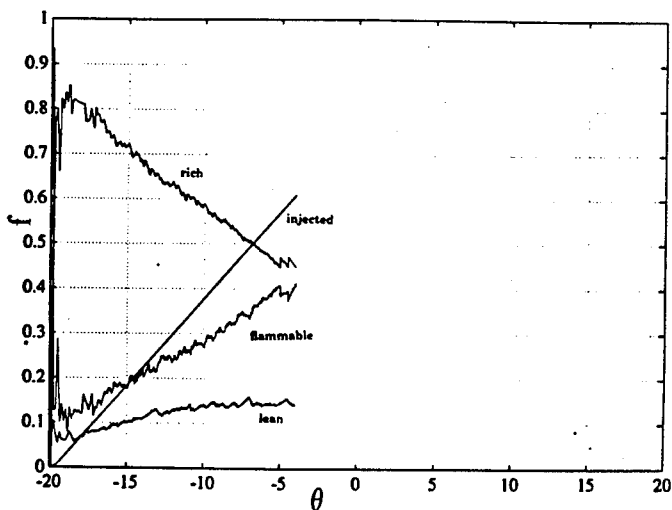


Fig.14: "f -  $\theta$ " plot for gas injection into a cylindrical bowl with a conical gas jet and with the turbulence length scale increased by a factor of 2 over the reference case.

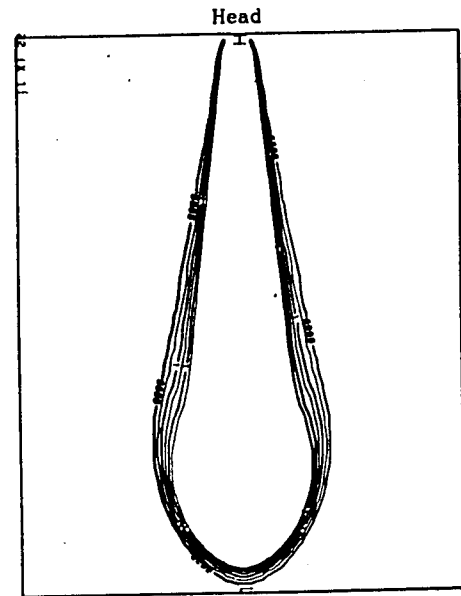
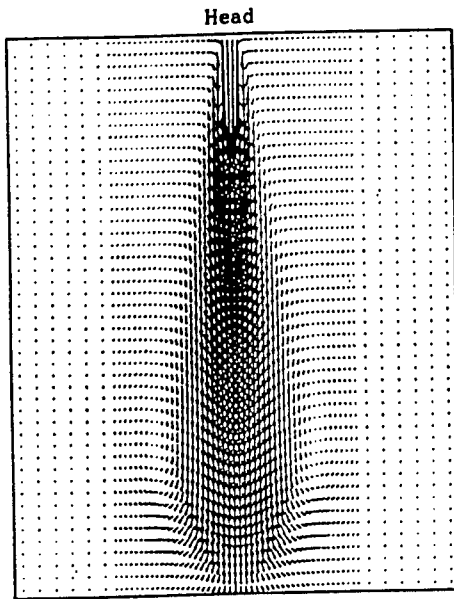


Fig.15: Velocity flowfield and equivalence ratio contour plots for gas injection into a fixed volume, 2ms after the start of injection.

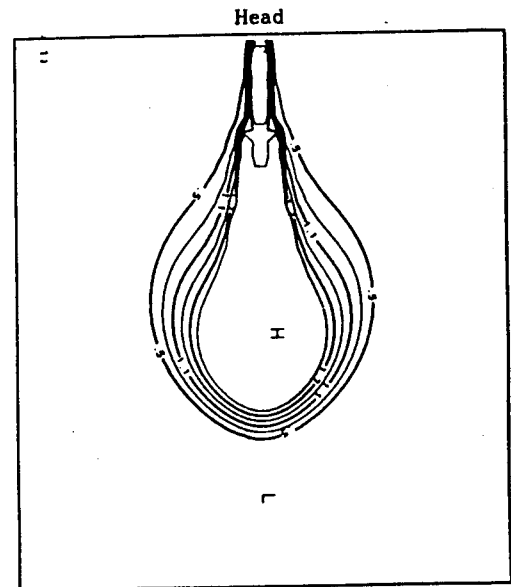
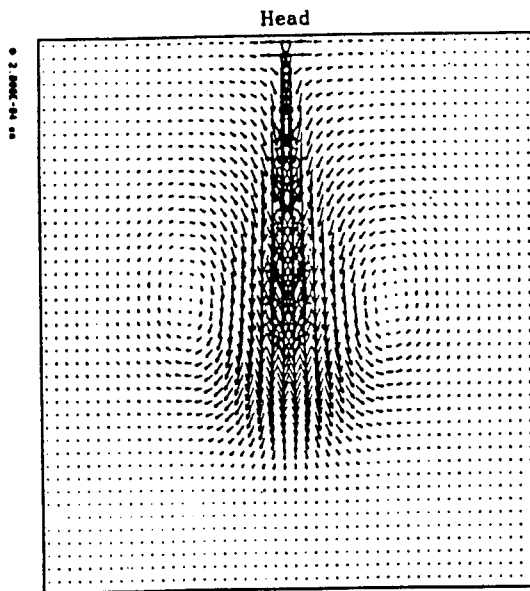


Fig.16: Velocity flowfield and equivalence ratio contour plots for direct injection of liquid into a fixed volume, 2ms after the start of injection.

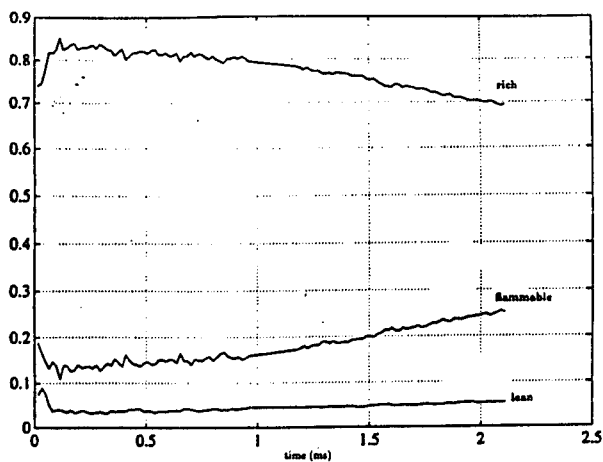


Fig.17: "f -  $\theta$ " plot for gas injection into the fixed volume.

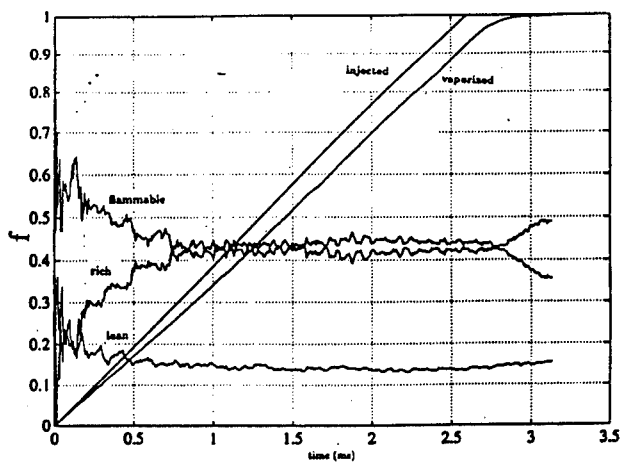


Fig.18: "f -  $\theta$ " plot for direct injection of liquid into the fixed volume.

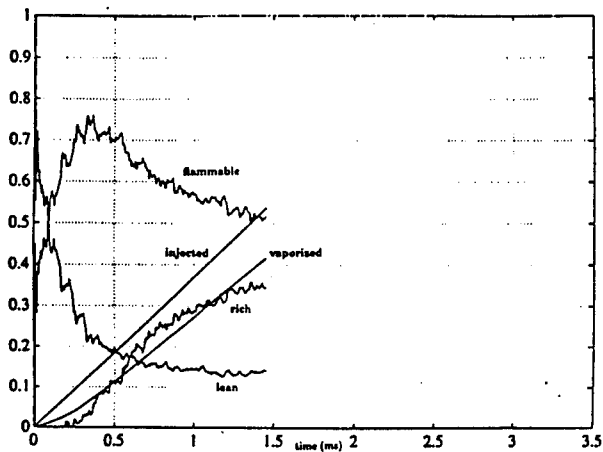


Fig.19: "f -  $\theta$ " plot for direct injection of liquid into the fixed volume with the Sauter Mean Radius of the initial drops increased by a factor of 10.

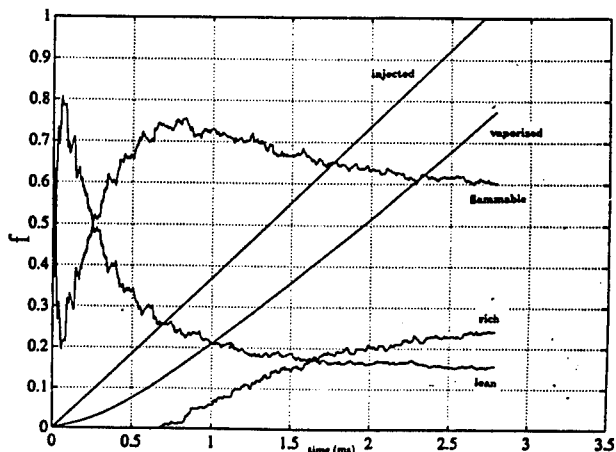


Fig.20: "f -  $\theta$ " plot for direct injection of liquid into the fixed volume with the Sauter Mean Radius of the initial drops increased by a factor of 25.

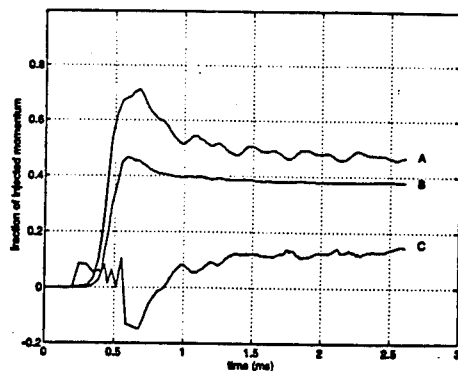


Fig.21: Fraction of injected fuel momentum in fuel (curve A), ambient gas (curve B) and in the pressure difference (curve C) at 3.2cm from the injector for gas injection into the fixed volume.

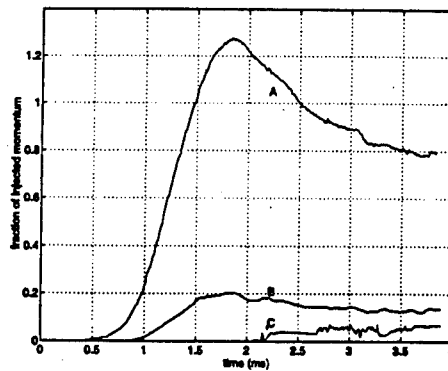


Fig.22: Fraction of injected fuel momentum in fuel (curve A), ambient gas (curve B) and in the liquid phase (curve C) at 3.2cm from the injector for liquid injection into the fixed volume.

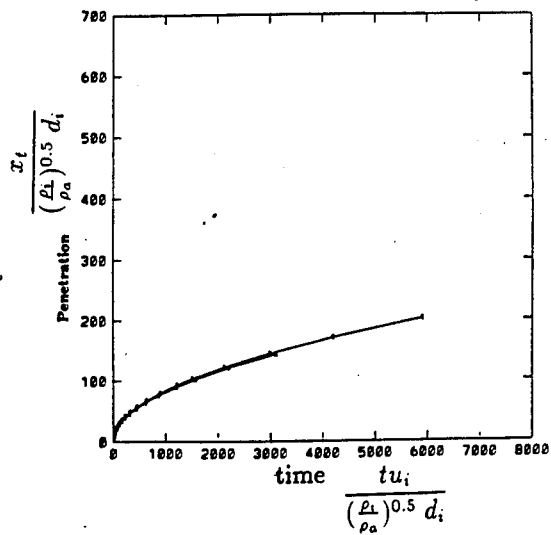


Fig.23: Penetration of gas jets for gas injection into an infinite environment.

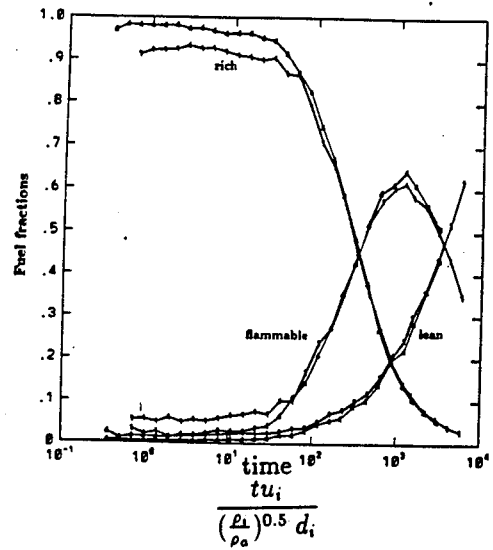


Fig.24: "f -  $\theta$ " plot for gas jet in an infinite environment.

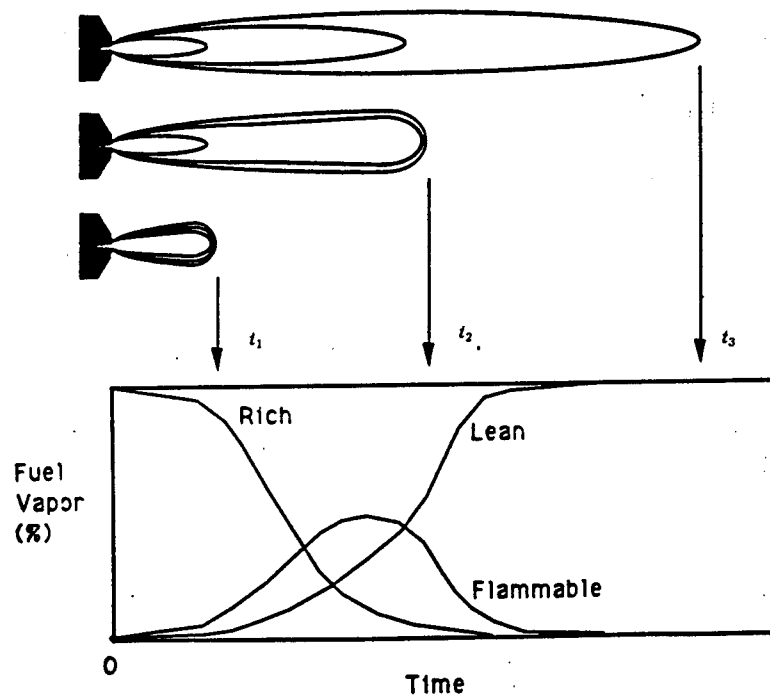


Fig.25: A schematic of the development of a gas jet.

## **High-Speed Four-Color Infrared Digital Imaging for Studying In-Cylinder Processes in a DI Diesel Engine**

K. T. Rhee

Department of Mechanical and Aerospace Engineering  
Rutgers, The State University of New Jersey  
Piscataway, NJ 08855

Four geometrically identical digital IR images of in-cylinder events are simultaneously obtained in respective spectral bands, which is individually triggered by the crank-angle signal generated from the host direct injection (DI) diesel engine.

A new spectrometric information processing algorithm is developed in order to determine distributions of temperature and species in the combustion chamber using the measurements.

**Apparatus Construction.** The improved engine apparatus having optical access has recently been incorporated with a new electronic controlled fuel injection system fabricated in our laboratory. This system at present delivers a injection pressure of as high as 170 MPa (25,000psi), which will be increased to well over 200MPa in the next system.

While our early two-color imaging system was employed in engine studies, development of the four-color spectral imaging system has been performed at the same time.

This includes: (a) a newly developed reflective optical arrangement having three custom-made spectral beam splitters; (b) four IR imaging camera heads; (c) new electronic packages having printed boards (unlike the hand-wired electronic boards employed in the previous systems) for driving the camera heads and simultaneously retrieving the output from the cryogenically cooled imagers; and (d) several new computer programs for image processing and display.

**Experimental Results.** The present ARO-sponsored study has been joined by Ford Motor Co. and Texaco Research Center in order to study SI engine combustion by using this new diagnostic system.

(1) SI engine combustion has been the subject to initially study by using this new tool because its in-cylinder environment is easier to manage than its counter part, the CI engine. This co-sponsored work is being directed to investigation of several engine events, including the knock processes, flame kernel growth, deposit image, and cold start.

(2) The most significant finding from the DI diesel engine study reported in the previous period was the low temperature inferred in the regions near the axis of the spray plume, which has been further studied in order to explain the reasons.

Among the possible reasons are: The fuel/air in the regions are at speeds too high to permit stable formation of reaction fronts, which seems to be supported by our video movie produced using the new electronic fuel injector and the four-color system. The other reason is that the fuel vaporization results in lower temperatures than required for self-ignition in the regions. The next possible reason is that the combination of the above effects. That is, even though the mixtures attain either marginally or sufficiently high temperatures for self-ignition, it will be difficult to produce established reaction fronts when the reactive mixture is at high speeds along the axis.

**Future Activities.** Since our imaging system is now operational, which we will continue to improve, we will obtain measurements and analyze them using our new process software in order to implement the project goal.

The variables to be immediately studied include different injector tips provided by Cummins Engine and new fuels expected from the DOE Alternative Fuels Utilization Program.

## **Summary of Presentation**

- o. Objectives**
- o. Methods**
- o. Analysis of Methods**
- o. Progress**
- o. Future Activities**

### **Objectives**

- 1. Develop a New High-Speed Multispectra IR Imaging System for Engine Studies.**
- 2. Develop Spectrometric Data Analysis Algorithm.**
- 3. Investigate In-Cylinder Processes of a DI Diesel Engine during the Entire Cycle Period:**
  - . Residual Gas Behaviors,**
  - . Temporal and Spatial Temperature Distributions,**
  - . Combustion Product Distributions,**
  - . Heat Transfer, and Others.**

### **Work Tasks**

- 1. A New Multispectra Imaging System.**
- 2. Conventional Two-Color Method for Solid Wall.**
- 3. New Dual-Band Method for Gaseous Mixtures.**
- 4. A New Electronic-Controlled Fuel Injection System.**
- 5. Bench Test and Engine Experiment.**



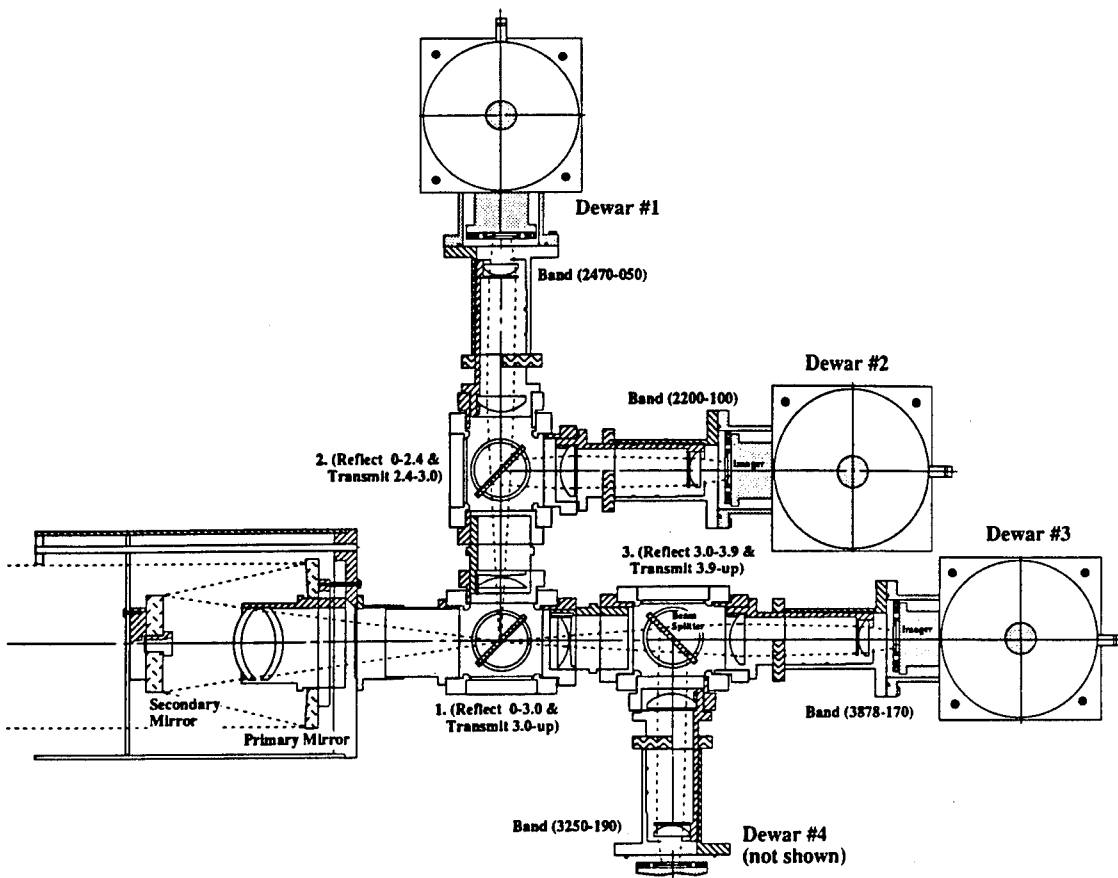


Fig. 1. Assembly Drawing of Four-Color Imaging System with Reflective Optics Arrangement

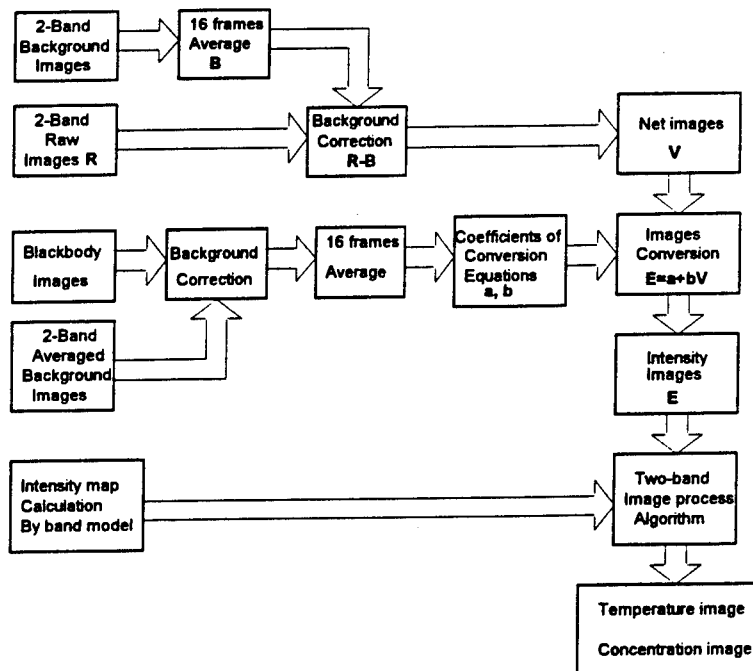


Fig. 2. Flow-Chart of the Dual-Band Quantitative Imaging.

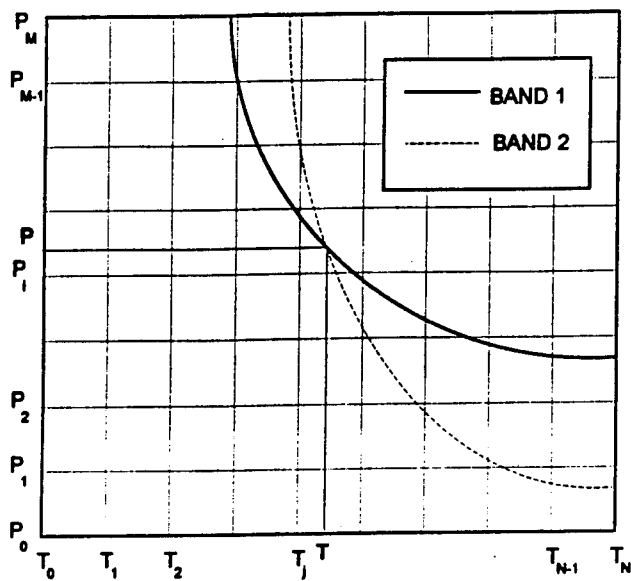


Fig. 3. Dual-Band Spectrometry Algorithm.

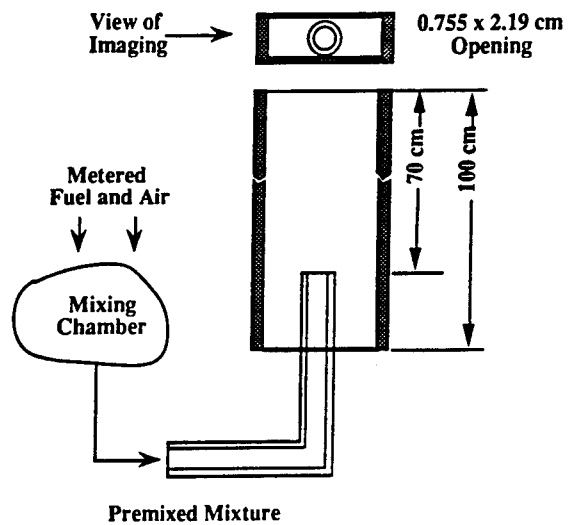


Fig. 4. Poiseuille Burner for  $H_2$ -Air Flame.

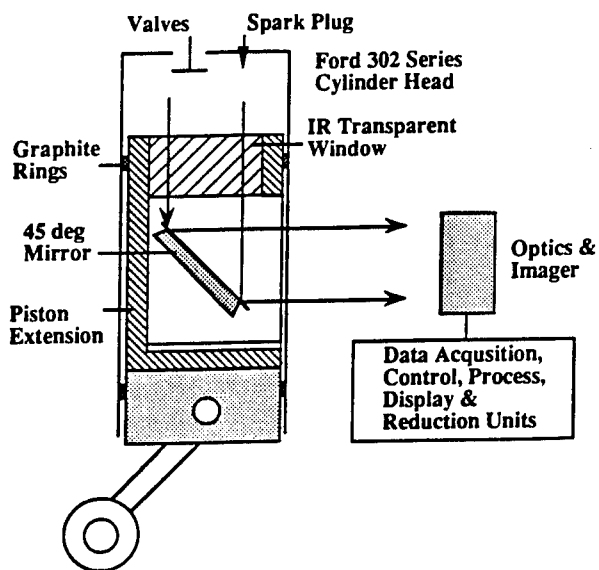


Fig. 5. Schematics of SI Engine Apparatus.  
(Co-Sponsors: Ford Motor and Texaco)

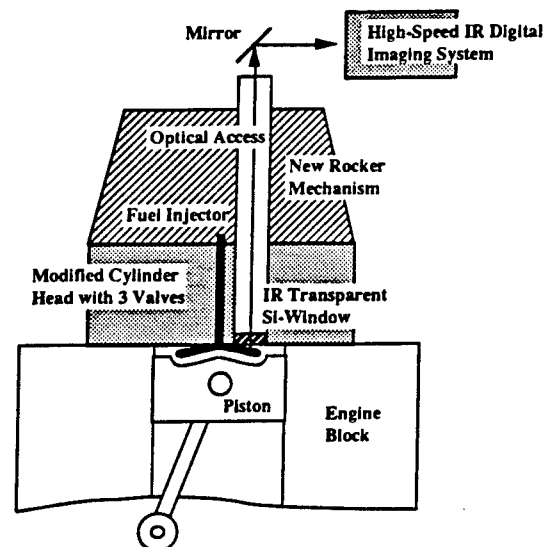


Fig. 6. Diesel Engine with Optical Access.  
(ARO Combustion Research)

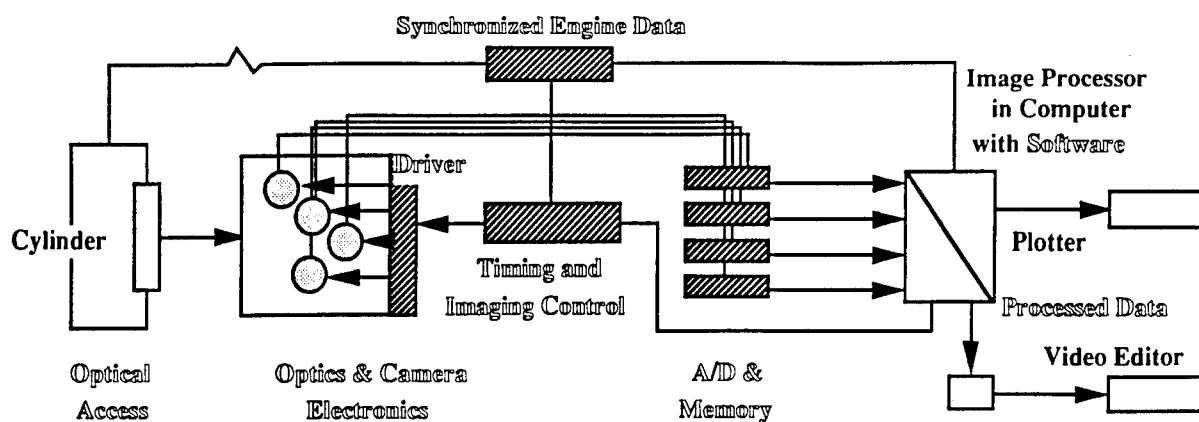


Fig. 7. Four Color-Imaging System Lined up with an Engine Apparatus.

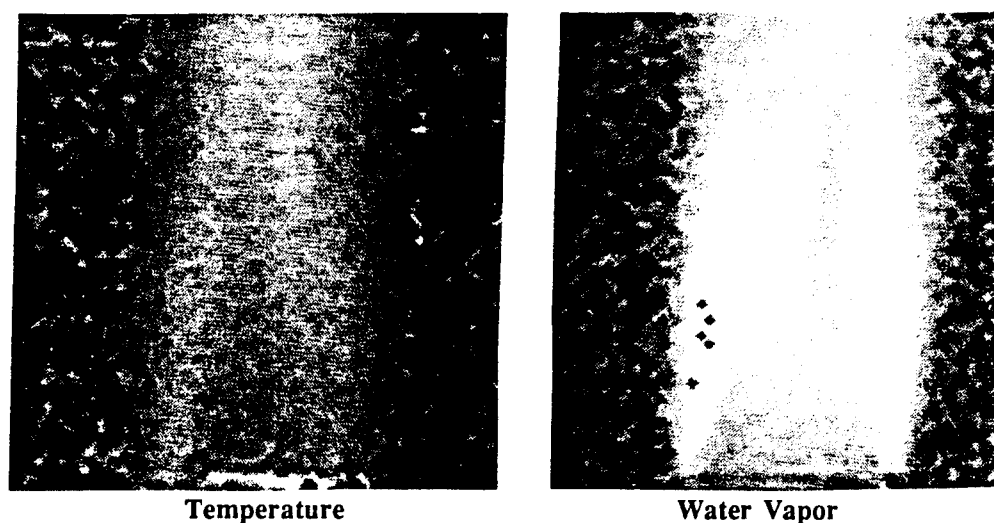


Fig. 8. Instantaneous Quantitative Flame Images of Hydrogen-Air Burner (Fig. 4).

- o. 500rpm
- o. Propane-Air
- o. Spark Ignition at 6bTDC (-6)

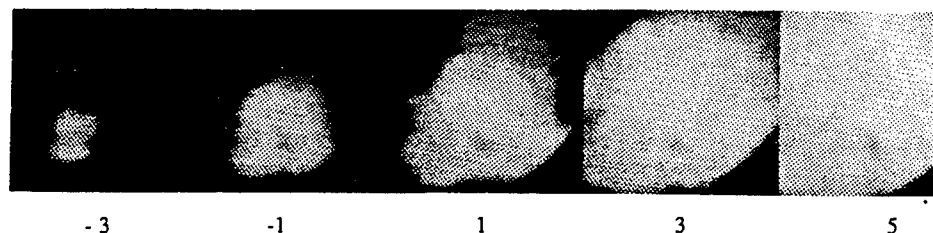
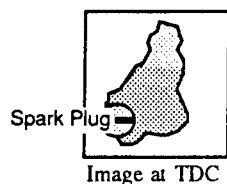
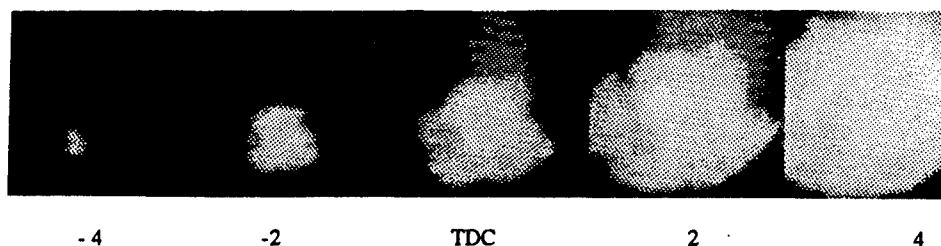
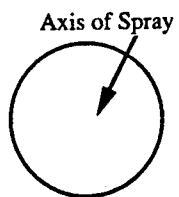


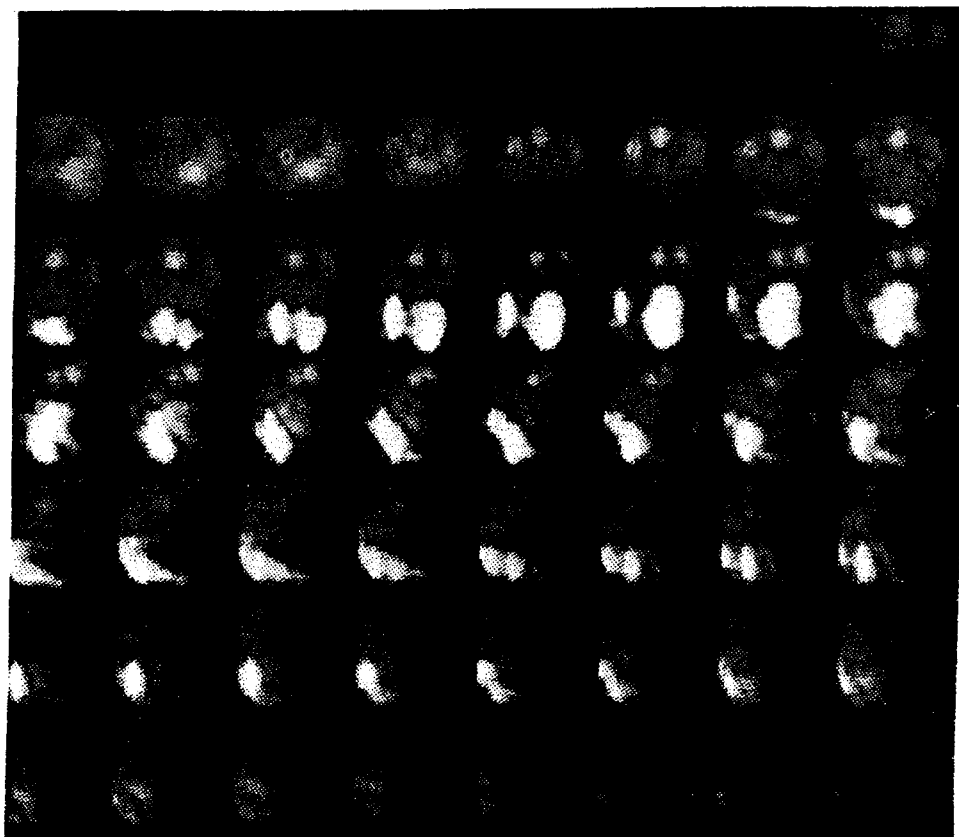
Fig. 9. High-Speed IR Images of Flame Kernel Growth in an SI Engine (Fig. 5).



o. Imaging  
at 20bTDC  
with 2.5CA  
Intervals,

o. 500rpm.

2.4 $\mu$ m  
Band



3.8 $\mu$ m  
Band

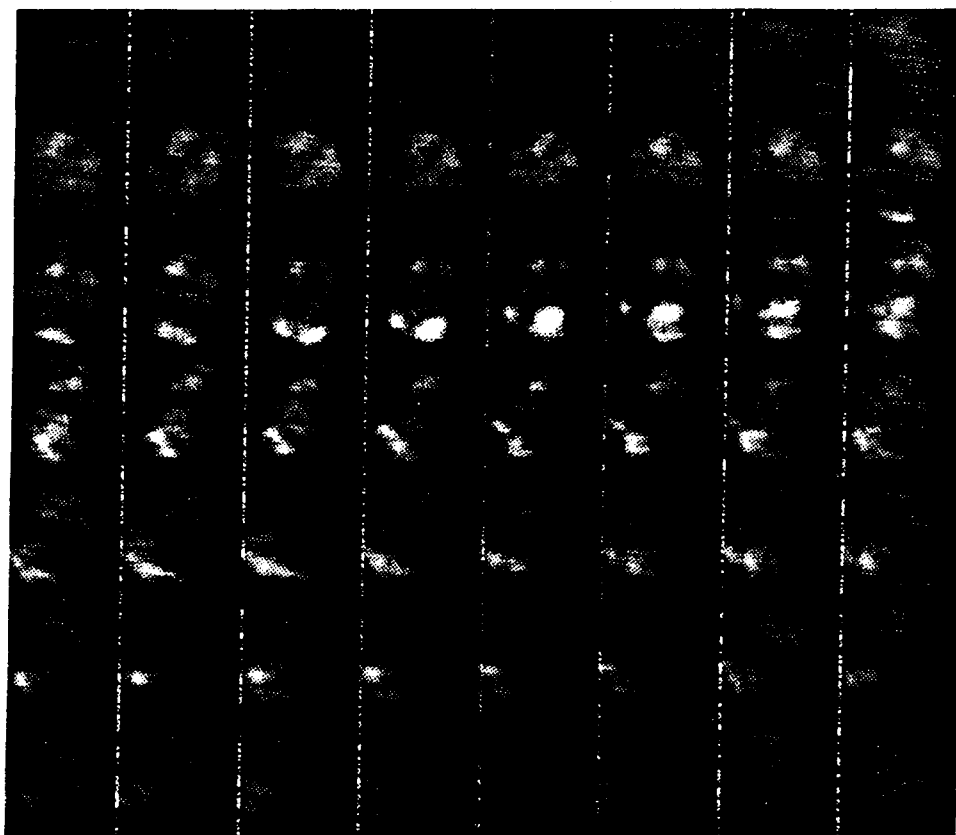


Fig. 10. High-Speed Spectral IR Images of a CI Engine Combustion with an Electronic Controlled Fuel Injector (170 MPa, Injection Pressure).

## Combustion Instability During Cold Starting of Diesel Engines

N. A. Henein, M. Lai  
Center for Automotive Research  
Wayne State University  
Detroit, MI 48202

Combustion instability during cold starting of diesel engines causes many problems such as long periods of cranking and the emission of excessive amounts of unburned fuel in the form of white smoke, stalling after an instable combustion or a complete failure of the engine to start. Such problems are of major concern to engine manufacturers and specially to the Army under the critical field operating conditions.

The objectives of this research program are: i- to investigate the nature of combustion instability, its randomness, and dependence on the fuel properties and engine design. ii- to investigate the causes of combustion instability and iii- to propose solutions.

Tests are conducted on three single cylinder, direct injection, four-stroke-cycle, diesel engines of different designs. The first is a TACOM research engine, water cooled, connected to an electric dynamometer for motoring and power absorption, equipped with an endoscope. The second is an industrial stand-alone engine equipped with its electric starter, battery and fuel tank. Both these engines are installed in a cold room where the ambient temperature can be controlled between the normal room temperature and  $-50^{\circ}\text{C}$ . The cold starting tests are conducted after the engines are soaked for 6 to 8 hours. The third engine is an AVL 520 water cooled engine modified for optical access through the piston top, all around the top of the cylinder and through the cylinder head. The engine is connected to an electric dynamometer for motoring. The intake air temperature is controlled. Fuel injection occurs only for two consecutive cycles while the engine is being motored. Traces are taken for the fuel pressure before the injector and for the cylinder gas pressure. The diagnostic instrumentation includes the following: (a) a high speed movie camera to study the spray parameters such as penetration, angle, impingement on and reflection off the walls of the combustion chamber, start of the ignition process, flame propagation and smoke intensity, (b) Exciplex LIF to study spray evaporation (without combustion) in a nitrogen atmosphere. (c) High speed video for 2-color pyrometry for simultaneous flame temperature measurements, and OH chemiluminescence imaging. (d) Lase Incandescence Imaging (LII) to investigate the spatial distribution of soot in the spray.

The experimental results on the three engines indicated the following: (a) Combustion instability is not a random process and combustion may occur every sixteen, twelve, eight or four strokes depending on the ambient temperature. (b) Combustion instability is not engine or fuel specific. (c) Combustion instability is caused by a combination of factors related to engine dynamics and combustion kinetics, during the transient cold starting process.

High speed photographs of the two consecutive cycles were obtained at different intake air temperatures:  $23^{\circ}\text{C}$ ,  $18^{\circ}\text{C}$  and  $13^{\circ}\text{C}$ . At  $23^{\circ}\text{C}$  the engine fired and combustion was stable in the two consecutive cycles. At  $18^{\circ}\text{C}$  the engine fired in the first cycle and misfired in the second cycle. At  $13^{\circ}\text{C}$  the engine misfired in the two cycles.

Future plans are for the use of different laser based techniques to investigate the cause(s) of combustion instability.

## OVERALL GOAL

IMPROVE THE COLD STARTING OF MILITARY DIESEL ENGINES.

## BACKGROUND

1. DIESEL COLD STARTING PROBLEMS INCLUDE:
  - . LONG PERIOD OF CRANKING AND THE EMISSION OF EXCESSIVE AMOUNTS OF UNBURNED FUEL, (WHITE SMOKE).
  - . STALLING AFTER AN INSTABLE COMBUSTION.
  - . COMPLETE FAILURE OF THE ENGINE TO START.
2. MOST OF THE PROBLEMS ARE RELATED TO AN INSTABLE COMBUSTION PROCESS.

## OBJECTIVES

TO ANSWER THE FOLLOWING QUESTIONS:

1. IS COMBUSTION INSTABILITY DURING COLD STARTING A RANDOM PROCESS ?
2. IS COMBUSTION INSTABILITY CAUSED BY A FAILURE OF THE AUTOIGNITION PROCESS ?
3. IS COMBUSTION INSTABILITY SPECIFIC TO ONLY SOME FUELS ?
4. IS COMBUSTION INSTABILITY SPECIFIC TO ONLY SOME ENGINES ?
5. WHAT IS THE EFFECT OF TEMPERATURE ON COMBUSTION INSTABILITY ?
6. WHAT ARE THE CAUSES OF COMBUSTION INSTABILITY ?

## APPROACH

### THEORETICAL

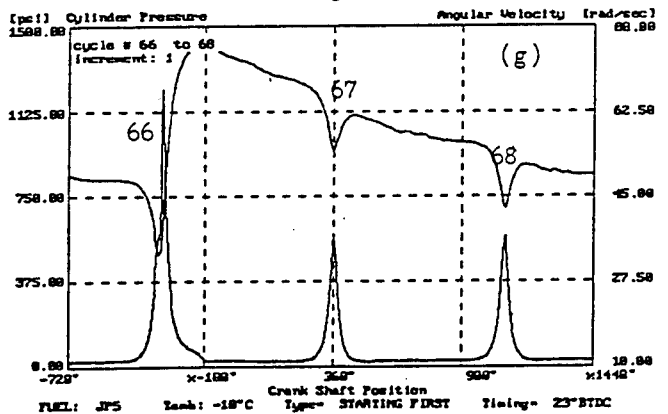
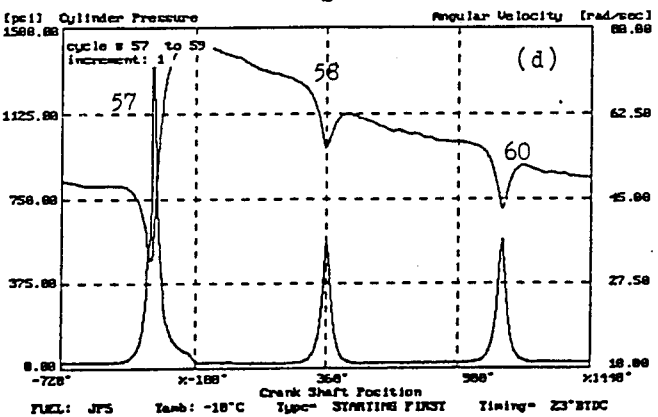
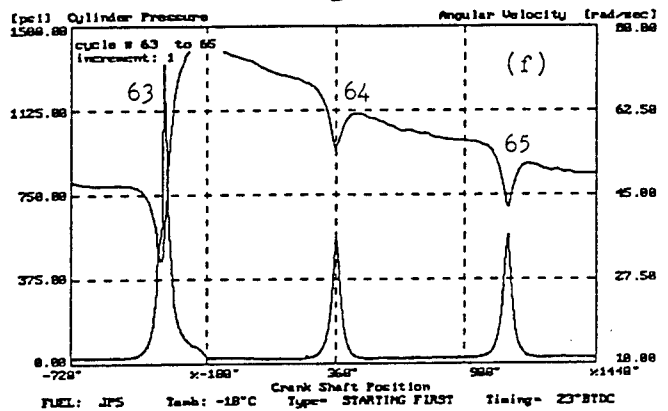
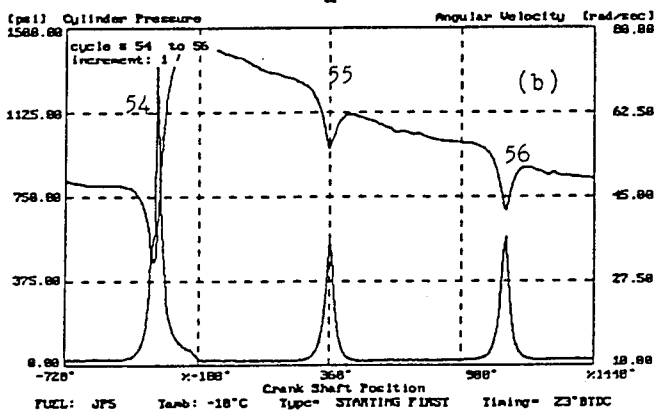
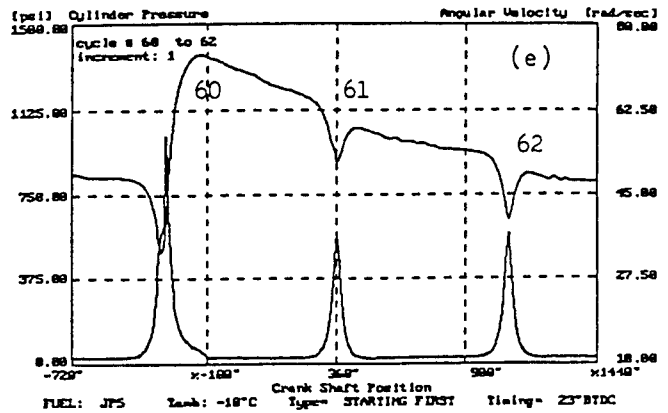
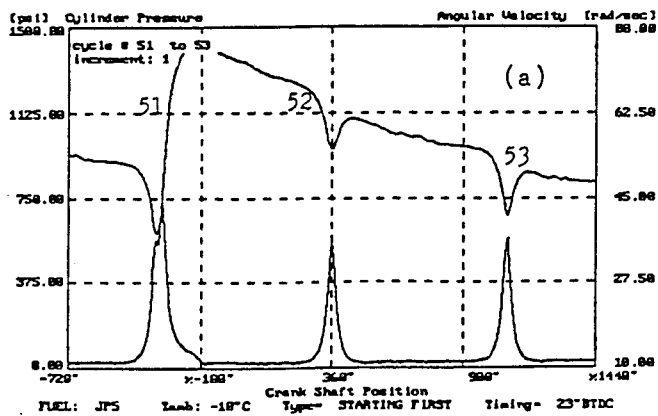
- . ANALYZE THE COMBUSTION PROCESS UNDER THE TRANSIENT THERMAL AND DYNAMIC ENGINE CONDITIONS DURING COLD CRANKING AND STARTING.
- . DEVELOP A MATHEMATICAL MODEL FOR THE ENERGY RELEASE IN SUCCESSIVE ENGINE CYCLES, CONSIDERING THE FOLLOWING:
  - . INSTANTANEOUS ANGULAR VELOCITY
  - . INSTANTANEOUS BLOWBY
  - . INSTANTANEOUS FUEL INJECTION
  - . INSTANTANEOUS BURNING RATES



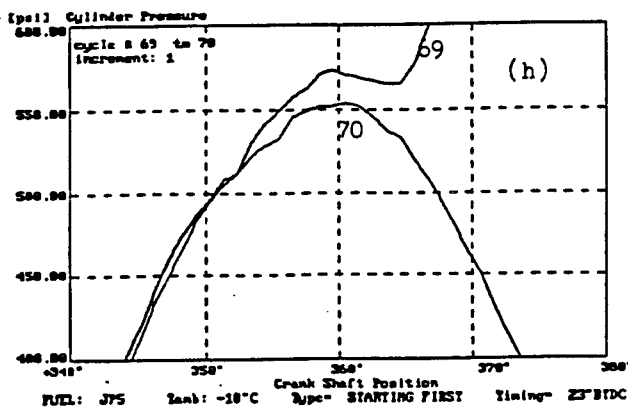
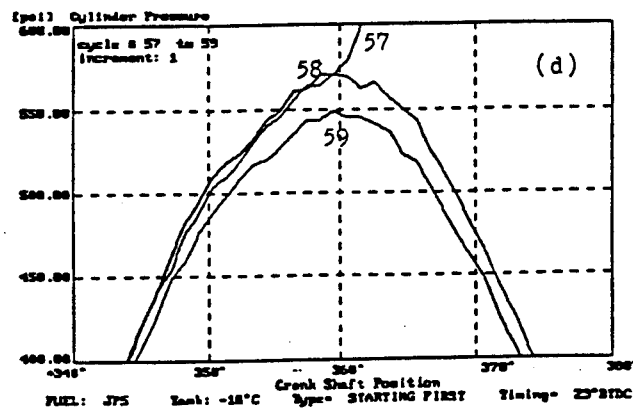
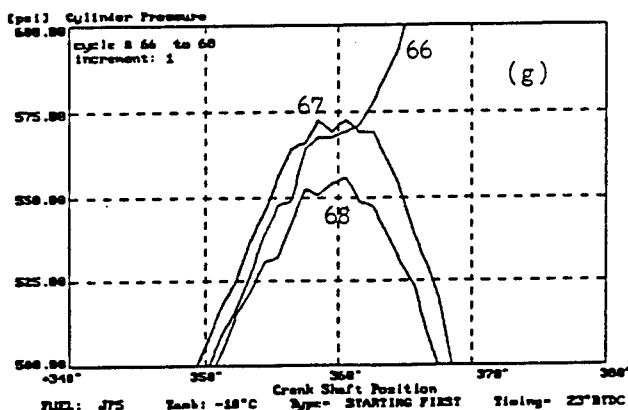
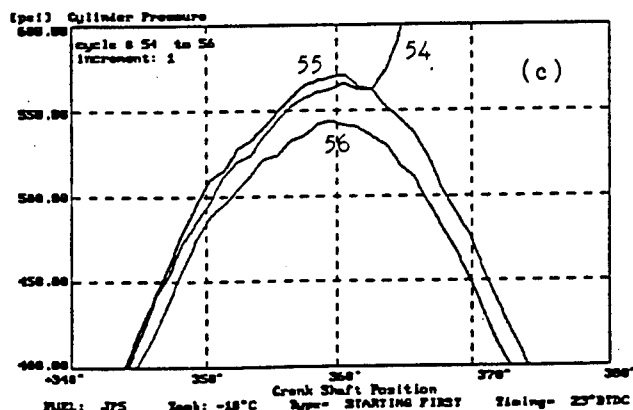
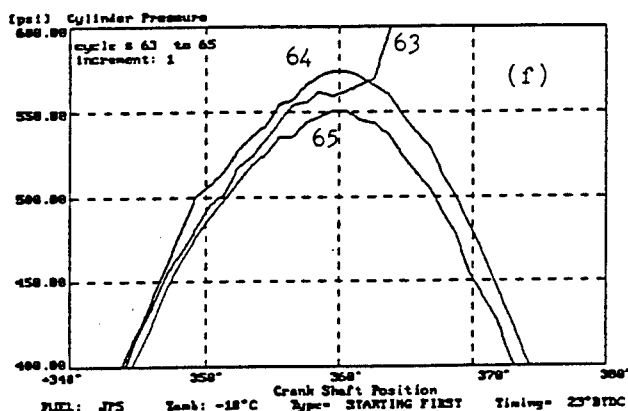
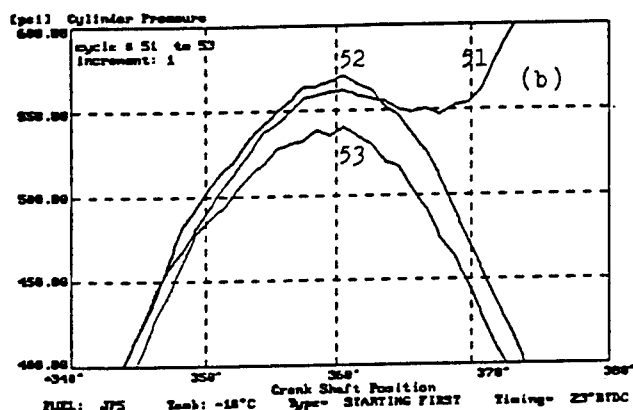
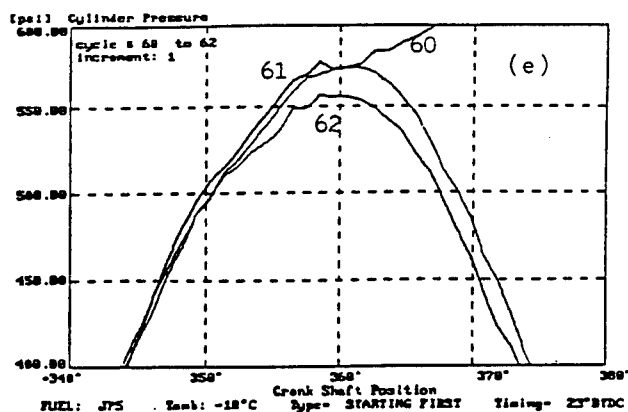
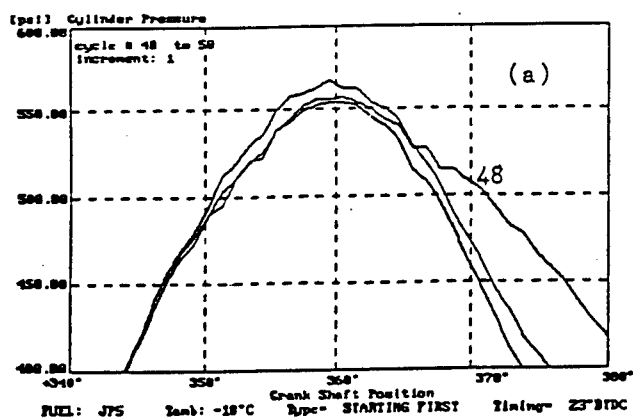
## EXPERIMENTAL

### ENGINES: DIRECT INJECTION, 4-STROKE-CYCLE

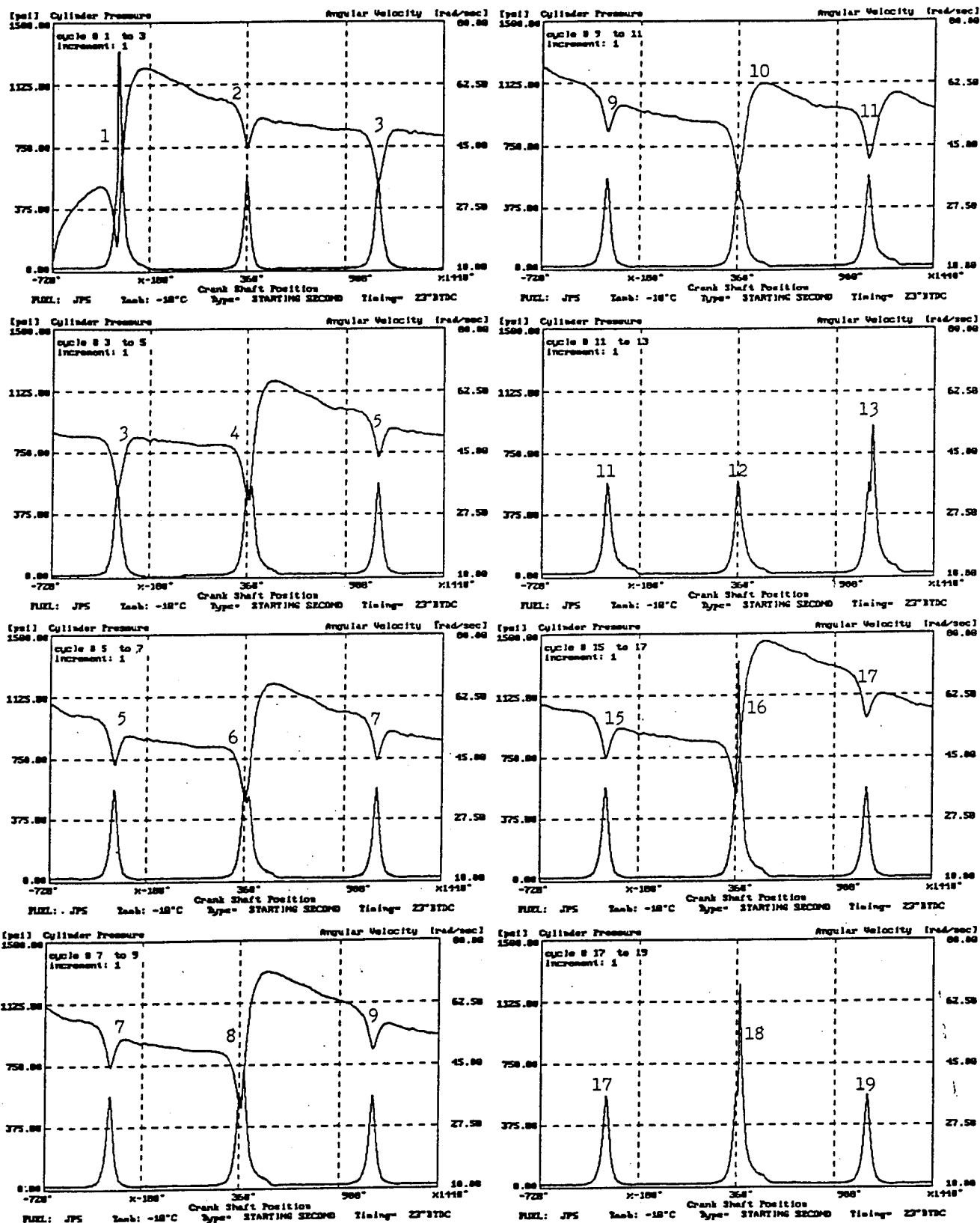
- (i) TACOM, DYNAMOMETER DRIVEN, WATER COOLED, WITH AN ENDOSCOPE FOR IN CYLINDER IMAGING.
- (ii) DEUTZ, STAND-ALONE, AIR COOLED.
- (iii) AVL, MODIFIED FOR OPTICAL ACCESS, DYNAMOMETER DRIVEN, WATER COOLED.
  - . HIGH SPEED MOVIE CAMERA
  - . EXCIPLEX LIF
  - . HIGH SPEED 2-COLOR PYROMETRY
  - . LASER INCANDESCENCE IMAGING



(P -  $\theta$ ) AND ( $\omega$  -  $\theta$ ) TRACES FOR DEUTZ ENGINE,  
OPERATING ON 12-STROKE-CYCLE



## DETAILED (P - $\theta$ ) TRACES FOR THE 12-STROKE-CYCLE OPERATION



(P -  $\theta$ ) AND ( $\omega$  -  $\theta$ ) TRACES FOR DEUTZ ENGINE,  
OPERATING ON 8-STROKE-CYCLE

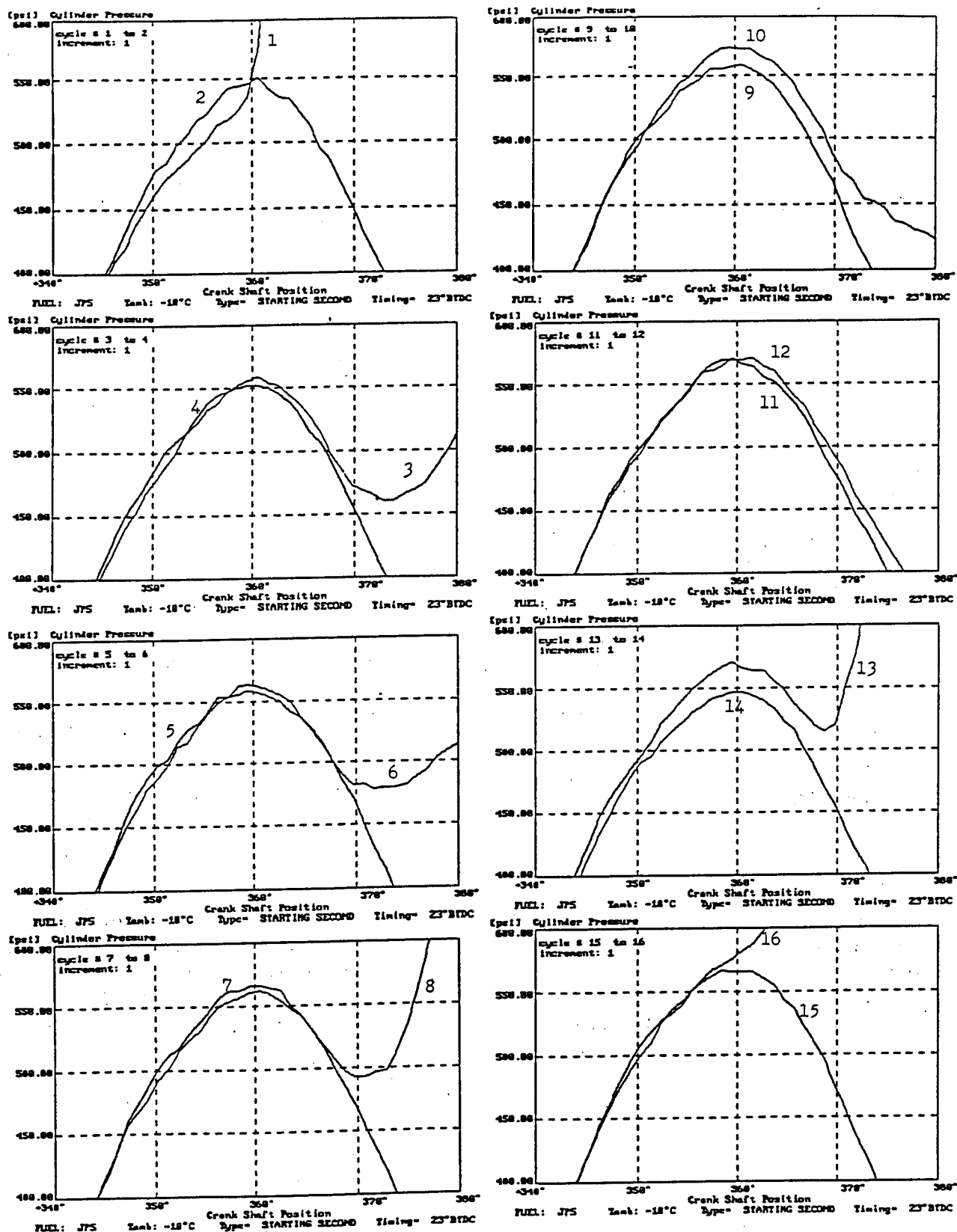
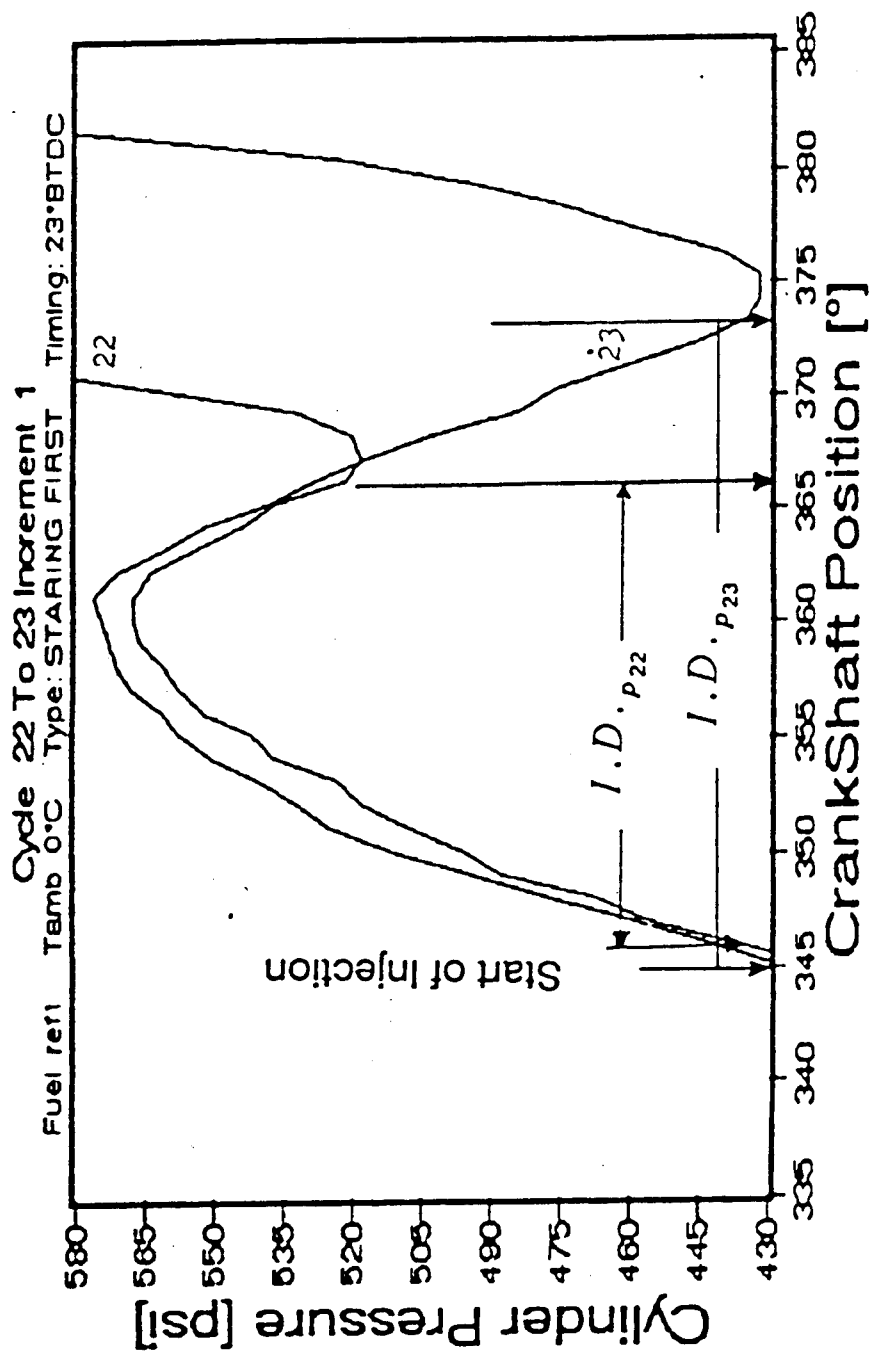


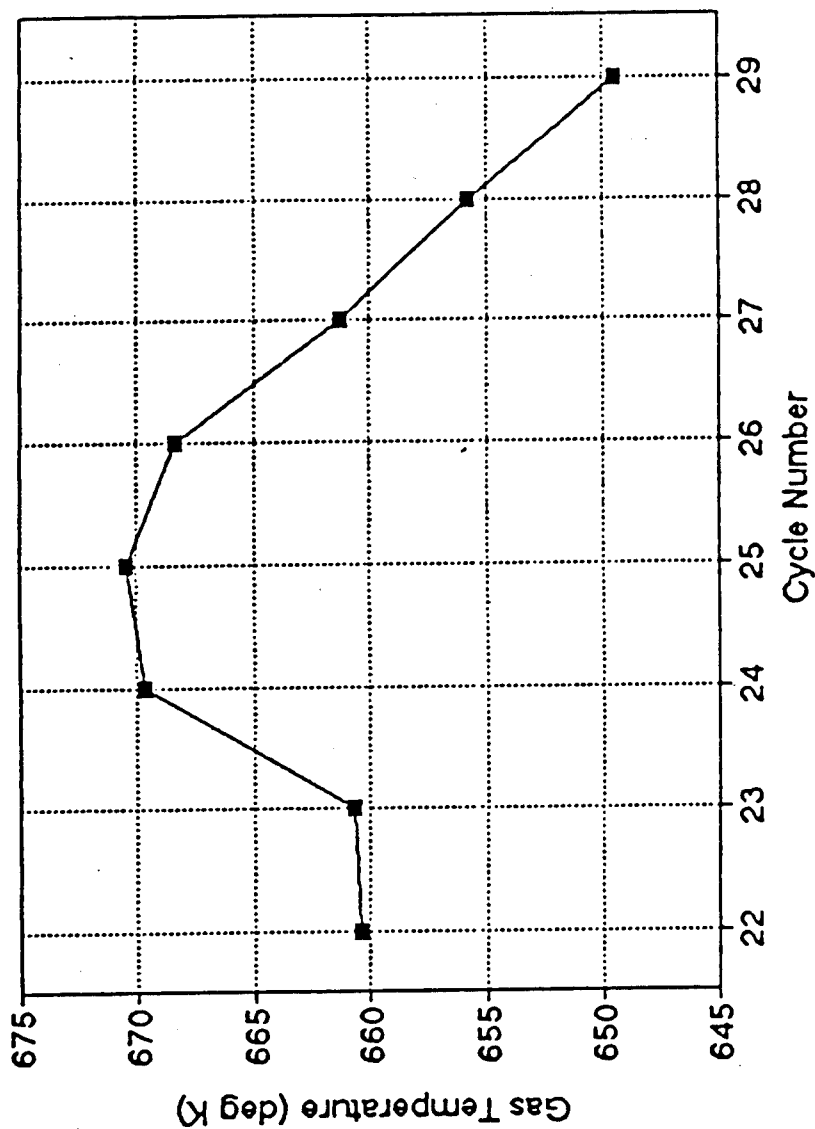
Fig 14: Detailed ( $P - \theta$ ) Traces for the 8-Stroke-cycle Operation

## DETAILED ( $P - \theta$ ) TRACES FOR THE 8-STROKE-CYCLE OPERATION



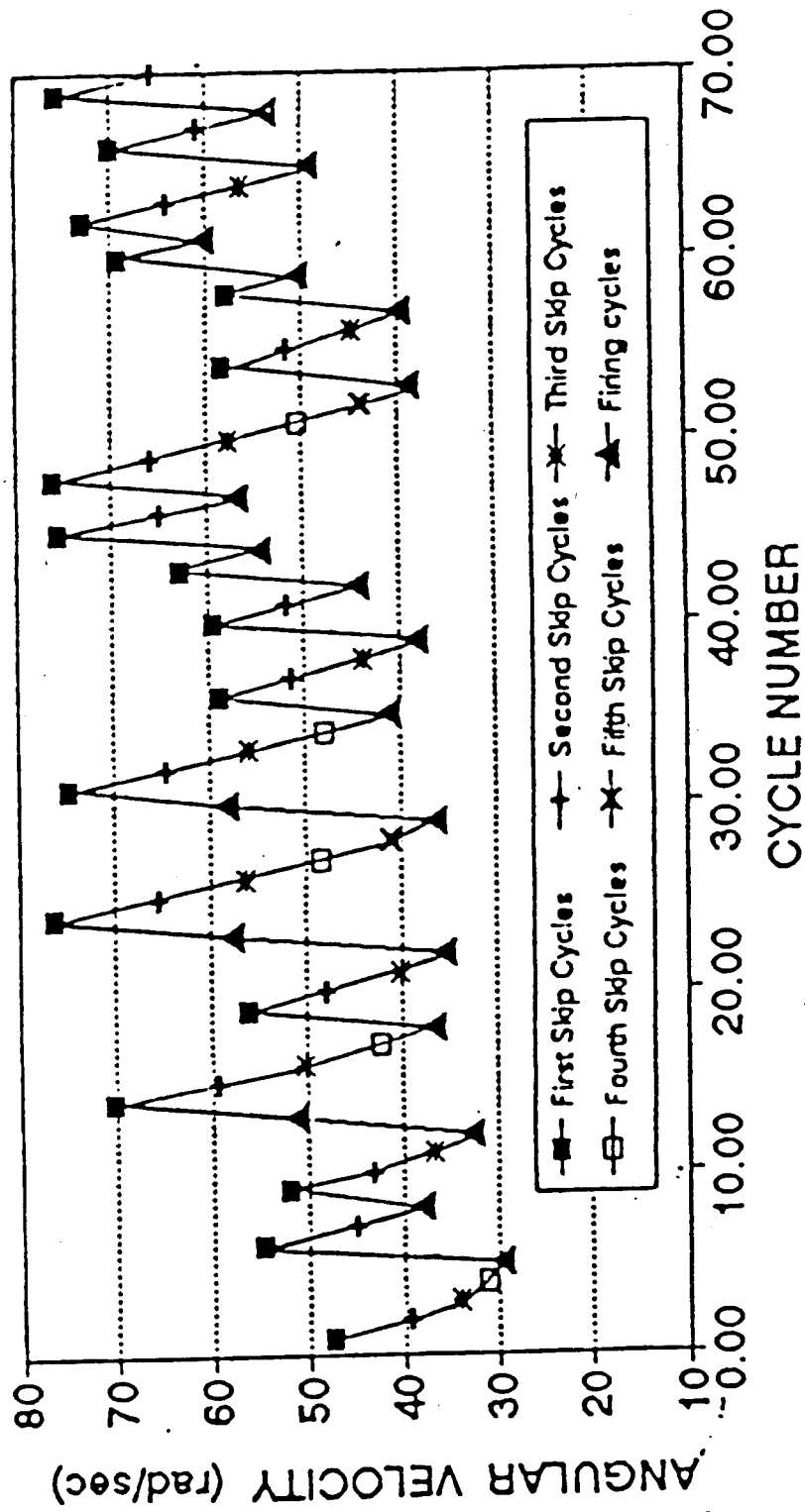
Tambient = 0°C, Fuel = Ref1, Timing = 23°BTDC

CYLINDER PRESSURE FOR CYCLES 22 TO 23, 25° FROM TDC  
[DEUTZ ENGINE]



$T_{\text{ambient}} = 0^{\circ}\text{C}$ , Fuel = Ref1, Timing =  $23^{\circ}\text{BTDC}$

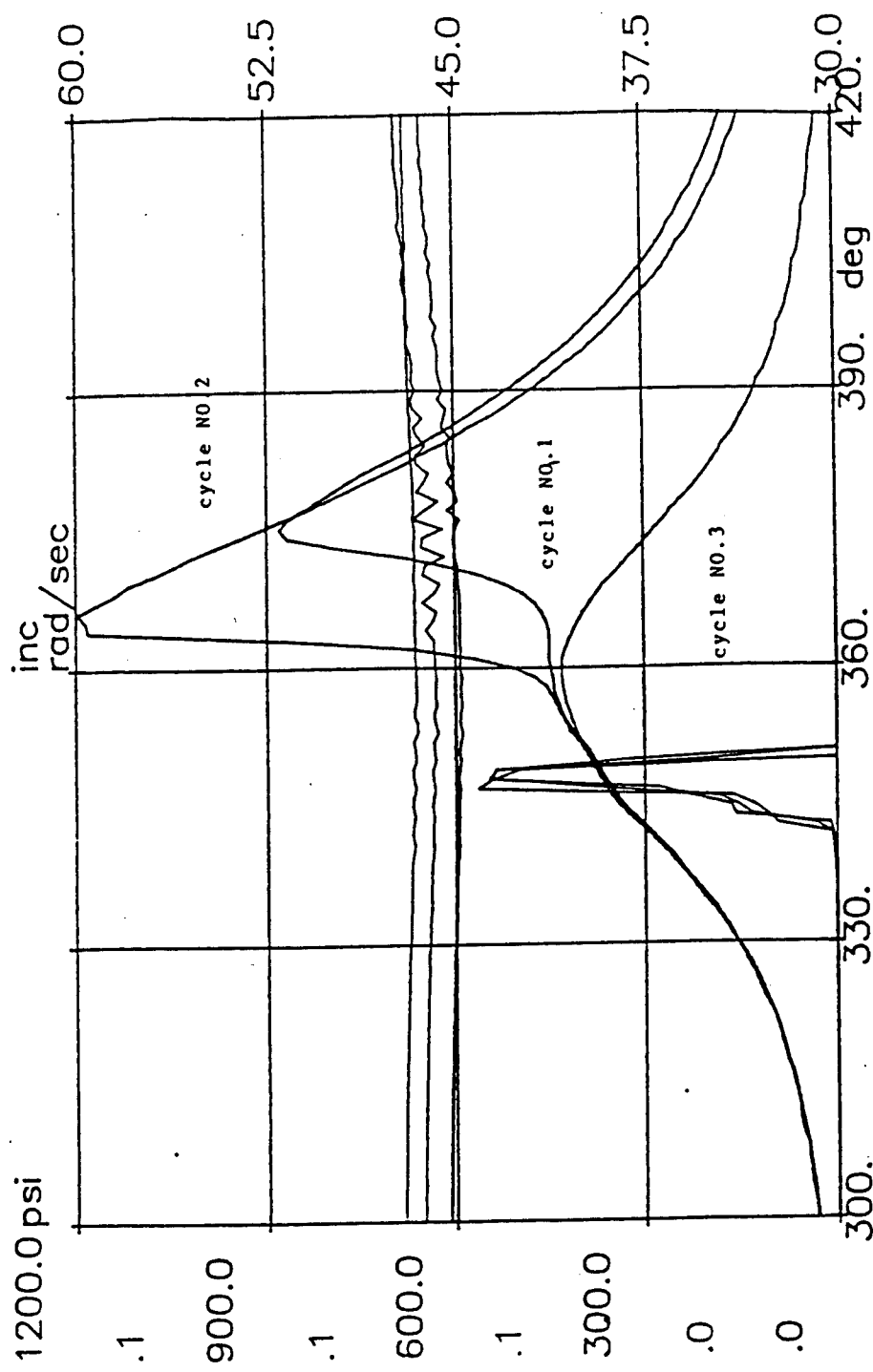
CYLINDER GAS TEMPERATURE AT START OF INJECTION  
FOR CYCLES 22 TO 29 [DEUTZ ENGINE]



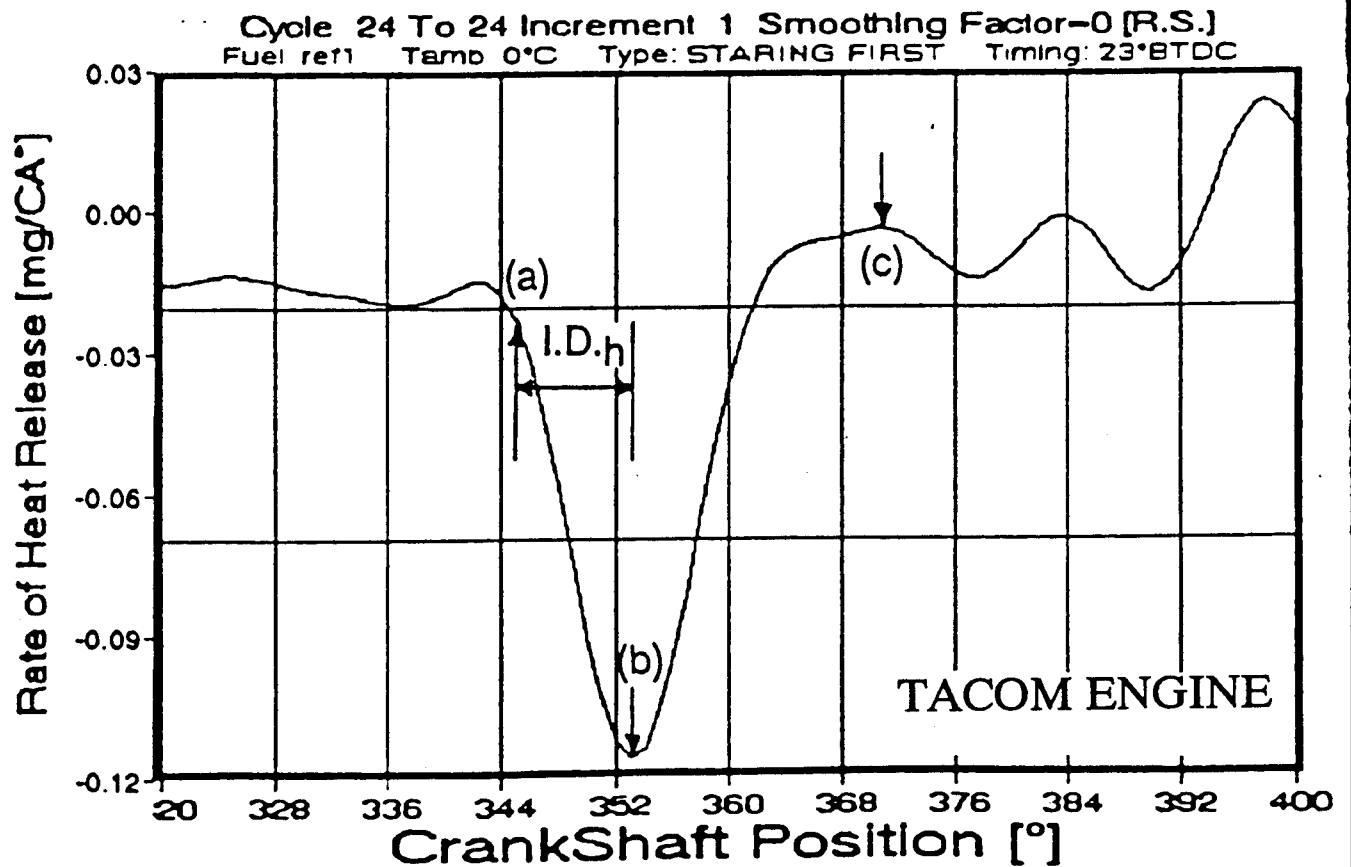
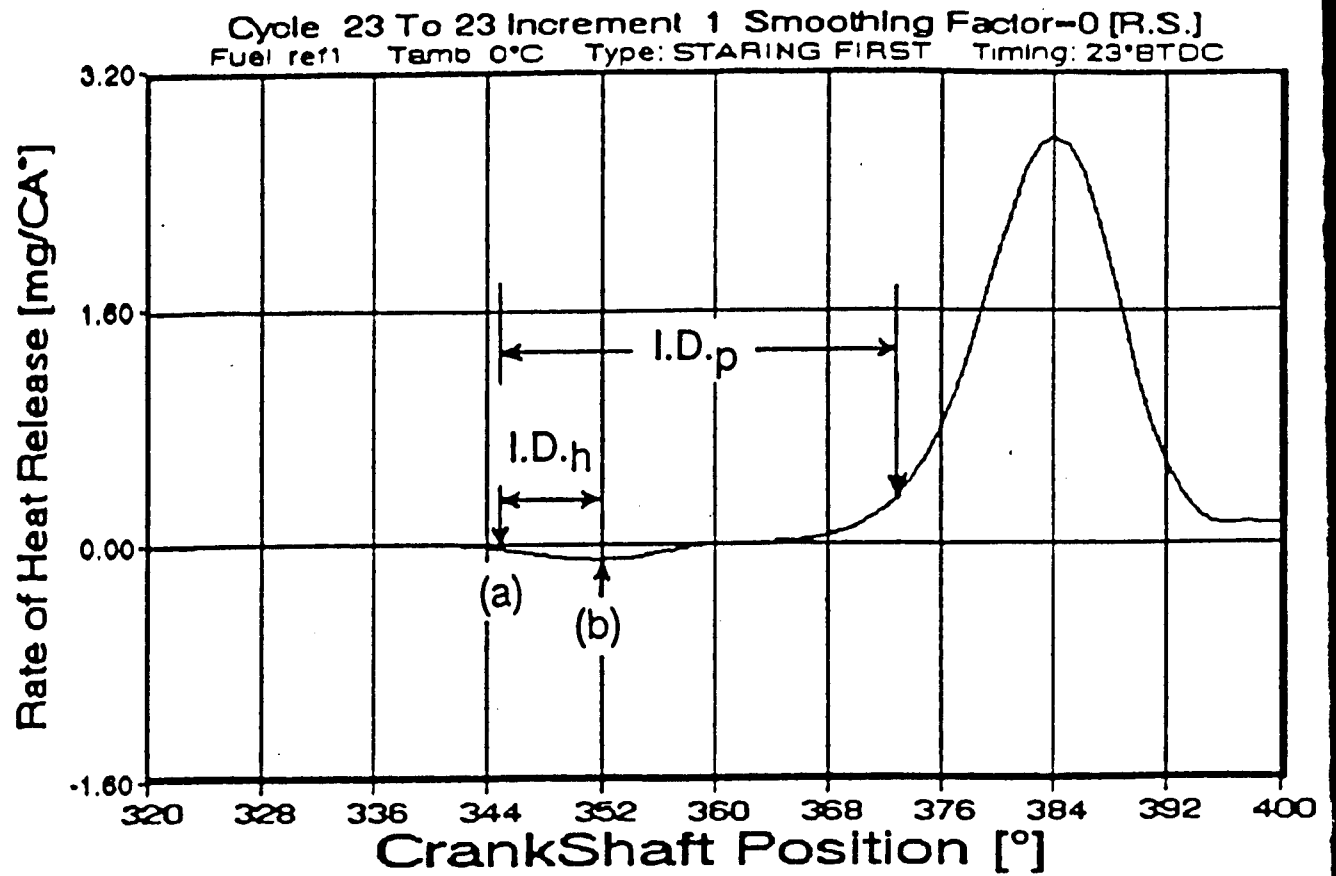
$T_{\text{ambient}} = 0^{\circ}\text{C}$ , Fuel = Ref1, Timing =  $23^{\circ}\text{BTDC}$

# MINIMUM INSTANTANEOUS ANGULAR VELOCITY FOR 70 CYCLES [DEUTZ ENGINE]

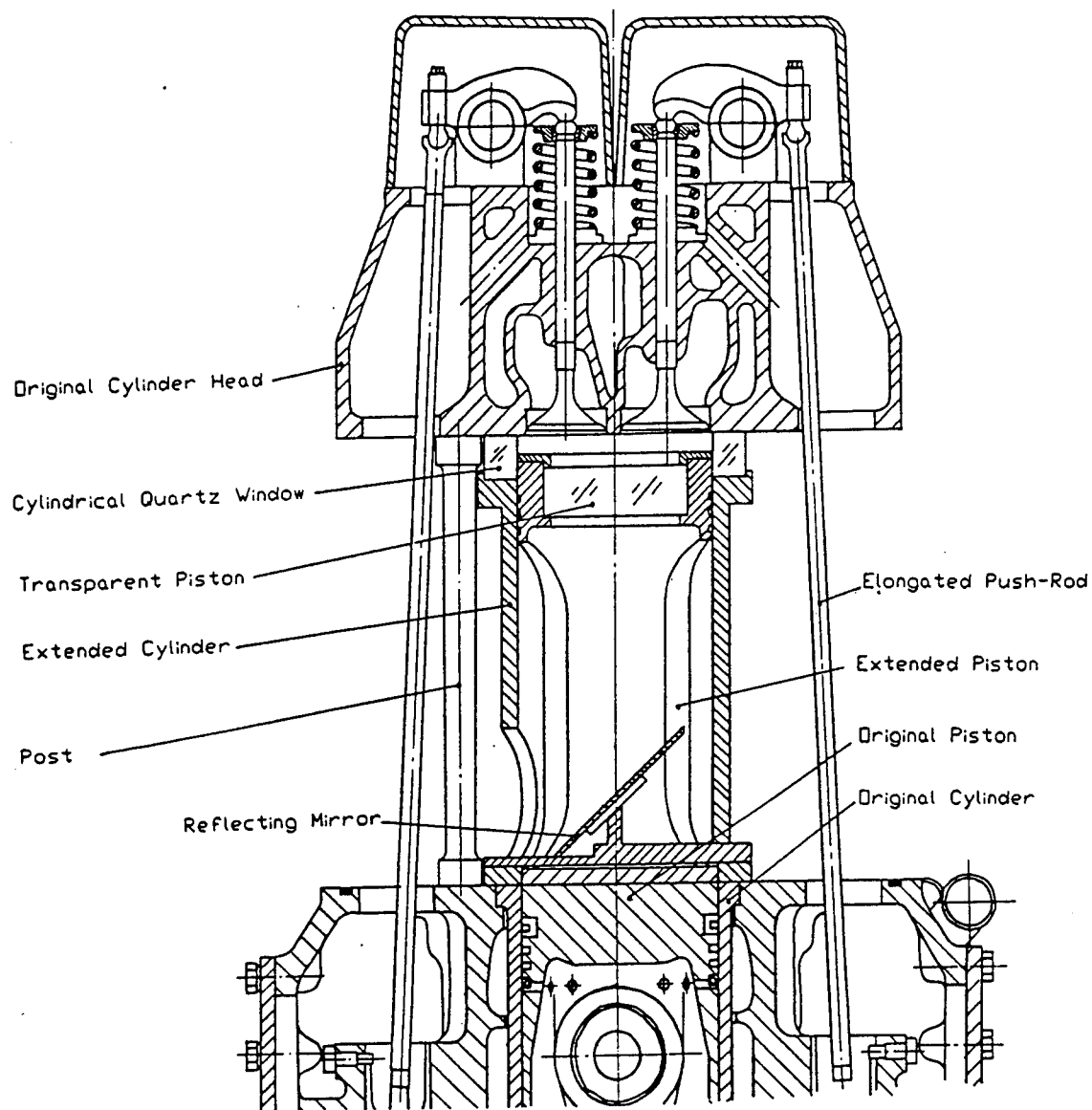




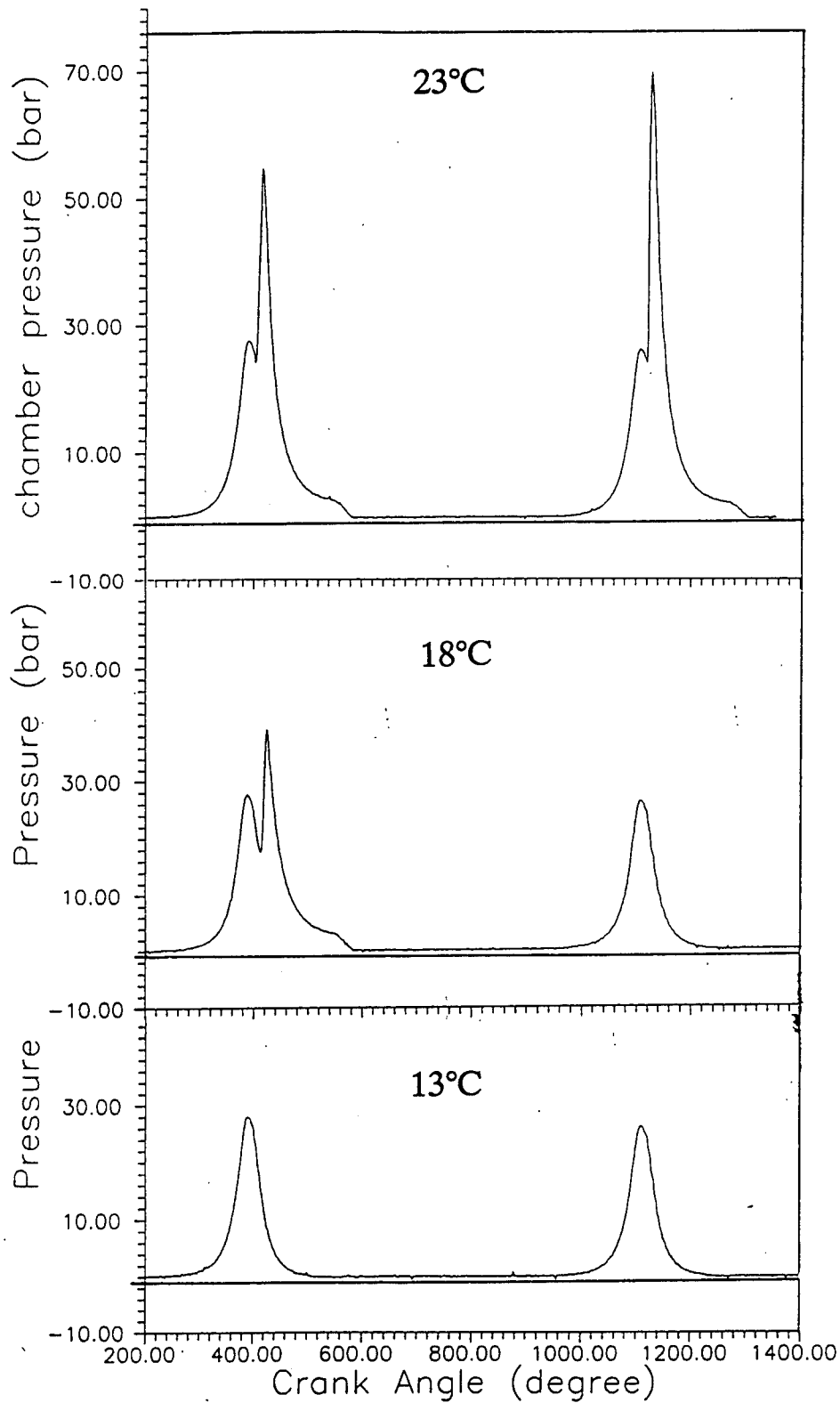
## COMBUSTION INSTABILITY DURING COLD STARTING IN TACOM ENGINE



RATE OF HEAT RELEASE FOR CYCLES 23 AND 24



**MODIFIED AVL ENGINE: EXTENDED  
CYLINDER/PISTON AND HEAD ASSEMBLY**



**EFFECT OF INLET AIR TEMPERATURE ON  
COMBUSTION STABILITY [OPTIC ACCESS ENGINE]**

## CONCLUSIONS

- 1- COMBUSTION INSTABILITY DURING COLD STARTING IS NOT A RANDOM PROCESS. ENGINE MAY OPERATE ON A 16, 12, 8 OR 4-STROKE-CYCLE, DEPENDING ON THE AIR TEMPERATURE.
- 2- COMBUSTION INSTABILITY DURING COLD STARTING MAY NOT BE CAUSED BY A FAILURE OF THE AUTOIGNITION PROCESS.
- 3- COMBUSTION INSTABILITY DURING COLD STARTING IS NOT ENGINE OR FUEL SPECIFIC.
- 4- COMBUSTION INSTABILITY DURING COLD STARTING IS CAUSED BY A COMBINATION OF FACTORS RELATED TO ENGINE DYNAMICS AND COMBUSTION KINETICS.

## Effect of Thin Ceramic Coatings on Combustion and Emissions in a DI Diesel Engine

D. E. Klett  
Mechanical Engineering Department  
North Carolina A&T State University  
Greensboro, NC 27411

E. M. Afify  
Mechanical and Aerospace Engineering Department  
North Carolina State University  
Raleigh, NC 27607

An experimental and analytical study on the effect of thin ceramic coatings on soot and NO<sub>x</sub> emissions and performance of a direct injection diesel engine is being conducted jointly between North Carolina A&T State University and North Carolina State University.

Performance and emissions data have been gathered on a normally aspirated Ricardo Hydra single cylinder DI engine with various combinations of ceramic coatings installed. Thin ceramic thermal barrier coatings were applied to the piston crown and bowl, the head and valves, and the cylinder liner. The coated piston and head were run singly and in combination with the cylinder liner to investigate the effects of these different coated surfaces on emissions and performance for two different pure hydrocarbon fuels, hexadecane and dodecane. Coating the piston crown alone results in generally lower cylinder pressure, lower brake specific fuel consumption and lower NO<sub>x</sub> emission compared to the baseline engine. Soot emission is typically increased below 2000 RPM and decreased above 2000 RPM. Coating the head alone reduces cylinder pressure, but generally increases specific fuel consumption and NO<sub>x</sub> and soot emissions.

The analytical portion of the study involved modifications to the KIVA-II code and its use to model the Hydra engine with the thermal coatings. Modifications to the code include incorporation of an eddy-break-up combustion model to replace the standard Arrhenius single reaction model. A time dependent combustion surface temperature was also incorporated to simulate the effects of thermal barrier coatings on cylinder temperature, pressure and NO<sub>x</sub> production. A soot model was added to the code following the work of Magnussen and Hjertager. The EBU model gives better results for the diffusional portion of the combustion process, but fails to adequately model the premixed combustion, typically resulting in a lower predicted peak cylinder pressure (and temperature) than predicted by the single reaction model and shown by experiments. Consequently, the EBU model also under-predicts NO emission to a greater degree than the SR model. The KIVA-II modeling has led to an understanding of the effect of coating the piston on NO production. The hotter piston crown warms the intake air, shortening ignition delay and decreasing the ratio of premixed to diffusion combustion, ultimately resulting in lower peak cylinder temperature and reduced NO. The KIVA-II results agree reasonably well with the experimental data for cylinder pressure and NO and soot emission.

The work is continuing with the use of JP-8 fuel. Performance and emissions will be compared between the baseline engine and with the various coated surfaces with JP-8 as the fuel.

- **INVESTIGATED EFFECTS OF THIN THERMAL BARRIER COATINGS ON VARIOUS SURFACES ON PERFORMANCE AND EMISSIONS OF THE RICARDO HYDRA DI ENGINE**
- **TESTS WERE MADE WITH VARIOUS COMBINATIONS OF SURFACE COATINGS**
  - **PISTON CROWN**
  - **CYLINDER HEAD AND VALVE FACES**
  - **PISTON, HEAD AND CYLINDER LINER**
- **EFFECT ON BSFC, IGNITION DELAY, SMOKE, NOX**
- **EXPERIMENTAL RESULTS COMPARED WITH KIVA-II MODELING RESULTS**
- **KIVA-II MODEL INCLUDES EDDY-BREAK-UP COMBUSTION MODEL, SOOT MODEL AND COATED SURFACE THERMAL MODEL**
- **WORK IS CONTINUING CURRENTLY WITH JP-8 FUEL**

## THERMAL BARRIER COATINGS

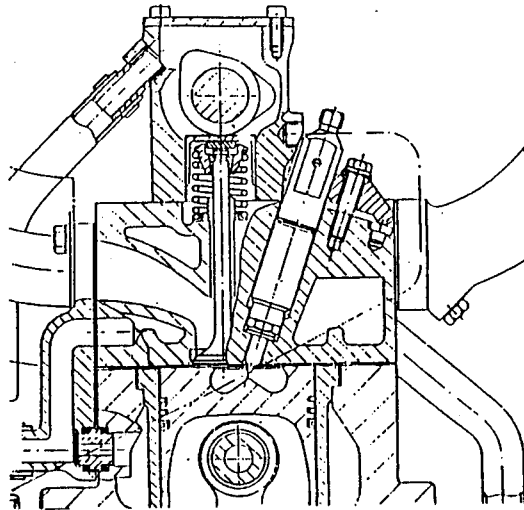
Piston Crown - 0.25 mm slurry sprayed PSZ  
 85% Cubic Zirconia, calcium partial stabilization  
 10% Tungsten Cobalt Chrome powder  
 5%  $\text{Cr}_2\text{O}_3$

Cylinder Liner - 0.75 mm Plasma Sprayed YSZ above TRR  
 0.2 mm slurry sprayed PSZ wear coat over  
 entire liner surface

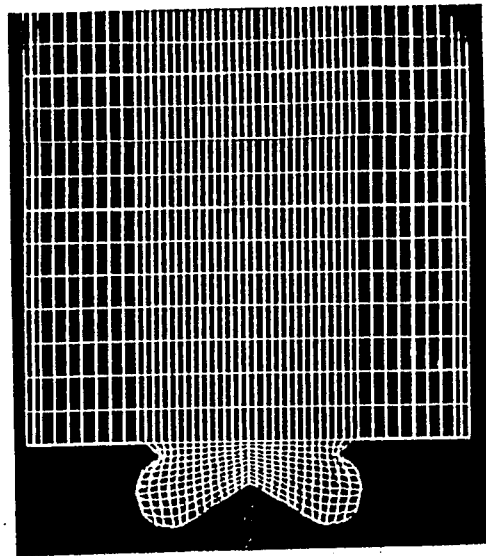
Head and Valves - 0.5 mm TBC with hollow Alumina spheres  
 65% Silica  
 15% PSZ  
 7% Tungsten Cobalt Chrome powder  
 8%  $\text{Cr}_2\text{O}_3$   
 5% Alumina spheres

TEST MATRIX				
Inj Timing (Deg BTDC)	16	18	20	22
BMEP (BAR)	2.24	3.35	3.91	4.47
Speed (RPM)	1000	1500	2000	2500
Engine Build	Baseline	Coated Piston	Coated Head	Coated Piston, Head, Liner

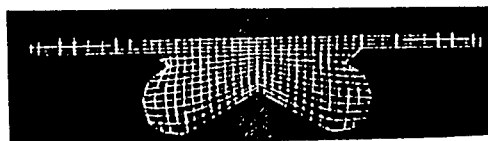




Cross Section of Ricardo Hydra DI Diesel Combustion Chamber

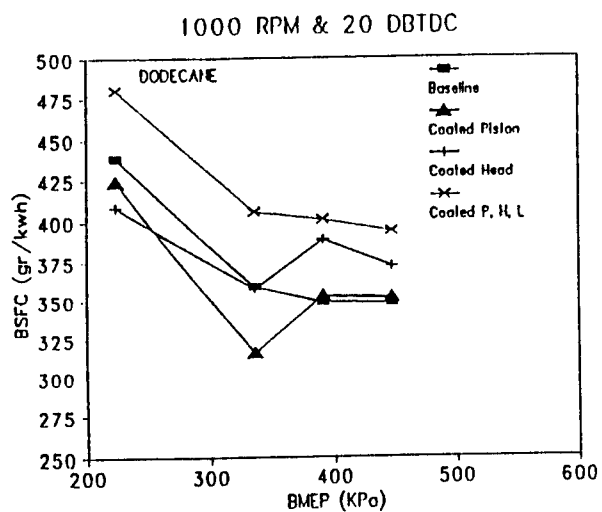


At 138 DBTDC

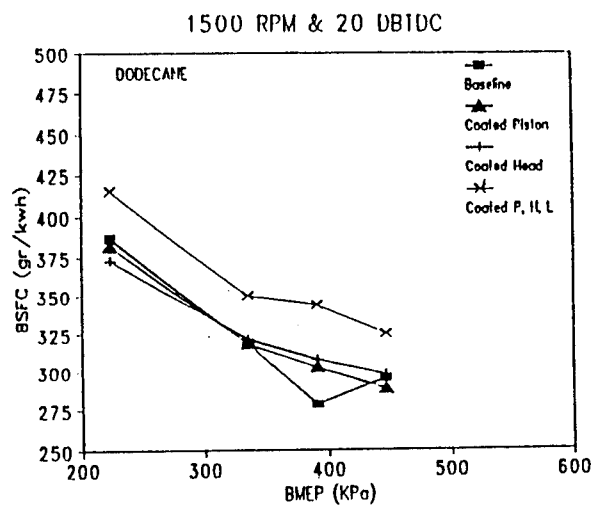


At TDC

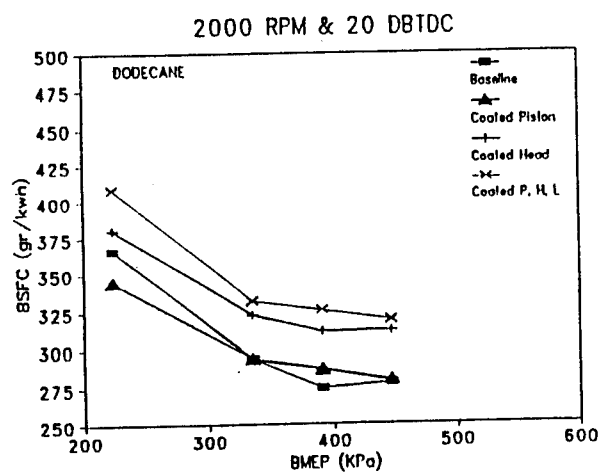
Computational Mesh Used to Model Ricardo Hydra DI Engine



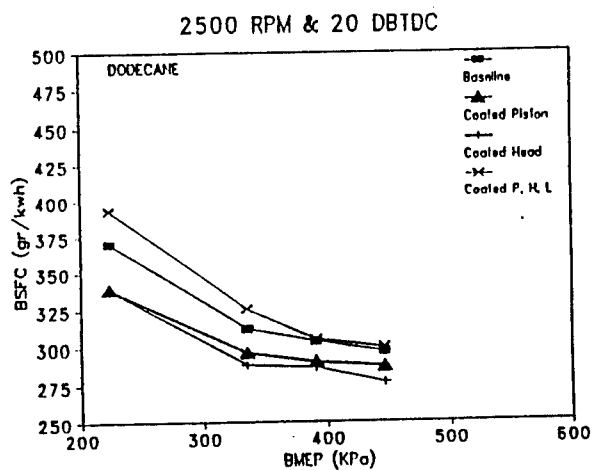
(a)



(b)

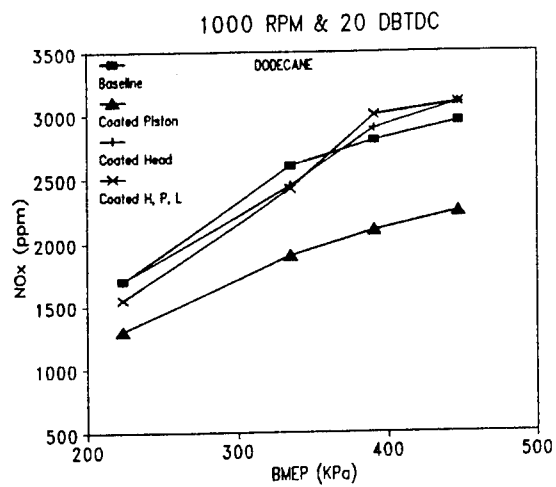


(c)

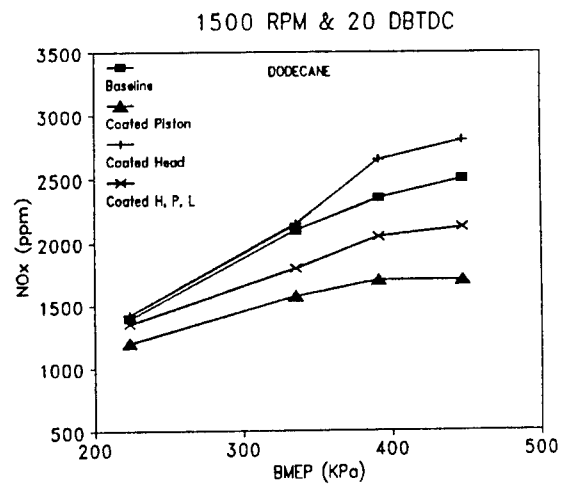


(d)

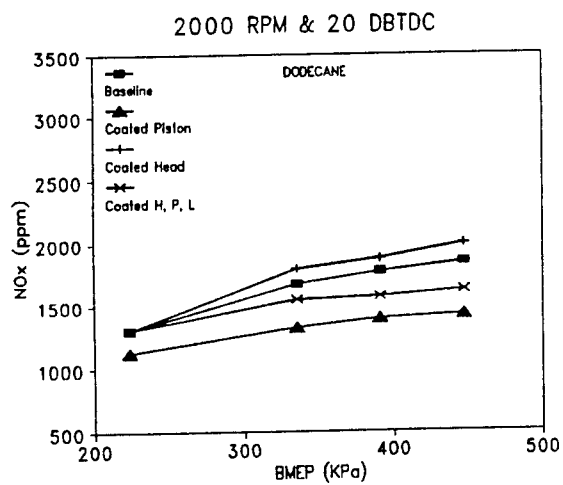
BSFC Versus Load for Dodecane Fuel at 20 Degrees BTDC



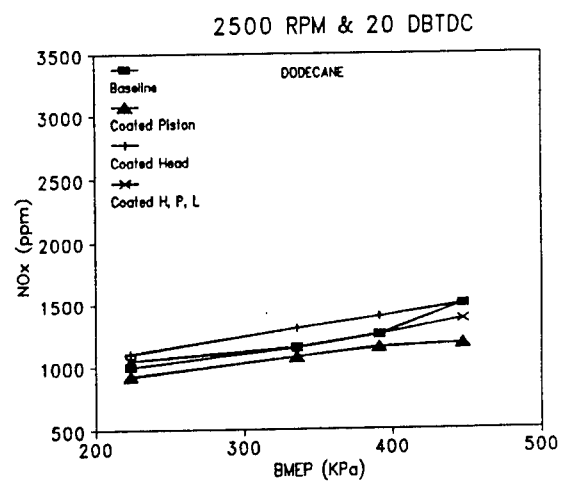
(a)



(b)

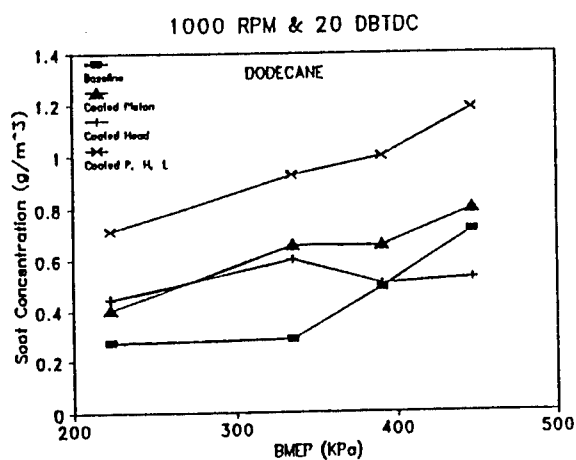


(c)

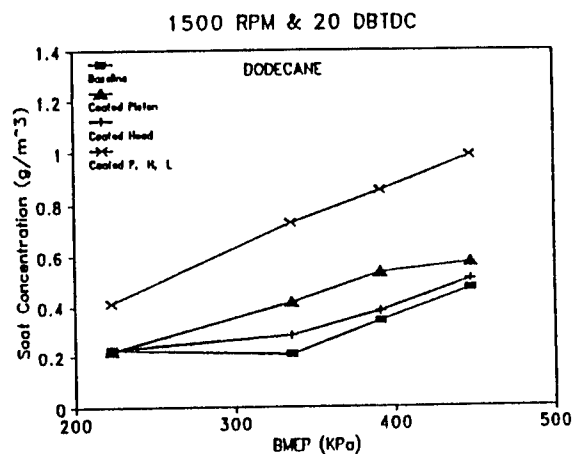


(d)

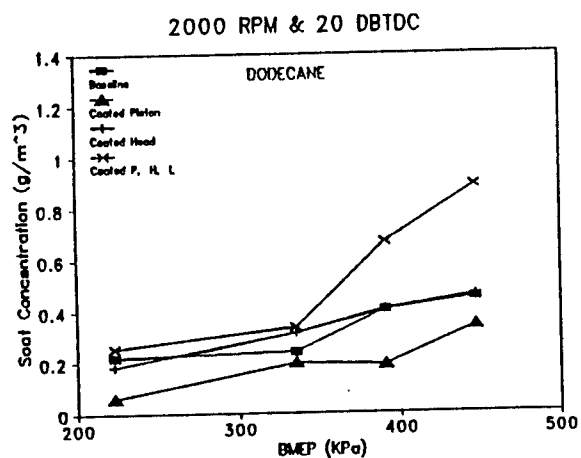
# NOx Versus Load for Dodecane Fuel at 20 Degrees BTDC



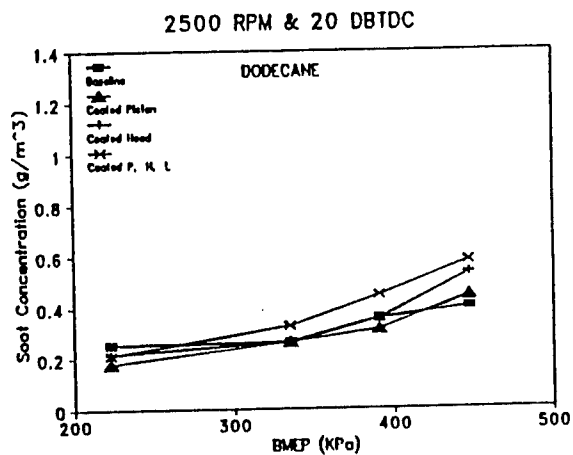
(a)



(b)

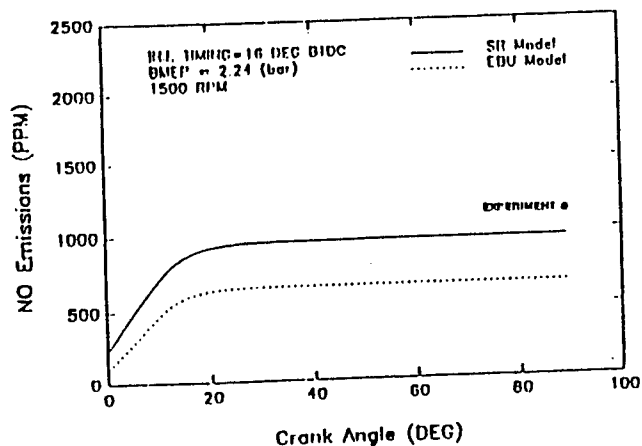


(c)

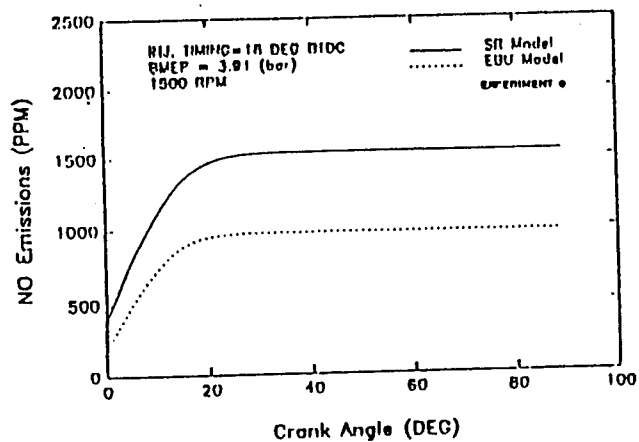


(d)

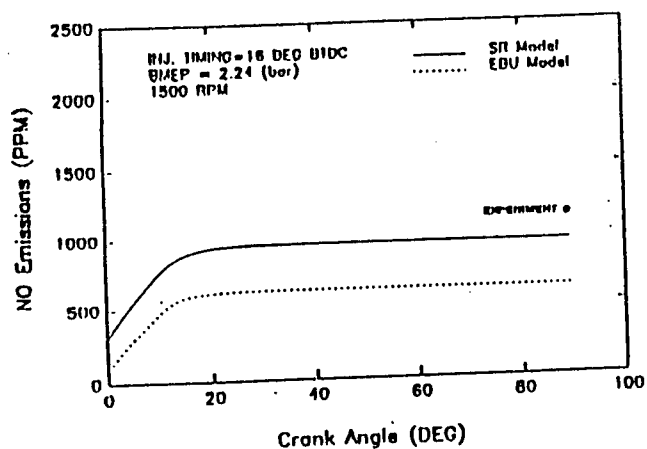
Soot Concentration Versus Load for Dodecane at 20 DBTDC



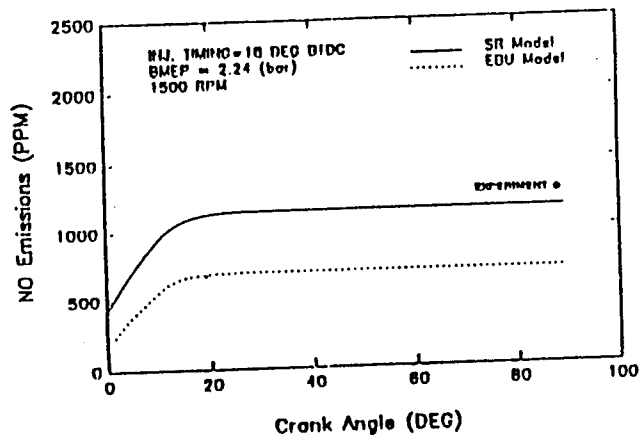
NO Emission Versus Crank Angle For Hexadecane Fuel  
1500 RPM, 16 Deg BTDC, 223 KPa BMEP



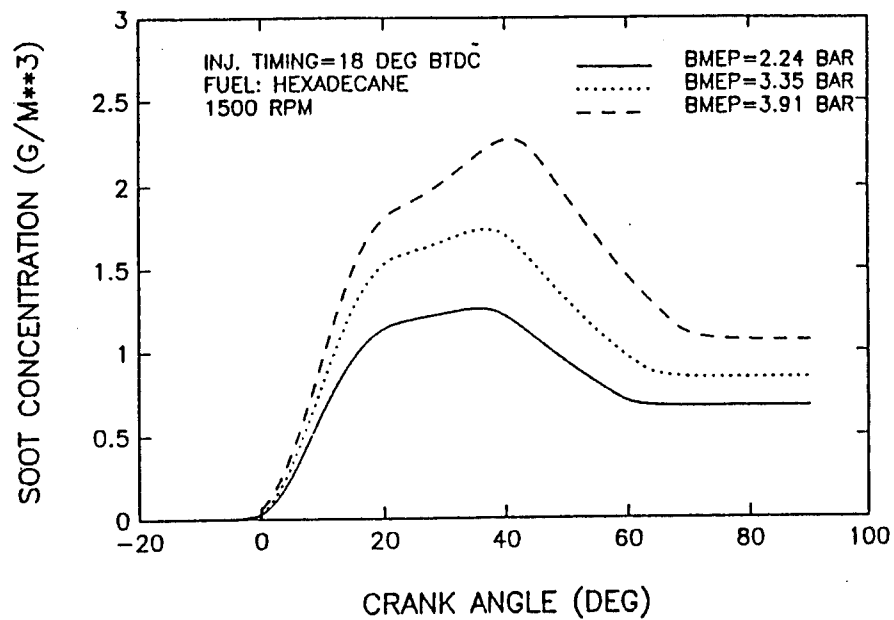
NO Emission Versus Crank Angle for Hexadecane Fuel  
1500 RPM, 18 Deg BTDC, 391 KPa BMEP



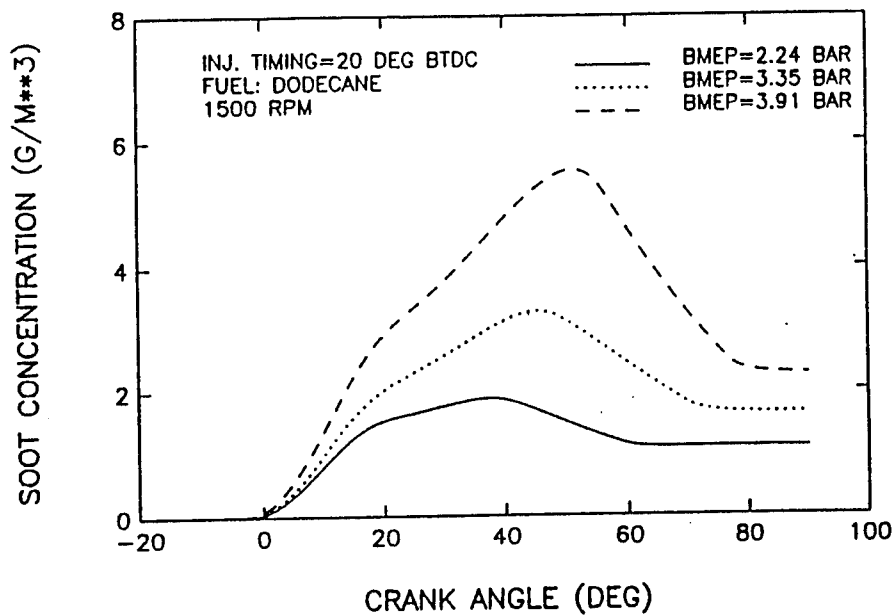
NO Emission Versus Crank Angle For Dodecane Fuel  
1500 RPM, 16 Deg BTDC, 223 KPa BMEP



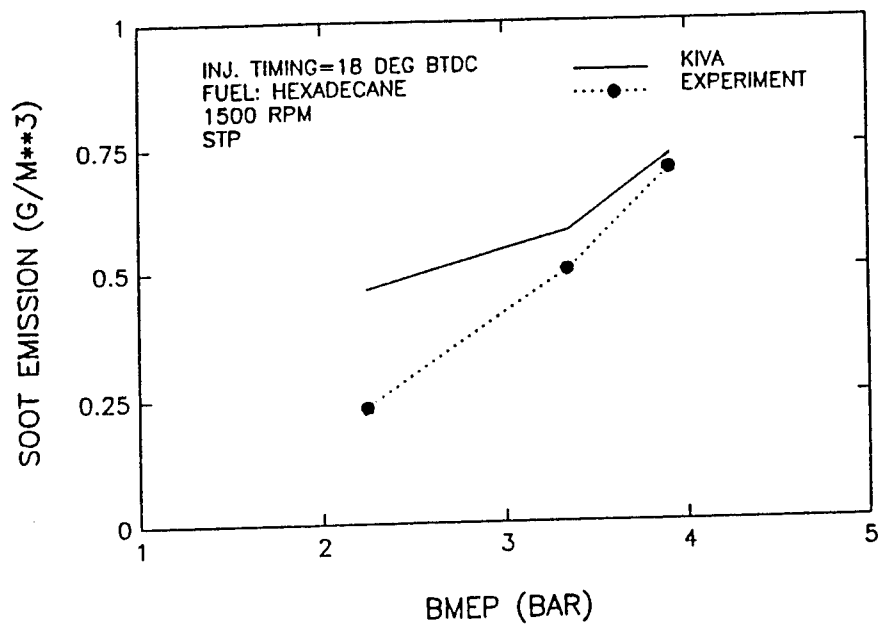
NO Emission Versus Crank Angle for Dodecane Fuel  
1500 RPM, 18 Deg BTDC, 223 KPa BMEP



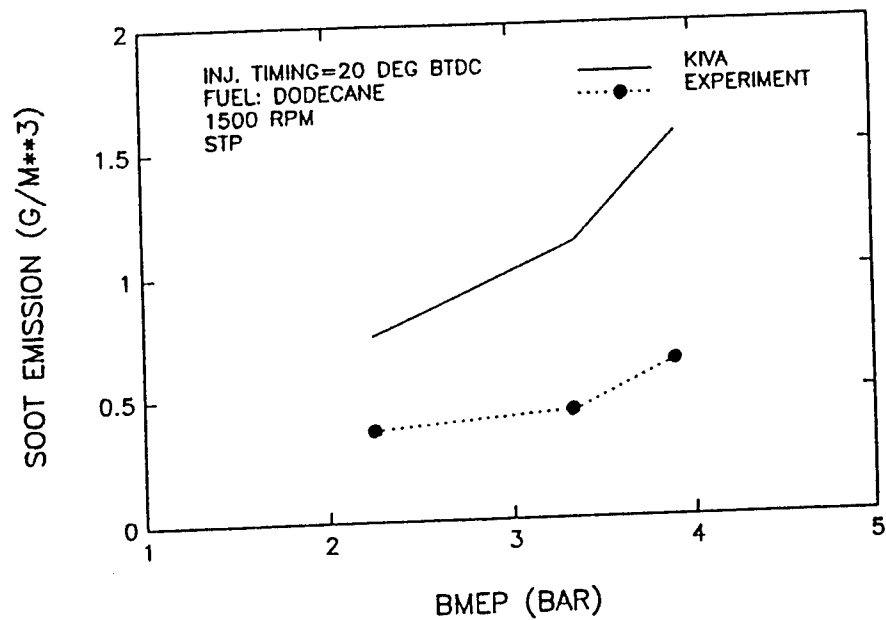
Soot Concentration Versus Crank Angle for Hexadecane



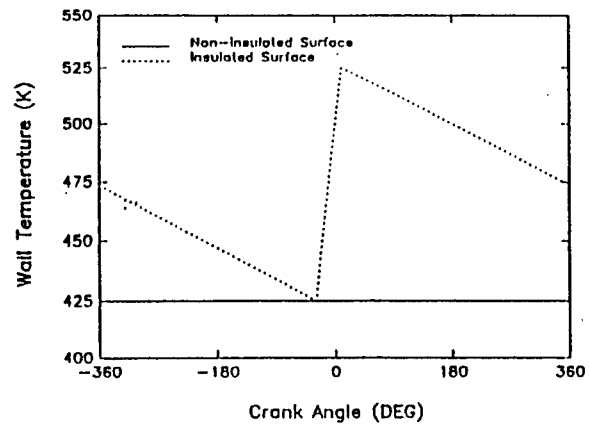
Soot Concentration Versus Crank Angle for Dodecane



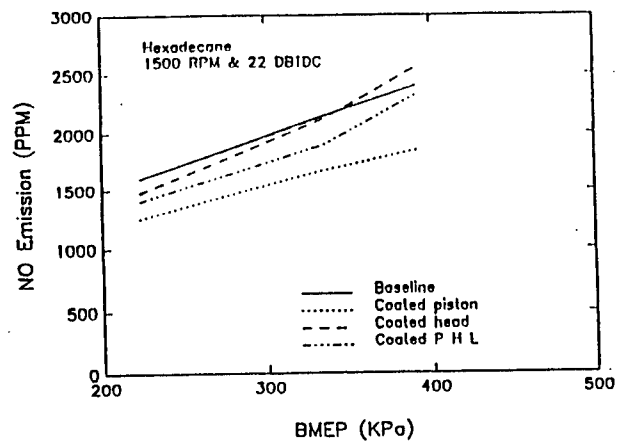
Soot Emission Versus Load for Hexadecane



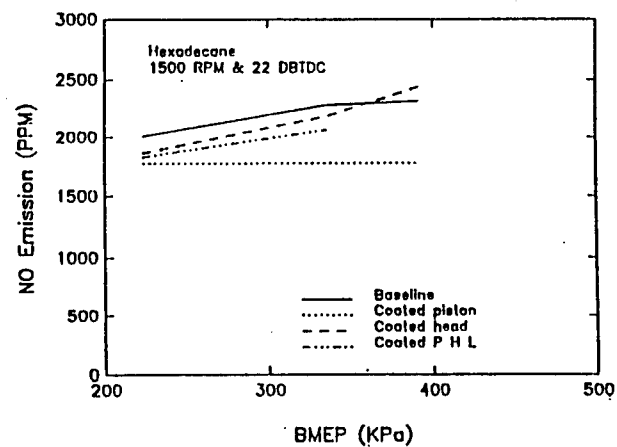
Soot Emission Versus Load for Dodecane



Assumed Coated Surface Temperature Versus Crank Angle Profile

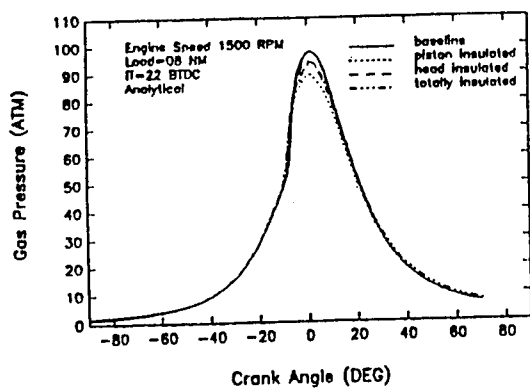


Experimental Results For NO Emission Versus Load  
For Hexadecane at 1500 RPM and 22 DBTDC Injection Timing

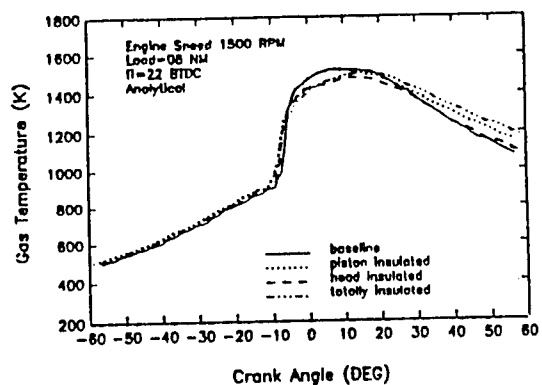


KIVA Results For NO Emission Versus Load  
For Hexadecane at 1500 RPM and 22 DBTDC Injection Timing

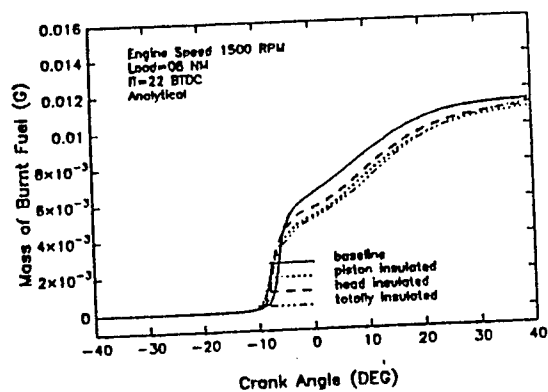




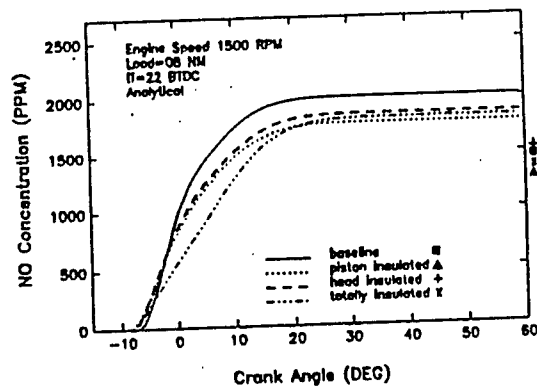
Cylinder Gas Pressure Versus Crank Angle



Cylinder Gas Temperature Versus Crank Angle

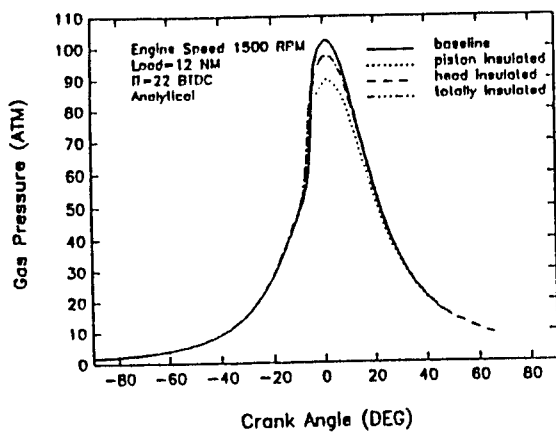


Mass of Fuel Burnt Versus Crank Angle

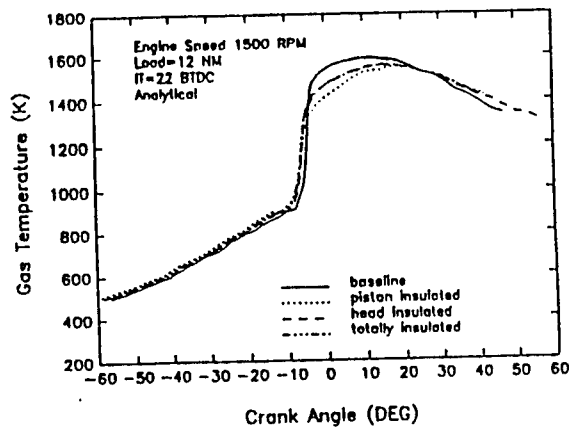


Nitric Oxide Concentration Versus Crank Angle

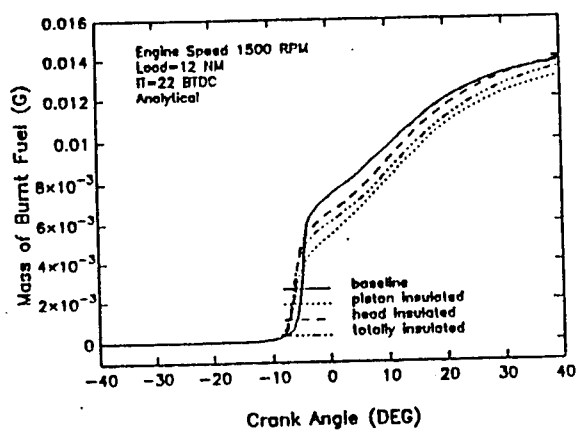
KIVA Results for 1500 RPM, 22 DBTDC and 223 KPa BMEP Load (8 NM Torque)



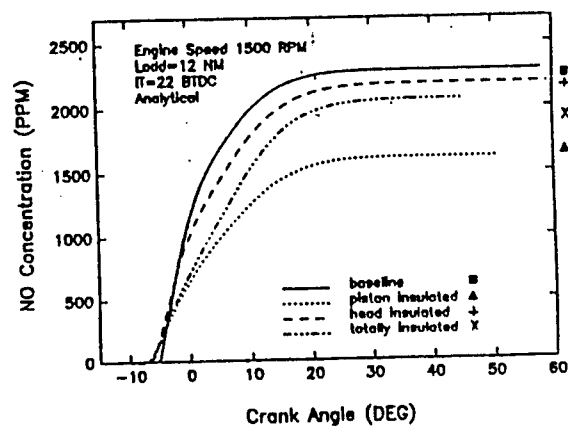
Cylinder Gas Pressure Versus Crank Angle



Cylinder Gas Temperature Versus Crank Angle

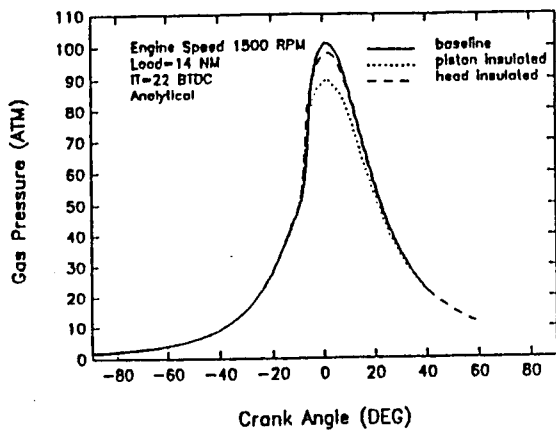


Mass of Fuel Burnt Versus Crank Angle

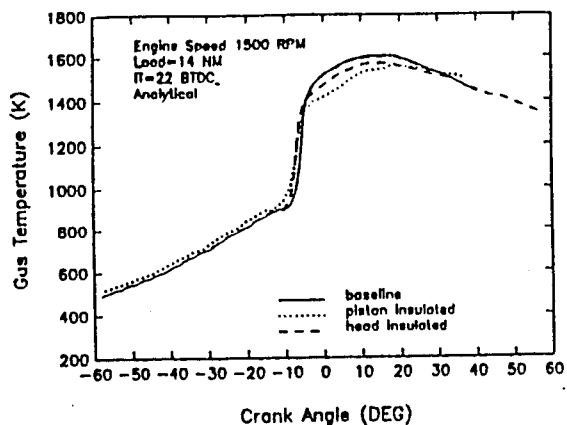


Nitric Oxide Concentration Versus Crank Angle

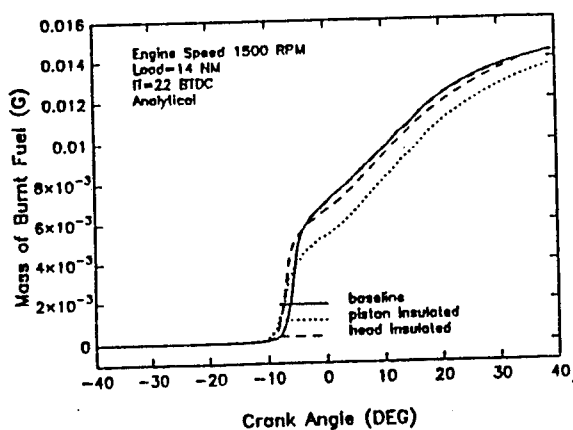
KIVA Results for 1500 RPM, 22 DBTDC and 335 KPa BMEP Load (12 NM Torque)



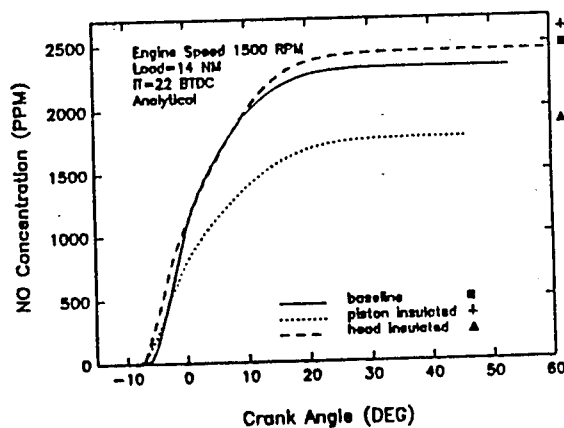
Cylinder Gas Pressure Versus Crank Angle



Cylinder Gas Temperature Versus Crank Angle



Mass of Fuel Burnt Versus Crank Angle



Nitric Oxide Concentration Versus Crank Angle

KIVA Results for 1500 RPM, 22 DBTDC and 391 KPa BMEP Load (14 NM Torque)

## DIESEL COMBUSTION MODELING AT THE ENGINE RESEARCH CENTER

C. J. Rutland and R. D. Reitz  
Engine Research Center  
Department of Mechanical Engineering  
University of Wisconsin - Madison  
Madison, WI 53706

Modeling diesel combustion presents several unique challenges. In addition to turbulence effects that must be considered, the combustion occurs in several distinct phases: ignition, premixed, and diffusion. The combustion models also rely heavily on accurate spray breakup and evaporation models to predict the gaseous fuel distributions prior to combustion.

At the ERC two major combustion modeling approaches are being pursued. The first is a characteristic time scale based model. This approach has been under development for some time and is performing very well for a variety of engine conditions. The second approach is based on flamelet concepts and attempts to model the physics more directly. This method is newer and still under development, but is performing fairly well for several cases. The flamelet approach offers more potential as turbulence modeling moves towards large eddy simulations and as emissions models are coupled into combustion models.

Both approaches use ignition modeling based on the Shell low temperature multi-step kinetics model. This is a reduced mechanism consisting of eight reactions using fuel, oxygen and five generic, intermediate species. The model was designed to simulate auto-ignition and has been adjusted to work well for diesel ignition over a wide range of conditions.

In the time scale based combustion model the reaction rate is determined by the product of an inverse time scale and the difference between the local species mass fractions and their local thermodynamic equilibrium values. The time scale is a linear combination of a global, Arrhenius reaction time scale and a turbulent mixing time scale. The Arrhenius time scale represents the laminar burning and the mixing time scale represents the turbulent, diffusion combustion. An exponential sliding factor is used to smoothly transition between the time scales.

The flamelet model uses a similar global Arrhenius reaction for the premixed combustion. However, for the turbulent diffusion combustion, a coherent flamelet model is used. In this approach, the reaction rate is the product of a flame area per unit volume and a laminar, flamelet consumption rate. The flame area is determined from a transport equation that includes turbulent mixing and terms that represent flame area sources and sinks. The main source of flame area is turbulent stretching. Sink or destruction mechanisms are included for flame sheet collisions, reactant depletion, front propagation, and wall effects.

Both combustion modeling approaches require criteria and mechanisms for modeling the transition between the different types of burning. The main criteria for the end of ignition and start of premixed burning is the local temperature. In the flamelet model this is augmented by a second criterion based on heat release rates.

The transition between premixed combustion and turbulent diffusion burning is more difficult. In the time scale model it is handled by monitoring the amount of local combustion products to indicate the progress of the reaction. In the flamelet model, the transition uses a Damköhler number criterion and occurs when the mixing time is slow compared to the reaction time scale. Then, premixed burning can continue with previously vaporized fuel, but as the remaining fuel vaporizes it goes into the turbulent diffusion model.

Overall, the combustion models compare very well with engine data. The flamelet model has shown good agreement on several cases to date and is able to accurately capture the different types of combustion. The time scale model has shown excellent agreement for a wide range of injection timings and pressures, and for many difficult to model split injection cases.

Work supported by: ARO Contract # DAAL03-92-G-0122, DOE/NASA Lewis Contract # NAG3-1087, Caterpillar; with computational resources provided by TACOM, Cray Research, and SDSC.

# Diesel Combustion Modeling at the Engine Research Center

**C. J. Rutland**

**R.D. Reitz**

**Engine Research Center University of Wisconsin - Madison**

**Work Supported by: ARO Contract # DAAL03-92-G-0122,  
DOE/NASA Lewis Contract # NAG3-1087  
Caterpillar**

**Computational Support from: TACOM, Cray Research, and SDSC**

## Diesel Combustion

### Spray

- Atomization
- Breakup
- Vaporization



### Combustion

- Ignition
- Premixed burning
- Diffusion burning

} kinetics controlled  
} mixing controlled

## **Spray Modeling**

---

- **Atomization and breakup models**
  - Use unstable wave growth analysis
  - Provides breakup time scale and droplet size
- **Drag modified to include droplet distortion**
- **Breakup parameters adjusted for wall interactions**
- **Multi-component vaporization completed and currently being tested**

## **Combustion Modeling Approaches**

---

- **Characteristic Time Scale Approach**
  - Very well developed
  - Performing very well over a wide range of engine conditions
- **Flamelet Approach**
  - Newer model
  - Good performance on several cases
  - Offers more potential:
    - Better fit with large eddy simulations
    - Better coupling to emissions models

## Ignition Modeling

- **Based on Shell Model**
  - Low temperature, multi-step kinetics
  - Uses Fuel, Oxygen and 5 generic species
  - Has 8 reactions representing initiation, branching, propagation and termination
- **Modified for Diesel Ignition**
  - Validated using bomb data for diesel fuel
  - Applied independently in each grid cell

## Characteristic Time Scale Combustion Modeling

- **Uses Local and Equilibrium Concentrations**

$$Rate = \frac{\text{Local concentration} - \text{Equilibrium concentration}}{\tau_{\text{laminar}} + f \tau_{\text{turbulent}}}$$

- **Uses Characteristic Laminar and Turbulent Time Scales**

$$\tau_{\text{laminar}} = A \exp(E/RT)$$

$$\tau_{\text{turbulent}} = C_2 k / \epsilon \quad (f = \text{delay coefficient})$$

## Flamelet Modeling

- Premixed Combustion
  - Uses same laminar global reaction model as the characteristic time scale approach
  - Premixed burning can continue in same cell in which diffusion combustion has begun
- Diffusion Combustion
  - Based on coherent flamelet approach
  - Reaction rate uses local chemistry and flame area per unit volume

$$Rate = \rho V_D \Sigma$$

## Diffusion Combustion Model

- Laminar Mass Burning Rate:  $\rho V_D$ 
  - From 1D analysis of diffusion flame
  - Uses modified local concentrations
- Flame Area:  $\Sigma$ 
  - Obtained from turbulent transport equation

$$\frac{\partial}{\partial t}(\bar{\rho}\tilde{\Sigma}) + \nabla \cdot ((\bar{\rho}\tilde{\Sigma})\tilde{u}) = \nabla \cdot \left( \frac{\mu_{turb}}{\sigma_s} \nabla \left( \frac{\bar{\rho}\tilde{\Sigma}}{\bar{\rho}} \right) \right) + \alpha \bar{\rho} \tilde{\epsilon}_s \tilde{\Sigma} - \beta f(\tilde{\Sigma}^2)$$

- Source for  $\Sigma$  from turbulent stretching
- Destruction of  $\Sigma$  from:
 

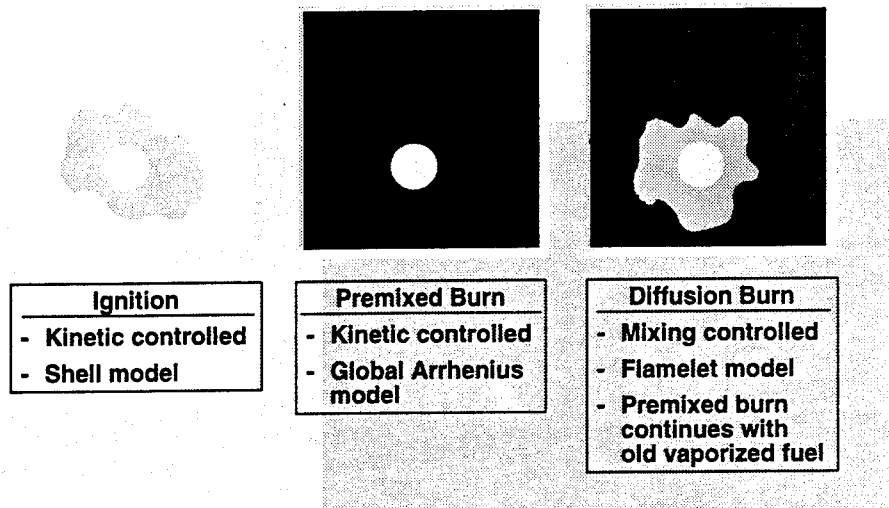
reactant depletion	wall effects
flame interaction	over stretching



## Diesel Flamelet Modeling

- Vaporizing Fuel
  - Initially, the vaporizing fuel goes to premixed burning
  - After diffusion flame is established in a cell, vaporizing fuel goes to diffusion burning
- Implementation
  - Transport equation for vaporized premixed fuel mass fraction
  - Transport equation for inerts to determine actual flame stoichiometry

## Physical Interpretation



## Ignition to Premixed Transition

- **Local Temperature Criteria**
  - Switch to high temperature kinetics (premixed combustion) when  $T > 1000 \text{ K}$
  - Used by both modeling approaches
- **Heat Release Rate Criteria (flamelet approach)**
  - Use linear combination of ignition and premixed heat release rates during transition
  - Helps prevent instabilities during transition

## Premixed to Diffusion Transition

- **Characteristic Time Scale Approach**
  - Combine laminar and turbulent time scales with exponential sliding factor,  $f$
  - Transition factor increases as reaction progresses
  - Reaction progress monitored by products
- **Flamelet Approach**
  - Mixing controlled: diffusion flame initiated when local Damköhler number becomes large

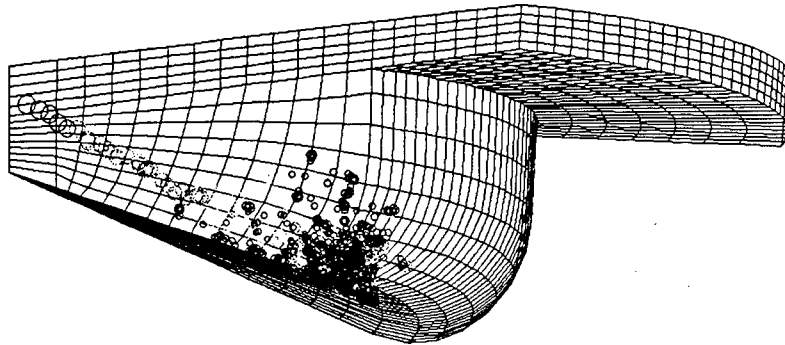
$$Da = \frac{A \exp(-E_A/RT)}{\varepsilon/k}$$

- Initial flame area equal to local drop surface area

## Engine Simulations

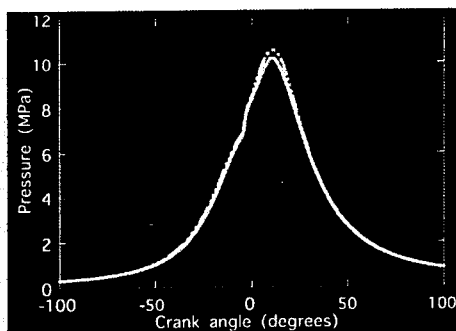
- **Caterpillar Engine**
  - Compression ratio 14.5
  - Displacement 2.44 liters
  - Injector 6 holes, up to 90 MPa
  - Speed and equiv ratio 1600 rpm, 0.48

single cylinder 3406

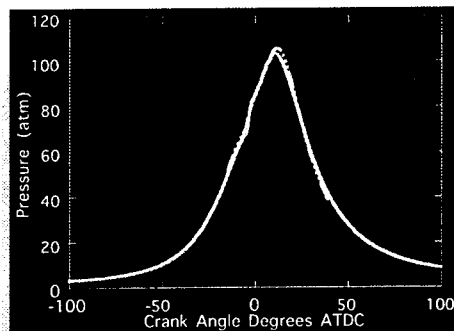


## Pressure Traces

Characteristic Time Scale



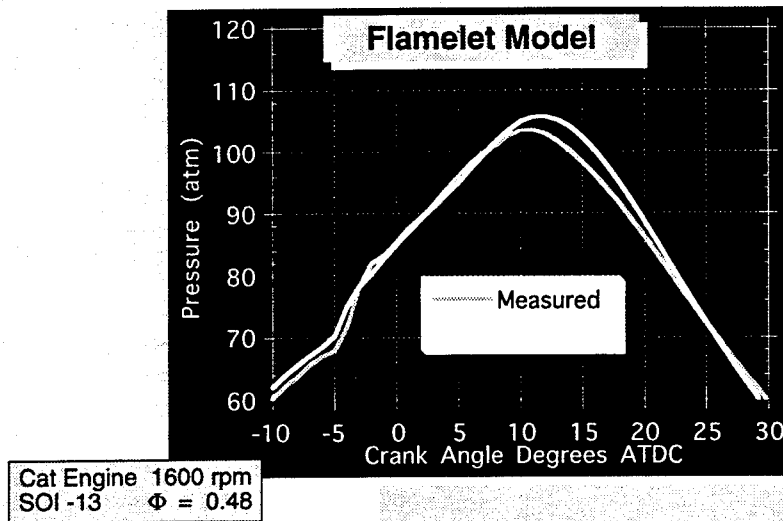
Flamelet



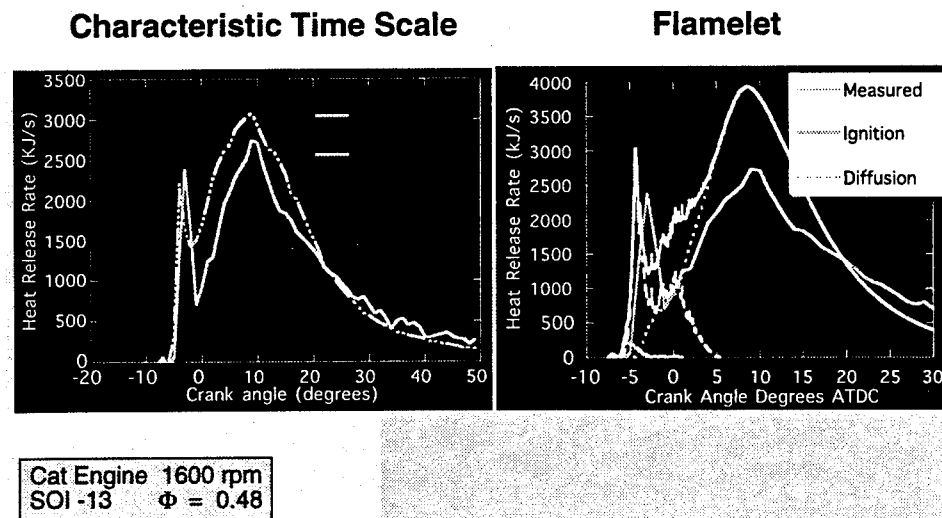
Cat Engine 1600 rpm  
SOI -13  $\Phi = 0.48$

— Computed  
— Measured

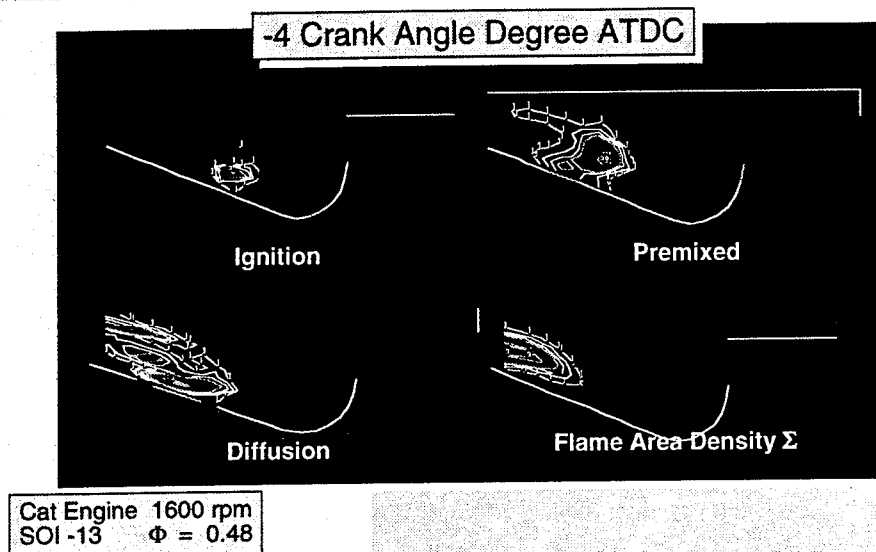
## Detail of Pressure Trace



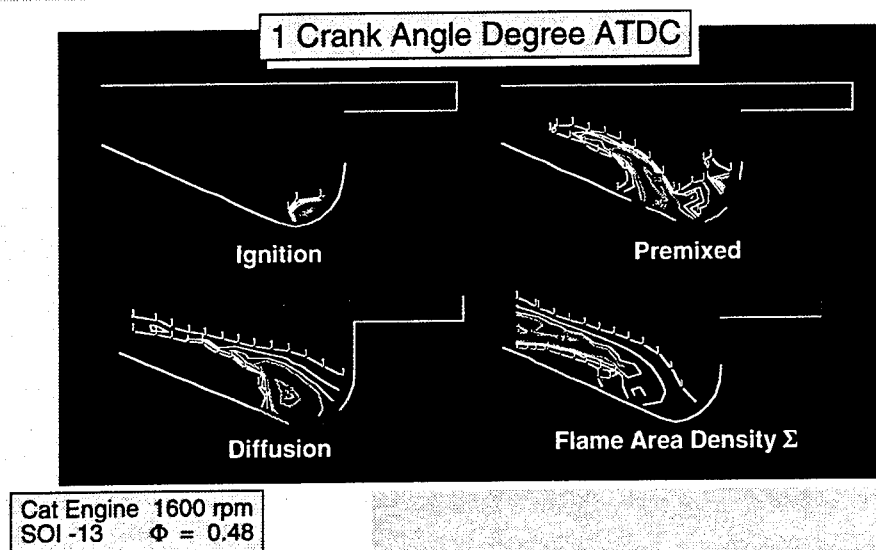
## Heat Release



## Heat Release Contours: Flamelet



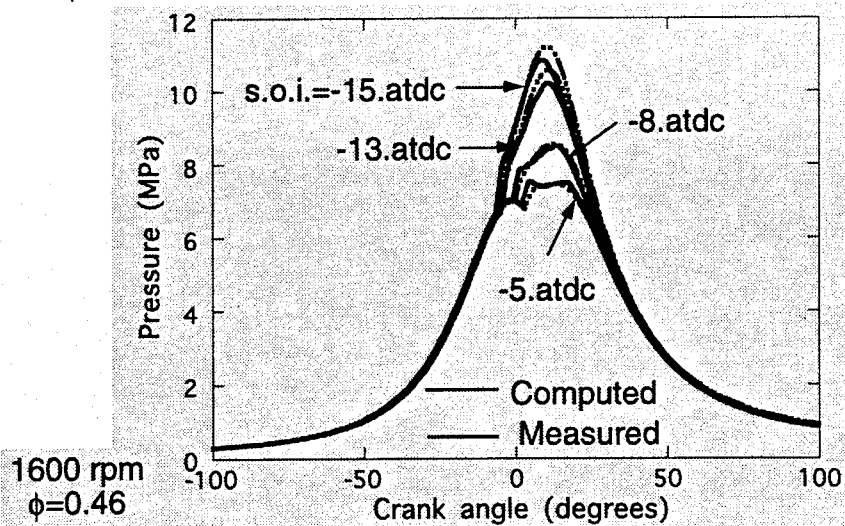
## Heat Release Contours: Flamelet



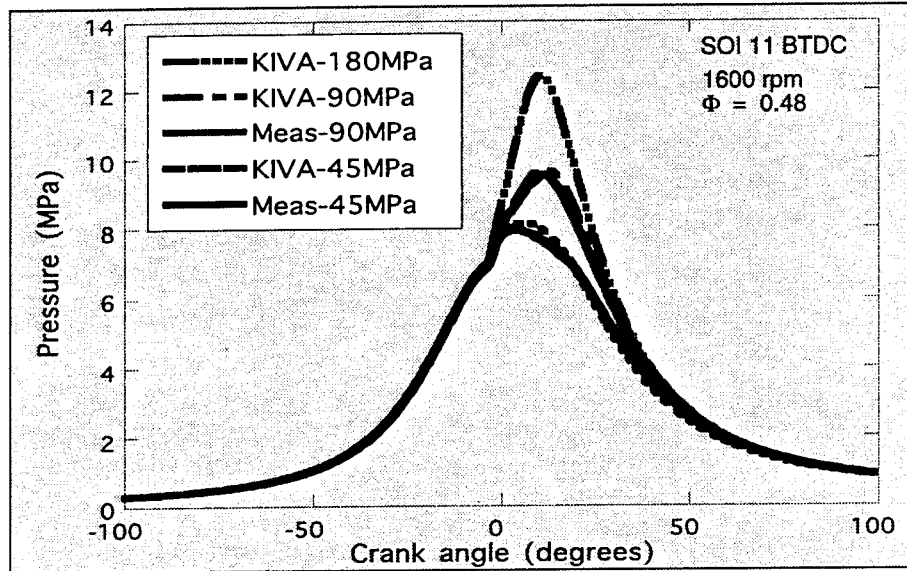
## Detailed Results from the Characteristic Time Scale Model

- Effects of Injection Timing
- Effects of Injection Pressure
- Results of Emissions Modeling
- Split Injection Results
- Alternative Turbulence Modeling

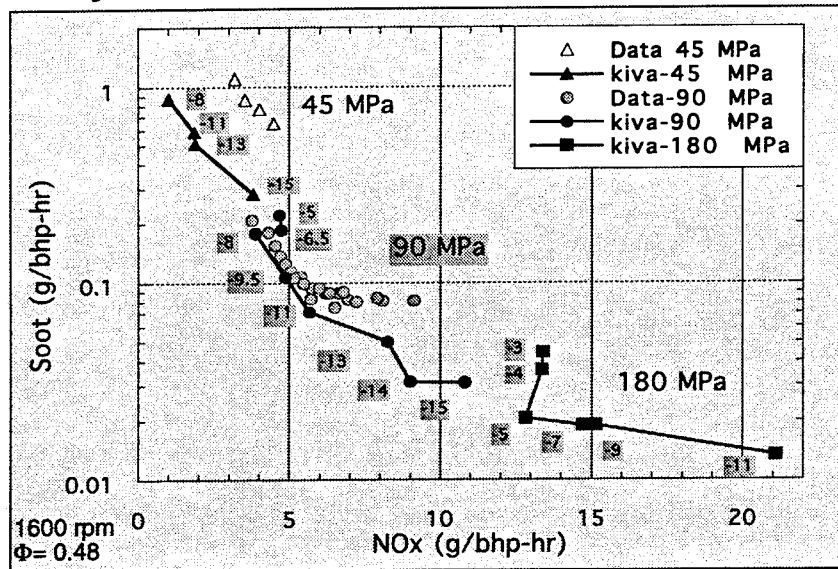
### Effects of Injection Timing



## Effects of Injection Pressure



## Injection Pressure and Emissions



## Emissions Modeling

Temperature

H= 2370 K

L= 958 K

NOx-Mass Fraction

H=0.60 g/kg

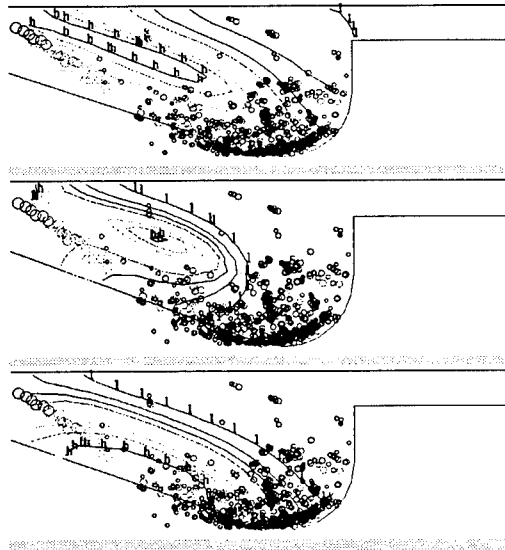
L=0.06 g/kg

Soot-Mass Fraction

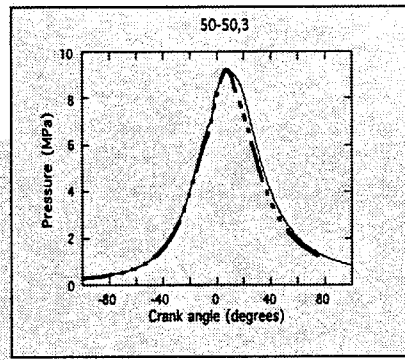
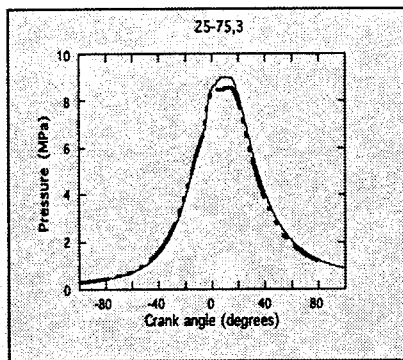
H=0.80 g/kg

L=0.08 g/kg

Cat Engine 7<sup>0</sup> ATDC



## Split Injection Results



50% - 50%

25% - 75%

3 degree dwell

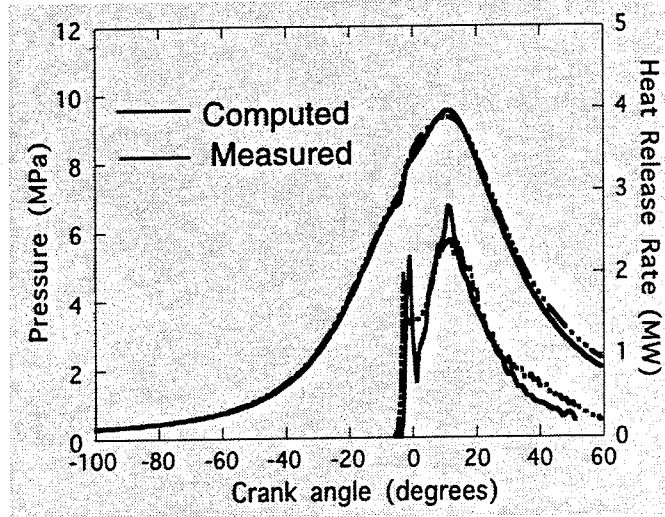


— Computed  
- - - Measured



## Alternative Turbulence Model

Results for RNG modification of  $\epsilon$  equation



## Summary

- Two Approaches to Combustion Modeling
  - Characteristic time scale and flamelet methods
  - Both methods perform well
- Modeling Provides Important Information
  - Effects of injection pressure and timing
  - Detailed information about flow, heat release and emissions
- Future Directions
  - Improve burning transitions
  - Improve spray models
  - Improve turbulence and spray mixing models

## List of Invitees

John Abraham  
University of Minnesota  
463 Mechanical Engineering  
111 Church Street, S.E.  
Minneapolis, MN 55455  
Tel (612) 625-3864  
Fax (612) 624-1398

E.M. Afify  
North Carolina State University  
Dept. of Mech. and Aero. Engrg.  
Raleigh, NC 27650  
Tel  
Fax

John Bailey  
Caterpillar Tractor Co.  
Research, General Offices  
100 N.E. Adamms, Tech. Center  
Peoria, IL 61629  
Tel  
Fax

Josette Bellan  
Jet Propulsion Laboratory  
Mail Stop 125/214  
4800 Oak Grove Drive  
Pasadena, CA 91109  
Tel (818) 354-6959  
Fax (818) 354-8153

Waldo Acosta  
Army Research Laboratory  
Vehicle Propulsion Directorate  
Lewis Research Center  
21000 Brookpark Road  
Cleveland, OH 44135-3127  
Tel  
Fax

Sandeep Ahuja  
Drexel University  
32 and Chestnut St.  
Philadelphia, PA 19104  
Tel (215) 895-1231  
Fax (215) 895-1264

Rodica Baranescu  
Navistar International  
Engine Division Engineering  
10400 West North Avenue  
Melrose Park, IL 60558  
Tel  
Fax

James E. Bennethum  
General Motors Corporation  
Detroit Diesel Division  
13400 W. Outer Drive, RO3-B  
Detroit, MI 48239  
Tel  
Fax

Robert Bill  
Army Research Lab.  
Vehicle Propulsion Directorate  
Lewis Research Center  
21000 Brookpark Road  
Cleveland, OH 44135-3127  
Tel (216) 433-3694  
Fax (216) 433-3720

Bob Bolton  
Aviation Advanced Tech. Center  
ATTN:SAVDL-ATL-ATP  
Fort Eutis, VA 22060  
Tel  
Fax

Gary Borman  
U of Wisconsin-Madison  
Engine Research Center - ERB  
1500 Johnson Drive  
Madison, WI 53706  
Tel (608) 263-1616  
Fax (608) 262-6707

C. T. Bowman  
Stanford University  
Department of Mechanical Engrg.  
Stanford, CA 94305  
Tel (415) 723-1745  
Fax (415) 723-1748

Michael Binder  
CERL  
P.O. Box 9005  
Champaign, IL 61826-9005  
Tel  
Fax

Jay P. Boris  
Naval Research Lab.  
Code 6400  
Washington, DC 20375  
Tel (202) 767-3055  
Fax (202) 767-4798

Claus Bornake  
University of Michigan  
Dept. of Mechanical Engrg.  
Ann Arbor, MI 48109  
Tel  
Fax

Frediano V. Bracco  
Princeton University  
Dept. of MAE  
Princeton, NJ 08544-5263  
Tel (609) 258-5191  
Fax (609) 258-6109

Kenneth Brezinsky  
Princeton University  
Dept. of MAE  
Princeton, NJ 08544-5263  
Tel (609) 258-5225  
Fax (609) 258-6109

William L. Brown, Jr.  
Caterpillar Inc.  
Technical Center  
PO Box 1875  
Peoria, IL 61656-1875  
Tel  
Fax

Walter Bryzik  
Army Tank Command  
ATTN: DRSTA-RGD  
Propulsion Systems Division  
Tank Automotive Command  
Warren, MI 48397-5000  
Tel (810) 574-6461  
Fax (810) 574-5054

H.F. Calcote  
AeroChem Research Lab.  
P.O. Box 12  
Princeton, NJ 08542  
Tel (609) 921-7070  
Fax (908) 329-8292

Nicholas P. Cernansky  
Drexel University  
Dept. of Mech. Engrg.  
Philadelphia, PA 19104-2884  
Tel (215) 895-2284  
Fax (215) 895-1978

George E. Cheklich  
Army Tank Command  
ATTN: DRSTA-RGE  
Tank-Automotive Command  
Warren, MI 48397-5000  
Tel  
Fax

Norman Chigier  
Carnegie Mellon University  
Department of Mechanical Engrg.  
Pittsburgh, PA 15213-3890  
Tel (412) 268-2498  
Fax (412) 268-3348

Peck Cho  
Michigan Technical University  
ME & EM  
1400 Townsend Drive  
Houghton, MI 49931-1295  
Tel (906) 487-2891  
Fax (906) 487-2822

Ken Choi  
Drexel University  
Dept. of MEM  
Market & 32 St  
Philadelphia, PA 19104  
Tel (215) 895-1586  
Fax

Charles Church  
SARD-TL  
Room 3E374  
Pentagon  
Washington, DC 20310-0103  
Tel  
Fax

John M. Clarke  
Caterpillar Inc.  
Technical Center  
PO Box 1875  
Peoria, IL 61656-1875  
Tel (309) 578-3913  
Fax (309) 578-4233

R.S. Cohen  
Temple University  
Dept. of Mech. Engrg.  
Philadelphia, PA 19122  
Tel (215) 204-6245  
Fax (215) 204-6936

Meredith B. Colket, III  
United Tech Research Center  
441 Silver Lane  
MS #30  
East Hartford, CT 06108  
Tel (203) 727-7481  
Fax (203) 727-7852

Peter DeBarber  
MetroLaser, Inc.  
18006 Skypark Circle, Suite 108  
Irvine, CA 92714-6428  
Tel (714) 553-0688  
Fax (714) 553-0495

John Dec  
Sandia National Laboratories  
Division 8362  
P.O. Box 969  
Livermore, CA 94550-0969  
Tel (510) 294-3269  
Fax (510) 294-2276

Richard A. Dobbins  
Brown University  
Division of Engineering  
Providence, RI 02912  
Tel (401) 863-2653  
Fax (401) 351-0742

Michael C. Drake  
General Motors Research Labs  
Physical Chemistry Dept.  
Box 9055  
Warren, MI 48090-9055  
Tel (313) 986-1320  
Fax (313) 986-8697

Frederick L. Dryer  
Princeton University  
D-316 Engineering Quadrangle  
Princeton, NJ 08544-5263  
Tel (609) 258-5206  
Fax (609) 258-1939

Alan C. Eckbreth  
United Tech Research Center  
MS 88  
Silver Lane  
East Hartford, CT 06108  
Tel (203) 727-7269  
Fax (203) 727-7911

Gordon England  
General Dynamics  
Vice President-Research and Engrg.  
PO Box 2074  
Warren, MI 48090-2074  
Tel  
Fax

G.M. Faeth  
The University of Michigan  
Aerospace Engineering  
550 E. University  
Ann Arbor, Michigan 48109-1092  
Tel (313) 764-7202  
Fax (313) 936-0106

Patrick Farrell  
U of Wisconsin - Madison  
Engine Research Center-ERB  
1500 Johnson Drive  
Madison, WI 53706  
Tel (608) 263-1686  
Fax (608) 262-6707

Philip G. Felton  
Princeton University  
MAE Department  
D326 Engrg. Quad.  
Princeton, NJ 08544  
Tel (609) 258-4672  
Fax (609) 258-6109

Patrick F. Flynn  
Cummins Engine Co  
P.O. Box 3005 - MC50181  
Columbus, IN 47201  
Tel  
Fax

Dave Foster  
U of Wisconsin-Madison  
Engine Research Center - ERB  
1500 Johnson Drive  
Madison, WI 53706  
Tel (608) 263-1617  
Fax (608) 262-6707

Michael Frenklach  
Penn State University  
202 Academics Projects Building  
University Park, PA 16802  
Tel (814) 864-4392  
Fax (814) 865-3075

Dennis H. Gibson  
Caterpillar Inc.  
Technical Center  
PO Box 1875  
Peoria, IL 61656-1875  
Tel  
Fax

Irvin Glassman  
Princeton University  
Department of Mech. & Aero. Engrg.  
P O Box CN5263  
Princeton, NJ 08544-5263  
Tel (609) 258-5199  
Fax (609) 258-6109

Alessandro Gomez  
Yale University  
Department of Mechanical Engrg.  
P O Box 2159YS  
New Haven, CT 06520  
Tel  
Fax

Jayavant P. Gore  
Purdue University  
School of Mechanical Engineering  
1003 Chaffee Hall  
West Lafayette, IN 47907-1003  
Tel (317) 494-1452  
Fax (317) 494-0530

F. C. Gouldin  
Cornell University  
Dept. of Mech & Aero Engrg  
Upson Hall  
Ithaca, NY 14853  
Tel (609) 255-5280  
Fax (609) 255-1222

Marvin Gunn, Jr.  
U.S. Department of Energy  
Energy Conservation  
and Utilization Tech., C-12  
1000 Independence Avenue, SW  
Washington, DC 20585  
Tel  
Fax

A.K. Gupta  
University of Maryland  
Dept. of Mechanical Engrg.  
College Park, MD 20742  
Tel (301) 405-5276  
Fax (301) 314-9477

Nabil S. Hakim  
General Motors Corporation  
Detroit Diesel Division  
13400 W. Outer Drive, RO3-B  
Detroit, MI 48239  
Tel  
Fax

D.L. Harrington  
G M Research Labs  
Fluid Mechanics Department  
12 Mile & Mound Rd.  
Warren, MI 48090  
Tel  
Fax

Naeim A. Henein  
Wayne State University  
Department of Mechanical Engrg.  
Center for Automotive Research  
Detroit, MI 48202  
Tel (313) 577-3887  
Fax (313) 577-3881

John H. Johnson  
Michigan Technological University  
Dept. of Mech. & Engrg. Mechanics  
Houghton, MI 49931  
Tel (906) 487-2551  
Fax (906) 487-2822

K. Kailasanath  
Naval Research Laboratory  
Code 4410  
Washington, DC 20375  
Tel (202) 767-2402  
Fax (202) 767-4798

C.W. Kauffman  
The University of Michigan  
Gas Dynamics Laboratories  
Dept. of Aerospace Engrg.  
Ann Arbor, MI 48109  
Tel (313) 936-0104  
Fax (313) 763-0578

Ian M. Kennedy  
University of California  
Mech. Engrg. Dept.  
Davis, CA 95616  
Tel (916) 752-2796  
Fax (916) 752-4158



Lawrence A. Kennedy  
Ohio State University  
Dept. of Mechanical Engineering  
206 West 18th Ave.  
Columbus, Ohio 43210  
Tel (614) 292-5782  
Fax (614) 292-3163

Merrill K. King  
NASA Headquarters  
300 E St., S.W.  
Code SNB, Rm. 4T86  
Washington, DC 20546  
Tel (202) 358-0817  
Fax

David B. Kittleson  
University of Minnesota  
Mechanical Engineering  
111 Church Street Southeast  
Minneapolis, MN 55455  
Tel  
Fax

David Klett  
NC A&T State University  
Dept. of Mech. Engrg.  
Greensboro, NC 27411  
Tel (910) 334-7620  
Fax (910) 334-7417

Tom G. Kreutz  
Princeton University  
Department of Mech & Aero Engrg  
Princeton, NJ 08544  
Tel (609) 258-5643  
Fax (609) 258-6233

Roger Krieger  
General Motors Research Corp.  
Fluids Mechanics Dept. Res. Labs  
Warren, MI 48090-9055  
Tel (313) 986-0012  
Fax (313) 986-0176

V.C. Arun Kumar  
Drexel University  
4400 Spruce St., #E-4  
Philadelphia, PA 19104  
Tel (215) 895-1245  
Fax (215) 895-1264

S.H. Harvey Lam  
Princeton University  
Department of MAE  
Princeton, NJ 08544  
Tel (609) 258-5133  
Fax (609) 258-6109

Moshe Lavid  
Energia Inc.  
P O Box 1468  
Princeton, NJ 08543  
Tel (609) 799-7970  
Fax

Chung K. Law  
Princeton University  
Dept. of MAE  
Princeton, NJ 08544-5263  
Tel (609) 258-5271  
Fax (609) 258-6233

Albert Lee  
NIST  
Chemical Science & Technology Lab  
Process Measurements Division  
Bldg. 221/B-312  
Gaithersburg, MD 20899  
Tel (301) 975-5190  
Fax (301) 869-5924

M.E. LePera  
U.S. Army Belvoir Research  
and Development Center  
ATTN: DRDME-GL  
Fort Belvoir, VA 22060  
Tel  
Fax

Sid J. Lestz  
Belvoir Fuels and Lubricants  
Research Facility  
Southwest Research Institute  
P.O. Drawer 28510  
San Antonio, Texas 78284  
Tel  
Fax

Houliang Li  
Drexel University  
32 & Chestnut St  
Philadelphia, PA 19104  
Tel (215) 895-1251  
Fax (215) 895-1264

S.P. Lin  
Clarkson University  
Dept. of Mech. Engrg.  
Potsdam, NY 13676  
Tel (315) 268-6584  
Fax (315) 268-6438

Milton J. Linevsky  
National Science Foundation  
1800 G. Street, NW  
Washington, DC 20550  
Tel (202) 357-9609  
Fax (202) 357-5184

Oscar P. Manley  
U.S. Department of Energy  
Office of Basic Energy Sciences  
Div. of Engrg. Math. & Geosciences  
Washington, DC 20545  
Tel (301) 903-5822  
Fax

David Mann  
Army Research Office  
P O Box 12211  
Research Triangle Park  
NC 27709-2211  
Tel (919) 549-4249  
Fax (919) 549-4310

Jay Martin  
U of Wisconsin-Madison  
Engine Research Center - ERB  
1500 Johnson Drive  
Madison, WI 53706  
Tel (608) 263-9460  
Fax (608) 262-6707

James Marzik  
US Army Research Laboratory  
Materials Technology Directorate  
Watertown, MA 02172  
Tel  
Fax

Thomas W. McCormick  
Drexel University  
1080 Holly Tree Rd  
Abington, PA 19001  
Tel (215) 895-1248  
Fax (215) 895-1264

John McVey  
United Tech. Research Center  
East Hartford, CT 06108  
Tel  
Fax

A.M. Mellor  
Vanderbilt University  
Dept. of Mech. Engrg.  
Box 1592, Station B  
Nashville, TN 37235-1592  
Tel (615) 343-6214  
Fax (615) 343-6687

Lynn S. Melton  
U of Texas at Dallas  
Dept. of Chemistry  
Richardson, Texas 75083-0688  
Tel (214) 690-2913  
Fax (214) 690-2925

James Mengenhauser  
STRBE-VFH  
Belvoir RD&E Center  
Ft. Belvoir, VA 22060  
Tel  
Fax

Richard B. Miles  
Princeton University  
Department of MAE  
Princeton, NJ 08544  
Tel (609) 258-5131  
Fax (609) 258-6109

David L. Miller  
Drexel University  
Mechanical Engrg. Department  
32 & Chestnut St  
Philadelphia, PA 19104  
Tel (215) 895-2429  
Fax (215) 895-1478

Hukam C. Mongia  
Allison Gas Turbine  
P O Box 420  
Indianapolis, IN 46206-0420  
Tel (317) 230-2000  
Fax

Clifford Moses  
Southwest Research Institute  
6220 Culebra Road  
San Antonio, TX 78238  
Tel (512) 522-2370  
Fax (512) 522-5720

Edward J. Mularz  
Army Research Laboratory  
Vehicle Propulsion Directorate  
Lewis Research Center  
21000 Brookpark Road  
Cleveland, OH 44135-3127  
Tel (216) 433-5850  
Fax (216) 433-3000

Henry Newhall  
Chevron Research Co.  
576 Standard Avenue  
Richmond, CA 94802  
Tel  
Fax

Anthony K. Oppenheim  
U of California at Berkeley  
Dept. of Mech. Engrg.  
Berkeley, CA 94720  
Tel (415) 642-0211  
Fax (415) 642-1246

Elaine S. Oran  
Naval Research Labs.  
Code 4404  
Washington, DC 20375  
Tel (202) 767-2960  
Fax (202) 767-4798

William C. Pfefferle  
Precision Combustion  
25 Science Park  
New Haven, CT 06511  
Tel (203) 786-5215  
Fax (203) 786-5214

Rolf Reitz  
U of Wisconsin-Madison  
Engine Research Center - ERB  
1500 Johnson Drive  
Madison, WI 53706  
Tel (608) 262-0145  
Fax (608) 262-0167

Gabriel Roy  
Office of Naval Research  
Code 1132P  
800 North Quincy Street  
Arlington, VA 22217  
Tel (703) 696-4406  
Fax (703) 697-0934

Donald J. Patterson  
University of Michigan  
Dept. of Mech. Engrg.  
Automotive Laboratory  
North Campus  
Ann Arbor, MI 481098  
Tel  
Fax

Roy J. Primus  
Cummins Engine Co  
M.C. 50180  
P.O. Box 3005  
Columbus, IN 47202-3005  
Tel (812) 377-7094  
Fax (812) 377-7808

K.T. Rhee  
Rutgers University  
Dept. of Mech. & Aero. Engrg.  
P.O. Box 909  
Piscataway, NJ 08855  
Tel (908) 932-3651  
Fax (908) 932-5313

Gary A. Ruff  
Drexel University  
MEM Department  
32nd and Chestnut St  
Philadelphia, PA 19104  
Tel (215) 895-1373  
Fax (215) 895-1478

Christopher J. Rutland  
U of Wisconsin - Madison  
Engine Research Center-ERB  
1500 Johnson Drive  
Madison, WI 53706  
Tel (608) 262-5853  
Fax (608) 265-2316

Joseph J. Sangiovanni  
United Tech Research Center  
411 Silver Lane  
MS 30  
East Hartford, CT 06108  
Tel (203) 727-7328  
Fax (203) 727-7852

Domenic A. Santavicca  
Penn State University  
314 Mechanical Engrg. Building  
University Park, PA 16802  
Tel (814) 863-1863  
Fax (814) 865-3389

R.J. Santoro  
Penn State University  
Dept. of Mech. Engrg.  
University Park, PA 16801  
Tel (814) 863-1285  
Fax (814) 865-2165

Robert F. Sawyer  
U of California, Berkeley  
Dept. of Mechanical Engineering  
Berkeley, California 94720, USA  
Tel (510) 642-5573  
Fax (510) 339-3915

Hratch G. Semerjian  
NIST  
Chemical Science & Technology  
221/B306  
Gaithersburg, MD 20899  
Tel (301) 975-2609  
Fax (301) 926-5002

K. Seshadri  
U of California, San Diego  
Dept. of Applied Mechanics  
and Engineering Sciences B-010  
La Jolla, CA 92093  
Tel (619) 534-4876  
Fax (619) 534-5354

Steve Shepard  
U.S. Army  
ATTN: AMSTA-RSA  
Tank- Automotive Command  
Warren, MI 48397-5000  
Tel  
Fax

Dennis Siebers  
Sandia National Laboratories  
Division 8362  
P.O. Box 969  
Livermore, CA 94550-0969  
Tel (510) 294-2078  
Fax (510) 294-1004

Harold Simmons  
Parker Hannifin Corp  
Gas Turbine Fuel Systems, Div.  
17325 Euclid Ave  
Cleveland, OH 44143  
Tel (216) 531-3000  
Fax

H. Singh  
N C A&T State University  
College of Engineering  
Architectural Engrg. Dept.  
Greensboro, NC 27411  
Tel  
Fax

W. A. Sirignano  
U of California at Irvine  
305 Rockwell Engineering Center  
Irvine, CA 92717-2700  
Tel (714) 856-6002  
Fax (714) 856-7966

Young-Hoon Song  
Penn State University  
15 Research Bldg. E  
University Park, PA 16802  
Tel (814) 863-6075  
Fax (814) 865-3389

R.J. Tabaczynski  
Ford Motor Corp.  
Engine Research Dept.  
Village Plaza, Suite 800  
23400 Michigan Avenue  
Dearborn, MI 48124  
Tel (313) 337-3495  
Fax (313) 323-1875

Julian M. Tishkoff  
Aerospace Sciences Directorate  
Office of Scientific Research  
Bolling Air Force Base  
Washington, DC 20332  
Tel (202) 767-0465  
Fax (202) 767-4988

James Trolinger  
MetroLaser  
18006 Skypark Circle 108  
Irvine, CA 92715  
Tel (714) 553-0688  
Fax (714) 553-0495

Wing Tsang  
NIST  
Chemical Kinetics Division  
Gaithersburg, MD 20899  
Tel (301) 975-2507  
Fax

Arjun Tuteja  
Southwest Research Institute  
6220 Culebra Road  
P.O. Drawer 28510  
San Antonio, TX 78228-0510  
Tel  
Fax

Mark Valco  
NASA Lewis Research Center  
Vehicle Propulsion Directorate  
Army Research Laboratory  
MS 86-6  
Cleveland, OH 44135-3127  
Tel  
Fax

Charles K. Westbrook  
Lawrence Livermore Natl. Lab.  
P O Box 808  
Livermore, CA 94550  
Tel (415) 422-4108  
Fax (415) 422-8511

F. A. Williams  
U of California at San Diego  
Dept. of AMES, B-010  
La Jolla, CA 92093  
Tel (619) 534-5452  
Fax (619) 534-5354

Michael Winter  
United Tech Research Ctr.  
411 Silver Lane  
East Hartford, CT 06108  
Tel (203) 727-7805  
Fax (203) 727-7911

William Wintucky  
NASA Lewis Research Center  
MS 86-6  
21000 Brookpark Road  
Cleveland, OH 44141  
Tel  
Fax

Christopher H. Wood  
Drexel University  
115 N 34th St  
Philadelphia, PA 19104  
Tel (215) 895-1251  
Fax (215) 895-1264



Roger Woodward  
Phillips Laboratory  
OLAC, PL/RKFA  
10 East Saturn Blvd  
Edwards AFB, CA 93524-7660  
Tel (805) 275-6234  
Fax (805) 275-6233

Richard A. Yetter  
Princeton University  
Department of MAE  
Princeton, NJ 08544  
Tel (609) 258-2947  
Fax (609) 258-1939

Ronald E. York  
General Motors Corporation  
Allison Gas Turbine Operations  
PO Box 420, Speed Code U-25  
Indianapolis, IN 46206-0420  
Tel  
Fax